Spray Development and Combustion in Direct-Injection Diesel Engines

by

Sung Taek Cho
B.A. MSc



Department of Mechanical Engineering
Imperial College of Science, Technology and Medicine
University of London

Thesis submitted for the degree of
Doctor of Philosophy
in the University of London
and for the
Diploma of Membership of the Imperial College

August 1999

BIBL
LONDON

ABSTRACT

This thesis presents an experimental study performed in a Ricardo Hydra single-cylinder and a Volkswagen four-cylinder, purpose-built optically accessible high-speed direct-injection diesel engines and focused on the effect of the exhaust gas recirculation (EGR), boost pressure, inlet swirl, fuel delivery, injection pressure and nozzle configuration on spray development, combustion and exhaust emissions. The investigations were conducted by means of analysis of cylinder pressure, measurement of exhaust emissions, visualisation of fuel spray and combustion, and characterisation of in-cylinder soot concentration.

The results of these investigations have confirmed that an increase in the EGR rate is associated with longer ignition delay, lower NO_x and higher smoke emissions, while increasing the inlet boost pressure resulted in shorter ignition delay, higher engine efficiency, lower smoke number, and a small effect on NO_x unlike increasing swirl which resulted in a significant increase in NO_x levels. These results imply that the combination of EGR and supercharging can provide a convenient way of reducing NOx emissions without any significant deterioration in engine efficiency and smoke emissions. In addition, visualisation of the sprays generated by an inclined multi-hole nozzle has revealed that an increase in boost pressure resulted in reduced spray tip penetration and a wider cone angle due to the enhanced air entrainment at the higher in-cylinder gas densities.

In addition to the exhaust smoke levels, the in-cylinder planar soot concentration which was characterised by laser-induced incandescence (LII) and laser-induced scattering (LIS) showed that the smoke level increase with increasing EGR rate is the result of the enhanced soot formation and shorter soot oxidation period due to the reduction of oxygen concentration and the prolonged ignition delay.

The effect of injection pressure and nozzle configuration on spray development, combustion and exhaust emissions was investigated in the same Hydra single-cylinder engine which was modified to incorporate a four-valve head with a centrally positioned vertical multihole injector connected to an advanced electronic rotary pump. The visualisation of the six sprays has confirmed that a centrally positioned vertical injector provides an even distribution of the sprays with an associated improved air-fuel mixing and minimisation of local hot spots. The results also showed that the higher injection pressure resulted in faster

spray tip penetration and earlier impingement of the fuel on the wall and dispersion along the wall, which resulted in a significant reduction in ignition delay.

Overall, the higher injection pressure and smaller nozzle hole resulted in shorter ignition delay, lower smoke levels but higher NO_x emissions due to the improved fuel atomisation. However, further increase in injection pressure resulted in no improvement in the smoke-NO_x trade-off curve due to the increased wall impingement, while a smaller nozzle hole counterbalances this effect leading to reduced NO_x and smoke levels.

ACKNOWLEDGEMENTS

I would like to thank my supervisor Professor C. Arcoumanis for the guidance, advice and encouragement he provided throughout my study at Imperial College.

Further, I would like to thank Dr. Arun. Nagwaney for introducing me to practical engine research using laser diagnostic techniques. The assistance of Dr. Xu during the LII and LIS experiment is deeply appreciated. I would like to thank Dr. Paul Cutter and Dr. Stuart Whitelaw for their assistance, discussion and many useful suggestions throughout the study. Further, the technical assistance of Harmindar Flora, Ian Wright, Fred Hall and Phil Proctor is most appreciated. I am particularly grateful to Dr. H. S. Yi for his important contribution to the work.

Specially, I would like to thank Dr. J. P. Hong, a general manager of Lucas Diesel Korea for the financial support and encouragement he provided during the course of project.

Finally, I would like to thank my wife, parents and sister for supporting my work during my stay in London.

TABLE OF CONTENTS

ABSTRACT 2
ACKNOWLEDGEMENTS 4
TABLE OF CONTENTS 5
LIST OF TABLES 8
LIST OF FIGURES 9
LIST OF SYMBOLS 13

CHAPTER 1 INTRODUCTION AND LITERATURE REVIEW

1.1 Introduction 15
1.2 Literature review 18
1.2.1 Spray development 18
1.2.2 Combustion development 22
1.2.3 Pollutant formation and exhaust emissions 25
1.2.4 Exhaust gas recirculation 30
1.2.5 Supercharging and turbocharging 37
1.3 Outline of thesis 39

CHAPTER 2 THE ROLE OF EGR AND SUPERCHARGING IN DIRECT INJECTION DIESEL ENGINES

2.1 Introduction 67
2.2 Experimental system 68
2.2.1 Test engines and test conditions 69
2.2.1.1 Four-cylinder engine 69
2.2.1.2 Single-cylinder engine 71
2.2.2 NO_x and smoke measurements 73
2.2.3 Visualisation of spray and combustion 74
2.2.3.1 Four-cylinder engine 74
2.2.3.2 Single-cylinder engine 75
2.3 Results and Discussion 75
2.3.1 Spray development 76
2.3.1.1 Four-cylinder engine 76

2.3.1.2 Single-cylinder engine 76
2.3.1.3 Spray tip penetration 77
2.3.2 Auto-ignition and flame development 79
2.3.3 Combustion and emissions 80
2.3.2.1 Effect of EGR 81
2.3.2.2 Effect of supercharging 85
2.3.3.3 Effect of swirl 88
2.3.3.4 Combined effect of EGR and supercharging 89
2.3.3.5 Effect of injection timing 92
2.4 Summary 93

CHAPTER 3 EFFECT OF EGR ON IN-CYLINDER SOOT DISTRIBUTION

3.1 Introduction 116
3.2 Imaging diagnostics 118
3.2.1 Laser induced incandescence (LII) 118
3.2.2 Laser induced scattering (LIS) 123
3.3 Experimental system 125
3.3.1 Test engine and test conditions 125
3.3.2 Laser sheet and optical set-up 127
3.3.3 Timing, triggering 130
3.3.4 Image processing 131
3.3.5 Uncertainties 132
3.4 Results and discussion 133
3.5 Summary 138

CHAPTER 4 THE ROLE OF INJECTION PARAMETERS IN A DIRECT-INJECTION DIESEL ENGINETo

4.1 Introduction 155
4.2 Experimental system 158
4.2.1 Engine and fuel injection system 158
4.2.2 Optical system 160
4.2.3 Test conditions 160
4.3 Results and discussion 161
4.3.1 Measurement of injection pressure, injection rate and needle lift 161

4.3.2 Spray and flame development 163
4.3.3 Combustion and Emissions 166
4.3.3.1 Effect of injection pressure 166
4.3.3.2 Effect of nozzle configuration 169
4.3.3.3 Effect of injection rate 170
4.3.3.4 Effect of nozzle protrusion into cylinder 171
4.4 Summary 172

CHAPTER 5 CONCLUSIONS AND RECOMMENDATIONS FOR FURTHER WORK

5.1 Conclusions 198
5.2 Recommendations for future work 200

REFERENCES 202

LIST OF TABLES

Table		Page
1.1	Literature review	40
1.2	Summary of new and proposed European emission standards for passenger car diesel vehicles	66
2.1	Geometric characteristic and operating conditions of the four-cylinder VW 1.9L engine	95
2.2	Geometric characteristic and operating conditions of the single-cylinder Hydra engine	96
2.3	Intake mass flow rate of air	97
3.1	Test conditions for LII and LIS experiment	140
4.1	Geometric characteristics of the modified four-valve single-cylinder Hydra engine	173
4.2	Test conditions of the modified Hydra engine	173

LIST OF FIGURES

Figure		Page
2.1	Schematic and photograph of the VW 1.9L HSDI diesel engine	98
2.2	Schematic of the supercharged Ricardo DI diesel engine incorporating EGR and the orientation of the sprays in the cylinder head	99
2.3	Comparison of spray images for different intake air charge conditions with 0% EGR rate at 5°bTDC; four-cylinder engine	100
2.4	Spray tip development at various engine operating conditions; single-cylinder engine	101
2.5	Spray tip penetration at different engine operating conditions; single-cylinder engine	102
2.6	Drum camera sequence of a complete cycle of sprays #2 & #3 at 1200rpm engine speed, 20mm^3/inj. and swirl ratio of 2.2 with various booster pressures; single-cylinder engine	103
2.7	Auto-ignition for various engine operating conditions in the four-cylinder engine	104
2.8	Flame development for various engine operating conditions in the four-cylinder engine	104
2.9	Cylinder pressure and heat release rate curves at engine speed of 1200rpm at various EGR rate and fuel delivery; single-cylinder engine	105
2.10	Start of ignition plotted against EGR rate for various fuel deliveries under NA conditions; single-cylinder engine	106
2.11	IMEP plotted against EGR rate for various fuel deliveries under NA conditions; single-cylinder engine	106
2.12	Bosch smoke number and NO_x concentrations plotted against EGR rate for fuel deliveries and swirl ratios under NA conditions; single-cylinder engine	106
2.13	Cylinder pressure and heat release rate curves at engine speed of 1200rpm and at various boost pressures and fuel deliveries; single-cylinder engine	107
2.14	Start of ignition plotted against boost pressure for various fuel deliveries and swirl ratios; single-cylinder engine	108

Figure		Page
2.15	IMEP plotted against boost pressure for various fuel deliveries and swirl ratios; single-cylinder engine	108
2.16	Bosch smoke number and NO_x concentrations plotted against boost pressure for various fuel deliveries and swirl ratios; single-cylinder engine	108
2.17	Cylinder pressure and heat release rate curves at engine speed of 1200rpm for various swirl ratios; single-cylinder engine	109
2.18	Start of ignition plotted against swirl ratio for various EGR rates and boost pressures; single-cylinder engine	110
2.19	IMEP plotted against swirl ratio for various EGR rates and boost pressures; single-cylinder engine	110
2.20	Bosch smoke number and NO_x concentrations plotted against swirl ratio for various EGR rates and boost pressures; single-cylinder engine	110
2.21	Cylinder pressure and heat release rate curves at engine speed of 1200rpm at various EGR rates and boost pressures; single-cylinder engine	111
2.22	Start of ignition plotted against EGR rate for various boost pressures	112
2.23	IMEP plotted against EGR rate for various boost pressures	112
2.24	Bosch smoke number and NO_x concentrations for various EGR rates and boost pressures; single-cylinder engine	113
2.25	Start of ignition, cylinder pressure and heat release rate curves at engine speed of 1500rpm for various engine operating conditions; four-cylinder engine	114
2.26	Bosch smoke number NO_x concentrations; four-cylinder engine	115
3.1	Photograph of the exhaust gas recirculation system in VW 1.9L HSDI diesel engine	141
3.2	Cylinder head and piston-bowl geometry of VW 1.9L HSDI diesel engine: optical access through quartz side-window in the liner and a pair of quartz plates in the piston-bowl side wall	141
3.3	Piston-bowl image with identified landmarks	142
3.4	Experimental set-up for the LII and LIS experiment	142
3.5	Lens arrangement for LII and LIS laser sheet	143
3.6	Optical access into the test engine	143
3.7	Specification curves for optical filters used in the LII and LIS experiment	144

Figure		Page
3.8	Unmodified (left) and processed (right) LIS image	145
3.9	Spray images obtained with high-speed CCD camera (IMACON 468) at 1000rpm with 0% EGR rate	146
3.10	Flame images obtained with high-speed CCD camera at 1000rpm	147
3.11	Flame images obtained with high-speed CCD camera (IMACON 468) at 1000rpm with time resolution of 0.25° CA	148
3.12	Cycle-to-cycle variation of LII images at 1000rpm with 0% EGR rate during main combustion period	149
3.13	Cycle-to-cycle variation of LII images at 1000rpm with 50% EGR rate during main combustion period	150
3.14	Cycle-to-cycle variation of LIS images at 1000rpm with 0% EGR rate during main combustion period	151
3.15	Cycle-to-cycle variation of LIS images at 1000rpm with 50% EGR rate during main combustion period	152
3.16	LII images at 1000rpm with 12mm^3/st of fuel delivery after main combustion	153
3.17	LIS images at 1000rpm with 12mm^3/st of fuel delivery after main combustion	154
4.1	Schematic of the four-valve engine incorporating a high pressure injection pump and the orientation of sprays in the cylinder head	174
4.2	Injection pressure, needle lift and injection rate profiles for the normal and doubled pump speeds	175
4.3	Injection pressure, needle lift and injection rate profiles for 20mm^3/inj and 25mm^3/inj of fuel delivery	176
4.4	Injection pressure and injection rate profiles for the different nozzle configurations	177
4.5a	Spray development for different injection pressure at engine speed of 1200rpm with S nozzle	178
4.5b	Spray development for different injection pressure at engine speed of 1200rpm with L nozzle	179
4.6	Spray tip penetration for different injection pressure and nozzle configurations	180
4.7	Flame development for different injection pressure at engine speed of 1200rpm with S nozzle	181

Figure		Page
4.8	Cylinder pressures and heat release rates for normal and doubled pump speed at various engine operating conditions	182
4.9	Effects of injection pressure on NOx emissions at various engine operating conditions	183
4.10	Effects of injection pressure on smoke emissions at various engine operating conditions	184
4.11	Effects of injection pressure on smoke-NOx trade-off curves at various engine operating conditions	185
4.12	IMEP calculated from the cylinder pressures at 3 bTDC injection timing for various engine operating conditions	186
4.13	Cylinder pressures and heat release rates for different nozzle configurations at various engine operating conditions	187
4.14	Effect of nozzle configuration on NOx emissions at various engine operating conditions	188
4.15	Effect of nozzle configuration on smoke emissions at various engine operating conditions	189
4.16	Effect of nozzle configuration on smoke-NOx trade-off at various engine operating conditions	190
4.17	Injection pressure and injection rate profiles for the normal pump speed with S nozzle and the doubled pump speed with L nozzle	191
4.18	Cylinder pressures and heat release rates for different injection rates at various engine operating conditions	192
4.19	Effect of injection rate on NOx emissions at various engine operating conditions	193
4.20	Effect of injection rate on smoke emissions at various engine operating conditions	194
4.21	Effect of injection rate on smoke-NOx trade-off curves at various engine operating conditions	195
4.22a	Effect of nozzle protrusion on exhaust emissions at various engine operating conditions; S nozzle	196
4.22b	Effect of nozzle protrusion on exhaust emissions at various engine operating conditions; L nozzle	197

LIST OF SYMBOLS

The symbols used in the thesis are listed below, together with the most commonly used units and values, where applicable. In cases where a symbol has been used with more than one meaning, the appropriate definition is given in the accompanying text.

SYMBOLS

$K_{abs}(a)$	Mie absorption efficiency;
a	radius of soot particle, cm (typical $<1 \times 10^{-5}$ cm);
q	peak laser intensity, W/cm^2;
T_o	ambient flame temperature, K (typical 1500-2000 K);
T	temperature of particle, K;
K_a	thermal conductivity of air, $W\ cm^{-1}\ K^{-1}=5.83 \times 10^{-5}\ (T/273)^{0.82}$;
G	geometry-dependent heat transfer factor = $8f\cdot(\gamma+1)/\alpha$;
K_n	Knudsen number = $\gamma/L = \gamma/2a$;
γ	C_p/C_v (=1.40 for air);
λ	mean free path, cm = $2.355 \times 10^{-8}\cdot T$ for air at 1 atm;
L	characteristic length; cm = $2a$ for sphere;
ΔH_v	heat of vaporisation of carbon, J/mol = 7.78×10^{-5};
W_s	molecular weight of solid carbon = 12g/mol;
σ_{sb}	Stefan-Boltzmann constant;
M	mass particle, grams;
t	time, sec;
c_s	specific heat of carbon = 1.90 $J\cdot g^{-1}\cdot K^{-1}$;
ρ_s	density of solid carbon = 2.26 $g\cdot cm^{-3}$;
ρ_v	density of carbon vapour = PWv/RT;
W_v	molecular weight of vapour taken as 36 g/mol;
U_v	velocity of vapour;
R	gas constant = 8.31 $j\cdot K^{-1}\cdot mol^{-1}$;
δ	absorption length parameter;

ABBREVIATION

aTDC	After top dead centre
BMEP	Break mean effective pressure
BSFC	Break specific fuel consumption
bTDC	Before top dead centre
CA	Crank Angle
CCD	Charge couple device or combustion chamber for disturbance
DI	Direct injection
EGR	Exhaust gas recirculation
$EINO_x$	Emission index of NO_x (grams of NO_x per kg of fuel)
EOI	End of injection
FID	Flame ionisation detector
FIE	Fuel injection equipment
FWHM	Full width at half maximum
GLI	Grey level intensity
HBW	Half-band width
HS	High-speed
IDI	Indirect injection
IMEP	Indicated mean effective pressure
LIF	Laser-induced fluorescence
LII	Laser-induced incandescence
LIS	Laser-induced scattering
LWP	Long wave pass
NA	Naturally aspirated
NO_x	Nitrogen oxides
rpm	Revolutions per minute
SOI	Start of injection
SWP	Short wave pass
TDC	Top dead centre
VW	Volkswagen

CHAPTER 1

INTRODUCTION AND LITERATURE REVIEW

1.1 INTRODUCTION

In the past, the emphasis in developing reciprocating engines was mainly on specific power and fuel efficiency with little concern about the environment. Recently it has become more important and urgent to reduce the environmental pollution levels caused by vehicle exhaust gases, as the emission regulations are becoming more stringent.

It is well known that diesel engines offer superior fuel consumption than gasoline engines of equivalent capacity but their relatively high exhaust levels of oxides of nitrogen (NO_x) and particulates are a serious drawback in improving their sales position and image between customers. Nevertheless, over the last few years, the share of diesel engine market for light duty automotive applications has been significantly increased by virtue of their inherent superior fuel economy, durability and lower gaseous emissions, while maintaining their traditional role as power plants of heavy duty vehicles. Furthermore, recent emphasis in Europe on reducing CO_2 emissions because of their greenhouse effect is expected to increase the sales of diesel engines in the light duty automotive market.

From the two available types of diesel engine, indirect injection diesels have been until recently favoured for light duty automotive applications because of their relatively low levels of noise and exhaust emissions compared with the direct injection engine which was traditionally confined to medium and heavy duty applications. However, in general, direct injection diesel engines have a compact shape of combustion chamber compared with indirect injection diesels incorporating a pre-chamber. This indicates that there is a relatively low heat loss to the cooling system due to the smaller surface area of the combustion chamber, and the absence of any pressure drop associated with the motion of the air from the pre-chamber to the main chamber. The end result is higher fuel efficiency by 10 to 15 percent and less CO_2 emissions compared with indirect injection diesel engines. These advantages of the direct injection type have encouraged its application to the light duty automotive sector with sizes recently approaching 1 litre engines. At the same time the HSDI engines are able to match the

IDI engine in terms of maximum rated engine speed by careful attention to the fuel injection and air motion, while keeping good starting performance.

As the only diesel engine type available in all sizes and covering a wide range of applications, the HSDI engine has attracted a lot of attention in terms of improving engine performance and reducing exhaust gaseous and particulate emissions. Many of the features imported from larger sizes or even from gasoline engines have been employed in today's advanced HSDI engines and numerous investigations on ways to optimise the combustion system have been carried out. As a result, significant improvements have been achieved in controlling noise and exhaust gaseous emissions but further reductions particularly in particulates and oxides of nitrogen are required to meet the forthcoming EURO 3 and EURO 4 emission regulations.

From the results of on-going research, a strategy for future DI diesel engines has been suggested and investigated with the aim of optimising various combined effects over a range of load and speed operating conditions (see for example, Needham and Whelan, 1994; Menne *et al.*, 1994). An optimised engine should thus be turbocharged and intercooled, equipped with electronically controlled fuel injection system capable of creating high injection pressures and multiple injections while incorporating four valve cylinder heads with central vertical injection, a re-entrant axisymmetric combustion chamber, exhaust gas recirculation (EGR) and an oxidation catalyst with or without a particulates trap.

One of the most cost-effective methods for reducing NO_x levels is exhaust gas recirculation (EGR), which has become a standard feature of passenger car diesel engines. However, there are limits to the amount of exhaust gas that can be reintroduced into the engine before power output and fuel economy are adversely affected and there are also further limitations due to the wear implications of the recirculated soot particles. The effects of EGR on NO_x, particulates and fuel consumption have been investigated in detail (Ladommatos *et al.*, 1996a and 1996b) but there are still a number of unresolved questions about the mechanisms that affect the gas temperature, soot distribution and flame luminosity, NO_x formation, fuel consumption and emissions, that need further investigation under naturally aspirated but mainly under high boost pressure conditions.

The primary purpose of supercharging or turbocharging is to increase the engine power output by allowing to burn more fuel with increasing air mass entering the engine cylinder. In addition, it has complementary effects on exhaust gas emissions by affecting spray characteristics and combustion. From the viewpoint of environmental pollution, the

turbocharging system is often employed as an effective means for reducing the levels of particulate emissions. Combining the turbocharging system with high pressure fuel injection and/or a four-valve cylinder head having a central vertical injector has been suggested as a method to achieve further reduction in exhaust gas emissions without significant deterioration in engine performance (Endo *et al.*, 1991, Daisho *et al.*, 1994). Furthermore, extensive application of electronics to various aspects of the automotive diesel engine, such as the fuel injection system, EGR and turbocharger, offer promise to improve engine performance and reduce raw emissions.

High pressure injection incorporating a central and vertical injector in a four-valve engine is considered the most effective way to improve the NO_x and particulates trade-off without any deterioration in fuel consumption. It results in improved atomisation of the fuel spray so that significant reduction in particulates can be achieved, while retarding injection timing or employing EGR can also suppress NO_x emissions.

In order to achieve further reductions in the NO_x and particulates emissions, it is essential to understand the principle of the formation and oxidation/reduction of soot and NO_x. Also it is necessary to understand the individual and combined effects of additional parameters on the fuel spray characteristics and combustion and, in turn on engine performance and exhaust gas emissions.

For the purpose of understanding the NO_x and soot formation and the effects of various parameters on engine performance and exhaust emissions, an extensive investigation was performed on the spray development and combustion in two optically accessible engines, using laser-based techniques through windows in the piston and liner. A 1.9L four-cylinder and a single cylinder DI engine were used first to investigate the individual and combined effects of EGR and supercharging on spray, combustion and emissions by means of a combination of spray and combustion visualisation, combustion pressure analysis and emission measurements. In addition, the effects of EGR on soot formation and oxidation were investigated in the four-cylinder engine by laser induced incandescence and laser induced scattering combined with combustion pressure analysis. Further, the effects of injection parameters on spray characteristics, combustion and emissions were investigated in the same single cylinder engine by incorporating a 4-valve cylinder head, electronically controlled fuel injection pump with central, vertical injector and an axisymmetric piston-bowl with a transparent flat base.

The remainder of this introductory chapter is divided into two sections. The following Section 1.2 is a literature review in the form of a discussion of the in-cylinder processes (spray development and combustion), exhaust emissions, EGR and supercharging in diesel engines with Table 1.1 providing a summary of the more recent and relevant literature on the subject of this thesis. Section 1.3 presents the objectives of the research programme as well as an outline of the subsequent four chapters.

1.2 LITERATURE REVIEW

1.2.1 Spray Development

The fuel is injected into the cylinder of a diesel engine through a nozzle having a large pressure differential across its orifice. These large pressure differences across the injector nozzle are required so that the injected liquid fuel will enter the chamber at sufficiently high velocity relative to air to achieve fine atomisation for rapid evaporation and effective interaction between sprays and in-cylinder air through enhanced entrainment. The improved air fuel mixing process affects ignition delay, combustion and pollutant formation in a number of ways. Hence extensive research has been performed on spray characteristics and spray structure with the ultimate objective to understand and predict the transient fuel spray development in the engine cylinder.

Laser diagnostics have been extensively used as experimental point and planar techniques for understanding the 3-D spray behaviour; point measuring techniques include Laser Doppler Velocimetry (LDV) or Phase Doppler Anemometry (PDA) while whole field visualisation requires various optics and a light source or laser. There are a number of differences between experimental techniques for spray visualisation. Direct spray photography, for example, cannot image droplet vaporisation and therefore reveals only the effect of temperature on liquid spray tip penetration compared to shadowgraphy which allows identification of the fuel vapour formed as part of the spray head. Also recently 2-D planar imaging techniques such as LIF (see for example, Senda *et al.*, 1992) or LIS (see for example, Espey and Dec, 1995) have started being used to investigate the spray characteristics.

Many varieties of fuel injection systems are being used to supply the engine with fuel in quantities exactly metered in proportion to the power required and at exactly the right time, so that the engine can deliver its power output within the limits prescribed for fuel

consumption and exhaust emissions. They can be divided into distribution type pump, in-line type pump, unit injector and common rail systems depending on their operating mechanism. In all systems their basic function is to provide repeatable but, according to the engine condition, variable start of injection, injection rate and injected quantity, with a further requirement the generation of good spray quality (Kent *et al.*, 1995). Recently electronics have been applied to fuel injection systems which allows more flexible control of fuel quantity and timing, even multiple injections, thus resulting in significant improvements in engine performance and emissions. The diesel fuel is pressurised through the injection system before being injected through the nozzle holes at high speed. The liquid fuel exiting from the orifice is atomised into small sized droplets which traverse the combustion chamber in the time available utilising the surrounding air charge. During their propagation into the combustion chamber, fuel droplets are vaporised at a rate depending on their size and mix with air in the so-called air entrainment process which leads to more air-mass within the spray, larger spray angle, lower spray tip velocity and enhanced evaporation of the total fuel mass (Heywood, 1988). The droplet size is strongly affected by the transient injection pressure, the injection rate, needle lift and nozzle orifice area during the injection period. On the other hand, the droplet size distribution at a location in the spray varies with time and, in general, many different sizes of droplets exist ranging from 5 to 150 μm but with the majority less than 20 μm (Hentschel, 1996). On average, the droplet sizes decrease at higher injection pressures and smaller nozzle hole diameters (Arai, 1984; Hiroyasu, 1989). Extensive parametric studies of spray characteristics have been performed over the years and empirical equations on spray tip penetration have been suggested by many researchers (Wakuri *et al.*, 1960; Dent, 1971; Arai *et al.*, 1984). The studies revealed that droplet size, spray tip penetration and spray cone angle are affected by one or more of the following variables: fuel properties (mainly viscosity), time from SOI, nozzle diameter, pressure difference between fuel and gas, and gas properties (mainly density, temperature and pressure). It is commonly accepted that spray tip penetration is reduced with decreasing gas temperature (Yule *et al.*, 1985; Yunyi and Xuanming, 1993; Espey and Dec, 1995; Verhoeven *et al.*, 1998) and with increasing gas density and pressure (Yunyi and Xuanming, 1993; Naber and Siebers, 1996) due to the higher level of aerodynamic resistance. It was also found that spray angle decreases with increasing gas temperature, fuel viscosity and droplet size (Arai *et al.*, 1984), while it increases with increasing gas density (Yunyi and Xuanming, 1993; Verhoeven *et al.*, 1998) and injection pressure (Yoshikawa *et al.*, 1988; Su and Farrell, 1998).

During diesel engine operation, the most dominant factor influencing the spray behaviour is gas density and temperature. Gas temperature affects spray formation in two ways; firstly, it has a direct influence on droplet atomisation and vaporisation, and secondly it affects gas density. The effect on the former seems to be more significant than the latter (Baert and Vermeulen, 1993). On the other hand, others (Yule *et al.*, 1985) have described the effect of temperature as being mainly through its influence on density. It seems that detecting the effect of temperature on spray development depends on the photographic system used, i.e. whether this is shadowgraphy (Verhoeven *et al.*, 1998) or direct spray photography (Baert and Vermeulen, 1993). Thus although the spray tip penetration of the liquid fuel may decrease, the overall spray tip penetration including the fuel vapour seems to remain the same with increasing gas temperature. It was further suggested (Yunyi and Xuanming, 1993) that the enhanced vaporisation due to the increased temperature could even result in a small reduction in the spray tip penetration. This could be attributed to the evaporating fuel cooling the gas mixture within the spray and hence increasing its density, thus resulting in reduced spray tip penetration (Naber and Siebers, 1996). Similarly, the wider spray angle with increasing temperature has been attributed to the larger spray volume obtained through vaporisation of the smaller fuel droplets present at the edges of the spray. On the other hand, in Yule *et al.* (1985) a reduction in spray angle with increasing temperature was observed and it was attributed to the decrease in gas density, increase in vaporisation rate and reduced droplet sizes associated with increasing temperature at constant pressure. Solbrig and Litzinger (1990) also examined the effect of intake charge temperature at constant density on spray development, with a two-component fuel using shadowgraphy, and only a very small effect on fuel penetration was observed.

When the liquid fuel is exposed to the surrounding gas through an orifice under pressure, the high velocity of the injected liquid relative to the gas commences the atomisation process. This is manifested as a disruption of the consolidating influence of surface tension, which is a liquid property of prime importance along with viscosity, by the action of internal and external forces. Surface tension tends to pull the liquid into the form of a sphere having minimum surface energy. The disintegrating process from a liquid column into fine droplets appears as soon as the liquid is injected at a sufficiently high injection pressure. Any subsequent surface instabilities are due to the combined effects of hydrodynamic and aerodynamic forces. A liquid core is currently expected for at least the submillimeter range downstream of the nozzle tip (Tsue *et al.*, 1992) but independently of the question of whether

and upto which distance a liquid core exists within the spray core, the evaporation process continues leading to the liquid and gas phases having different tip penetration characteristics (Baritaud *et al.*, 1994), with the gas phase penetrating into the piston bowl for a longer period of time as compared to the liquid phase. The size of spray droplets along the centre of a non-evaporating diesel spray generally decrease with distance, pass through a minimum and then slowly increase towards the spray tip (Yeh *et al.*, 1993b). The amount of spray impingement on the wall varies depending on the engine geometry and the fuel delivery system. When the dense spray impinges, it is expected that further active evaporation of the droplets is taking place due to mixing with the surrounding air caused by the 'wall jet vortex' (Senda *et al.*, 1992). Recently all research on spray characteristics is related to gaseous or particulate emissions. For example, the nozzle hole shape can influence the droplet size and the exhaust emissions as determined by Yoda *et al.* (1995) who found that a nozzle shape that reduces droplet size and increases spray angle can also lower smoke emissions. Further, multi-stage injection offers advantages as it decreases noise, smoke, and NO_x emissions due to the lower injection rates during the main injection period (Ashley *et al.*, 1995).

A new strategy of fuel introduction into the cylinder is under development since the electronically controlled injection pump has appeared. High pressure injection systems are needed as the diameter of the piston-bowl increases, the airflow is reduced and the smoke generation is inversely proportional to injection pressure (Krill, 1995), possibly because of the reduced droplet size (Nishijima *et al.*, 1995). Injection pressures up to 134MPa were found to result in higher vapour concentrations and increased vapour regions due to improved fuel atomisation and higher droplet velocities (Yeh *et al.*, 1993a). However, as very high injection pressures lead to high maximum temperatures which increase NO_x emissions, the timing of injection has to be controlled carefully (Krill, 1995). Generally, a reduction in NO_x and particulates can be achieved by retarding and advancing the injection, respectively (Montgomery and Reitz, 1996).

Many researchers have investigated reducing NO_x and combustion noise with multiple injections. The term 'multiple' injections has a broad meaning which includes pilot injection, split injection and other injections with many separate sprays. High injection pressure along with multiple injections has been shown to be an effective way to improve engine combustion emissions (Tow *et al.*, 1994; Montgomery and Reitz, 1996). An optimised pilot injection results in lower levels of NO_x emissions and noise as a result of suppressing the high initial rate of heat release at the start of combustion (Shundoh *et al.*, 1992; Russell and Lee, 1995;

Shiozaki *et al.*, 1998). Yoshizu *et al.* (1991) have reported that the spray penetration is shorter and the spray angle is narrower for a pilot injection system than for a standard single injection system. A split injection changes the spray mixing, vaporisation and fuel distribution and it has a significant impact on peak combustion pressure and rate of pressure rise (Bower and Foster, 1993). Farrell *et al.* (1996) have found that the near spray angles for the multiple injections decreases within every split injection interval and increases during each time spacing between injection intervals and also after the end of injection. They have considered this variation is good for the fuel spray and ambient air mixing, indicating the reason why high injection pressure coupled with selected multiple injections strategies can reduce the emissions and particulates for engine combustion. An optimised combination of EGR and multiple injection has shown to result in improved fuel consumption and decreased NO_x and particulate emissions over the entire operating map (Montgomery and Reitz, 1996).

1.2.2 Combustion Development

The combustion process in a diesel engine can be divided into four stages. It begins with ignition delay of a few crank angle degrees followed by the premixed combustion phase. In the premixed period, the fuel mixed with air within the flammability limits during the ignition delay period is burned rapidly, which results in a high pressure rise. At the next stage, the burning rate is controlled by the rate of air fuel mixture in the mixing controlled combustion phase. Finally, the combustion process ends with the late combustion period promoting more complete combustion and less dissociated product gases. The mechanism of combustion process has not been well understood because the unsteady, turbulent and high pressure field of the diesel flame is a poorly accessible environment. Numerous investigations have been devoted to reveal the combustion process by means of analysis techniques varying from in-cylinder pressure and constituents analysis to various optical techniques, such as normal photography, shadowgraphy and shilieren, including several laser techniques.

Ignition delay in a diesel engine is defined as the time (or crank angle) interval between SOI and the start of combustion, which is usually taken as the time when the injector needle lifts off its seat as determined by a needle lift sensor. It has been argued that it is more precise to determine the start of combustion as the minimum point on the heat-release curve (Dec and Espey, 1995) or the minimum cylinder pressure gradient. Flame luminosity detectors have also been used to determine the first appearance of the flame; generally the

time of appearance of the flame happens later than the point of pressure rise and results in greater uncertainty in the determination of ignition delay.

Both physical and chemical processes affect ignition, hence the total ignition delay is considered to be the summation of the chemical ignition delay and the physical ignition delay (Amann and Siegla, 1982). The physical ignition delay is the time interval during which the liquid droplets leave the exit of the nozzle, are heated up by the compressed air, evaporate and mix with air while the chemical ignition delay results from the pre-reactions that precede auto-ignition. The chemical ignition delay results from the pre-combustion reactions of the fuel, air and residual gas mixture which lead to autoignition. The chemical process consists of an initiating reaction (where highly reactive intermediate radicals are produced from stable molecules of fuel and oxygen), propagation reactions (where radicals react with the reactant molecules) and termination reactions (where the propagating radicals are removed) (Heywood, 1988). The gaseous fuel-air mixture autoignites when the energy released by reaction as heat is greater than the heat lost to the surrounding gas, which results in the mixture temperature increasing and accelerating rapidly towards the self-ignition temperature. Though ignition occurs in vapour phase regions, oxidation reactions can proceed in the liquid phase as well as between the fuel molecules and the oxygen dissolved in the fuel droplets. Also larger hydrocarbon molecules can be cracked into smaller molecules. Overall, both physical and chemical processes depend on the cylinder charge temperature and pressure.

The next combustion stage is pre-mixed combustion which is also known as uncontrolled combustion because, once combustion has been triggered, it proceeds very quickly through this stage at a rate that is not externally controllable but rather determined by conditions prevailing in the spray at the end of the ignition delay. This pre-mixed combustion begins with an early blue flame which is difficult to be visualised due to its low luminosity (Heywood, 1988) and hence only very sensitive photographic systems (Kamimoto *et al.*, 1987), laser illumination (Dec and Espey, 1995) or an apparent heat-release analysis (Kamimoto and Kobayashi, 1991) can be employed for this very early part of the combustion phase. Dec and Espey (1995) have considered the chemiluminescence process to occur due to the decay to an equilibrium energy level of the combustion radicals previously raised to an excited state by energetic chemical reactions. They also found the signal to result mainly from OH, CH and C_2 radicals in the near ultra-violet wavelengths; further, chemiluminescence marks the start of the exothermic chemical reactions, i.e. ignition, and continues throughout the combustion heat release process. The first sites of chemiluminescence appear at several

points in the downstream region of the fuel jets and by the end of the pre-mixed burn period the soot distribution pattern shows higher concentration of small soot particles in the leading portion of the jet than in the upstream areas and larger soot particles at the periphery of the spray jet. According to Dec and Espey (1995) the processes leading to this distribution are the following: first fuel-rich pre-mixed burning results in formation of small soot particles across the jet cross-section with these particles increasing in concentration and also slowly increasing in size as pre-mixed burning continues. The pre-mixed burning further causes the jet to expand and the conditions for forming a diffusion flame at the periphery of the jet are established. Here, soot forms on the fuel-rich side of the diffusion flame hence resulting in a different soot particle size class. The time scale for chemiluminescence relative to heat release is difficult to be determined since the first detection of signal is dependant on the experimental equipment employed but generally the first appearance of chemiluminescence occurs before the minimum of the heat-release curve with soot luminosity occurring later (Dec and Espey, 1995).

Within the diffusion combustion stage the rate controlling process is turbulent mixing which provides the necessary similarity to steady turbulent diffusion flames (Kamimoto and Kobayashi, 1991) sometimes employed for simplified diesel flame-like experiments. The diffusion flame formed inside the cylinder of a diesel engine was analysed by Dec and Coy (1996), Kosaka *et al.* (1996) and Corcione *et al.* (1996) all employing OH radical imaging besides other optical techniques. The OH PLIF signal is generated mainly in the reaction zone of high-pressure diffusion flames and shows a large change in signal strength from the flame zone to the surrounding gas (Dec and Coy, 1996); further, a correlation was found between the OH concentration and the soot temperature as determined by the two-colour method (Corcione *et al.*, 1996). According to Dec and Coy (1996) and Kosaka *et al.* (1996), the diffusion flame seems to be limited to the periphery of the flame plume until major soot obscuration occurs. The flame appears to be very thin (less than 120μm) especially at the leading edge of the jet (Dec and Coy, 1996); the reasons are low shear rates and turbulence due to the development of an opposed flow stagnation point between the jet flow and the relative flow of surrounding air at the centre of the leading jet. Along the sides of the jet the higher shear forces possibly lead to larger-scale turbulent structures and generally higher turbulence levels which result in the diffusion flame rolling and folding up (Dec and Coy, 1996).

1.2.3 Pollutant Formation and Exhaust Emissions

Soot

The soot generated during the combustion process is not uniquely defined. It normally looks black and consists mainly of carbon but it is not very different from graphite. Apart from carbon, soot particles also contain up to 10 % mole hydrogen, and even more soon after formation. The soot formation process comprises the particle generation and surface growth stages, which are often followed by soot oxidation (Haynes and Wagner, 1981). The eventual emission of soot will depend on the balance between the processes of formation and burnout.

The first stage is the particle inception stage, whereby the first condensed phase material is generated from the fuel-molecules via oxidation and /or pyrolysis. Such products typically include various unsaturated hydrocarbons which are relatively stable with respect to decomposition to their elements; these products are often considered the most likely precursors of soot in the flame.

The following condensation reaction of these gas-phase particles leads to the appearance of the first recognisable soot particles, which are very small (d<20Å) and called soot nuclei. The bulk of the solid phase material is generated by surface growth which involves the attachment of gas phase species to the particles and their incorporation into the particulate phase. Surface growth reactions lead to an increase in the amount of soot but the number of particles remains unchanged by this process. The opposite is true for growth by coagulation, where particles collide and coalesce, thereby decreasing the number of particles but the amount of soot remaining constant. Particle growth is the result of simultaneous surface growth reaction and coagulation. The elementary soot particles exhibit a size distribution, usually not far from log-normal, and the particles collected from a wide variety of combustion processes do not differ much in size being typically 200~400Å in average diameter (Palmer and Cullis, 1965). The agglomeration of the primary particles apparently begins within the combustion chamber, even within a few crank angle degrees aTDC. Further agglomeration may occur in the exhaust and sampling systems.

The soot formation mechanism is considered to be independent of engine load but the amount of soot formed increases at higher engine loads by raising the chamber temperature and promoting soot burnout (Li and Wallace *et al.*, 1995b) and decreases at lower engine speeds due to the reduction in the burnout time (Quoc *et al.*, 1991). The majority of soot is formed during the diffusive combustion of the last burning stage, where fuel is injected into a gaseous environment already depleted of oxygen through combustion of the previously

injected fuel (Amann and Siegla, 1982) and where the local C/O ratio is above a critical value (Li and Wallace, 1995a). Experimentally, the limits of soot formation usually coincide with the onset of luminosity and this occurs not at C/O ≅ 1 but usually in the vicinity of C/O=0.5 (Haynes and Wagner, 1981). Kamimoto *et al.* (1987) found that the mean equivalence ratio averaged over a cross section perpendicular to the spray axis is almost stoichiometric or below in the sooting region. According to Dec (1992), the first soot occurs at random locations and shortly thereafter small soot particles develop throughout the cross section of the leading portion of the flame, which arise from the fuel rich premixed phase; significantly larger soot particles appear around the periphery of the jet, presumably from the initial stage of diffusion combustion. Significant soot formation at the region of the jet periphery could be explained by the gas temperature and local equivalence ratio in the flame as the two key factors being mainly responsible for soot formation (Won *et al.*, 1992). Kamimoto and Yagita (1989) have showed that soot concentration is maximum when both temperature and equivalence ratio reach maximum values of 2200K and 1.7, respectively.

It is estimated that about 20~30% of the carbon contained in the original fuel develops into soot (Kamimoto and Kobayashi, 1991); however, particle oxidation can occur at each stage of particle generation and growth, especially in the premixed-burning/burned gas zone as air is entrained (Li and Wallace, 1995a), with the final exhaust soot emissions being dependent on the balance between the two processes of formation and oxidation. It is expected that soot oxidation is promoted at flame temperatures above 1800~1900K and ceases between 30°CA aTDC (Matsui *et al.*, 1982) and 50°CA aTDC (Li and Wallace, 1995b). Oxidation takes place where soot and/or soot precursors are burned in the presence of oxidants for carbon to form products such as CO and CO_2. Neoh *et al.* (1981) found OH to be a comparatively effective soot oxidant, particularly at rich equivalence ratios. This oxidation process is enhanced by low production of soot during the formation and growth processes, small particle diameters, large concentrations of the predominant oxidation species, high temperatures (Smith, 1981) and high turbulence levels. Once gas temperatures fell down to a certain level as a result of mixing and cylinder gas expansion, soot oxidation terminates despite the continued drop in equivalence ratio. This is well explained by three routes of unburned soot particles generation, that is quenching due to contact with wall surfaces, quenching due to detachment from the main flame and survival in the main flame due to slow oxidation rate (Kamimoto and Yagita, 1989). According to in-cylinder gas sampling studies and optical measurements, the exhaust soot levels are reached after about 12°CA aTDC

(Shimazaki *et al.*, 1996) and up to 50°CA aTDC (Li and Wallace, 1995b), respectively; a homogenous gas mixture in the combustion chamber, however, is found only after about 30°CA and 35°CA aTDC according to Li and Wallace (1995b) and Quoc *et al.* (1991), respectively. However, adsorption and condensation of hydrocarbons can lead to formation of new particles in the exhaust system.

In order to improve the understanding of the soot formation mechanism, diagnostics which have high temporal and spatial resolution are desirable. Numerous efforts have been devoted to the study of soot formation in diesel flames by means of various optical techniques. Recently, two dimensional visualisation techniques using a laser sheet have been applied to diesel flames in order to investigate the soot distribution with high spatial resolution. Laser induced incandescence (LII) was developed as a method to visualise soot in an optically accessible engine (zur Loye *et al.*, 1990, Dec *et al.*, 1991). Pinson *et al.* (1993) developed a method to obtain quantitative distributions of soot particle size and number density by calibrating the simultaneous LII and LIS imaging technique. These techniques have provided detailed information for soot formation and oxidation in diesel engines. Tree and Fostier (1994) have found that the peak soot diameters were a range of 30~50 nm and peak soot diameter and soot volume fraction increase with increasing equivalence ratio. Shioji *et al.* (1995) have reported that the increased injection pressure and reduced nozzle orifice diameter enhanced soot oxidation. Won *et al.* (1992) applied double pulsed laser sheet during a short time and two intensified gated camera for LIS and LII techniques to estimate the velocity vectors of soot particles in unsteady spray flames. They have found that soot is mainly formed in the periphery of the flame tip where the air entrainment is relatively small and flame temperature favours soot formation and it is conveyed to the flame periphery by large scale vortices formed in the flame head.

Oxides of Nitrogen

Nitric oxide is the predominant gaseous pollutant produced in engines, with nitric oxide (NO) and nitrogen dioxide (NO_2) grouped together as NO_x and attributed to three formation mechanisms.

Their principal source is the oxidation of atmospheric nitrogen, which is known as thermal NO_x. As explained by the extended Zeldovich mechanism for combustion of near stoichiometric fuel-air mixtures, thermal NO_x is formed by reactions during high temperature

processes generating both oxygen and nitrogen atoms and molecules through dissociation which subsequently result in formation of nitric oxide.

$$O + N_2 = NO + N \qquad (1.1a)$$

$$N + O_2 = NO + O \qquad (1.1b)$$

$$N + OH = NO + H \qquad (1.1c)$$

The initial NO formation rate may be derived by considering the rate constants for the NO formation mechanism, i.e.

$$\frac{d[NO]}{dt} = \frac{6 \times 10^{16}}{T^{1/2}} \exp\left(\frac{-69.090}{T}\right)[O_2]_e^{1/2}[N_2]_e \qquad (1.2)$$

where T is temperature and t is time. It is clear that there is a strong dependence of d[NO]/dt on temperature through the exponential term. In diesel engines NO_2 can be 10 to 30 percent of the total exhaust NO_x emissions, while chemical equilibrium considerations indicate that for gases at typical flame temperatures the NO_2/NO ratio should be small and NO_2 can be converted from NO through

$$NO + H_2O = NO_2 + OH \qquad (1.3a)$$

$$NO + OH = NO_2 + H \qquad (1.3b)$$

The other two NO_x formation mechanisms, comprise prompt NO_x formed by chemical reactions in thin oxygen-poor flame layers of premixed combustion, and fuel NO_x from the fuel bound nitrogen formed during combustion at relatively low temperature; both are of small significance in diesel engines. Thus, NO_x is primarily formed during the premixed flame combustion process in the vicinity of combustion regions especially at high temperatures and in presence of O_2 and N_2, that is in lean flame regions. Therefore, NO_x formation in cylinders can be suppressed by better control of air-fuel mixing, the premixed combustion process with respect to local oxygen/nitrogen concentrations and local temperatures.

Overall, control of NO_x formation in diesel engines is fundamentally difficult because the high thermal efficiency of the diesel cycle stems from the otherwise undesirable high peak temperatures and suppression of NO_x has the tendency to cause an increase in particulates. Thus any actions to reduce NO_x formation should be considered together with their effect on engine performance and particulate emissions.

Hydrocarbons

Unburned hydrocarbon (HC) emissions in diesel engines result from two main sources: firstly from excessive fuel mixing that leads to fuel/air ratios surpassing the lean combustion limit during the ignition delay period and secondly from insufficient fuel mixing due to the low nozzle exit velocities later in the combustion process (Heywood, 1988). The total hydrocarbon emissions are, however, a measure of combustion inefficiency and not necessarily an index of pollutant emission according to Heywood (1988). Regarding the CO formation, Heywood (1988) comments that CO is formed during combustion when rich fuel-air mixtures have insufficient oxygen to burn fully all the fuel-carbon to CO_2; the CO emission is hence controlled by the local fuel/air equivalence ratio with the dissociation of the high-temperature combustion products generally ensuring high CO levels.

Increasingly stringent emission standards will possibly require the reduction of CO by 50%, of HC+NO_x by 67% and of particulates by 75% to reach the proposed Stage 4 (2005) regulations starting from today's Stage 2 (1996) levels (Table 1.2). Various strategies for achieving the necessary reductions have been suggested and partly tested for reducing particulates and HC emissions in a HSDI diesel engine (Horrocks, 1993). The main ones being examined include: optimisation of fuel injection and improved atomisation of the fuel spray; small sac volume or VCO injection nozzle; minimisation of the parasitic volumes in the combustion chamber; minimisation of the contribution of lubricating oil; incorporation of central injector and combustion chamber; application of modulated and possibly filtered EGR (Khalil *et al.*, 1995); use of electronic controls for good conformity of production, rapid engine warm-up and finally use of an oxidation catalyst and/or a particulate trap. Cold start conditions result in emissions of white smoke which consist mainly of gaseous unburned HC but also particulates (Yassine *et al.*, 1996) and these emission depends strongly on the number of misfires during cranking of the engine. To achieve the necessary reduction in NO_x emissions it is currently suggested to reduce the combustion temperature by one or more of the following ways (Tsujimura, 1994): retarding injection timing from optimum, injection rate shaping, lowering the intake air temperature through turbo-charging and intercooling, water injection into intake air, fuel composition changes and by applying EGR. Further research is being conducted to develop after-treatment devices to remove NO_x emissions by "selective catalytic reduction", NO_x trap and "catalysed thermal decomposition" (Horrocks, 1993). Emission reduction strategies also consider changes to the fuel injection equipment.

1.2.4 Exhaust Gas Recirculation

A fraction of the engine exhaust gases is often recycled to the intake to dilute the fresh mixture for control of NO_x emissions. EGR rate is defined as the percent by mass of the total intake mixture which is recycled exhaust, i.e.

$$EGR(\%) = \left(\frac{m_{EGR}}{m_i}\right) \times 100 \qquad (1.4a)$$

where m_{EGR} is the mass of exhaust gas recycled, and m_i is the inducted mass per cycle. An alternative definition of EGR rate is also used based on the ratio of EGR to fresh mixture (fuel and air),

$$EGR^*(\%) = \left(\frac{m_{EGR}}{m_a + m_f}\right) \times 100 \qquad (1.4b)$$

where m_a and m_f is the mass of air and mass of fuel, respectively. The exhaust gas can be recycled up to about 30%, then the burned gas fraction during compression approaches 30 to 40% including the residual fraction of a few percent from previous cycles (Heywood, 1988). The recirculated gas consists of N_2, CO_2, H_2O and O_2 (Heywood, 1988) and its temperature is higher than that of surrounding air.

The effects of the ratio of the recycled exhaust gas to intake charge on the NO_x and/or soot formation process can be explained in various ways. The introduction of EGR mainly involves the replacement of inlet oxygen with CO_2 and water vapour; the reduction in oxygen in the inlet charge is called the dilution effect. The higher specific heat capacities of CO_2 and water vapour in comparison to that of the replaced oxygen results in the thermal effect. There is also the chemical effect of EGR as these EGR constituents dissociate at the high temperatures of the combustion process. EGR can have an additional effect on combustion if the exhaust is recirculated without being cooled, mainly, the increase in inlet charge temperature associated with the use of hot EGR.

Dilution Effect of EGR

The reduction in oxygen concentration in the combustion chamber due to EGR influences the flame temperature that controls NO_x formation. Tsunemoto and Ishitani (1980) have concluded that the effect of EGR on NO reduction is explained by the reduction in the O_2 rate in the intake charge. Their explanation is based on Khan *et al.* (1973) who assumed that the

fuel spray structure is not changed considerably through EGR at the first stage of combustion which represents the main stage of NO formation. The oxygen reduction through EGR leads to an increase in the extent of the fuel rich zone around the spray centre; further, assuming that NO is formed where the excess air factor is about 1 (in the reaction zone enveloping the core), the NO formation zone decreases in size (hence reducing the NO emissions). Additionally, the size increase of the fuel rich zone decreases the reaction temperature because of the reduced oxygen. This leads to an increase of the heat transfer from the NO formation zone to the fuel rich zone and therefore to a reduced temperature of the NO formation zone (hence reduced NO emissions). Further, Tsunemoto and Ishitani (1980) found that a reduction in NO emissions can be attributed to the increased ambient humidity which could contribute to the reduction in oxygen in the incoming charge.

For experimentation purposes, either burned gas (residual gas or recirculated gas) or single substances is used for dilution. Ladommatos *et al.* (1996) showed that the dominant effect of CO_2 on emissions is through the reduction in oxygen concentration in the inlet charge, as CO_2 gas is used for dilution. Plee *et al.* (1981) have reported that the flame temperature has the major influence on NO_2 emissions while particulate and CO emissions are mainly influenced by oxygen mole fraction in the inlet charge, through experiments varying the inlet charge. Mitchell *et al.* (1993) also found that the flame temperature rather than the oxygen availability is the dominant factor for NO_x formation, according to experiments where the inlet charge to a DI diesel engine was diluted with nitrogen or CO_2. Lida and Sato (1988) reported that oxygen enrichment of the inlet charge resulted in a decrease in ignition delay, an increase in NO_x emissions, and a reduction in particulate emissions when the injection timing was kept constant, where the increase in NO_x from the shortening ignition delay could arise from the knock-on effect that short ignition delays have on raising cylinder gas pressure and, hence, temperature.

The EGR-induced reduction in the flame temperature results in a decrease in NO emissions as modelled by the extended Zeldovich mechanism (Equation 1.1) with Equation (1.2) showing a strong temperature dependence in the exponential term (Heywood, 1988) and a relatively small influence of the oxygen and nitrogen concentrations (Plee *et al.*, 1981). The correlation between NO_x emissions and the calculated flame temperature was experimentally confirmed by Mitchell *et al.* (1993) and Plee *et al.* (1981). The correlations between T_f and NO_x emissions, and between T_f and carbon emissions were developed from experiments by Plee *et al.* (1981), i.e.

$$EINO_x \propto e^{-\frac{38700}{T_f}} \qquad (1.5)$$

$$EIC \propto e^{\frac{48900}{T_f}} \qquad (1.6)$$

It was also suggested that the effect of EGR and gas addition is rather stronger on the oxidation process than on the formation one. The higher sensitivity of soot oxidation than of soot formation towards the reduction in combustion temperature was confirmed by Lapuerta *et al.* (1995) in a combined exhaust emission and modelling study on the effects of EGR. On the other hand, Lida (1993) revealed that soot formation was enhanced for a higher surrounding gas temperature, whereas soot oxidation was higher for higher flame temperature. The results reported by Röpke *et al.* (1995) were also in agreement with other results, where oxygen availability controlled the flame temperature and, thereby, NO_x formation. The reduction in NO_x formation associated with lower flame temperature was suggested to be due to the reduction in dissociation of CO_2 and water to form atomic oxygen that is required for NO_x formation.

Thermal Effect of EGR

The core flame temperature is independent of the engine operating condition with the maximum being about 2360K (Quoc *et al.*, 1991); however, EGR does reduce the flame temperature, first by increasing the heat capacity of the cylinder charge per unit mass of fuel (Heywood, 1988) and second by increasing the mass of inert gases present during combustion (Röpke *et al.*, 1995). Other investigators also showed that main effect of EGR on combustion and emissions was through its high heat absorbing capacity which reduces the combustion temperature. The higher heat absorbing capacity of EGR was attributed to the high specific heat capacity of the recirculated CO_2 and H_2O and also to the dissociation of these gases (Torpey *et al.*, 1971; Ohigashi *et al.*, 1971; Dürnholz *et al.*, 1992; Ladommatos *et al.* 1998a); Tsunemoto and Ishitani (1980) found a maximum increase in the heat capacity of about 2% for a DI engine. Dürnholz *et al.* (1992) have considered the reduction in the calculated adiabatic combustion temperature caused mainly by the higher molar heat capacity of the recirculated exhaust gas as compared with air. They differentiated between a not significantly changing 'mean maximum combustion temperature' and a 'local maximum temperature' which has to be reduced in order to explain the reduction in NO_x. Similarly, Plee *et al.* (1981) found that EGR changes the calculated stoichiometric flame temperature. EGR also lowers the

oxygen concentration due to dilution of the intake charge (Plee *et al.*, 1981). Röpke *et al.* (1995) have determined the peak flame temperature by a 5-colour technique at a non-identified location and found it decreasing from about 2620K to 2470K and down to 2410K as the EGR-rate increased from 0% to 30% and 50%, respectively. It was also reported that a remarkable reduction in the surrounding gas temperature at TDC resulted when CO_2 was added to the inlet charge of a rapid compression machine, and that the surrounding gas temperature which also affected the ignition delay period was one of the major factors that influence soot formation in diesel combustion. (Lida, 1993). On the other hand, Wilson *et al.* (1974) pointed out that the effect of the higher heat capacity of diluted gases on the flame temperature is much less than that of reduction in oxygen, that is, the thermal effect of EGR is very low and is offset by the high temperature of the recirculated gases when hot EGR is used.

Chemical Effect of EGR

The dissociation of CO_2 at high the temperature of combustion was reported by Röpke *et al.* (1995) as the mechanism that provides atomic oxygen that could increase the NO_x formation according to the Zeldovich mechanism. The dissociation of CO_2 was also shown (Mitchell *et al.*, 1993, Lida, 1993) to cause a reduction in soot formation in diesel combustion. Mitchell *et al* (1993) suggested that this could be due to the increase in premixed burning associated with the longer ignition delay and the enhancement of soot oxidation.

Inlet Charge Temperature Effect

The recirculation of the uncooled exhaust gas raises the temperature of the inlet charge well above the ambient temperature, especially for high EGR fractions. Plee *et al.* (1981) have found an increase of 5°C at 30% EGR with only a minor effect on the exhaust particulates or gaseous emissions. The increase of the in-cylinder air temperature due to EGR is relatively small compared to the temperature increase due to compression; Roller *et al.* (1995) found an increase from 425K at 284°CA to 560K at 320°CA without EGR, which could explain the relatively small influence of this variable on exhaust emissions. Torpey *et al.* (1971) compared the emissions of hot and cooled EGR and found that the hot EGR resulted in higher NO_x and lower unburned hydrocarbon emissions in comparison to cold EGR. Similar results were also reported by Dürnholz *et al.* (1992) and Röpke *et al.* (1995). However, both have noticed diminishing NO_x levels with increased EGR which they attributed to thermal throttling when hot EGR was used. Thermal throttling is known as the reduction in inlet

charge mass as a result of increased inlet temperature, since the intake volume of the engine is fixed.

In addition to these observations, there are numerous general effects of EGR on spray development, combustion and emissions which are interrelated. It is expected that EGR influences spray development, that is spray tip penetration and spray angle, through the changes in the thermodynamic and flow conditions at the start of injection induced by changes in the intake charge temperature and composition. The intake parameters affected by EGR include the bulk intake charge temperature, which increases through mixing of the fresh air with the hot exhaust gases, the pressure of the intake charge and its density which is affected by the increased temperature of the charge and the recirculation of soot particles. The composition of the intake stream also changes. In view of the simultaneous variation of more than one parameter, it is difficult to harmonise the conflicting influences of EGR and decide on the preferred conditions at the start of injection for reduction of NO_x and soot emissions. Even the effect of EGR on the spray characteristics is not straightforward, since the various parameters such as temperature, density and pressure of the cylinder charge at the time of fuel injection and auto-ignition, have to be changed considerably in order to identify any measurable influences. With the currently preferred, due to its convenience, method of uncontrolled EGR, the inlet gas temperature increases and the flame combustion temperature decreases, thus the overall effect concerning the effect of temperature on spray development becomes very small. Regarding density changes induced by EGR no clear trends have been reported, due to the competing influences of decreased density resulting from the increased temperature and increased density because of the additional soot particles present in the recirculated gas. It is expected, however, that the density change due to the effect of the higher charge temperatures is less important.

Ignition delay is affected by two opposite phenomena caused by EGR, that is on the one hand the increased average intake gas temperature leading to an expected shortening and on the other hand the decrease in the O_2 content due to dilution with CO_2 and N_2 which is equivalent to a lowering of the air-fuel ratio and leading to an expected lengthening of ignition delay. Using the addition of single-component gases to a rapid compression machine with non-impinging sprays, Iida (1993) has found that ignition delay increases with decreasing O_2 from 25% to 17% and with increasing CO_2 up to 19%, respectively. Machanon *et al.* (1994) reported a slight increase in ignition delay with EGR and concluded a predominance of the dilution effect over the manifold temperature increase in terms of emissions production; that

EGR tends to increase ignition delay was also found by Daisho *et al.* (1994), Machacon *et al.* (1994), Röpke *et al.* (1995) and Ladommatos *et al.* (1998a, b). Using simulated EGR Mitchell *et al.* (1993) found an increase of ignition delay with both nitrogen and carbon dioxide dilution; however, the influence of CO_2 was stronger than that of NO_x. In Kwon *et al.* (1991) a combustion bomb study with residual gases showed a decrease in ignition delay until the residual gases were increased to 4%, with a subsequent increase in ignition delay as the percentage of residual gases was increased further. It was thus concluded that the residual gas could control the ignition delay but not the ignition mechanism of the spray and that it is the chemical ignition delay which is increasing with decreasing O_2 concentration rather than the physical ignition delay. A minor lengthening of the ignition delay was caused by increasing the CO_2 and CO concentrations. Ignition delay was decreased non-uniformly by adding hydrocarbons such as C_2H_6 and C_3H_8.

Clearly EGR has an effect on particulate emissions. In Machanon *et al.* (1994) and Ladommatos et al. (1998a) it is reported that EGR increases the exhaust particulate emissions, mostly caused by an increase in the dry-soot component of the particulates. Plee *et al.* (1981) confirmed the classic trade-off between NO_x and particulate emissions, that is that EGR increases particulates carbon content and CO emissions but reduces NO_x emissions. Hiroyasu *et al.* (1980) have tried to explain the increase in the exhaust gas smoke levels through EGR with a combination of experiments performed in a diesel engine and a diffusion flame of similar combustion characteristics. It was concluded that the observed increase in combustion duration led to soot oxidation being still in progress at exhaust valve opening, which stopped the oxidation process prematurely because of the temperature and pressure drop leading to a quenching effect. Ladommatos *et al.* (1996b) have confirmed that the particulate emissions increases with CO_2 and N_2 replacing oxygen in the inlet charge, which indicates that the oxygen availability plays a vital role in the formation and oxidation of particulates. However, in-cylinder soot emissions do not seem to change by the dilution of the intake charge with nitrogen and carbon dioxide dilution leads to reduced in-cylinder soot emissions as well as to NO_x reductions (Mitchell *et al.*, 1993). In Mitchell *et al.* (1993) the soot volume fraction was measured by the soot extinction method based on the Rayleigh approximation over a motored cycle following a firing cycle and visible light images were obtained with a single-shot per cycle CCD camera. It was reported that simulated EGR decreases the flame luminosity in intensity and duration when the dilution agent is either N_2 or CO_2 (Mitchell *et al.*, 1993). The decrease in luminosity was attributed to a decrease in combustion temperature for

nitrogen dilution and to a decrease in the in-cylinder soot mass and temperature for CO_2. The luminosity intensity is a function of the amount of soot present in the cylinder and the temperature of the soot to the fourth power. The in-cylinder soot concentration did not seem to change appreciably with nitrogen diluting the intake charge (O_2 reduced from about 21% to 15%); this was used to explain the luminosity reduction as being caused primarily by a temperature decrease. However, the addition of CO_2 decreased the soot concentration substantially. Possible explanations include the increased ignition delay and associated increase in the premixed burn fraction which eliminates much of the fuel rich areas required for soot production; that carbon dioxide retards the formation of soot precursors; or that CO_2 accelerates the oxidation of soot. This is confirmed by Ladommatos *et al.* (1996b) who explained this with chemical effect. The observed decrease in luminosity with increasing EGR-rates was also observed by Röpke *et al.* (1995) who attributed it to the decrease in flame temperature. Three studies were reported about the effect of EGR (Shiozaki *et al.*, 1996), simulated EGR (Mitchell *et al.*, 1993) and the surrounding gas (Iida, 1993) on combustion based on the use of optical techniques inside the cylinder. Shiozaki *et al.* (1996) found by applying the two-colour method in a four-cylinder diesel engine incorporating uncontrolled EGR that the mean flame temperature decreased as EGR rate increased from 0% to 25%, but the soot concentration (*KL*-factor) increased only until EGR rate increased up to 20% with similar soot levels observed at 25% as at 0% rate.

The influence of EGR on in-cylinder pressure is not clear: for example Mitchell *et al.* (1993) found the maximum cylinder pressure and the rate of pressure rise to increase with N_2 dilution, while CO_2 dilution resulted in reduction of the maximum pressure and increase of the pressure gradient. On the other hand, Dürnholz *et al.* (1992) did not find the maximum combustion pressure to change significantly with EGR; the improved air/fuel mixing due to the longer ignition delay times was suggested as a possible reason. Iida (1993) has confirmed using the two-colour technique in a rapid compression machine with non-impinging sprays that soot is reduced with carbon dioxide addition

The effect of EGR on specific fuel consumption has to be taken into account when establishing a cost-benefit analysis of this particular emission control approach. The effect is small or even negligible at lower loads and EGR levels (Mitchell *et al.*, 1993) and Levendis *et al.* (1994) have observed no penalty in fuel efficiency at 15% EGR-rate; similarly Machacon *et al.* (1994) found the specific fuel consumption little changed. Tsunemoto and Ishitani (1980) experienced a decrease in engine output which was correlated to a decrease in the

oxygen concentration in the exhaust gas; it was further suggested that the decrease in BMEP is usually accompanied by an increase in smoke, which was confirmed in their experiments.

A further effect of EGR should be noted, namely that EGR increases the in-cylinder wall abrasion (Daisho *et al.*, 1994). Akiyama *et al.* (1987) have showed that cylinder wear is increased above normal levels under low-water temperature conditions and the mechanism suggested was corrosive wear of the cast iron liner. The reasoning is that combustion SO_x is increased by EGR and this leads to increased formation of sulphuric acid through the reaction of the condensed water on the surface of the cylinder.

1.2.5 Supercharging and Turbocharging

The primary purpose of supercharging is to increase the mass of air trapped in the cylinders of the engine by raising air density, which allows more fuel to be burnt, hence increasing the power output of the engine for a given swept volume while keeping the efficiency of the engine unchanged. A compressor is used to achieve the increase in air density which, when driven from the crankshaft of the engine, the system is called 'mechanically driven supercharging' or often just 'supercharging', while it is called 'turbocharging' when the compressor is driven by a turbine which itself is driven by the exhaust gas from the cylinders. Turbocharging is more efficient than mechanical supercharging since the power required for driving the compressor is extracted from the exhaust gas energy rather than the crankshaft. However the turbine imposes a flow restriction to the exhaust system, and therefore the exhaust manifold pressure will be greater than the atmospheric pressure.

In general, the turbocharger is not ideally suitable for vehicle engine operation because its performance is very dependent on the mass flow rate of the exhaust gases while a vehicle engine is required to run over a wide range of speed and loads which affect the air flow rate. Therefore, careful attention should be paid to the matching of the turbocharger with the engine for better turbocharger efficiencies and improved engine performance.

Since the inlet and exhaust pressures are above ambient and more fuel is burnt in the engine, the cylinder pressure throughout the cycle and particularly during combustion is substantially higher in the case of the supercharged cycle. Therefore the compression ratio of the engine must be reduced to prevent an excessive maximum cylinder pressure being achieved. However, the process of compression raises the temperature as well as the pressure. Since the objective is to increase the inlet air density, a charger air cooler is often used to cool

the air between the compressor delivery and the cylinder, so that the pressure increase is achieved with the maximum rise in density. A further advantage of charge cooling is that the lower inlet gas temperature at the cylinders will result in lower temperatures throughout the working process of the engine which reduce thermal loading.

Recently a diversity of high-boost turbocharging systems have been developed, such as exhaust waste gate control turbocharging, variable geometry turbocharging (VGT), axial-radial turbocharging, sequential turbocharging and two-stage turbocharging, in order to achieve better efficiencies and lower levels of exhaust gas emissions, especially at low engine speed without over-speeding the turbocharger at high engine speed; some of these turbocharging systems have already been adopted for use in vehicles. VGT and the sequential turbocharging would have basically similar performance characteristics. In either turbocharging system, the charge air pressure can be increased by decreasing the turbine capacity in the low engine speed range, and the over-speed condition in turbocharging can be improved by increasing the turbine capacity in the high speed range. The turbocharging efficiency can be also enhanced over a wide range of engine speeds. In the variable geometry turbocharging, the turbine capacity is continuously variable, while it is changed stepwise in sequential turbocharging. When the turbine capacity is changed, the recovery of the temporary torque drop is one of the technical problems in the sequential turbocharging system (Tajima *et al.*, 1991). The structure of the turbocharger is rather complex in VGT, whereas the intake and exhaust piping layouts are more complex in the sequential turbocharging. In the two-stage turbocharging, the charged air pressure is theoretically two times higher than that in the single-stage turbocharging over a wide range of engine speeds. In practice, the charge air pressure is not doubled due to the restriction by the outlet temperature of the high pressure stage compressor. To overcome this restriction, an intercooler may be fitted at the outlet of low pressure stage compressor in addition to the aftercooler. All these turbocharging systems are regarded as effective methods for improvement of combustion and reduction in exhaust gas emissions. Uchida *et al.* (1992) found that ignition delay was shortened and the peak value of the heat release rate during the premixed combustion period was reduced with supercharging; and that supercharging resulted in a significant reduction of smoke levels due to improvement in air-fuel mixing and a slight increase in NO_x emissions. Further, the insensitivity of NO_x emissions to supercharging was suggested to be due to the reduced combustion as a result of the increased charge. It was also reported that the EGR rate limited

by misfiring can be more widely expanded as the boost pressure increases (Uchida *et al.*, 1993)

From the viewpoint of environmental pollution, the turbocharging system is often employed as an effective means for reducing the levels of exhaust gas emissions. Adapting the turbocharging system with a high pressure fuel injection system and/or a four-valve cylinder head having a central vertical injector has been suggested as a good method to achieve further reductions in exhaust gas emissions without significant deterioration in engine performance (Endo *et al.*, 1991; Daisho *et al.*, 1994).

1.3 OUTLINE OF THESIS

The aim of the present work is to examine factors affecting spray development, combustion and emissions in HSDI diesel engines. Detailed experiments were carried out in an optical diesel engine of production geometry by applying a range of mainly optical but also probe techniques.

The thesis consists of five chapters of which Chapter 1 serves as an introduction, while it provides a brief literature review of combustion, emissions and the effect of EGR and supercharging in diesel engines as well as providing an overview of the remaining chapters.

Chapter 2 describes the effect of exhaust gas recirculation (EGR) and supercharging on spray, combustion and emissions on the basis of results obtained from the experiments conducted in a four-cylinder (VW 1.9 L) and a single-cylinder (Hydra) HSDI diesel engines. The techniques used for spray, flame visualisation and combustion analysis are also presented.

Chapter 3 describes the effect of EGR on soot formation on the basis of a feasibility study of laser-induced incandescence (LII) and laser-induced scattering (LIS) techniques (semi-quantitative soot concentration measurements) conducted in the four-cylinder VW engine.

Chapter 4 describes the effect of various injection parameters on the basis of the results obtained from experiments conducted in a four-valve single-cylinder engine converted from the two-valve Hydra and incorporating an electronically controlled injection system.

Finally, Chapter 5 summarises the main findings of this research programme and suggests further experiments which can provide additional insight into the in-cylinder processes in HSDI diesel engines.

Table 1.1 Literature review

Author(s)	Experimental set-up + experimental technique	Main findings
Akiyama *et al.* (1987)	♦ engine bench tests with varying EGR-rate, cooling water temperature and fuel sulphur content	◊ EGR increases cylinder wear, especially under low water temperatures, due to corrosive wear of the cast iron as EGR increases SO_x which leads to formation of sulphuric acid by reacting with condensed water on cylinder surface
Arai *et al.* (1984)	♦ High pressure chamber ♦ Laser diffraction	◊ SMD decreases with increasing injection pressure ◊ SMD at low injection pressure decreases with increasing ambient pressure ◊ SMD decreases with decreasing nozzle hole diameter ◊ SMD increases rapidly when viscosity of liquid is higher than certain value
Amann and Siegla (1982)	♦ literature review	◊ majority of soot is formed during the diffusive burning of the last burning stage ◊ soot mass is reduced within cylinder by dehydrogenation but mainly by oxidation ◊ oxidation of soot is quenched by falling temperature due to mixing with colder cylinder air and expansion of cylinder volume
Arcoumanis *et al.* (1991)	♦ Hydra DI diesel, single-cylinder engine, unit injector ♦ high-speed cine-camera spray visualisation ♦ spray tip penetration measured by two-beam deflection and axial droplet velocities measured by LDV under atmospheric conditions	◊ spray penetration dependent on engine speed rather than load ◊ higher engine speeds result in higher line pressures and higher peak droplet velocities ◊ spray unaffected by swirl, and only after impingement influence of swirl can be noted

Author(s)	Experimental set-up + experimental technique	Main findings
Arcoumanis *et al.* (1994)	♦ 1.9L four-cylinder VW HSDI DI diesel engine ♦ re-entrant combustion chamber ♦ laser Doppler velocimeter (LDV) for fuel spray droplet and in-cylinder air flow velocity ♦ intensified CCD camera	◊ maximum droplet velocities in the engine are about 7 times lower than those in the atmospheric spray. ◊ mean radial droplet velocities near the piston wall at the time of spray impingement are about 23 and 26 m/s for idle and low load conditions while the rms velocities are about 10 m/s in the main body of the sprays.
Arcoumanis *et al.* (1995a)	♦ Bosch VE rotary distributor pump driven by D.C. motor ♦ impinging onto heated and unheated flat plates under cross-flow air ♦ phase-Doppler anemometer	◊ characteristic roll-up vortices are formed at the head of the wall-jet. ◊ cross-flow results in the formation of a droplet cloud on the downstream side of the spray. ◊ cross-flow results in higher overall mean droplet velocities and diameters. ◊ raising wall temperature increases the number of droplets at the front of the wall-jet atomises without direct wall contact, but this effect was reduced at cross-flow.
Arcoumanis *et al.* (1995b)	♦ 1.9L four-cylinder VW HSDI DI diesel engine ♦ re-entrant combustion chamber ♦ adjustable EGR system ♦ intensified CCD camera ♦ Two colour method	◊ core temperature of the flame is at about 2230K at 0% EGR. ◊ increasing EGR decreases the core flame temperature on average 50K-100K. ◊ increasing EGR tends to delay and reduce the overall formation of soot. ◊ elevated temperature and KL-factors are concentrated near the piston-bowl wall. ◊ increasing EGR leads generally to an increase in fragmentation of the temperature and KL-factor distribution.

Author(s)	Experimental set-up + experimental technique	Main findings
Arcoumanis *et al.* (1995c)	♦ 1.9L four-cylinder VW HSDI DI diesel engine ♦ re-entrant combustion chamber ♦ adjustable EGR system ♦ intensified CCD camera ♦ different type of fuel ♦ hot and cold EGR	◊ spray tip penetration is not influenced significantly by EGR. ◊ spray angle increases slightly with EGR at idle conditions. ◊ auto-ignition sites increase in number and spread in space at higher EGR rates. ◊ independent of the charge intake temperature and fuel type, increasing EGR leads to: decreasing NO_x and O_2 and increasing soot, CO, CO_2 and HC concentrations. ◊ hot EGR leads to higher soot, CO, CO_2 and HC emissions. ◊ cold EGR gives lower NO_x emissions.
Baritaud *et al.* (1994)	♦ optical DI diesel engine with single hole injector and no spray impingement ♦ fuel is n-heptane ♦ laser induced exciplex technique for spray structure and penetration with engine running on nitrogen ♦ natural flame images for determining auto-ignition sites triggered by photo-diode responding to first soot ♦ LDV of motored airflow ♦ simultaneous self-ignition and Mie-scattering visualisation	◊ radial turbulence intensity is almost linear with engine speed ◊ liquid jet is discontinuous and shows sheared layers with ambient air rolled into the vortices ◊ change of droplet size along spray axis ◊ change in temperature from 713K to 900K leads to reduced liquid tip penetration but similar gas phase penetration ◊ liquid and gas phase progress together at start of injection after which the liquid spray stops progressing (after 20mm) and the gas phase continues ◊ ignition starts mostly in region of maximum vapour concentration at the tip of the liquid phase ◊ increasing chamber pressure, temperature and engine speed result in shortening the ignition delay and reducing the spatial scatter of auto-ignition sites ◊ larger cycle-to-cycle variations for the gas phase than for the liquid

Author(s)	Experimental set-up + experimental technique	Main findings
Campbell *et al.* (1995)	♦ single-cylinder optical two-stroke DI diesel engine ♦ piloted diesel fuel spray ♦ exciplex imaging of liquid and fuel distribution ♦ fuel and dopant injected into nitrogen environment	◊ pilot injection improves impingement characteristics as less fuel is accumulated near wall and hence possibly less hydrocarbon emissions ◊ in planar images the area spread rate instead of the spray tip penetration should be measured ◊ the gas phase expands linearly (at a higher rate than the liquid phase) and reaches 0 velocity at impingement; the liquid phase spreads linearly with a decreasing slope until impingement
Corcione *et al.* (1996)	♦ optical diesel engine at 2000rpm ♦ flame emissivity and absorption measurements (including two-colour method) at 153 measurement locations ♦ OH detected at 309.6nm and CH at 432.4nm ♦ high-speed photography of spray and flame development	◊ combustion starts in region downstream of spray and proceeds to involve entire chamber volume ◊ OH radicals are present in region of fuel thermal pyrolysis, which is induced by the radiation of the surrounding flame, rather than in region of burned gas ◊ OH concentrations follow trends of soot temperatures
Corcione and Valentino (1994)	♦ motored diesel engine with compression ratio of 21:1 between 1000-3000rpm ♦ high squish re-entrant combustion chamber ♦ cycle-resolved LDV measurements of tangential velocity, plane 5mm below cylinder head	◊ linear dependence of mean swirl motion and turbulence on engine speed ◊ spectrum of instantaneous velocity does not hold Kolmogorov's 5/3 law (isotropic turbulent flow)

Author(s)	Experimental set-up + experimental technique	Main findings
Daisho *et al.* (1994)	♦ single-cylinder DI diesel engine with supercharger and EGR-system ♦ rapid compression and expansion machine ♦ high-speed cine camera ♦ emission measurements of soot, NO_x and HC ♦ combustion modelling	◊ EGR significantly reduces NO_x, possibly due to decreased burned gas temperature ◊ EGR tends to increases ignition delay ◊ EGR increases in-cylinder abrasions ◊ supercharging can reduce deterioration of combustion and thermal efficiency both being caused by increasing EGR ◊ supercharging increases air entrainment in the fuel spray, hence increasing evaporation and reducing ignition delay
Dec and Espey (1995)	♦ single-cylinder DI diesel engine at 1200rpm ♦ reference fuel and low sooting fuel ♦ imaging of natural chemiluminescence, LII and LIS	◊ first chemiluminescence occurs at multiple points downstream of fuel jets prior to first apparent heat release and well before detection of soot luminosity ◊ first soot occurs at random locations ◊ small soot particle develop throughout cross-section of leading portion of fuel spray possibly arising from fuel-rich premixed burning; higher soot particle concentration towards the front of jet and lower concentration upstream ◊ larger soot particle appear around periphery of spray jet possibly caused by the initial diffusion combustion

Author(s)	Experimental set-up + experimental technique	Main findings
Dec and Coy (1996)	♦ single-cylinder, heavy-duty DI diesel engine at 1200rpm ♦ low-sooting fuel and reference fuel ♦ compression ratio increased to 16:1 by increasing intake air temperature and pressure ♦ planar LIF of OH radicals	◊ OH PLIF signal confined to flame front ◊ diffusion flame develops around periphery of the downstream portion of the reacting fuel jet ◊ diffusion flame remains at jet periphery until considerable soot formation occurs ◊ maximum flame thickness is estimated to be 120μm ◊ source of small soot particles throughout cross-section of the vapour region of the fuel jet are generated within fuel-rich premixed flame region ◊ NO production by the Zeldovich mechanism occurs only in thin zone at jet periphery on the air side of the diffusion flame where temperatures are high and O_2 is present
Hardalupas *et al.* (1992)	♦ temporal and spatial measurement of size and velocity of fuel spray droplets with phase-Doppler anemometer	◊ spray becomes finer with increasing distance from the injector and tend to be better atomised on the periphery ◊ larger droplets move faster than the smaller droplets ◊ during spray movement away from the nozzle, larger droplets tend to concentrate at the edge because the smaller droplets lose momentum faster and hence are overtaken
Herrmann and Dürnholz (1995)	♦ concept of four valve technology	◊ higher volumetric efficiency in the medium and high speed range ◊ vertical and central injector presents a more regular spray propagation in combination with symmetric air motion in the piston bowl ◊ more regular fuel distribution leads to a optimal mixture formation and a combustion with extremely low smoke level and low fuel consumption

Author(s)	Experimental set-up + experimental technique	Main findings
Hiroyasu and Ari (1989)	♦ pressurised vessel ♦ Fraunhofer diffraction optical technique (He-Ne laser) ♦ determine new empirical equations for SMD of diesel spray with liquids of different viscosity and surface tensions	◊ SMD increases with increasing ambient pressure at a high injection velocity ◊ SMD decreases with increasing ambient pressure at a low injection velocity ◊ effect of surface tension on SMD is great when injection pressure is relatively low ◊ surface tension has a smaller effect on SMD under higher injection pressure conditions ◊ under a low effective injection pressure, an increase in ambient pressure results in a significant decrease in SMD ◊ under a high effective injection pressure, SMD increases with increasing ambient pressure ◊ induced a generalised empirical SMD form
Horrocks (1993)	♦ summary of diesel emission standards	◊ see Table 1.2
Iida (1993)	♦ rapid compression machine with non-impinging sprays ♦ two-colour method for in-cylinder soot concentration estimates ♦ variation in O_2 concentration through addition of single substances	◊ increasing O_2 concentration from 17% to 25% increases maximum flame temperature and extinction rate of soot during later stage of combustion (proportional to soot oxidation rate) and decreases peak *KL*-factor ◊ CO_2 addition combined with O_2 reduction has soot reduction effect despite lower flame temperature ◊ CO_2 addition with constant O_2 level decreases *KL*-factor ◊ addition of Argon (25.9%) increases surrounding gas temperature at TDC by 100K, the flame temperature by 180K and increases also the *KL*-factor ◊ soot present in all of spray flame, with high density soot later located in flame tip

Author(s)	Experimental set-up + experimental technique	Main findings
Kamimoto *et al.* (1987)	♦ rapid compression machine with quiescent atmosphere ♦ injection pressure from 30-110MPa ♦ evaporating and non-evaporating spray and flame imaging	◊ increasing injection pressure leads in non-evaporating spray to decreasing SMD ◊ length of liquid phase of evaporating spray stays almost constant with varying injection pressure ◊ increased premixed initial combustion with increasing injection pressure ◊ increasing injection pressure reduces soot concentration in flame, possibly caused by above observations
Kamimoto *et al.* (1989)	♦ fuel (n-tridecane) injected into N_2 environment at room temperature and a pressure of 1.5MPa ♦ non-evaporating transient dense sprays ♦ shadow-picture of spray based on light extinction in order to determine SMD of droplets in spray	◊ increasing injection pressure results in reduction of overall SMD ◊ smaller droplet sizes are found in the peripheral region of the spray rather than in the central region
Kamimoto and Kobayashi (1991)	♦ literature summary covering air motion, spray development, combustion phenomena and emissions in diesel engines	◊ various, see accompanying text

Author(s)	Experimental set-up + experimental technique	Main findings
Khalil *et al.* (1995)	♦ 65kW diesel engine Caterpillar 3304 four cylinder engine at 1800rpm ♦ exhaust emission measurements of NO_x, CO and particulates ♦ four ceramic filters, with pressure drop of 91mbar at 2m/s face-velocity ♦ periodic (at 100mbar pressure drop after 2h) back-pulsing of compressed air for filter regeneration	◊ at full load and 30% EGR: 75% reduction in NO_x, CO reduces to initial value through oxidation catalyst (open channel monolith type) placed downstream of filter; particulate filter with efficiency of more than 99% ◊ EGR more effective at higher engine loads (higher equivalence ratios) ◊ CO unaffected up to 10% EGR, then increasing if no oxidation catalyst is utilised
Kosaka *et al.* (1996)	♦ rapid compression machine ♦ fuel is mixture of 90% paraffin hydrocarbon and 10% polypropylene-glycol because of low sooting properties ♦ simultaneous LIF of OH and LIS imaging	◊ in the quasi-steady region and in the leading portion of the flame soot exists mainly in the central portion and is surrounded by OH which exists mainly in the periphery of the flame ◊ soot and OH exist separately in a diesel flame
Kwon *et al.* (1991)	♦ high pressure, high temperature constant volume combustion bomb with variable residual gas and single component addition ♦ phototransistor measurements of ignition delay	◊ reduction of ignition delay until residual gases reach 4%, followed by increase in ignition delay as residual gases are increased further ◊ CO and CO_2 addition increase ignition delay ◊ C_2H_6 and C_3H_8 addition reduce ignition delay

Author(s)	Experimental set-up + experimental technique	Main findings
Ladommatos *et al.* (1996a)	♦ Ford 2.5L DI diesel Engine ♦ reduce the inlet charge oxygen ♦ cylinder-pressure and exhaust gas emissions measurements	◊ dilution of the inlet charge oxygen has little effect on the engine power output and thermal efficiency, but it has a detrimental effect on combustion and emission ◊ change on ignition delay associated with the inlet charge dilution has minor effect on combustion and emissions ◊ inlet charge temperature mainly affects the smoke and the dry soot emission
Ladommatos *et al.* (1996b)	♦ Ford 2.5L DI diesel Engine ♦ replacing the inlet charge oxygen with CO_2, N_2+Ar, CO_2 +Ar and N_2 +He ♦ cylinder-pressure and exhaust gas emissions measurements	◊ in replacing oxygen in the inlet charge with CO_2 the dilution effect was found to be the most significant factor influencing the combustion characteristics and emissions ◊ the dissociation of the CO_2 resulted in the lowering of both NO_x and particulates ◊ the thermal effect of CO_2 was the least effect on emissions and combustion

BIBL
LONDON

Author(s)	Experimental set-up + experimental technique	Main findings
Ladommatos *et al.* (1998a)	♦ Ford 2.5L DI diesel Engine ♦ control the inlet charge ♦ heat release analysis ♦ exhaust gas emissions measurements	◊ lower oxygen available for combustion, associated with EGR, results in and prolonged ignition delay period shifting the combustion further towards the expansion stroke ◊ it leads to lower thermal NO_x formation and lower rate of soot oxidation ◊ less oxygen results in reduced the peak rate of pre-mixed burning and increased diffusion burning , consequently lower NO_x and higher particulates ◊ increase in inlet charge temperature, associated with EGR, results in increase in combustion temperature and longer diffusion period due to the shortened ignition delay, consequently increase in the formation of both NO_x and particulate emissions ◊ effect of inlet charge throttling due to hot EGR is minor
Ladommatos *et al.* (1998b)	♦ Ford 2.5L DI diesel Engine ♦ control the inlet charge ♦ cylinder-pressure and exhaust gas emissions measurements	◊ thermal throttling effects of EGR (lower trapped charge mass and higher inlet temperature) cause an increase in the NO_x emissions ◊ reduction in inlet charge mass also lowers the engine output power due to its lowered cylinder gas peak pressure
Ladommatos *et al.* (1998c)	♦ Ford 2.5L DI diesel Engine ♦ control of inlet charge temperature (40-120°C) ♦ control of charge mass rate (10-8.5 g/s) ♦ UHC, NO_x and VOF measurement	◊ increased inlet charge temperature results in an increase in NO_x and interestingly in particulates due to prolonged diffusion-burning period, but a decrease in UHC. ◊ reduced inlet air flow-rate results in a small increase in NO_x due to the competing influence between the lowered heat absorbing capacity and the reduction of oxygen, and a substantial increase in particulates and UHC due to the reduction of oxygen concentration.

Author(s)	Experimental set-up + experimental technique	Main findings
Lapuerta *et al.* (1995)	♦ single-cylinder DI diesel engine ♦ supercharger and EGR-system ♦ exhaust gas measurements ♦ phenomenological combustion model	◊ effect of EGR on NO_x emissions mainly through reduction of adiabatic flame temperature due to O_2 reduction in intake charge ◊ increase in smoke emissions with EGR influenced by more parameters than only O_2 concentration, for example mass ratio between injected fuel and trapped oxygen is correlated with smoke emissions ◊ soot oxidation is more sensitive than soot formation to reduction in combustion temperature due to presence of inert gas
Lee and Tien (1981)	♦ development of dispersion model for optical constants of soot in HC flames ♦ in-situ flame transmission measurements	◊ optical properties of soot are relatively insensitive to temperature changes at elevated temperatures ◊ optical properties are relatively independent of fuel H/C ratio ◊ optical properties of soot and carbon are not identical ◊ derivation of total emissivity of soot cloud in Rayleigh limit
Levendis *et al.* (1994)	♦ single-cylinder DI diesel engine with EGR-system ♦ ceramic filter to remove particulates ♦ exhaust emission measurements of NO_x and unburned HC	◊ at 15% EGR-rate no fuel penalty is observed ◊ EGR is more effective regarding NO_x reduction at higher loads than at lower loads ◊ EGR-rates up to 15% do not change substantially unburned HC emissions
Li and Wallace (1995a)	♦ phenomenological model for soot formation and oxidation and comparison with experimental data, for example obtained by the two-colour method	◊ cylinder volume divided into four zones: rich fuel spray core, premixed-burning/ burned gas zone, mixing controlled burning zone, lean air zone. ◊ soot formation occurs in mixing controlled burning zone where local C/O ratio is above a critical value ◊ soot oxidation occurs in premixed-burning/burned gas zone as air is entrained

Author(s)	Experimental set-up + experimental technique	Main findings
Li and Wallace (1995b)	♦ single-cylinder DI diesel engine (Lister ST-1) ♦ two-colour method at three test lines for soot temperature and concentration measurements ♦ re-calibration of probes to take account of soot deposits ♦ exhaust soot concentration measurement by direct sampling method	◊ change in calibration with engine running time is linear and usually less than 5% for presented tests ◊ power spectrum of two-colour signal can provide swirl ratio ◊ data-averaging (as compared to result-averaging) of two-colour information results in elimination of measurement noise ◊ soot formation starts early in premixed burn period, is rapid and can be associated with heterogeneity of early combustion; soot formation mechanism is independent of engine load but amount of soot formed increases with engine load ◊ soot oxidation is slower than formation and becomes dominant at end of mixing-controlled combustion period ◊ good correlation between in-cylinder soot concentration at 50°CA aTDC and exhaust soot concentration as soot oxidation stops around 1800K which usually corresponds to about 50°CA aTDC and as homogenous in-cylinder mixture after 35°CA aTDC ◊ soot formation mainly around 2300K with only small difference caused by load condition indicates difference between soot temperature and gas temperature with the burning particles being hotter than the gas due to the energy released by the surface reaction of soot oxidation

Author(s)	Experimental set-up + experimental technique	Main findings
Machanon *et al.* (1994)	♦ Yanmar DI diesel engine, 4-cycle, single-cylinder at 900rpm ♦ measurement of diesel particulate, dry-soot and soluble organic fraction emissions	◊ ignition delay slightly lengthens with increasing EGR ◊ specific fuel consumption little changed by EGR ◊ at retarded injection timing (later injection) EGR increases particulate emissions, mainly caused by an increase in dry-soot component ◊ usually the NO_x-particulate trade-off is present, but engine conditions exist (for example, low load with advanced injection timing) where particulate suppression (due to decreased SOF) or no effect on particulate levels are found ◊ the intake air dilution effect is considered dominant for the auto-ignition process since the ignition delay is increased despite the heating effect caused by increased intake temperature

Author(s)	Experimental set-up + experimental technique	Main findings
Matsui *et al.* (1982)	♦ DI diesel engine, single-cylinder, four-stroke ♦ direct in-cylinder sampling of soot ♦ two-colour method for measuring flame temperature and *KL*-factor at point locations; conversion of *KL*-factor to soot concentrations for quantification ♦ exhaust smoke emission measurements	◊ soot is formed in initial stage of diffusion burning followed by oxidation, which is terminated in the latter half of combustion period (at about 30°CA aTDC) ◊ soot oxidation is promoted at flame temperatures above 1800-1900K ◊ higher soot concentrations (measured by gas sampling) as piston-bowl wall is approached ◊ quantitative agreement between visible two-colour method and in-cylinder gas sampling for certain measuring points and crankangles ◊ *KL*-factors during second half of combustion period follow trend of exhaust smoke conditions for varying operating conditions ◊ maximum flame temperature is constant regardless of amount of fuel injected whereas the *KL*-factor increases ◊ advanced injection leads to earlier and higher maximum temperatures; further, maximum *KL*-factor is decreased, because premixed fraction is increased and flame temperature is too high for soot formation; additionally, the faster spray penetrates fuel pass measuring point into clearance volume

Author(s)	Experimental set-up + experimental technique	Main findings
Mitchell *et al.* (1993)	♦ single-cylinder, optical DI diesel engine, two-stroke ♦ 2-component fuel: 41% cetane and 59% heptamethylnonane ♦ one firing cycle followed by five motoring cycles ♦ simulated EGR with NO (hence O_2 reduction only and small change in specific heat) and CO_2 (hence O_2 reduction and increase in specific heat) dilutants ♦ constant start of combustion ♦ optical measurements on motoring cycle following firing cycle ♦ exhaust emission measurement of NO_x ♦ continuos wave Argon-ion laser at 488nm used for point measurement of soot extinction with Rayleigh approximation ♦ visible light photography with intensified CCD	◊ NO and CO_2 addition increase ignition delay, more severe for CO_2 dilutant ◊ NO dilution leads to increase in peak cylinder pressure and rate of pressure rise; CO_2 dilution leads to reduced peak cylinder pressure and increased rate of pressure rise ◊ NO dilution has no effect on indicated work; CO_2 dilution decreases parameter by 8-21% ◊ both dilutants lead to reduced luminosity and shorter duration of combustion, due to decrease in temperature for NO dilution and temperature and in-cylinder soot mass reduction for CO_2 dilution ◊ both dilutants drastically reduce NO_x emission, which correlates very well with calculated stoichiometric adiabatic flame temperature (which is close to max. temperature of premixed and mixing controlled phases), hence considered to be main mechanism for NO_x reduction ◊ N_2 addition does not affect in-cylinder soot levels; CO_2 addition reduces soot levels due to increased premixed burn fraction (hence less fuel rich areas which are necessary for soot formation) caused by longer ignition delays, or the dilutant retards soot precursor formation or it accelerates oxidation of soot

Author(s)	Experimental set-up + experimental technique	Main findings
Montgomery and Reitz (1996)	♦ single-cylinder, heavy-duty diesel engine at 1600rpm and 75% load ♦ electronically controlled common rail injector with multiple injection capability up to quadruple injections ♦ EGR-system ♦ exhaust emission measurements	◊ reduction of NO_x by retarding injection and reduction of particulate by advancing injection ◊ multiple high pressure injections reduce particulate emissions without significant penalty in NO_x ◊ EGR reduces NO_x emissions ◊ large pre-mixed burn results in more NO_x emissions ◊ combination of 10% EGR and optimised quadruple injection results in improved fuel consumption and decreased NO_x and particulate emissions over the entire engine operating map
Naber and Siebers (1996)	♦ constant-volume combustion chamber with common-rail injector ♦ parametric density variation from 3-200kg/m^3 for vaporising and 3-61kg/m^3 for non-vaporising sprays; further variables were orifice diameter, injection pressure and ambient gas temperature ♦ extinction and Schlieren imaging ♦ theoretical investigation of spray penetration	◊ increasing ambient gas density results in increased spray dispersion, hence more air entrainment and therefore in slower penetration velocity and reduced spray penetration ◊ vaporisation decreases penetration and dispersion by up to 20% relative to non-vaporising sprays; the evaporating fuel cools the gas mixture in the spray and hence increases its density and this leads to slower spray penetration; further, the increased density contracts the spray and hence the spray dispersion angle is reduced
Nishida *et al.* (1985)	♦ high-pressure bomb of 3MPa and 773K ♦ single- and double-pulsed holography to reconstruct shadow-, Schlieren- and micro-graphs	◊ increase in atmospheric temperature results in decrease of spray width

Author(s)	Experimental set-up + experimental technique	Main findings
Pierpont and Reitz (1995)	♦ single cylinder DI diesel engine with hydraulically actuated EUI ♦ cylinder-pressure and exhaust gas emissions measurements ♦ effects of injection pressure (72-160 bar), nozzle inlet condition (rounded edged, sharpen edged nozzle) and spray angle(125° and 140°)	◊ raising the injection pressure effectively reduces particulate emissions, however injection timing must be retarded resulting in an increases in BSFC in order to maintain the same NO_x level ◊ sharp-edged nozzles produce less particulate emissions ◊ spray angles with significant wall impingement compared to minimal wall impingement show little difference in emissions
Plee *et al.* (1981)	♦ single-cylinder 5.7L, V-8, diesel engine with EGR-system ♦ particulate and NO_x emission measurements ♦ luminosity probe	◊ for fixed SOC, EGR reduces NO_x and increases particulate emission possibly due to variation in the calculated stoichiometric flame temperature ◊ EIC ∝ exp (48900/T_f) ; soot oxidation is more strongly affected by EGR than formation ◊ $EINO_x$ ∝ exp (-38700/T_f) ◊ calculated burned gas temperature changes only little due to EGR ◊ O_2 variation did not effect ignition delay appreciably unless N_2 concentration was increased excessively ◊ air inlet temperatures increase by about 5°C at 30% uncontrolled EGR-rate ◊ 30% reduction in ambient O_2 concentration lengthens flame length by 40% (based on Spalding, 1955)

Author(s)	Experimental set-up + experimental technique	Main findings
Quoc *et al.* (1991)	♦ DI diesel engine, two-cylinder, made by Deutz ♦ two-colour method for determining temperature and *KL*-factor at two lines (above piston-bowl and piston crown, respectively) through cylinder head ♦ conversion of *KL*-factor to soot volume fraction ♦ exhaust measurement of Bosch smoke number	◊ radial stratification of soot concentration, with soot particles mainly present within piston-bowl ◊ heavy loads (i.e. varying fuel quantity) exhibit second stage of soot formation and oxidation due to lack of oxygen within the dilutant combustion gases entrailing in the spray towards end of injection ◊ about 35°CA aTDC mixing within combustion chamber results in homogeneity ◊ increase in engine speed reduces the oxidation of soot (as less time available for the kinetically controlled process) more than it increases the formation of soot (proportional to engine speed) ◊ the flame temperature is not correlated to the operating condition, the maximum temperature being about 2360K ◊ weighted mean soot volume fraction during combustion is correlated to exhaust soot levels for high soot conditions
Roller *et al.* (1995)	♦ four-cylinder, 1.9L DI diesel engine at 1000rpm motoring ♦ single-line laser-induced fluorescence of molecular oxygen	◊ the in-cylinder air temperature is measured to increase from 425K at 284°CA to 560K at 320°CA ◊ the measured temperatures agree with the calculated ones assuming polytropic compression

Author(s)	Experimental set-up + experimental technique	Main findings
Röpke *et al.* (1995)	♦ four-cylinder VW 1.9L DI diesel engine ♦ EGR-system, simulated and uncontrolled ♦ different fuels (diesel, n-heptane and 7D3N) and different intake temperatures (uncontrolled, 50K and 100K) ♦ in-cylinder flame temperature measurement by 5-colour method and flame imaging ♦ NO_x exhaust emission measurements ♦ 2-zone modelling of NO_x formation	◊ 2-step thermal dissociation reaction of CO_2 and H_2O leading to atomic oxygen is reason for the thermal sensitivity of NO formation ◊ EGR results in replacing O_2 by CO_2 and H_2O and this reduction in O_2, rather than the accompanying increase in molar heat capacity, is the dominant factor for lowering the flame temperature ◊ EGR decreases flame luminosity because of lower flame temperatures ◊ flame temperature is decreased from about 2620K to 2470K and 2410K as EGR-rate is increased from 0% to 30% and 50%, respectively ◊ EGR increases the ignition delay ◊ hot EGR leads to higher flame temperatures and hence more NO but also to reduced intake mass and hence lower air/fuel ratio and therefore to lower NO, the latter effect dominating from about 30% EGR-rate ◊ n-heptane produces less NO than diesel because an increase in H/C ratio at constant energy supply lowers the flame temperature since it determines the amount of combustion H_2O and hence the mass of the burning zone, the heat capacity and the amount of dissociation products

Author(s)	Experimental set-up + experimental technique	Main findings
Shimazaki *et al.* (1996)	♦ single-cylinder, two-stroke DI diesel engine at 1000rpm ♦ compression ratio 18.5 and SOI at 3°CA bTDC ♦ high-pressure fuel injection ♦ EGR-rates of 0%, 11% and 23% are tested; EGR level is controlled by amount of residual gas ♦ in-cylinder gas sampling ♦ high-speed cine photography	◊ no combustion close to nozzle tip during injection ◊ in-cylinder emissions seem to stabilise by about 12°CA aTDC for O_2, CO_2, NO_x and others ◊ 23% EGR-rate has a Bosch smoke number of 4.5 a compared to 0.5 for 0% EGR-rate at SOI; during main combustion the in-cylinder soot levels do not correlate with the expected trends caused by EGR but by 12°CA aTDC the Bosch smoke number seems to represent the trends of the exhaust gas concentrations ◊ in-cylinder NO_x levels are similar for 0% to 23% EGR-rates up to 9°CA aTDC after which the 0% and 11% EGR-rates show a rise in NO_x; the levels at 12°CA aTDC are 200ppm for 0% and 11% EGR-rates and 40ppm for 23% EGR-rate, this trend is followed by the exhaust gas concentrations
Shiozaki *et al.* (1998)	♦ 4 cylinder 2 valve engine ♦ 6 cylinder 4 valve engine with an endoscope ♦ 1 cylinder 4 valve engine with a common rail fuel injection system ♦ measurement of flame temperature and NO_x emissions	◊ temperature distribution of combustion flame is more uniform with 4 valve than with 2 valve ◊ maximum flame temperature with 4 valve engine is lower than that with 2 valve engine while the mean temperatures are same level ◊ NO_x emissions with 4 valve is lower than that with 2 valve ◊ flame temperature with pilot injection is reduced

Author(s)	Experimental set-up + experimental technique	Main findings
Shundoh *et al.* (1992)	♦ single-cylinder 4-valve DI diesel engine ♦ high injection pressure and pilot injection ♦ effects of heat insulation, compression ratio, pilot injection and swirl ratio ♦ cylinder-pressure and exhaust emission measurements	◊ shortening of ignition delay has little influence on combustion and emissions at the usual injection timing ◊ when the injection timing is retarded or when the original ignition delay is long, shortening of the ignition delay is effective to reduce combustion and NO_x emissions ◊ considerable retard of injection timing is possible by pilot injection ◊ combination of pilot injection and high injection pressure result in reduction of NO_x and smoke emissions without worsening the fuel economy
Smith (1981)	♦ literature review	◊ oxidation of soot can be enhanced by: low production of soot during the formation and growth processes, small particle diameter, large concentration of the predominant oxidation species and high temperature
Su and Farrell (1998)	♦ spray chamber having high gas pressure and density with laser light source for spray images and measuring droplet diameter using light extinction method ♦ high injection pressure (900-1600 bar) using hydraulically actuated EUI ♦ single cylinder DI diesel engine for performances and emissions measurements	◊ higher injection pressure results in a longer tip penetration length and narrower spray con angle ◊ overall average SMD for whole spray decreases with increasing the injection pressure ◊ higher injection pressures with accompanying shorter injection duration reduce particulate emissions and increase NO_x emissions for a constant injection timing and engine load

Author(s)	Experimental set-up + experimental technique	Main findings
Tree and Foster (1994)	♦ single-cylinder optical DI diesel engine ♦ simultaneous light scattering, extinction and radiation at point (5mm long and 1.5mm wide) near cylinder head ♦ semi-quantitative results of soot particle size, number density and temperature	◊ peak soot diameters in range of 30-50nm ◊ peak soot diameter, soot volume fraction and soot temperature increase with equivalence ratio ◊ soot cloud thickness of 0.4-0.6 times the length from the piston to the head ◊ optical point measurement of soot concentration gives similar peak values as point sampling, but higher ones than total cylinder sampling
Tsujimura (1994)	♦ VCO nozzle ♦ cylinder-pressure and exhaust emission measurements	◊ two ways to reduce emissions: 2 stage combustion (lean and rich) or lean combustion (at flame front) ◊ first possibility can be achieved relatively easily but there is fuel consumption penalty because of 2nd stage ◊ second possibility is technologically more difficult (high pressure injection, small nozzle holes and small combustion chamber diameter required) since fast air entrainment and vaporisation have to compete with rate of thermal decomposition and auto-ignition processes

Author(s)	Experimental set-up + experimental technique	Main findings
Tsunemoto and Ishitani (1980)	♦ engines: two naturally-aspirated IDI diesel engines, one DI diesel engine and one turbo-charged DI diesel engine ♦ emission measurements of NO, O_2, CO_2 and smoke density ♦ EGR-rates from 0-30%	◊ in-cylinder charge heat-capacity increases by a maximum of 6% at an EGR-rate of 40% ◊ reduction in NO dependent on rate of incoming O_2 and less on lowering of combustion temperature ◊ NO reduction due to increased ambient humidity (with increasing EGR) explained by reduction in incoming oxygen ◊ increase in smoke is usually accompanied by decrease in BMEP; both are caused by a reduction of exhaust O_2 due to EGR ◊ expected NO and BMEP reduction and increase in smoke can be predicted from experiments without EGR ◊ similar spray structure with and without EGR during first stage of combustion when large part of total NO is formed in region of excess air factor being about 1; reduction in O_2 leads to increase in fuel rich zone with increasing EGR, hence reduction in NO formation zone; further, fuel rich zone has lower temperature due to lack of oxygen, hence larger temperature difference between formation zone and rich zone which leads to heat transfer from high to low temperature region and hence lowering of temperature of NO formation zone

Author(s)	Experimental set-up + experimental technique	Main findings
Uchida *et al.* (1992)	♦ single-cylinder DI diesel engine with supercharging ♦ engine performance and exhaust emissions measurement ♦ in-cylinder air flow velocity measurement with hot-wire aneomometry	◊ supercharging reduces ignition delay and enhances diffusion combustion, resulting in fuel economy and reduced emissions except NO_x ◊ increasing injection rate reduces both particulate and NO_x emissions without deterioration of fuel economy ◊ combustion and emission characteristics is improved by supercharging more than by enhancing intake swirl
Uchida *et al.* (1993)	♦ single-cylinder DI diesel engine ♦ cylinder-pressure and exhaust gas emissions measurements	◊ ignition delay increases with increasing EGR rate ◊ limit of the EGR rate can be widely extended as the intake boost pressure increases
Verhoeven *et al.* (1998)	♦ high pressure and high temperature cell ♦ liquid spray images of the Mie scattering from fuel and tracer droplets, vapor spray images with a schlieren technique and flame images with high speed cine photography ♦ effects of chamber pressure, temperature and injection pressure on spray penetration, spray angle and ignition	◊ liquid penetration is strongly dependent on the gas temperature, gas density, fuel and nozzle hole size but only weak dependent on the injection pressure ◊ position of ignition is farther from the injector at higher injection pressure ◊ combustion propagates from a point in the center of the spray towards the tip of the spray plume
Wiartalla *et al.* (1995)	♦ model combustion chamber with quiescent airflow ♦ maximum air pressure is 6MPa and temperature is 900K ♦ non-impinging spray ♦ 1-D light extinction technique for soot measurement	◊ maximum soot mass concentration occurs on spray axis and decreases towards the spray edges ◊ soot formation is increased with higher early injection rates but is reduced with higher overall injection rates ◊ spray inclination angle influences soot formation and oxidation processes and a 4-valve configuration with central injection is recommended for soot emission improvements

Author(s)	Experimental set-up + experimental technique	Main findings
Yassine *et al.* (1996)	♦ single-cylinder DI diesel engine in cold room ♦ effects of fuel properties, design and operating parameters on formation and emission of white smoke ♦ real-time exhaust measurements of gaseous HC, solid and liquid particulates	◊ firing occurs in the first cranking cycle at normal room temperature and only after many misfirings at lower ambient temperatures ◊ first firing depends on fuel volatility in addition to cetane number ◊ white smoke depends on the number of misfired cycles ◊ solid particulate exhaust emissions decrease with drop in ambient temperature
Yule *et al.* (1985)	♦ non-impinging, non-combusting spray study ♦ spark photography, high speed cine photography and point photodiode measurement of spray shadow	◊ spray tip penetration reduces with increasing gas pressure ◊ reduced spray angle with increasing temperature from 290K to 373K ◊ increasing spray penetration with increasing gas temperature ◊ spray penetration and angle are mainly dependent on gas density with only weak dependence on secondary gas temperature effects like improved atomisation and vaporisation ◊ dense spray core is surrounded by well atomised sheet of droplets ◊ cycle-to-cycle variations of sprays

Legislation		CO g/km	NO_x g/km	$HC+NO_x$ g/km	Particulates g/km
EC passenger car 94/12/EC • current exhaust emissions standard	IDI Diesel	1.00	-	0.70	0.08
	DI diesel	1.00	-	0.90	0.10
EC draft limits for passenger car for stage 3 in 2000 • accompanied by a change in the test cycle • no concession in DI diesels	All Diesel	0.64	0.50	0.56	0.05
EC proposal limits for passenger car for stage 4 in 2005 • accompanied by a change in the test cycle • no concession in DI diesel	All Diesel	0.50	0.25	0.30	0.025

Table 1.2 Summary of new and proposed European emission standards for passenger car diesel vehicles

CHAPTER 2

THE ROLE OF EGR AND SUPERCHARGING IN DIRECT-INJECTION DIESEL ENGINES

2.1 INTRODUCTION

In order to meet the increasingly more stringent diesel engine emission regulations for the years 2000 and 2005, a significant reduction of the exhaust NO_x and particulate emissions is required. In the past, retarding the fuel injection timing has been adequate to reduce NO_x emission to acceptable levels, but this approach represents now only a short-term solution because of the associated reduction in fuel economy and increase of particulate emissions. More recently exhaust gas recirculation (EGR) has been increasingly used, since it represents a very cost-effective method for reducing the NO_x levels; EGR, by introducing part of the hot exhaust gases back into the engine, replaces a small quantity of oxygen in the inlet air by carbon dioxide and water vapour and reduces the mass of the trapped charge. Since the specific heat capacity of both carbon monoxide and water vapour is greater than that for oxygen, the gas temperatures within the engine cylinder during combustion are reduced, which, together with the reduction of the oxygen available for mixing, leads to reduction in the NO_x formation rate and, thus, NO_x levels in the exhaust. However, application of EGR is restricted to only low to medium loads due to an increase in smoke emissions and power reduction at high loads.

The in-cylinder air-fuel mixing process, which depends on the spray characteristics and degree of air entrainment, is one of the most important factors governing the combustion development, engine performance and level of exhaust emissions. Thus, a reduction in both fuel economy and NO_x emissions can be achieved, without any significant deterioration in the level of the other pollutants, through improvements in air-fuel mixing. In this respect, the effects of combustion chamber geometry are well known but it is important to further optimise other parameters such as the level of intake swirl, the EGR rate and the degree of supercharging or turbocharging for a given combustion chamber design.

The primary purpose of supercharging is to increase the mass of air trapped in the cylinders of the engine by raising air density, which allows more fuel to be burnt. This leads to an increase in engine power output for a given swept volume of the cylinders while keeping the efficiency of the engine unchanged. In addition to the significant improvement in engine power, there is little effect on NO_x emissions due to the higher in-cylinder air density affecting the heat capacity of the in-cylinder charge and reducing its ignition delay. On the other hand, induction swirl generally causes an increase in NO_x emissions by enhancing the air-fuel mixing during the premixed combustion phase.

Overall, supercharging can improve combustion by compensating for the thermal efficiency deterioration at higher EGR rates but it may lead to a small increase in NO_x levels. Thus, it becomes important to examine the combined effects of supercharging and EGR on sprays, combustion and emissions since it is expected that all future engines may operate at high boost pressures and EGR rates even at high loads. Here, these effects are investigated in a four-cylinder and a single-cylinder, high-speed, direct-injection optical engines where the spray development between naturally aspirated and supercharged engine conditions can be directly compared through spray imaging. This comparison concerning the influence of supercharging and EGR (separately and combined) on spray tip penetration and spray angle is complemented by measurements of in-cylinder pressure, heat release rate, ignition delay and exhaust gas emissions and by visualisation of flame development. The effects of EGR and supercharging on ignition delay, spray and flame development and exhaust gas emissions at various injection timings are investigated and compared in the two engines, while additional emphasis is placed on the individual effects of swirl ratio, boost pressure and fuel delivery as characterised in the single-cylinder engine.

2.2 EXPERIMENTAL SYSTEM

The geometry of the four-cylinder and single-cylinder research engines is considered to be representative of HSDI passenger car and light-duty production diesel engines, respectively. In order to control the EGR rate in both engines, two adjustable valves were installed, one on the exhaust pipe allowing very high EGR rates to be attained and the other on the exhaust gas return pipe connected to the inlet manifold. For supercharging, an air blower was attached to the inlet manifold providing a constant inlet boost pressure. An adjustable valve which varied the cross sectional area of the air blower outlet, thus varying the flow rate, allowed control of

the inlet boost pressure. In addition, a pressure gauge and an air flow meter were installed on the inlet manifold and the inlet pipe of the air blower to monitor the inlet boost pressure and EGR rate.

2.2.1 Test Engines and Conditions

A number of tests were carried out in a four-cylinder and a single-cylinder HSDI diesel engine to determine the effects of EGR and supercharging on the fuel spray development, combustion and NO_x/smoke emissions.

2.2.1.1 Four-cylinder engine

The four-cylinder engine used was a VW high speed, 1.9L direct-injection diesel engine with a helical intake port, a re-entrant combustion chamber and an inclined, slightly off-centre, 5-hole injection nozzle. The combustion chamber having optical access through quartz side windows and a flat piston window, is presented in Figure 2.1. The standard engine version had a scroll supercharger (G40) and an intercooler, however both were by-passed to allow optical measurements under repetitive short-term conditions. The main geometric characteristics and operating conditions of the engine are summarised in Table 2.1. The advanced engine version included a turbocharger and an EGR system. The turbocharger was, however, again by-passed since steady-state conditions were usually reached after more than 40 engine cycles and not more than about 15 cycles could be visualised, on average, without considerable window contamination by soot particles generated during combustion.

A typical mechanically controlled rotary-type Bosch VE fuel injection pump was used which was equipped with a single spring injector having a nominal nozzle opening pressure of 196 bar. The injector was positioned with an inclination of 26° to the cylinder axis so that the axes of the five sprays were uniformly oriented inside the piston bowl. The angle between the spray axis and the cylinder head is nominally 15° resulting in a spray cone angle of 150°.

The test bed used for engine installation is based on a DC dynamometer (Thrige-Scott) rated at 37 kW (415V/100A), which is operated through a thyristor control unit (SSD). This is necessary to allow the dynamometer to be used as a DC motor during motoring operation and as a DC generator when loading the engine. Unfortunately, the rating of the dynamometer is not high enough to achieve a stable speed above 2000rpm under firing

conditions. Thus, the engine speed of these experiments was maintained constant at 1500rpm to avoid any speed oscillations over 2000rpm.

A shaft encoder mounted on the cam shaft provided a single marker pulse per cycle and 2000 pulses with a time resolution of 0.36°CA while a Hall needle lift sensor fitted onto the injector provided information about the start of injection, which can be measured directly with an oscilloscope and recorded in the computer through the data acquisition system. The cylinder pressure was measured by a KISTLER pressure transducer which was installed in the cylinder liner. An AVL type 316 piezo-electric pressure transducer was mounted on the injection pump end using a threaded adapter to measure the injection line pressure. The chamber pressure transducer was placed flush with the inside of the liner and close to the cylinder head through one of the liner dummy windows. KISTLER 5007 charge amplifiers were used to convert the charge signal from the transducer into a measurable voltage for both measurements. The line pressure and cylinder pressure transducers with their corresponding charge amplifiers were calibrated using a hydraulic dead-weight test rig.

A personal computer was used for simultaneous data acquisition of the shaft-encoder, line pressure, needle lift, cylinder pressure, pulse-by-pulse laser power and camera timing signals using a data acquisition card (FLASH 12).

The four-cylinder engine was operated at three different injection timings of 2, 5 and 8 CAD before top-dead-centre (bTDC) at an engine speed of 1500rpm and fuel delivery of 15.5mm^3/inj, while a smaller quantity of 6.0mm^3/inj was also used for spray visualisation to avoid a quick window fouling. Three EGR rates of 0%, 15% and 30% were examined while a boost pressure of 0.1 bar was compared to the naturally aspirated case. Corresponding engine operating conditions for the single-cylinder engine included injection timing of 8 CAD bTDC, engine speed of 1200rpm and fuel delivery of 15, 20 and 25mm^3 / injection.

The EGR rate has been defined here as the percentage of exhaust gas mass in the inlet charge following the definition adopted by Hentchel and Röpke (1993), i.e.

$$EGR \text{ rate} = (1 - F / I_o) \times 100 \qquad (2.1)$$

This definition assumes that the total intake mass (I_o) remains constant for all the EGR rates at constant engine speed, load and cylinder boost pressure and, hence, at 0% EGR I_o is equal to the intake mass of fresh air (F). However, it should be stated that using this definition the volumetric efficiency of the engine might be different at different EGR rates due to the change of in let charge temperature.

2.2.1.2 Single-cylinder engine

The single-cylinder engine was a Ricardo Hydra, previously used by Arcoumanis *et al.* (1991, 1996) and in a slightly different form by Rao *et al.* (1992, 1993), that incorporates a combustion chamber and a two-valve cylinder head geometry similar to those of the Ford York 2.5 litre four-cylinder HSDI engine. A variable induction swirl port and an electronic unit injector (Lucas EUI 50) provided flexibility in controlling the operating conditions by enabling the swirl number to be varied between 1.6 and 3.0 and the fuel quantity and injection timing to be easily adjusted. Optical access, when required, was provided by a quartz window forming the bowl base of an extended piston; the optical piston was replaced by a similar extended piston incorporating a conventional metallic toroidal piston-bowl for the emission tests. The main geometric characteristics and operating conditions of the engine are summarised in Table 2.2.

The engine was motored by a 30 kW DC dynamometer and controlled by a thyristor circuit. Engine torque was measured by a transducer situated between a lever mounted on the dynamometer casing and the mounting frame, and calibrated to provide a digital readout. A piezoelectric pressure transducer was installed into the cylinder head to measure the combustion chamber pressure. For each test case, the data received from the pressure transducer and the shaft encoder were digitised and transferred to the hard disk of a personal computer using a data acquisition card.

Engine operating conditions included injection timing of 8 CAD before top-dead-centre (bTDC), engine speed of 1200rpm and fuel delivery of 15, 20 and 25mm^3 / injection. Three EGR rates of 0%, 20% and 40% were examined and four boost conditions including naturally aspirated, 0.3, 0.4 and 0.5 bar. The temperatures of the engine oil and cooling water were maintained at 85^0 C during all the tests while "SHELL Gas Oil SH" was used as fuel.

The rate of heat release and the IMEP were calculated from the ensemble-averaged cylinder pressure over 75 consecutive engine cycles which were sampled every 0.36 CAD using a piezoelectric pressure transducer installed into the cylinder head.

A schematic of the system for the single-cylinder engine, which is principally the same as for the four-cylinder engine, is shown in Figure 2.2. The EGR rate was controlled by means of two valves; the first was placed in the return pipe between the exhaust manifold and the inlet of the blower and the second in the exhaust pipe downstream of the return pipe. The

exhaust gases were connected upstream of the supply blower to enable them to recirculate at the higher boost pressures. Due to the length of the pipe connecting the exhaust manifold to the fan inlet, the engine was run for at least 15 seconds before any measurements were made in order to ensure that the air in the pipe was displaced by the exhaust gases. As a result of the quick window fouling before the system could reach steady state, it proved difficult to perform the photographic investigation of the diesel sprays and combustion flames within the firing engine operating at supercharged conditions with different EGR rates.

High-pressure air was supplied to the inlet manifold using a single-stage blower which provided the required air boost pressure for the single-cylinder engine up to an engine speed of 2400rpm. In this case, three different boost pressures were obtained by varying the size of the inlet hole of the blower. A Lucas air flow meter was used to measure the mass flow rate of air entering the blower at 1500rpm for the four-cylinder engine and at 1200rpm for the single-cylinder engine under three different inlet boost pressures. The EGR rate was then calculated from Equation (2.1) and the required rate for a given boost pressure was set by the adjustable valve. The measured values of the fresh air mass flow rates are given in Table 2.3. It should be noted that the boost pressures measured at the intake manifold were lower than those expected from the input air mass flow rate to the blower, especially at the higher boost pressures. For example, when the measured air mass flow rates increased by 31.3%, 44.8% and 67.2% the corresponding boost pressures increased by 30%, 40% and 50%, respectively. This difference is probably attributed to the loss in air mass due to the unavoidable blow-by resulting from the use of the graphite piston ring to enable dry lubrication of the optical engine. Since the loss in air mass increases as the cylinder pressure increases, this loss is more pronounced during compression. The motoring pressure measured was 34.0, 39.7, 42.3 bar and 44.7 bar corresponding to boost pressures of 0, 0.3, 0.4 and 0.5bar, respectively. On the other hand, the actual increases in air mass at the various boost pressures, which persist in the cylinder during the compression period, can be calculated from the measured motoring pressure; the relevant increases in air mass compared with the naturally aspirated (NA) conditions were estimated to be 13%, 19% and 24% at boost pressures of 0.3, 0.4 and 0.5 bar, respectively.

2.2.2 NO_x and Smoke Measurements

Oxides of nitrogen were measured with a Signal 4000 series chemiluminescent analyser. The NO in the exhaust gas sample stream reacts with ozone in a flow reactor. The reaction produces electronically excited NO_2 molecules which emit radiation as they decay to the ground state. The amount of radiation emitted is measured with a photomultiplier and is proportional to the amount of NO. The instrument can also convert any NO_2 in the sample stream to NO by decomposition in a heated stainless steel tube so that the total NO_x concentration can be determined. Since this instrument is very sensitive, it should be calibrated with a zero NO_x and a span gas of which NO_x concentration is already known, and needs to be supplied with ozone to initiate the chemiluminescent gas phase reaction between ozone and NO. It cannot be used for transient NO_x emission measurements since the dynamics of the analyser cause a distortion to the exhaust signal and it does not react instantaneously to NO_x concentration changes. In this experiment, the calibration of the chemiluminescent oxides of nitrogen analyser was carried out before every measurement using N_2 gas for zero setting and sample gas of 500 ppm NO_x for span.

A probe was fitted to the exhaust system at a position 250mm downstream of the exhaust valve, to allow samples of exhaust gas to be drawn. The chemiluminescence analyser provided information about the NO_x concentration in ppm while smoke measurements were obtained using a Bosch smoke meter positioned 1500mm from the exhaust valve. Smoke levels were measured for every test at the end of the NO_x measurements in order to provide sufficient time for the engine-out gases to fill the exhaust system. Five readings for each test were obtained; the highest and lowest were discarded and then the average of the remaining three was recorded. It should be noted that when NO_x emissions are measured in ppm, the total amount of NO_x varies depending on the amount of exhaust gases. Therefore, since the amount of exhaust gas increases with supercharging, the measured values of NO_x emissions in ppm were corrected by taking into account the volume increase by supercharging, thus allowing direct comparison of the amount of NO_x generated in each cycle. The corrected values are indicated as 'effective NO_x' in the relevant figures, where:

$$\textit{effective}\ NO_x\ (\text{ppm}) = \textit{Measured}\ NO_x\ (\text{ppm}) \times (I_{SC}/I_{NA})$$

where I_{SC} and I_{NA} present the air mass supplied into cylinder under supercharging and naturally aspirated conditions, respectively.

2.2.3 Visualisation of Sprays and Combustion

2.2.3.1 Four-cylinder Engine

Diesel sprays and combustion in the four-cylinder engine were observed through a transparent piston window using a high speed CCD camera (IMACON 468) which incorporates a prism to obtain six images from one incoming image and guide those to a separate second generation intensifier. The resolution of the individual sensors is 576×385 pixels (linear spatial resolution of about 0.2mm/pixel) at 8-bit and the light levels can be controlled by adjusting the intensifier gain separately from the exposure time. Also further light level control is provided through an iris inside the main camera body in addition to the camera aperture. The exposure time for each frame is variable from 10 ns to 1ms in 10 ns step and the maximum frame rate is 100 million pictures per second, which means that six frames from one cycle can be captured sequentially with a time interval of less than 10 ns.

All variables for each of the six images, that is intensifier gain, exposure time and delay time from the trigger, can be set on the camera set-up programme together with the timing of the flash light for illumination. The iris within the camera body was kept fully open for all tests, whereas the intensifier gain, the aperture and the exposure time were adjusted to obtain good illumination and adequate freezing of the images. The combination of the variables was optimised for each test case. For instance, higher intensifier gain and longer exposure time were chosen for the pictures at the beginning of combustion in order to detect the start of auto ignition more accurately. Since noise is amplified together with the real signal, the high intensifier gain is limited. The main trigger was provided directly from the shaft encoder of which the marker pulse was adjusted to rise at the top dead centre (TDC). Two synchronised flash lamps of about 2ms duration were used for the illumination of the sprays.

Due to the slow saving of the images on the computer hard disc, only one cycle-six image sequence could be taken per time. The limitation in the number of frames able to be captured within one cycle presents the acquisition of time-resolved images over the complete cycle. Also it should be noted that even though the iris, camera aperture and exposure timing were selected to be the same for all six sensors, slightly different light levels were registered due to the inherent differences in the optical system and the sensors themselves. A 75~300mm zoom lens was used with a focal length of 200mm while a dioptric close-up lens allowed

shortening of the focal length for adjusting the focus on the spray and the flame despite the positioning of the camera system close to the test bed.

2.2.3.2 Single-cylinder engine

Visualisation of the sprays exiting from the four-hole nozzle of the unit injector was performed under different boost pressures, swirl ratios and fuel quantities in the absence of EGR, by employing a Drum Camera (Oxford Lasers) to obtain 35mm images of the sprays prior to the start of combustion. Illumination of the spray was provided by a Copper-Vapour pulsed laser (Oxford Lasers CU15) at a frequency of 20 kHz. The laser light was directed towards the piston bowl through a quartz window in the piston base using an optical fibre which was positioned to scatter the laser light off the fuel spray. The laser was triggered by the shaft encoder, enabling the period between the start of injection and the start of combustion to be recorded in approximately 25 images. The system also benefitted from a high resolution Kodak T 35mm film and short film processing times. Flame visualisation studies were performed under naturally aspirated conditions at different EGR rates and for supercharging conditions in the absence of EGR. For the naturally aspirated conditions with EGR, the exhaust gases were connected closer to the intake manifold of the engine in order to reduce the number of cycles required to ensure stable EGR, thus helping to reduce window fouling. A CCD camera (Proxitronic HF-1) triggered from the shaft encoder was employed in conjunction with a frame grabber to provide a single digitised flame image per cycle. Since only a single shot could be taken per cycle with this CCD camera, each flame image in the sequence was obtained from a different cycle and at a different crank angle, while the spray sequences were obtained from the same cycle. Both spray images and flame images were recorded only after the engine had completed 15 firing cycles, thus enabling the combustion chamber walls to achieve their steady-state temperature prior to window fouling.

2.3 RESULTS AND DISCUSSION

Experiments were performed to quantify the effects of exhaust gas recirculation and supercharging on diesel spray and combustion characteristics, engine performance and exhaust emissions for various engine test conditions. This section presents the spray and combustion images, and an estimate of engine performance in terms of cylinder pressure,

IMEP, heat release rate, and exhaust emissions of NO_x and soot concentrations as quantified by a Bosch smoke meter. By examining the characteristics of the sprays first, the implications of their spatial and temporal development for combustion and exhaust emissions may become clearer.

The tests were performed for injection timings of 2, 5 and 8 CAD bTDC at a constant fuel delivery of 15.5mm^3/inj and an engine speed of 1500rpm in the four-cylinder VW engine and for a fuel delivery of 15, 20 and 25mm^3 / injection, a swirl ratio of 1.6, 2.2 and 3.0 and an engine speed of 1200 and 1800rpm in the single-cylinder Hydra engine.

2.3.1 Spray Development

2.3.1.1 Four-cylinder engine

The spray development for an injection timing of 5° bTDC in the absence of EGR under naturally aspirated conditions and with a time resolution of 0.2° crank angle is shown in Figure 2.3 together with the spray development for the same injection timing but without EGR under supercharged conditions. It should be noted that the sequence of images consists of pictures from two different cycles, since only six images per batch could be obtained from every cycle due to the limitation of the CCD camera (IMACON 468) used for this experiment.

The very first evidence of liquid emerging from the nozzle hole was observed at 355.2°CA, which is in good agreement with the needle lift profile acquired at the same time. It is interesting that the second spray from the top in the clockwise direction appears to have a smaller spray angle, faster penetration and a more clear boundary than others until it reaches the wall.

2.3.1.2 Single-cylinder engine

The drum camera was positioned and focused to provide visualisation of the four fuel sprays exiting the inclined injector, up to the point of wall impingement, in a sequence of approximately 20 images with a time resolution of 0.05ms (0.36 CAD at 1200rpm and 0.54 CAD at 1800rpm) for three fuel delivery rates and three swirl ratios at 1200rpm and 1800rpm. Images of the sprays with varying rates of EGR are not presented here since previous investigations have revealed that realistic levels of EGR have no measurable effect upon the spray angle and tip penetration (Arcoumanis *et al.*, 1995b; 1995c).

Spray images arranged sequentially after the start of injection are shown in Figure 2.4 for three fuel delivery rates, three swirl ratios, four boost pressures including the naturally aspirated condition and two engine speeds. On the basis of the spray orientation (Figure 2.2), it was expected that the development of sprays 1 & 4 would be similar but faster than that of sprays 2 & 3 due to the inclination of the injection hole. As can be seen from Figure 2.4, it is obvious that the development of all four fuel sprays is different from each other which could be the result of manufacturing tolerances in the injection hole geometry and hole position, exacerbated by the inclined orientation of the unit injector, as well as to cavitation onset in the sac volume and holes.

2.3.1.3 Spray tip penetration

The spray development in terms of tip penetration, estimated from the images of Figure 2.3 and Figure 2.4, is shown in Figure 2.5. It is presented as the best-fit curve for spray tip penetration, obtained by using a function of the form:

$$S = a + bt^{0.5} + ct + dt^2 \qquad \text{with } b, c, d > 0$$

where S is the spray tip penetration distance and t is the time after SOI. In the above equation, the justification for incorporating both a square term and a linear term is provided in the results of Arai *et al.* (1984), who suggested that the development of a diesel spray can be divided into two stages: a non-atomised spray with $S \propto t$ and an atomised spray with $S \propto t^{0.5}$.

The effect of the amount of fuel delivered by the unit injector on spray tip penetration (Figure 2.5c) was found to be negligible as the increase in fuel delivery is achieved through extension of the period of injection. The effect of swirl ratio also seems to have a small effect on the spray tip penetration rate (Figure 2.5d) unlike boost pressure which clearly has a stronger influence (Figure 2.5a, 2.5b, 2.5e). For example, an increase of the boost pressure from the naturally aspirated case to 0.5 bar has resulted in reduced spray tip penetration by nearly 40%. This is in agreement with the recent investigations by Naber and Siebers (1996) and Verhoeven *et al.* (1998) who showed that the effect of higher density within the combustion chamber is a larger spray angle and reduced tip penetration. Under supercharging conditions, Daisho *et al.*, (1986) reported that the spray volume changes only slightly whereas the spray penetration is greatly reduced; hence a fuel spray evaporates more rapidly due to an increase in the heat transfer between the ambient gas and the fuel droplets. As expected, the

rate of spray tip penetration increases with increasing engine speed (Figure 2.5f); however, the spray tip penetration distance could not be measured accurately close to the wall. Verhoeven *et al.* (1998) have reported that the injection pressure has only a small influence on liquid fuel penetration, while Kamimoto *et al.* (1987) reported that liquid penetration remained approximately constant for injection pressures between 26 and 110 MPa. Concerning the effect of density, the images sequence shown in Figures 2.4e~g corresponding to different boost pressures indicate no clear trend in the spray angle, probably due to the spray-to-spray variations inherent in inclined injectors. It should be noted that the obtained spray images are the result of light scattered by the fuel droplets rather than by the fuel vapour, although Baritaud *et al.* (1994) have identified that the liquid and gas phases penetrate at almost the same rate during the early period of injection.

Since in the Hydra engine the injector tip was slightly offset from the centre of the piston bowl, as shown in Figure 2.2, the spray impinged on the side wall of the bowl at an angle of approximately 15° to the horizontal plane and 10° to a vertical plane normal to the wall surface. As has been shown by Arcoumanis *et al.* (1995a), the impingement of a diesel spray onto a flat surface under atmospheric conditions results in a wall jet that moves rapidly along the wall, with much of the liquid moving as a film along the surface. A similar situation seems to occur within the engine as can be seen in more detail in Figure 2.6. The presented sequence shows spray #2 impinging on the wall and creating a wall jet, which is enhanced in the anti-clockwise direction due to the impingement angle, where it moves against the clockwise rotating swirl. On the other hand, sprays #3 and #4 are enhanced in the clockwise direction by the action of swirl. Upon exiting the injector, the sprays seem to be well atomised with an initial half cone angle of approximately 5°. Figure 2.6 also shows the spray development as a function of the inlet boost pressure. As the in-cylinder air density increases with boost pressure, the amount of fine droplets surrounding the dense core appears to increase, which indicates that the air-fuel mixing process is enhanced during spray penetration into air of higher density, and the size of the droplets is reduced due to the faster vaporisation rate. As a consequence, the smaller droplets lose their initial momentum and are separated from the main spray, which results in shorter ignition delay and reduction of smoke emissions. In contrast, during the early part of the diffusion combustion period, droplet vaporisation becomes slower since the in-cylinder temperature is reduced due to the increased amount of entrained air mass. Enlargement of the spray head seems to occur almost immediately after exiting the nozzle, due to the displacement of the fuel droplets towards the side of the

advancing spray tip. It appears that the size of the spray head becomes larger as the inlet boost pressure increases. Upon impact of the spray on the piston wall, a mist of droplets is formed around the impingement region, which are entrained within the roll-up vortices characterising the developing wall jet. The mist of droplets formed at the right side of the spray appears much denser and lasts longer than on the other side. This indicates that more droplets are concentrated towards the right hand side of the spray due to the particular impingement angle, which are prevented from spreading by swirl, while spreading of droplets by swirl is enhanced at the left side.

One of the main aims of this investigation was to examine the development of the sprays and their interaction with the piston bowl wall as a function of the swirl velocity. The obtained spray images have demonstrated a reduction in spray tip penetration induced by supercharging, which is generally associated with an increase in the spray width. Cossali *et al.* (1996) have confirmed in a constant-volume chamber that an increase in the gas density or temperature leads to an increase in the amount of air entrained within the injected spray; the majority of the air is entrained after the passage of the spray tip which accounts for the decrease in ignition delay associated with higher boost pressures. The work of Naber and Siebers (1996) has also revealed that the surrounding gas density has a significantly larger effect on tip penetration than on spray dispersion due to the relatively larger mass of entrained air at higher ambient air densities.

2.3.2 Auto-Ignition and Flame Development

The influence of EGR and supercharging on the auto ignition process and flame development was investigated on the basis of flame images obtained in the four-cylinder engine. The intensity of CCD camera used for capturing the auto-ignition was higher than that used for visualisation of flame development. In this experiment, the engine was operated at no load to avoid fast contamination of the piston window.

The first visible flame and its development under naturally aspirated and supercharging conditions for different EGR rates are shown in Figure. 2.7. Dec and Espey (1995) have reported that the chemiluminescence emission which is too weak to capture with a low intensified camera exists throughout the leading portion of the spray jet prior to the appearance of soot luminosity. Therefore, in this experiment, the comparison was performed on the basis of the visual flame captured by the given camera set-up. Overall, the first visible

flame appears earlier under supercharged conditions by 0.8°~1.2°CA than under naturally aspirated conditions as shown in Figure 2.7. When EGR was applied, the appearance of the first visible flame was delayed for all cases tested but the effect of EGR on ignition delay was rather small under supercharging conditions. Any differences in ignition delay for the different injection timings were hardly detected from these images. As shown in Figure 2.7, auto-ignition seems to occur at positions half way between the injection tip and the piston bowl wall for all sprays but a time difference. The flame propagates from each ignition site along its own spray axis and, interestingly enough, it is not transferred to adjacent sprays until the flame reaches the wall.

A sequence of flame images for two inlet charge conditions and different EGR rates is shown in Figure 2.8. It is apparently clear that the flames developed under supercharged conditions have higher luminosity throughout the combustion period than those under the naturally aspirated condition. This implies that supercharging may result in higher thermal efficiency. Sugihara *et al.* (1992) have found through analysis of the heat release rate that when the intake air quantity is increased, the combustion period is shortened due to the enhanced air-fuel mixing as a result of the higher air density, and results in improvement in combustion. It is clear that under naturally aspirated conditions the flame luminosity decreases with increasing EGR rate due to the reduced oxygen concentration. However, no clear influence is observed under the supercharged condition since the amount of air seems sufficient and the recycled exhaust gas contains enough oxygen concentration in the case of zero load. Daisho(1994) has suggested that the recirculated exhaust gas must be increased at higher boost pressures to allow reduction of NO_x to the same low levels as under naturally aspirated conditions, since the recycled gas contains more excessive oxygen.

2.3.3 Combustion and Emissions

The effects of EGR, supercharging, swirl and injection timing on combustion and emissions were investigated in both the four-cylinder and the single-cylinder engine. The effects of the first three parameters and the combined effect of supercharging and EGR will be discussed below on the basis of the results obtained in the single-cylinder engine while the effects of injection timing will be discussed in connection with the results obtained in the four-cylinder engine.

2.3.3.1 Effect of EGR

Plee *et al.* (1981) have identified the classic trade off between NO_x and particulate emissions in view of the fact that EGR increases the carbon content of particulates and CO emissions while it reduces NO_x levels. Since in the application of EGR some of the inlet air is replaced by recirculated exhaust gas, the fresh air available for combustion is reduced. If the amount of fuel supplied to the engine is constant, then the reduced air/oxygen available for combustion decreases the air-fuel ratio at which the engine operates. The reduction of the air-fuel ratio affects engine performance and exhaust emissions mainly through the oxygen concentration (dilution effect) and the heat absorbing capacity of the inlet charge (chemical effect). (Ladommatos *et al.*, 1998a~c) The change of the inlet charge temperature due to the introduction of the recirculated exhaust gas into the inlet air stream is another factor affecting combustion and exhaust emissions. As a result of all these changes, ignition delay is varied and, in turn, combustion and exhaust emissions are affected. In this project, the performance of the engine has been quantified in terms of cylinder pressure, the rate of heat release and the indicated mean effective pressure (IMEP) as a function of the EGR rate.

It has been well established that introducing EGR results in longer ignition delay, which varies with oxygen concentration. The delay time is slightly offset by the extra heat provided to the intake air by the hot exhaust gas. The heat release rate curves for various EGR rates are presented in Figures 2.9a~f together with the corresponding cylinder pressures; based on these the ignition timings are estimated and given in Figure 2.10. Ignition delay varied under naturally aspirated conditions from about 5 CAD at 0% EGR to about 8 CAD at 40% EGR but this had little effect on the duration of the premixed and diffusion phases of combustion. As a result of the prolonged ignition delay, the amount of fuel burned during the premixed combustion period increased and diffusion combustion was retarded. This observed increase in ignition delay associated with EGR implies that the fuel has more time to vaporise and mix. The increased amount of fuel injected during the ignition delay period results in a rapid temperature rise during the premixed combustion phase, which increases NO_x emissions. However, the influence of the increased premixed combustion phase on engine performance and exhaust emissions is relatively small compared with the suppression of the combustion temperature as a result of the reduction in the oxygen concentration and the delay in the start of the diffusion phase. The reduction in oxygen concentration available for combustion resulted in lower flame temperatures, while the effect of retarding the start of combustion depends on its timing relative to TDC, which is determined by the amount of

ignition delay and injection timing. In general, the injection timing is adjusted to position the peak pressure just after TDC for maximisation of the engine's power output. Therefore, an excessive delay of combustion due to EGR results in reduced amounts of fuel burned in the period around TDC, low in-cylinder gas temperatures and reduced NO_x emissions. The addition of CO_2 and H_2O from the exhaust gas to the inlet air also contributes to NO_x reduction by suppressing the gas temperature though their higher heat capacity.

From the heat release rate and cylinder pressure curves (Figure 2.9a~c), it is clear that the appearance of a peak in the heat release rate is also delayed with increasing EGR rate, and that the amount of this delay increases with increasing fuel delivery. The observed delay in the peak heat release was greater than the increase in ignition delay. For example, in the case of 20mm^3/inj of fuel delivery (Figure 2.9b), the peak heat release appears at about 4 CAD after the start of ignition at 40% EGR, while at 0% EGR it appears 3 CAD later. This indicates that flame propagation in the case of EGR becomes slower as a result of the reduced oxygen concentration despite the increased fuel injected during the prolonged ignition delay period. The overall slower flame propagation leads to further retardation in combustion, which in turns leads to reduction of the peak in-cylinder pressure and temperature.

The delay in the start of combustion and the suppression of its diffusion phase associated with EGR, resulted in reduction of the maximum cylinder pressure, with the peak reduced from 60 bar at 0% EGR to 55 bar at 40% EGR for the case of 20mm^3/inj, as shown in Figure 2.9b. It is thus well known that applying EGR results in some deterioration of the engine's power output or thermal efficiency. Ladommatos *et al.* (1996a) have confirmed that the dilution of the inlet charge by EGR resulted in lower oxygen availability and longer ignition delay, with an adverse effect on engine power output; however, the isolated effect on ignition delay was rather small. In these experiments, as can be seen in Figure 2.11, the IMEP calculated from the measured cylinder pressure tends to increase slightly with increasing EGR rate except for the case of 40% EGR and 25mm^3/inj where the maximum cylinder pressure was reduced. This is mainly attributed to the delay of the start of combustion from before TDC to after TDC. When combustion starts before TDC, the work done before TDC is considered as negative work in the IMEP calculation. However, when the start of combustion moves towards or after TDC, due to the increased ignition delay resulting from the higher EGR rate, it appears that IMEP increases with increasing EGR rate. As shown in Figure 2.10 under naturally aspirated conditions for 20mm^3/inj. of fuel delivery, the start of combustion is delayed from 3° bTDC at 0% EGR rate to 0.5° bTDC at 40% EGR rate. As a result, the IMEP

could be slightly enhanced at higher EGR rates due to the delay in the start of combustion which results in reduction of the negative work despite the slight reduction in the maximum cylinder pressure. Therefore, it is expected that when the injection timing at 0% EGR is retarded towards TDC or even after TDC, the IMEP will be reduced at higher EGR rates, as reported by Ladommatos *et al.* (1996a).

In the case of 25mm^3/inj of fuel delivery, however, IMEP is dramatically reduced at 40% EGR. Since the recirculated exhaust gas reduces the oxygen available for combustion at this high load, ignition delay becomes longer and combustion deteriorates. It can be seen from Figures 2.9d~f, that there is no difference in the start of combustion for the various fuel deliveries in the absence of EGR, but in the case of 40% EGR combustion starts later at higher rather than at lower loads. This late post-TDC combustion resulted in lower combustion pressures in addition to incomplete combustion. This reduction in combustion pressures seems to be too large to be compensated for by the reduction in the negative work due to the longer ignition delay associated with EGR. It can thus be argued that the effect of EGR on combustion pressure is greater at higher than at lower loads due to the more delayed combustion. The other effect of EGR on IMEP, a decrease in pumping loss from about -2kPa at 0% EGR to -1kPa at 40% EGR, might be considered negligible.

According to flame visualisation results not shown here, the intensity of the flame images becomes weaker at higher EGR rates, which implies lower flame temperatures as a result of the reduction in oxygen concentration. The first visible flame appears later at higher EGR rates, which is in agreement with the prolonged ignition delay indicated in the heat release rate curves. It can also be seen that flame development after the start of ignition is slower at 40% EGR than at 0% EGR, as deduced from the retardation in the appearance of the peak heat release at higher EGR rates. Concerning combustion, the results from this investigation are in agreement with those of Ladommatos *et al.* (1998), where it was identified that one of the main influences of EGR is ignition delay and the consequent timing of the combustion phases relative to TDC.

It can be seen from Figure 2.12a, representing the variation of NO_x emissions with EGR rates, that addition of EGR resulted in NO_x reduction regardless of fuel quantity and swirl ratio; this is due to the reduction in the available oxygen concentration and the delay in the start of combustion, despite the increased fuel quantity injected during the ignition delay period. The replacement of oxygen with CO_2 and H_2O from the exhaust gas also affects in-

cylinder gas temperatures through enhancement of the heat absorbed due their higher heat capacity. The rate of reduction in the NO_x exhaust concentration decreases as EGR rate increases; NO_x emissions are reduced from 500 ppm at 0% EGR to 140 ppm at 20% EGR, swirl ratio of 2.0 and 20mm^3/inj of fuel delivery. However, the additional reduction in NO_x levels was only 100 ppm when the EGR rate increased further to 40%.

The results in terms of the Bosch smoke number, being proportional to exhaust particulates, exhibit the typical trade-off between NOx and particulate emissions. As shown in Figure 2.12b, smoke emissions increase with increasing EGR rate over the fuel delivery range examined here. This is attributed mainly to the reduction in the oxygen concentration and the associated delay in combustion, despite the additional time available for the fuel to vaporise and mix with the air during the prolonged ignition delay period. Smoke emissions increase significantly at higher EGR rates, which indicates that EGR should be carefully controlled at each engine operating condition, especially at high loads. Smoke emissions seem to increase with increasing fuel delivery, and this increase becomes greater at high EGR rates.

It is interesting to note that NO_x emissions are slightly affected by increasing the fuel delivery from 20mm^3/inj to 25mm^3/inj (in the part load range) over all EGR rates (Figure 2.12a). The increased fuel quantity resulted in an increase in the diffusion combustion phase without any change in the premixed combustion period, with the extra fuel burned during the later part of the diffusion phase. This extended diffusion combustion has little influence on NO_x formation because the cylinder pressure and temperature during the later part of this phase are relatively low. On the other hand, since smoke formation is controlled by the air-fuel ratio, it increases with increasing fuel delivery (Figure 2.12b).

In the case of low loads (15mm^3/inj), NO_x emissions are less at 0% EGR but higher in the presence of EGR, relative to the case of 20 and 25mm^3/inj. Since there is no difference in the start of combustion between the different fuel deliveries at 0% EGR, lower NO_x levels result from less amount of fuel. However, as can be seen from Figures 2.9e~f, the delay in combustion at 15mm^3/inj due to EGR was very small compared to that at higher loads. As a result, in the case of 15mm^3/inj, combustion at high EGR rates was concentrated near TDC, while combustion at higher fuel quantities was shifted away from TDC. Combustion around TDC leads to higher NO_x levels due to its high combustion pressure/temperature although fuel delivery can be small. This indicates that the timing of combustion is the predominant parameter affecting the in-cylinder temperature rise and, thus, NO_x levels under low load conditions.

It is also interesting to note that at low loads (15mm^3/inj) the smoke emissions relatively decrease with increasing EGR compared to the higher loads. The same trend appears to be valid throughout the range of boost pressures and swirl ratios. It can be argued that the effect of improved air-fuel mixing during the prolonged ignition delay, associated with EGR, on the reduction in smoke levels is greater than the effect of the reduced oxygen concentration, since the oxygen content in the recirculated gas is not reduced significantly at low loads.

2.3.3.2 Effect of supercharging

The application of supercharging affects combustion and emissions in diesel engines in three ways; through an increase of the inlet charge mass, the oxygen concentration and the air-fuel mixing rates. Inlet charge mass and oxygen concentration increase in proportion to the inlet boost pressure. An increase of the heat absorbing capacity of the air in the cylinder due to the increased inlet charge mass affects NO_x emissions by reducing the gas temperature, while an increase of the oxygen concentration enhances auto-ignition and combustion and, consequently, affects exhaust emissions. It is also obvious that the air-fuel mixing rates are higher under supercharging conditions than under naturally aspirated conditions, particularly around TDC. Inlet airflow rates were measured for various inlet charge pressures using an air mass flow meter, and the results are shown in Table 2.3. The increased rate in inlet charge mass with increasing boost pressure should be the same as that of oxygen concentration.

The cylinder pressure and heat release rate curves are presented for various boost pressures and fuel deliveries in Figures 2.13a~f. The combustion pressure increases with increasing boost pressure for all fuel deliveries (Figure 2.13a~c). The ignition delay decreases with boost pressure, which leads to a reduction of the peak heat release rate affecting the exhaust emissions. However, there is little difference in the ignition delay between 0.3 and 0.5 bar of boost pressure (Figure 2.14). As shown in Figures 2.13d~f, under supercharging conditions, the variation in fuel delivery has no influence on ignition delay but the combustion period and peak pressure both increase with increasing fuel delivery. Similarly to the naturally aspirated condition, for the case of 15mm^3/inj the peak heat release rate is higher than at higher fuel deliveries, and there is short diffusion combustion implying that most of the fuel injected is burned during the premixed combustion period (Fig 9d~f).

It is shown in Figure 2.15 that IMEP increases with boost pressure for constant fuel delivery, due to the associated increase in the cylinder pressure as reported by Ladommatos *et*

al. (1998a). IMEP improvements are also induced by the higher oxygen concentration, the higher air-fuel mixing rate due to the increase in the inlet charge mass and the gas temperature rise due to the higher initial pressure during the compression stroke. According to flame visualisation not shown here, the intensity of the flame is higher at higher inlet boost pressures, which implies that combustion is enhanced with supercharging. In addition, the inversion of pumping loss from about -2kPa without boost pressure to 19, 26 and 31kPa with 0.3, 0.4 and 0.5 bar of inlet boost pressure, respectively, contributes to the observed improvement of IMEP; however, it should be noted that there is an offset by an increase in the negative work done before TDC. In addition, since the injection timing was kept constant in this experiment, the negative work done before TDC increases as ignition delay becomes shorter with increasing inlet boost pressure. Therefore, further improvement in IMEP can be expected if injection timing is adjusted under supercharging conditions by taking into account the shortened ignition delay.

Since supercharging reduces the ignition delay, the rise of heat release rate during the premixed combustion period is slower and the diffusion combustion period slightly advanced. Daisho *et al.* (1994) have confirmed that supercharging reduces the ignition delay, thereby reducing the premixed combustion phase, but also suggested that the total combustion period is shortened. Sugihara *et al.* (1992) reported that when the intake air mass increases, the combustion period is reduced due to overall improvements in combustion. In the present experiment, however it is hard to observe any reduction in the combustion period as a result of supercharging. What can be seen is that the heat release rate during the early part of the diffusion phase is slightly higher under supercharging conditions, which implies that a larger amount of the injected fuel is burned rapidly during the diffusion phase due to the enhanced air entrainment induced by inlet boost pressure. It should be noted that when the inlet boost pressure increases from 0.3 bar to 0.5 bar, there are still small changes in the IMEP and ignition delay values but the most significant changes are observed with 0.3 bar inlet boost pressure compared to the naturally aspirated case; in particular, IMEP is improved by about 15kPa at 0% EGR and 20kPa at 40% EGR when inlet boost pressure increases from 0 to 0.3 bar. Ignition delay was shortened by 1.5 CAD at 0% EGR and by 4 CAD at 40% EGR with a boost pressure of 0.3 bar, but no further shortening of the ignition delay was observed at the higher boost pressure of 0.5 bar. This implies that further increases in inlet boost pressure may not necessarily provide proportional improvements in engine performance. Sugihara *et al.* (1992) have reported that doubling the boost inlet pressure resulted in insignificant

improvements in combustion and no reduction in the total combustion period, especially at higher engine speeds. This indicates that boost pressure may require optimisation at each engine operating condition with regard to the EGR rate, for benefits to be accrued.

Ignition delay is also one of the most important parameters affecting the in-cylinder temperature during combustion, which consequently controls NOx formation. It is well known that ignition delay affects combustion in two ways; first, through the amount of fuel injected during the ignition delay period which determines the rate of temperature rise and, second, through combustion timing changes that affect the flame temperature depending on when combustion does take place relative to TDC. There is a consensus that under supercharging conditions ignition delay is shortened due to the increased oxygen concentration and enhanced air-fuel mixing rates. It seems that the effect of the reduced fuel injected during the ignition delay period on in-cylinder temperature is relatively small compared to the other two effects of supercharging; i.e. the increase in the heat absorbing capacity of the inlet charge and the resulting enhanced combustion. Thus, the increased charge mass has a higher heat absorbing capacity which reduces the in-cylinder gas temperature and associated NOx levels. On the other hand, the enhanced combustion resulting from the higher oxygen concentration increases the flame temperature and results in higher NO_x emissions. In addition, variation in the combustion timing and duration of the premixed and diffusion phases, due to the shortened ignition delay, is another factor affecting NO_x formation. Overall, the effects of the above four factors on in-cylinder temperature vary depending on the engine operating condition and, especially, injection timing which controls the all important start of combustion.

As seen in Figure 2.16a, NOx emissions under supercharging conditions do not increase significantly compared to those under naturally aspirated conditions, despite the higher flame intensity and temperature; NOx emission levels with supercharging are generally higher, but not by much, than those under naturally aspirated conditions. This indicates that on average, the higher flame temperature resulting from the increased oxygen concentration is offset by the higher heat capacity due to the increased inlet charged mass. Since the heat capacity is in proportion to the inlet charge mass, the effect of suppressing the gas temperature becomes greater as inlet boost pressure increases. The end result is that at the higher examined boost pressure of 0.5 bar, similar levels of NO_x emissions were measured to those with the lower boost pressure of 0.3 bar.

Smoke emissions are reduced as inlet boost pressure increases when the amount of fuel delivery is kept constant (Figure 2.16b), with only a small change in NOx emissions. Since smoke emissions are the result of incomplete combustion, the smoke number is reduced with supercharging due to the enhanced combustion induced by the increased oxygen concentration and improved air-fuel mixing; this leads to fast breakdown of fuel rich eddies and enhanced soot oxidation during the diffusion phase, with the consequence of lower smoke emissions. This trend is offset by reduced vaporisation of the fuel droplets, due to the shortened ignition delay, but its influence is relatively small compared to the effect of the increased oxygen concentration. The degree of smoke reduction appears to be proportional to the inlet boost pressure, implying that increased oxygen concentration is the most important method for controlling smoke levels despite its adverse effect on NO_x emissions.

Overall, it should be noted that all emission data were compared on the basis of constant fuel delivery which confirmed that, under supercharging conditions, NOx emissions are indeed slightly higher but the smoke levels decrease significantly when compared to the naturally aspirated conditions.

2.3.3.3 Effect of swirl

Intake swirl is another important parameter contributing to the air-fuel mixing process, which in turn controls combustion and emissions. As shown in Figure 2.17a~f for various EGR rates and boost pressures, the heat release rate curves start to rise slightly earlier and more rapidly with increasing swirl ratio, which implies that ignition starts earlier and combustion is enhanced at higher swirl levels. At the same time the peak value of the heat release rate is higher in the case of higher swirl, which implies that swirl enhances air-fuel mixing leading to shortened ignition delay and improved combustion. This effect on ignition is more pronounced at higher boost pressures but is reduced with increasing EGR rate, as can be seen in Figure 2.18.

As explained in the previous section, increasing the swirl ratio resulted in an increase in the negative work, because the start of combustion is advanced as a result of shortening the ignition delay. Nevertheless, IMEP tends to increase with increasing swirl ratio over the whole range of EGR rates and inlet boost pressures, due to the enhanced mixing process (Figure 2.19).

Despite the reduced amount of fuel injected during the shortened ignition delay period, the enhanced air-fuel mixing induced by swirl resulted in a rapid temperature rise during the

initial combustion phase. This, in turn, gave rise to a considerable increase in NOx emissions from 400 ppm at 1.6 swirl ratio to 600 ppm at 3.0 swirl ratio in the absence of EGR under naturally aspirated conditions (Figure 2.20a). The effect of swirl on NOx emissions decreased gradually with increasing EGR rate, showing no influence at the 40% EGR rate. Under supercharged conditions, a similar trend was observed except that a small effect of swirl on NOx emissions remained evident at 40% EGR.

It can be seen from Figure 2.18 that the start of auto-ignition was retarded at 40% EGR relative to 0% EGR under naturally aspirated conditions. On the other hand, at 40% EGR under supercharging conditions, where the prolonged ignition delay period was shorter than under naturally aspirated conditions, combustion is still taking place near TDC. The relationship between NOx emissions and intake swirl indicates that the effect of swirl is noticeable only near TDC and decreases as the start of combustion is retarded under the influence of EGR. From these results, it can be concluded that the effect of swirl on combustion development is related to the timing of fuel injection with respect to TDC, in agreement with Uchida *et al.* (1992) who showed that swirl has no significance when injection timing is retarded, implying that swirl is effective only near TDC.

Contrary to the NOx levels, smoke emissions decrease with increasing intake swirl through enhanced air-fuel mixing and soot oxidation. Overall, the effect of swirl on smoke emission remains similar throughout the EGR and inlet boost pressure range.

2.3.3.4 Combined effect of EGR and supercharging

The combined effect of EGR and supercharging on combustion parameters such as pressure and heat release rate are presented in Figures 2.21a~f. While the peak combustion pressure was reduced significantly at 40% EGR under naturally aspirated conditions relative to 0% (Figure 2.21a), a very small reduction was identified under supercharging conditions (Figure 2.21b~c). This implies that the dilution effect of EGR on combustion is reduced with increasing boost pressure, since combustion is still centered around TDC. It is also clear that the effect of EGR rate on ignition delay is considerably reduced under supercharging conditions, as a result of the higher oxygen concentration and enhanced air-fuel mixing induced by supercharging. As shown in Figure 2.21d, small differences are evident in the start of combustion between various boost pressure conditions in the case of 0% EGR; these differences become greater at higher EGR rates (Figure 2.21e~f). Overall, the reduction in the

peak heat release rate induced individually by EGR and supercharging remains valid even when the two are applied simultaneously.

It is shown in Figure 2.22, that the ignition delay increases from 5 CAD at 0% EGR rate to 8 CAD at 40% EGR rate under naturally aspirated conditions and from 4 CAD to just 5 CAD under an inlet boost pressure of 0.5 bar. As a result, the maximum cylinder pressure with 0.5 bar of inlet boost pressure is reduced by only 1.2%, from 69.5 bar at 0% EGR rate to 68.7 bar at 40% EGR rate but by 7.4%, from 59.6 bar at 0% EGR rate to 55.2 bar at 40% EGR rate, under naturally aspirated conditions.

The combined effect of EGR and supercharging on IMEP and, thus, engine efficiency is presented in Figure 2.23; in general, engine efficiency becomes worse as EGR rate increases. However, here IMEP increases slightly with increasing EGR rate in spite of the reduction in the oxygen concentration. As explained before, this is probably attributed to the lower negative work as a result of combustion taking place closer to TDC due to the prolonged ignition delay induced by the increased EGR rate. On the other hand, the reduction in oxygen concentration accompanying EGR can lead to deterioration in combustion, with associated lower combustion pressures and IMEP; however, for the present parametric range the deterioration in combustion is relatively small. For the case of high load (25mm^3/inj) at 40% EGR a significant loss in IMEP under naturally aspirated condition was observed with increasing EGR, but no effect or even a slight gain under supercharging conditions.

It can thus be concluded from the IMEP results, that the deteriorating effect of EGR on engine power and efficiency can be significantly reduced or even suppressed under high boost pressure. On this basis, it can be argued that under supercharging or turbocharging conditions, higher EGR rates can be applied at higher loads without any significant effect on engine efficiency and exhaust emissions compared to the naturally aspirated case. For this to happen, the start of injection should be adjusted to optimise engine combustion and performance over the complete speed and load range in terms of EGR rate.

The peak heat release rates are lower throughout the EGR range under supercharging relative to the naturally aspirated conditions, due to the shorter ignition delay and higher heat absorbing capacity of the charge that allows reduction of NOx emissions.

Overall, the combination of supercharging and EGR leads to a counterbalancing effect on ignition delay and smoke levels, while achieving a significant reduction in the exhaust NO_x concentration through mainly the reduced oxygen concentration associated with EGR; this is offset by boost pressure and the increased heat absorbing capacity of the inlet charge. Figures

2.24a~b show the levels of NOx and smoke emissions obtained when EGR and supercharging are applied at the same time. The results show that with supercharging, NO_x emissions decrease modestly with increasing EGR rate over the fuel delivery range while smoke increases, similarly to the naturally aspirated case. Also it can be seen that the effect of EGR on NO_x emissions remains consistent regardless of the inlet boost pressure, as a result of the combined effect of enhanced combustion, earlier combustion (shorter ignition delay) and higher heat capacity under supercharged conditions. While the effect of EGR on smoke varies with inlet boost pressure, overall the relative increase in smoke by increasing EGR was less at higher inlet boost pressure. On the other hand, the combined effect of supercharging and EGR was slightly different for different fuel delivery.

Figure 2.24c~d show the emission results as a function of fuel delivery under supercharging and EGR. Although less NO_x emissions were expected at lower fuel loads as a result of lower flame temperatures but no effect on ignition delay, the measured NO_x levels were rather higher with small fuel delivery at 20% and 40% EGR than with the large fuel delivery. On the other hand, smoke emissions increase in proportion to fuel delivery throughout the whole EGR range. Thus, the results confirm that NO_x is predominantly formed during the premixed combustion phase and the early part of the diffusion combustion period near TDC. At 0% EGR, increased fuel delivery resulted in lengthening of the diffusion combustion period but without any effect on the start of combustion. Therefore, if ignition timing is kept constant, the effect of the increased fuel on NO_x formation is not significant because the in-cylinder temperature during the later stage of the diffusion combustion period (where the additional fuel is burned) is relatively low due to the low cylinder pressure; in this case, NO_x is affected predominantly by the oxygen concentration and combustion timing. Since the exhaust gas contains less oxygen in the case of high fuel delivery ($25mm^3$/inj) than with small fuel delivery ($15mm^3$/inj), the former case leads not only to reduced oxygen concentration in the cylinder but also to further retardation of combustion, which results in lower flame temperature and lower NOx compared with the small fuel delivery.

Since smoke formation is mainly controlled by the oxygen concentration, it increases with increasing fuel delivery independent of the EGR rate. It is, however, interesting that at the lower load ($15mm^3$/inj), smoke emissions decrease with increasing EGR. The same trend appeared to be valid over the examined boost pressure and swirl ratio range (Figure 2.24b). This can probably be explained by considering that EGR results in prolonged ignition delay which allows enough time for fuel vaporisation and mixing, while the reduced oxygen

concentration seems to have a smaller influence since there may be enough oxygen for combustion of the relatively small amount of injected fuel.

As mentioned previously, all the emission results were interpreted on the basis of constant fuel delivery rather than on IMEP. The results have indicated that on the basis of constant fuel delivery, applying EGR under supercharging conditions results in only a slight increase of NOx emissions but a significant reduction in smoke emissions. Considering the significant improvements in IMEP introduced by supercharging, it can be argued that on the basis of constant IMEP, supercharging is capable of significant reduction in smoke levels but without an adverse effect on NOx emissions.

In general, the smoke levels limit the EGR rate that can be applied at each engine operating condition. However, smoke levels are much less under supercharging than under naturally aspirated conditions throughout the EGR range, and more so at 40% EGR. Therefore, higher EGR rates can in principle be applied at the same engine operating condition with inlet boost pressure, resulting in further suppression of NOx emissions while taking advantage of the power increases with supercharging. Daisho(1994) has suggested that recirculated exhaust gas must be increased to balance the NO_x increases at higher boost pressures as a result of the relatively higher oxygen concentration present in the recycled gas.

2.3.3.5 Effect of injection timing

It has been well established that advancing injection timing results in a decrease of ignition delay and an increase of the peak cylinder pressure as a result of placing combustion near TDC; this leads to an increase of NO_x levels and a decrease of smoke. Figure 2.25 presents the ignition delay, cylinder pressure and the heat release rate for different injection timings with two inlet charge conditions and three EGR rates in the four-cylinder engine. It is shown that the effects of EGR and supercharging were maintained over the whole range of injection timings tested. As expected, combustion started earlier under supercharging conditions than under naturally aspirated conditions for all injection timings; also the peak of heat release rate was lower under supercharging. There were significant reductions in ignition delay between 2° bTDC and 5° bTDC of injection timing but no further reduction at 8° bTDC.

The effective NOx and smoke emissions are plotted in Figure 2.26 against injection timing. Overall, NOx emissions increased and smoke decreased with advancing injection timing. Uchida *et al.* (1992) have reported that NO_x emission can be reduced almost in proportion to the EGR rate independent of injection timing. However, the increased rate of

NOx emissions with advancing injection timing was reduced significantly when EGR was introduced.

2.4 SUMMARY

It is well known that EGR, boost pressure and swirl are important parameters in modern direct-injection diesel engines, controlling spray development, combustion and exhaust emissions. The present results obtained in a four-cylinder and a single-cylinder optical research engines have revealed the degree to which these parameters affect engine efficiency, NO_x, and smoke emissions through changes on ignition delay, fuel quantity injected during the ignition delay period, heat absorbing capacity of inlet charge, effective compression pressure, oxygen concentration of inlet charge and charge temperature. The results of the present investigation have revealed the following;

1. Engine efficiency is predominantly affected by pumping loss, compression pressure (inlet charge mass) and combustion timing. In particular, IMEP increases with increasing inlet boost pressure depending on the timing of combustion but independent of the EGR rate.
2. NO_x emissions are affected predominantly by oxygen concentration, heat absorbing capacity of the inlet charge and timing of combustion. In particular, NO_x emissions decrease with increasing EGR but increase slightly with supercharging compared to their levels under naturally aspirated conditions.
3. Smoke levels are predominantly affected by oxygen concentration and ignition delay. In particular, smoke increases with increasing EGR, and decreases with increasing swirl ratio and, more so, with intake boost pressure.

Advanced direct-injection diesel engines are employing EGR under part-load conditions in order to reduce NO_x emissions and, in addition, low-level supercharging or turbocharging in order to overcome any loss in power output and to reduce smoke levels. It has been shown through the present investigation that the combination of EGR and supercharging can offer only advantages in that it allows a significant reduction in the NO_x levels and increase of power output while maximising the suppression of smoke emissions. In general, smoke levels which limit the EGR rate applied to each engine operating condition, are greatly reduced by supercharging compared to naturally aspirated conditions throughout the EGR range. Thus, at

each engine operating condition higher EGR rates may be applied in the presence of higher inlet boost pressure, which can lead to further reductions in NO_x emissions.

Finally, the consensus at present is that further reductions in smoke levels can be achieved in four-valve engines by using higher injection pressures in vertical injectors and a greater number of smaller nozzle holes, which combined can result in improved atomisation of the fuel spray and better fuel vaporisation without any adverse effect on ignition delay; the symmetric pattern of well-atomised multi-hole spray and the symmetric squish eliminate the need for strong induction swirl. Alternatively, the use of oxygenated fuels instead of diesel offer promise for almost elimination of particulate emissions, making possible the further reduction of NO_x levels through optimisation of a range of parameters including those examined in the present study.

Description	Specification
Displacement	1.9 litres
Bore	79.5 mm
Stroke	95.5 mm
Connecting rod length	144.0 mm
Compression ratio	19.5
Power Output	66 kW @ 4000rpm
Oil/Water temperature	85± 2 °C
Valve timing	IVO 11° CA bTDC IVC 25° CA aBDC EVO 40° CA bBDC EVC 10° CA bTDC
Geometry of the piston-bowl:	
Re-entrant diameter	37.0 mm
Maximum diameter at centre	40.8 mm
Depth	16.1 mm
Squish area	73.4 %
Fuel pump	VE Bosch pump
Injectors	5 hole x 0.184mm (diameter) x 1.0mm (length) x 150° (cone angle) opening pressure - 195 bar

Description	Test Conditions
Engine Speed	1500 rpm
Injection Timing	2°, 5° and 8° bTDC
Fuel Quantity	
Visualisation	6.0 mm^3/inj
Emissions Measurement	15.5 mm^3/inj
EGR Rates	0%, 15% and 30%
Boost Pressures	0 and 0.1 bar

Table 2.1 Geometric characteristics and operating conditions of the four-cylinder VW 1.9 L engine

Description	Specification
Bore	93.67 mm
Stroke	90.54 mm
Swept volume	0.624 litres
Connecting rod length	154.0 mm
Compression ratio	16.75
Cold piston to head clearance	1.2 mm
Oil/Water temperature	85± 2 °C
Valve timing	IVO 13° CA bTDC IVC 219° CA aTDC EVO 231° CA aTDC EVC 13° CA bTDC
Piston bowl	Cylindrical
Diameter	46.4 mm
Depth	16.1 mm
Fuel pump	Lucas EUI
Injectors	4 hole x 0.2mm (diameter) x 150° (cone angle) opening pressure - 250 bar VCO nozzle

Description	Tests Conditions
Engine Speed	1200rpm
Swirl Ratio	1.6, 2.2 and 3.0
Fuel Quantity	15, 20 and 25mm^3/inj
EGR Rates	0%, 20% and 40%
Boost Pressures	0, 0.3, 0.4 and 0.5 bar

Table 2.2 Geometric characteristics and operating conditions of the single-cylinder Hydra engine

Four-cylinder engine

Unit : kg/hr

	0% EGR	15% EGR	30% EGR
NA	84.9	72.2	59.3
0.1 bar	97.2	82.6	68.0

Single-cylinder engine

Unit : kg/hr

	0% EGR	20% EGR	40% EGR
NA	24.1	19.8	14.4
0.3 bar	31.7	26.3	19.1
0.4 bar	34.9	27.7	20.5
0.5 bar	40.3	32.0	24.5

Table 2.3 Intake mass flow rate of air

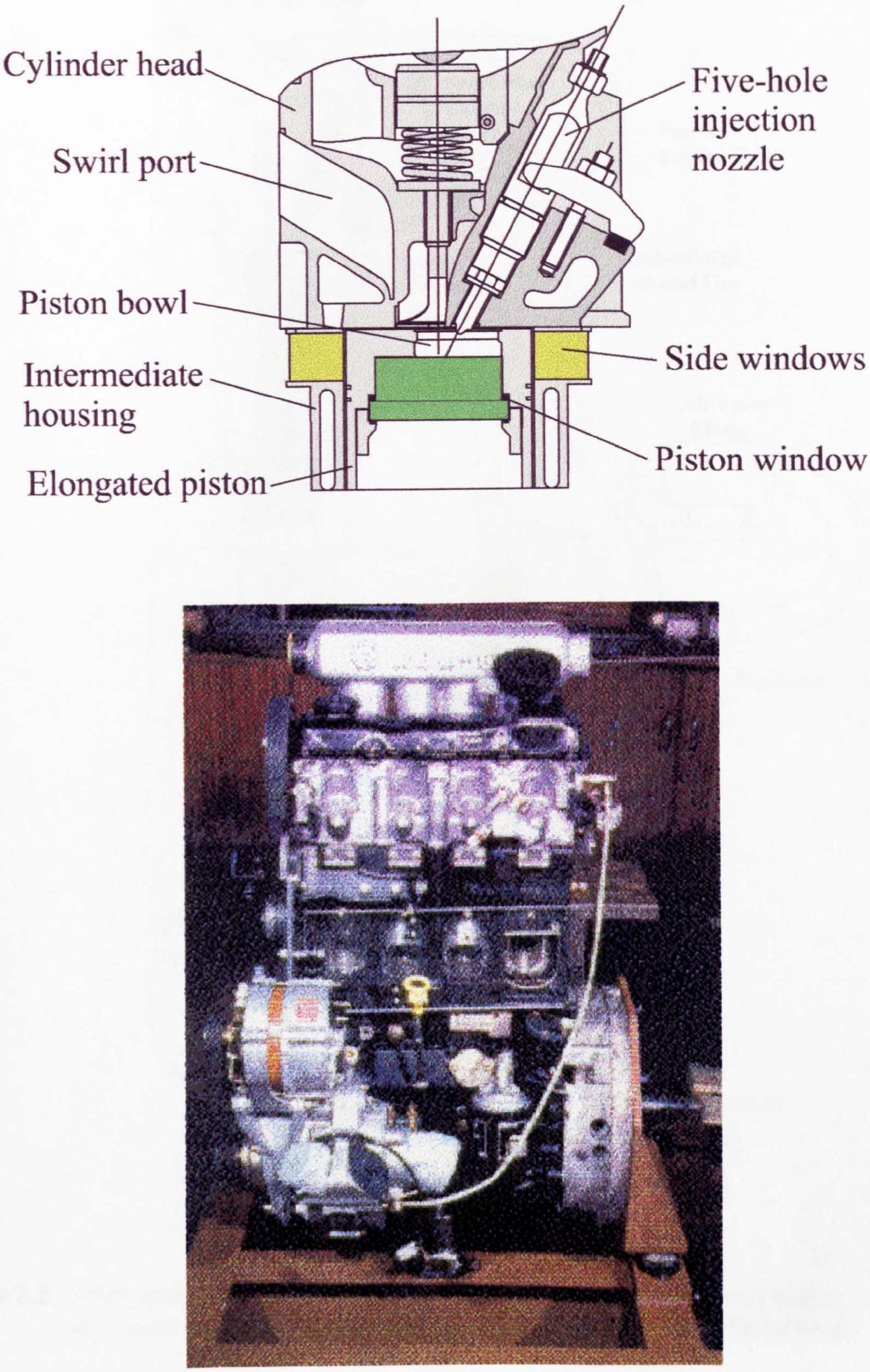
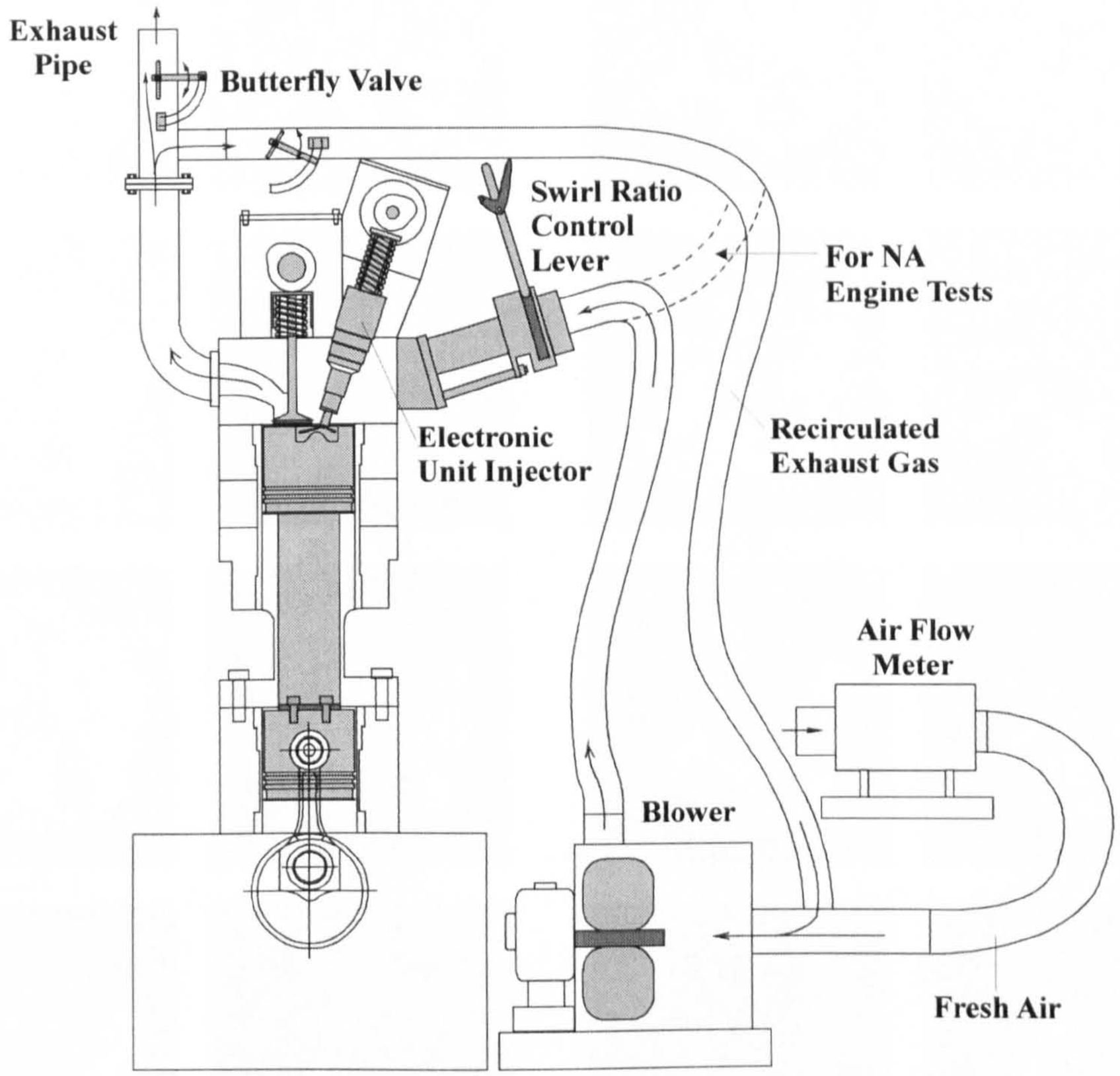


Figure 2.1 Schematic and photograph of the VW 1.9L four-cylinder HSDI diesel engine



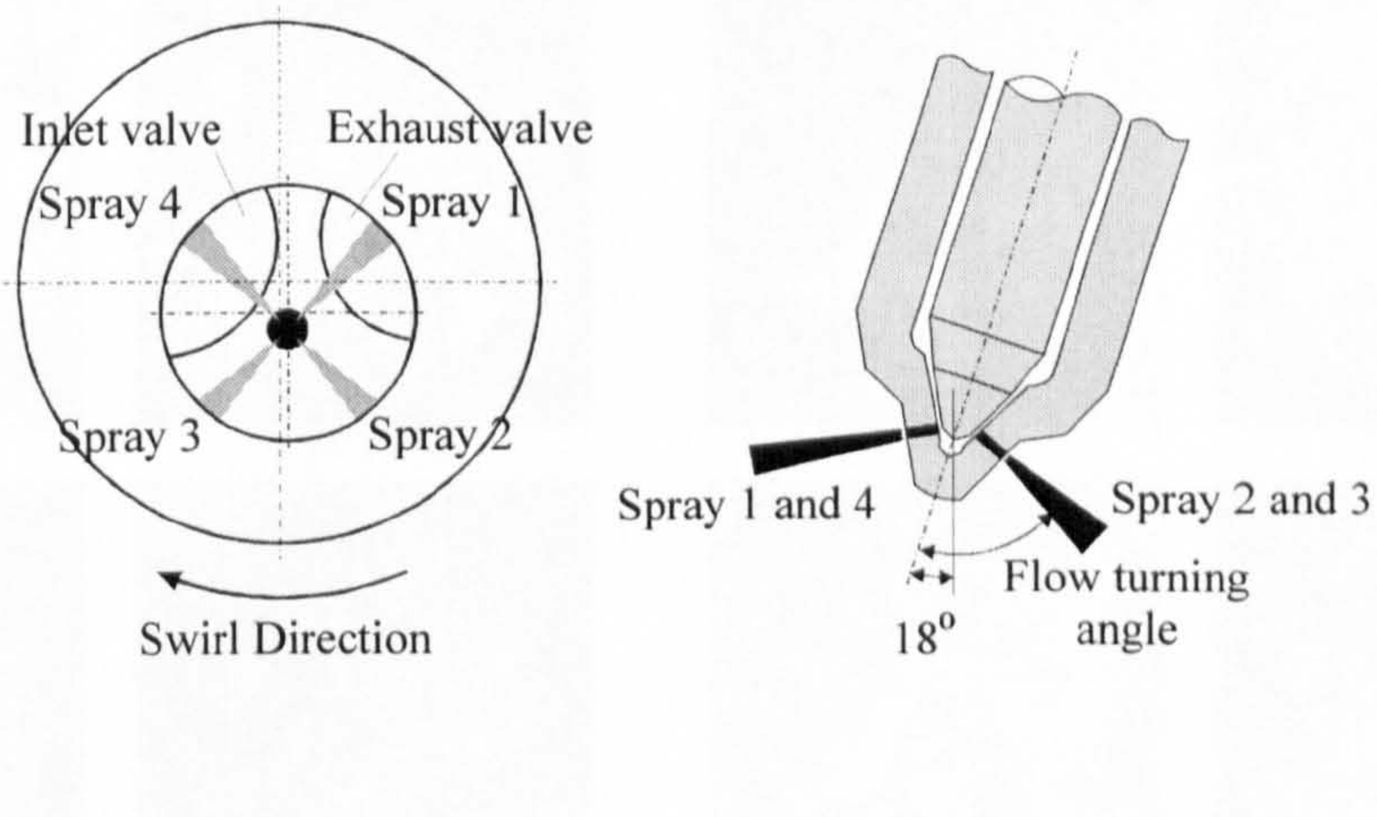


Figure 2.2 Schematic of the supercharged Ricardo single-cylinder DI diesel engine incorporating EGR and the orientation of the sprays in the cylinder head

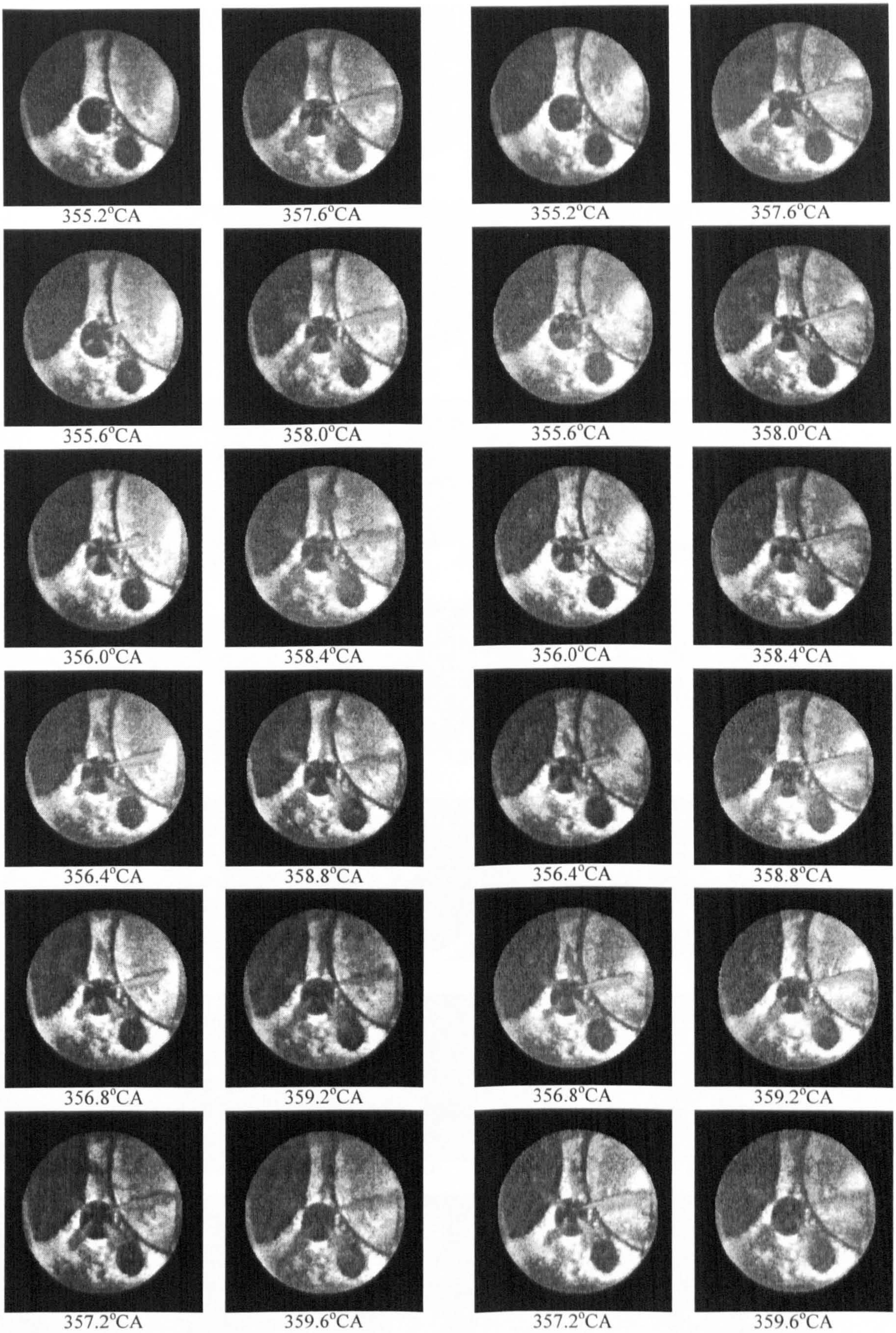


Figure 2.3 Comparison of spray images for different intake air charge conditions with 0% EGR rate at 5°bTDC; four-cylinder engine

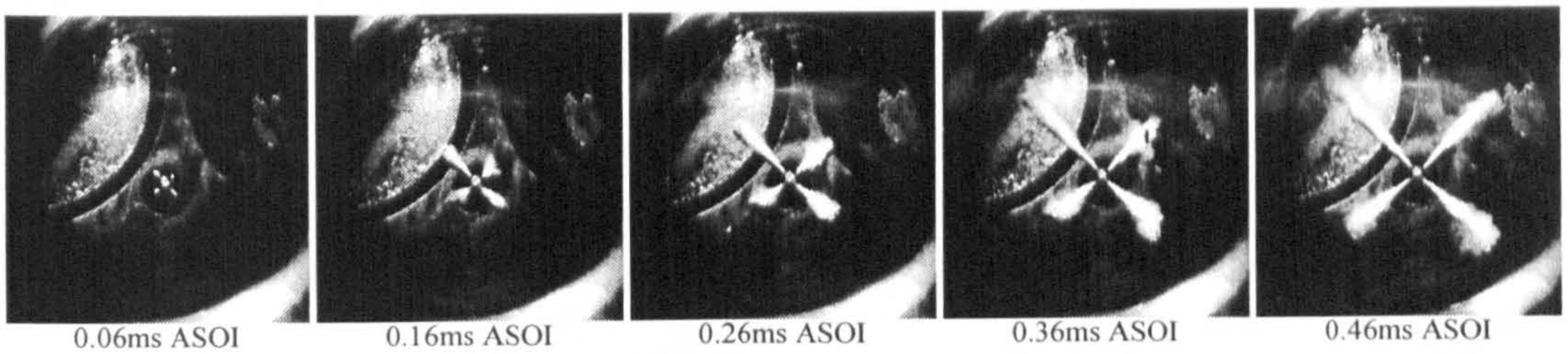
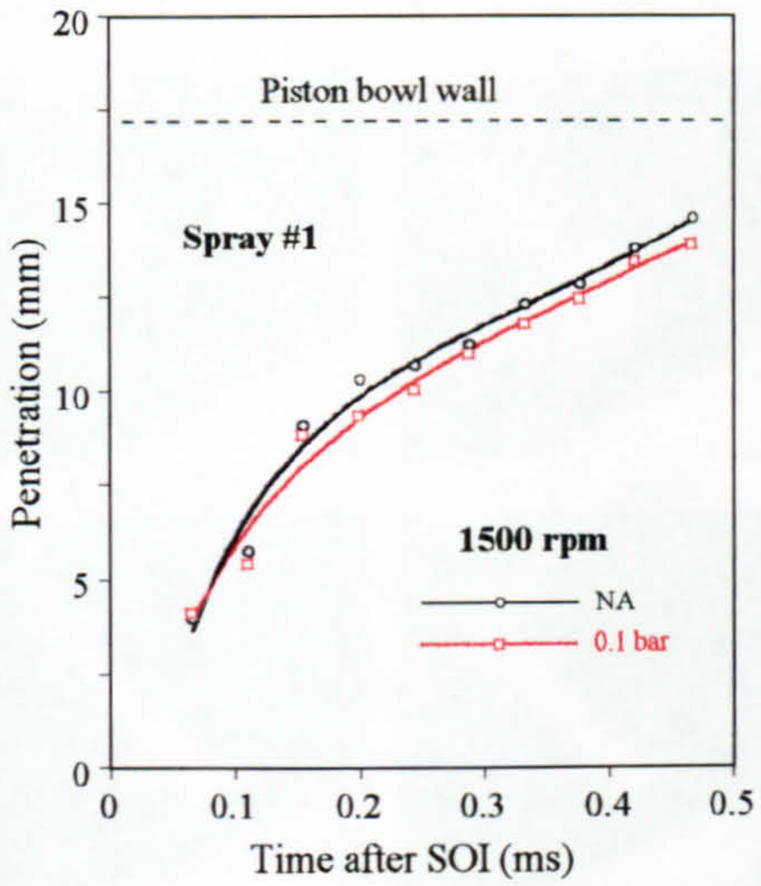
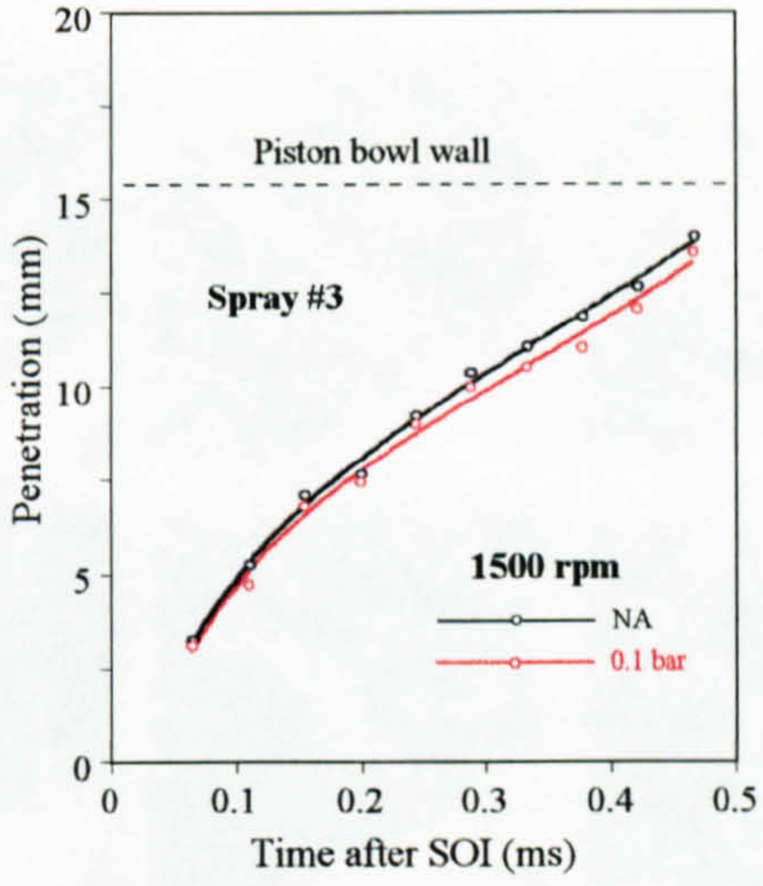


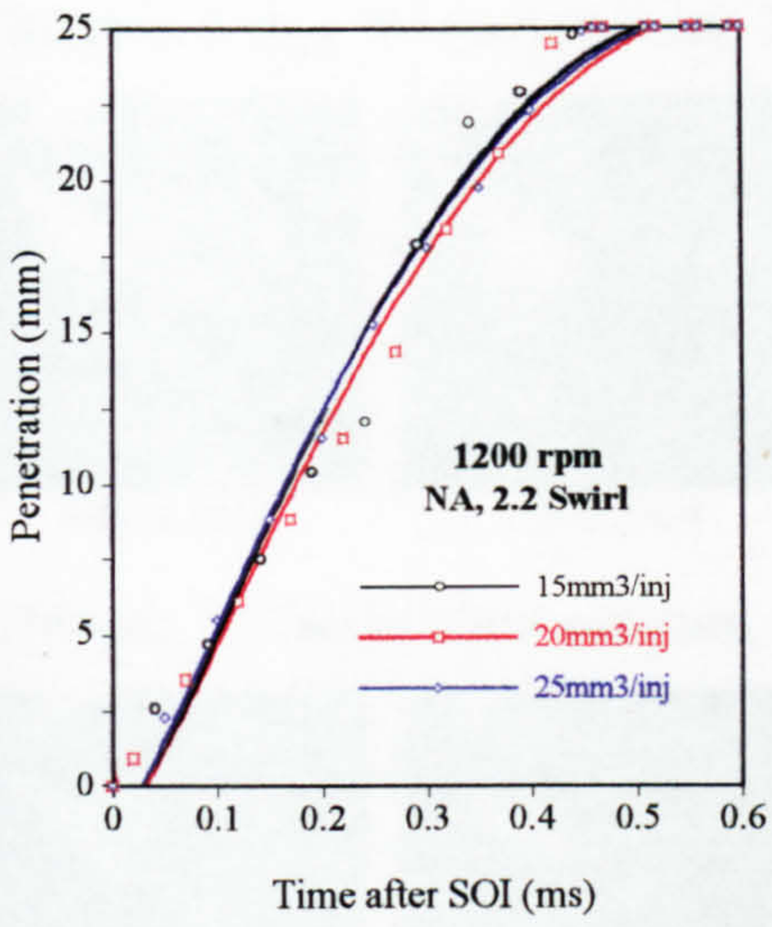
Figure 2.4 Spray tip development at various engine operating conditions; single-cylinder engine



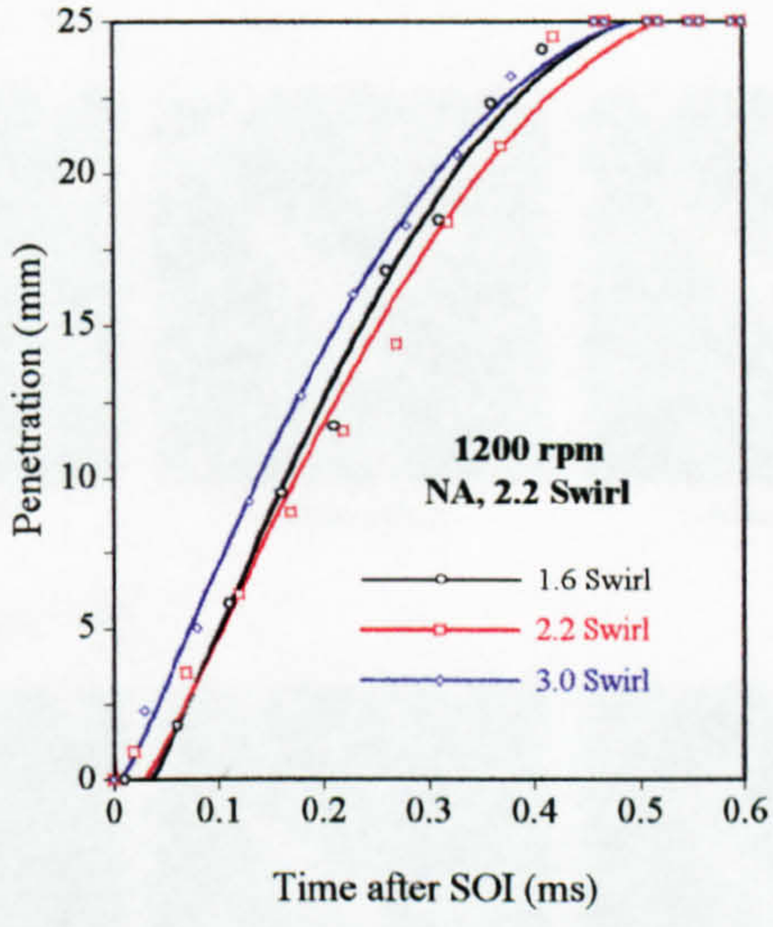
(a)



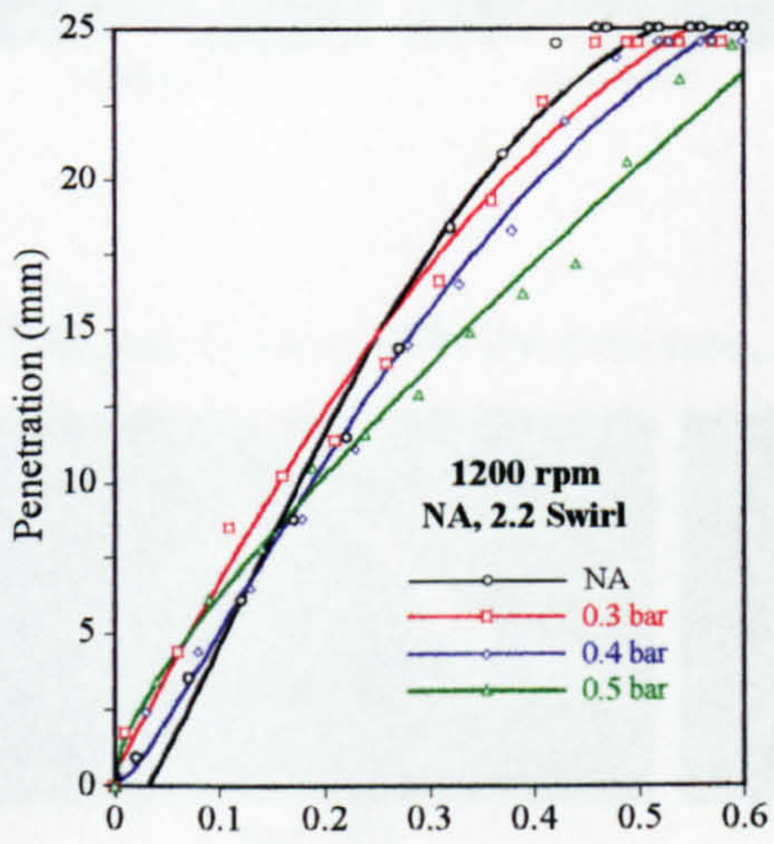
(b)



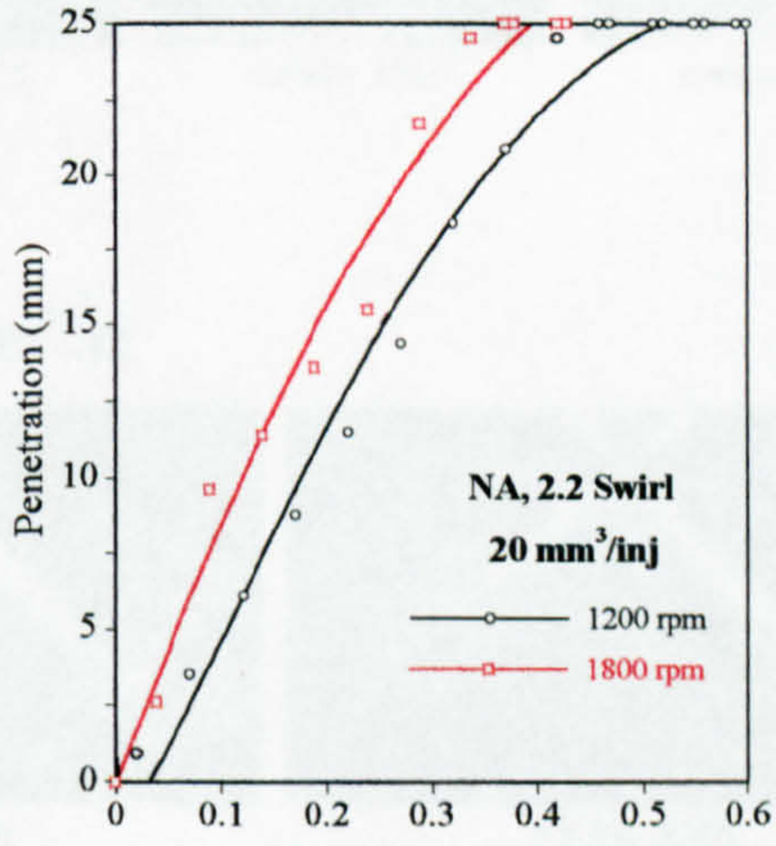
(c)



(d)



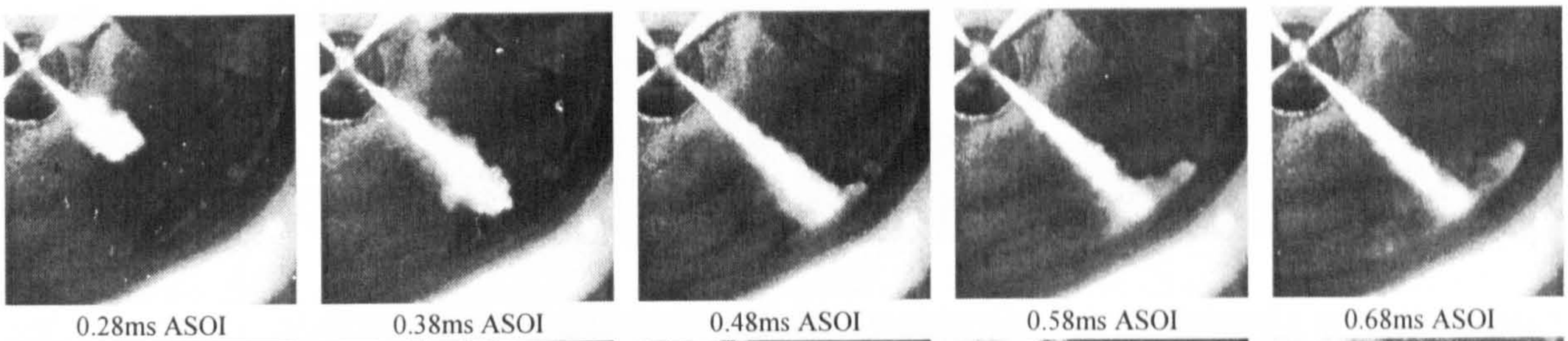
(e)



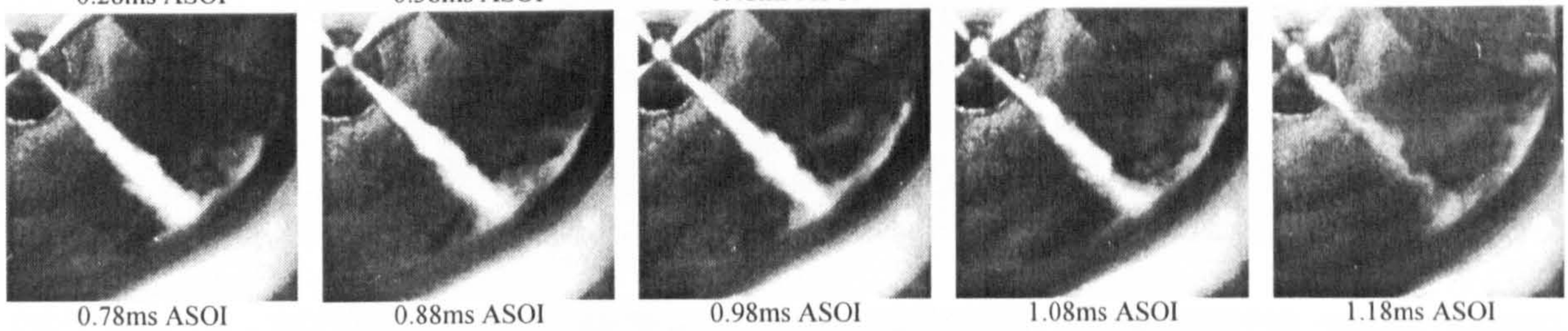
(f)

Figure 2.5 Spray tip penetration at different engine operating conditions
(a) (b) : four-cylinder engine, (c) - (f) : single cylinder engine

1200rpm, NA, 2.2 swirl, 20mm^3/inj

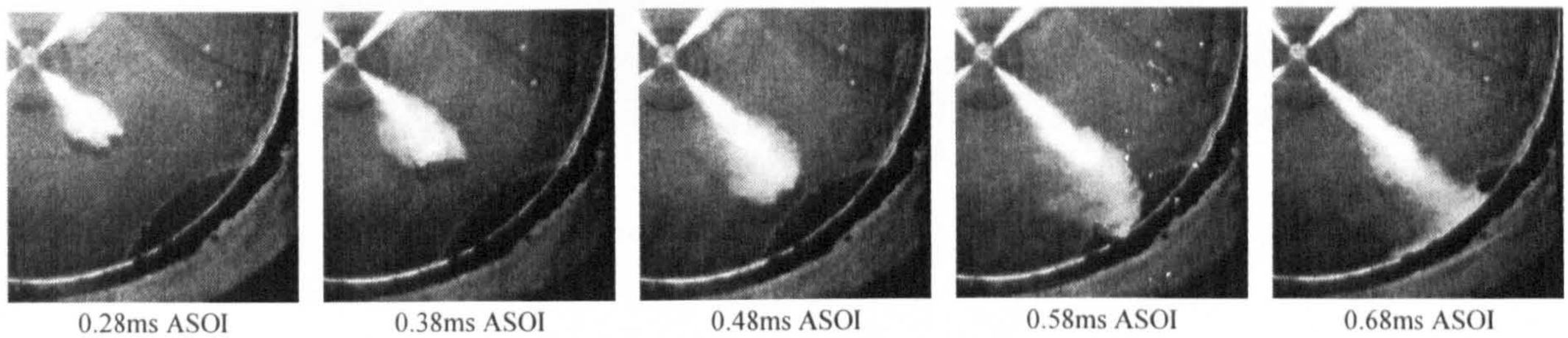


0.28ms ASOI 0.38ms ASOI 0.48ms ASOI 0.58ms ASOI 0.68ms ASOI



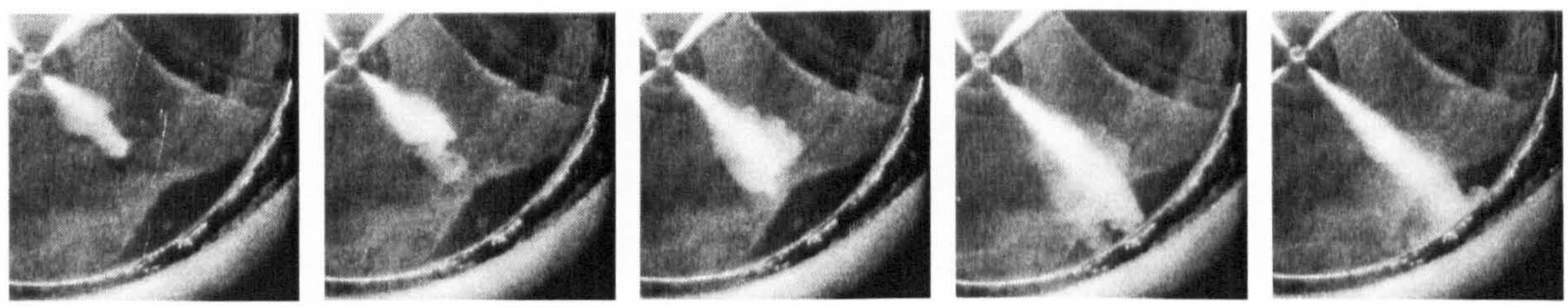
0.78ms ASOI 0.88ms ASOI 0.98ms ASOI 1.08ms ASOI 1.18ms ASOI

1200rpm, 0.4bar of boost pressure, 2.2 swirl, 20mm^3/inj



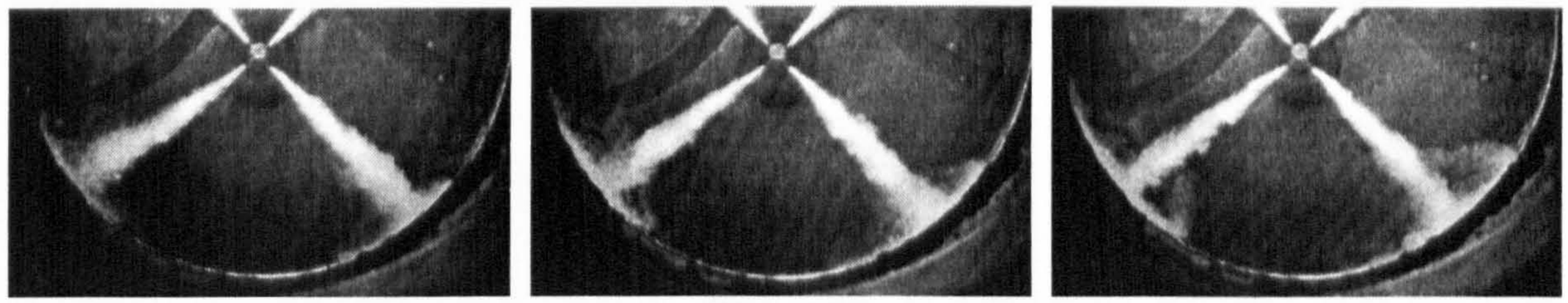
0.28ms ASOI 0.38ms ASOI 0.48ms ASOI 0.58ms ASOI 0.68ms ASOI

1200rpm, 0.5 bar of boost pressure, 2.2 swirl, 20mm^3/inj



0.28ms ASOI 0.38ms ASOI 0.48ms ASOI 0.58ms ASOI 0.68ms ASOI

1200rpm, 0.4 bar of boost pressure, 2.2 swirl, 20mm^3/inj



0.73ms ASOI 0.83ms ASOI 0.93ms ASOI

Figure 2.6 Drum camera sequence of a complete cycle of sprays #2 & #3 at 1200rpm engine speed, 20mm^3/inj. and swirl ratio of 2.2 with various boost pressures; single-cylinder engine

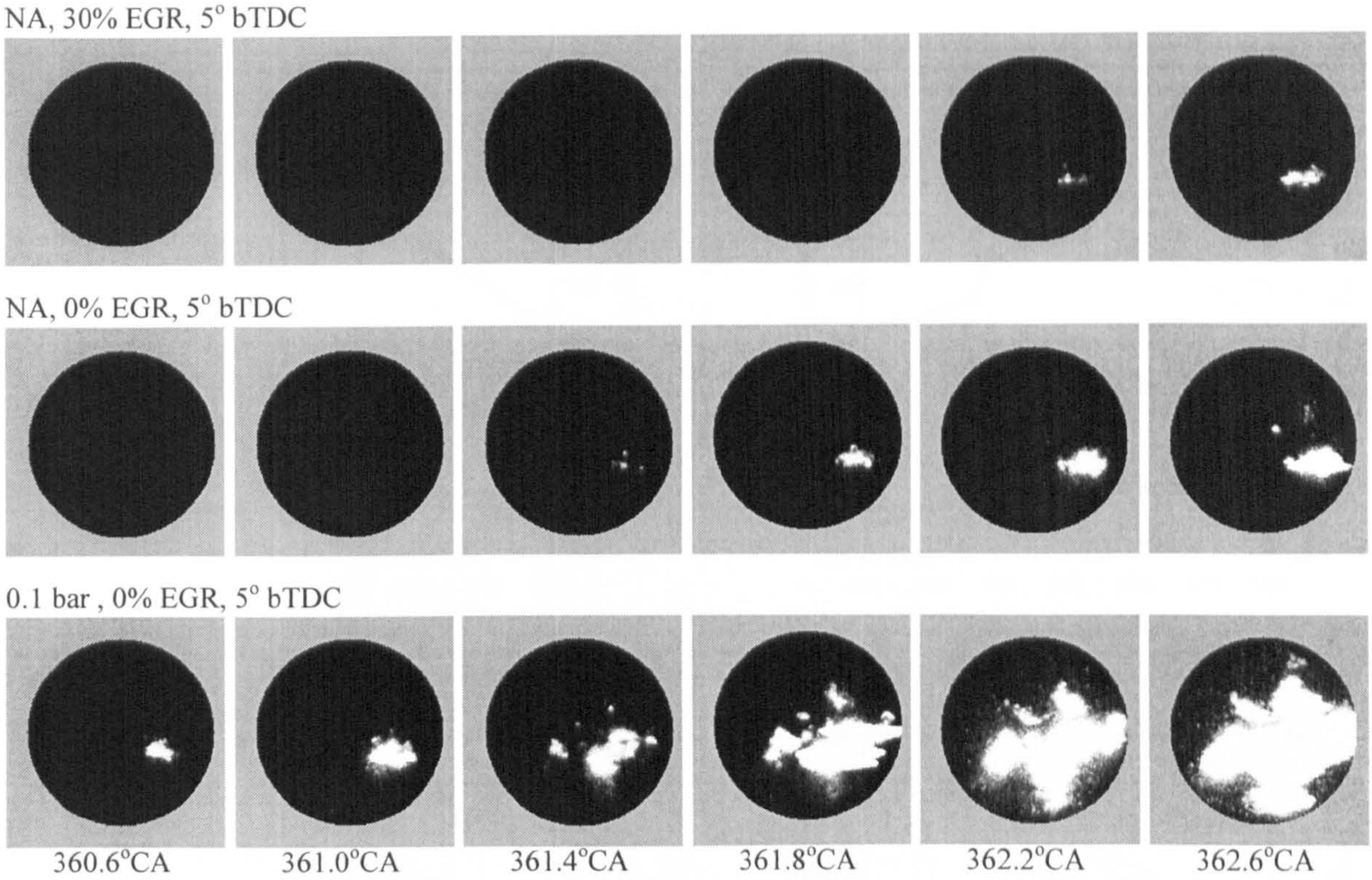


Figure 2.7 Auto-ignition for various engine operating conditions in the four-cylinder engine

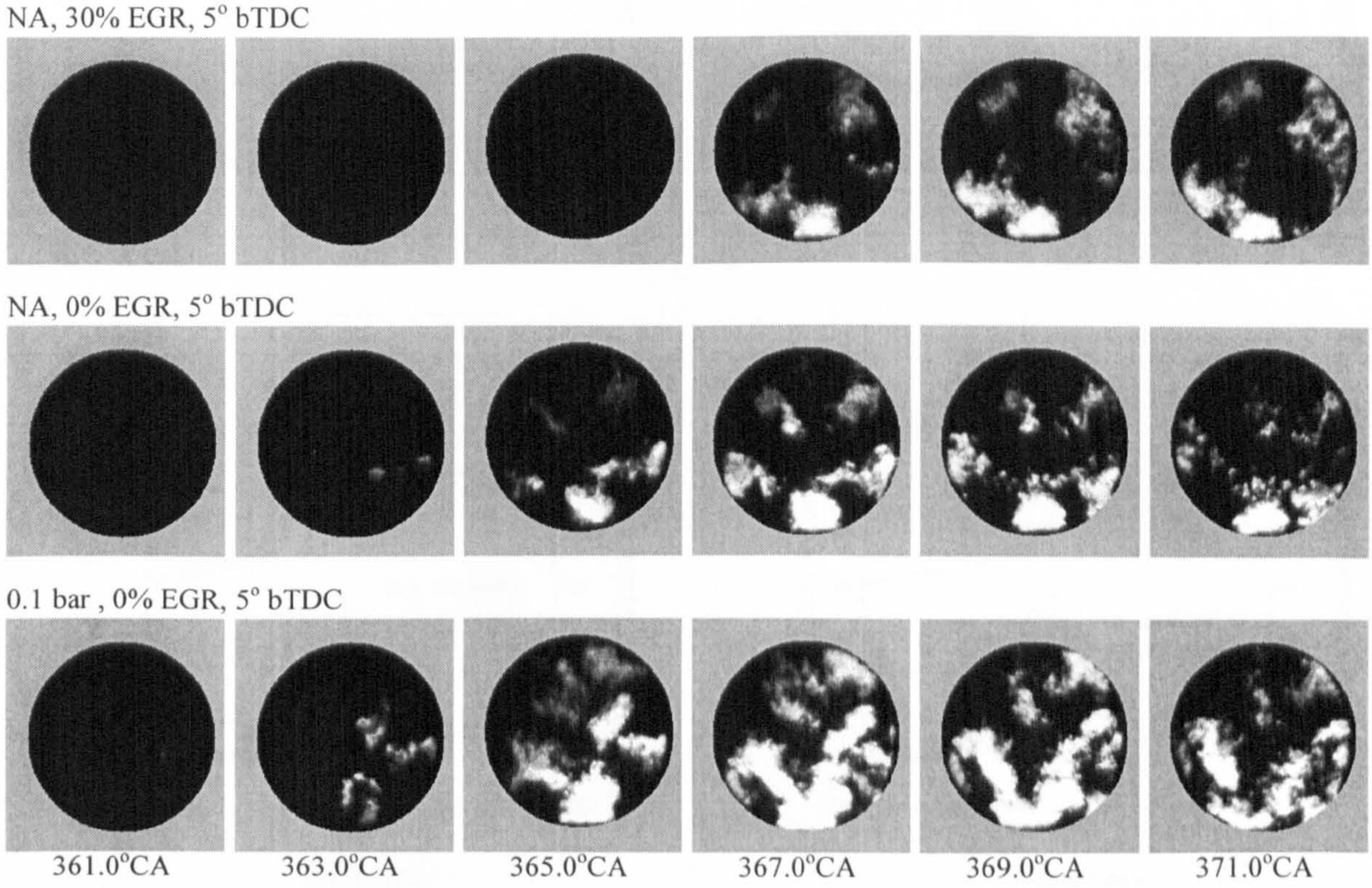


Figure 2.8 Flame development for various engine operating conditions in the four-cylinder engine

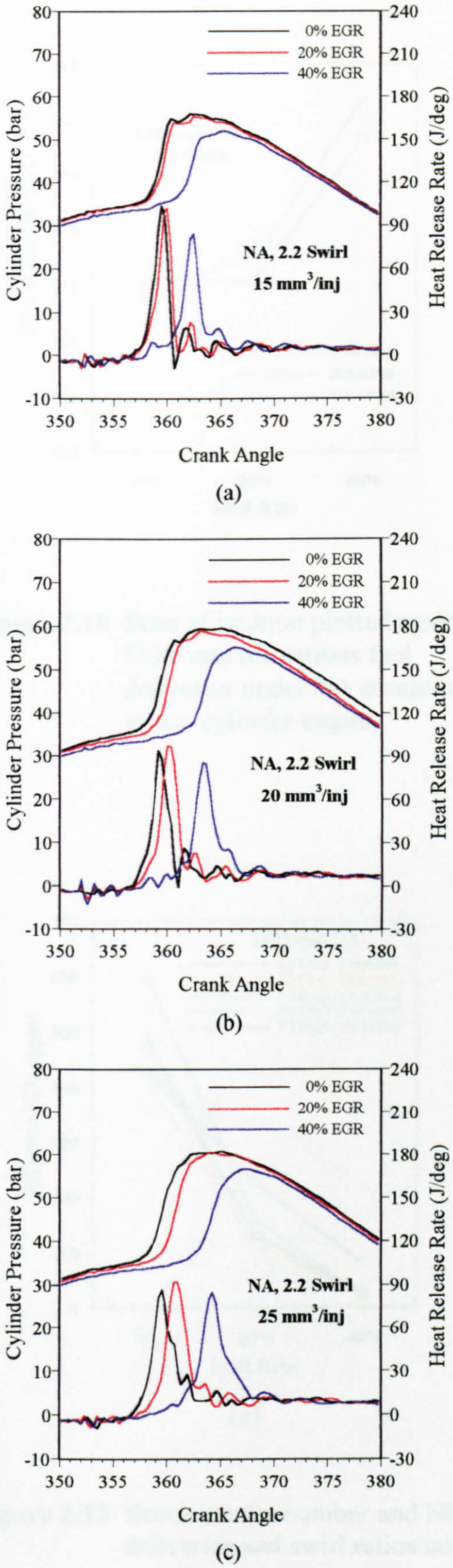


Figure 2.9 Cylinder pressure and heat release rate curves at engine speed of 1200rpm at various EGR rate and fuel delivery; single-cylinder engine

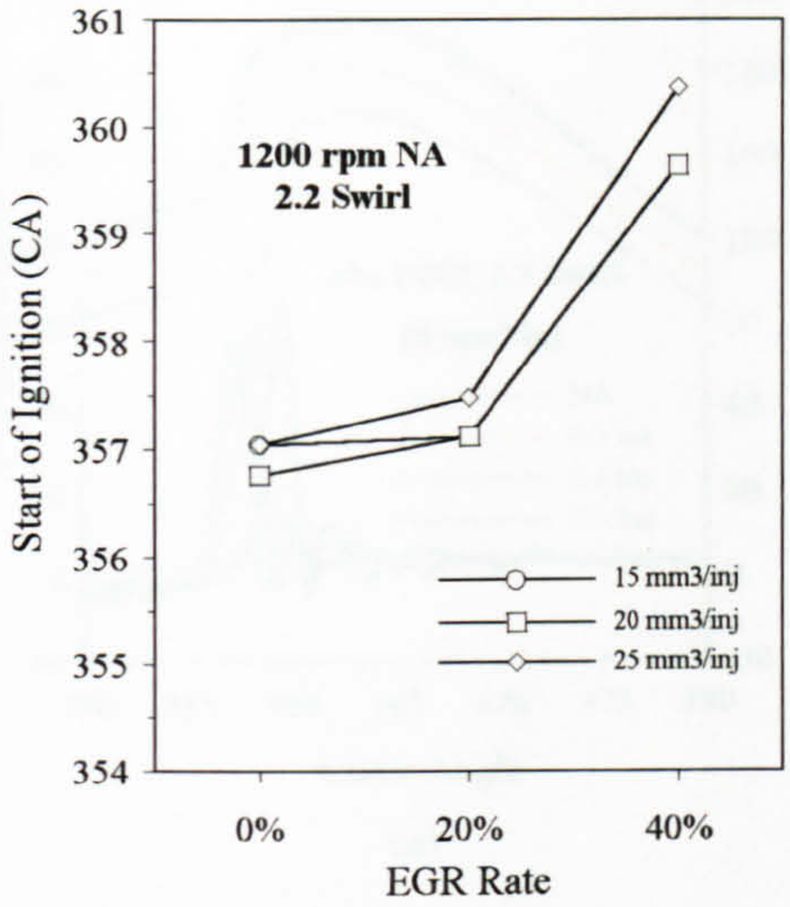


Figure 2.10 Start of ignition plotted against EGR rate for various fuel deliveries under NA conditions; single-cylinder engine

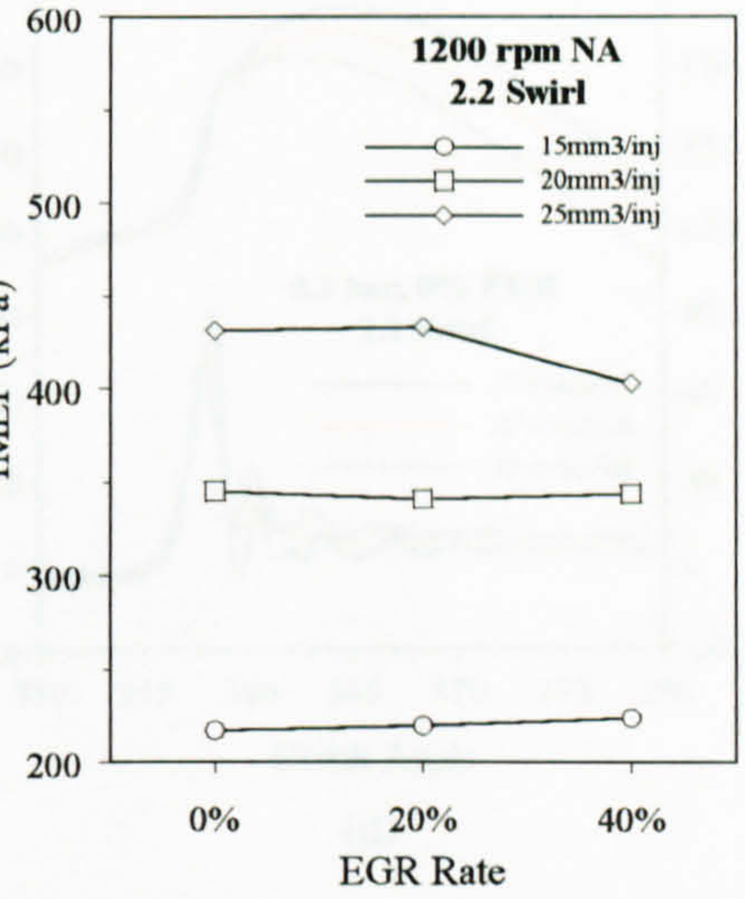
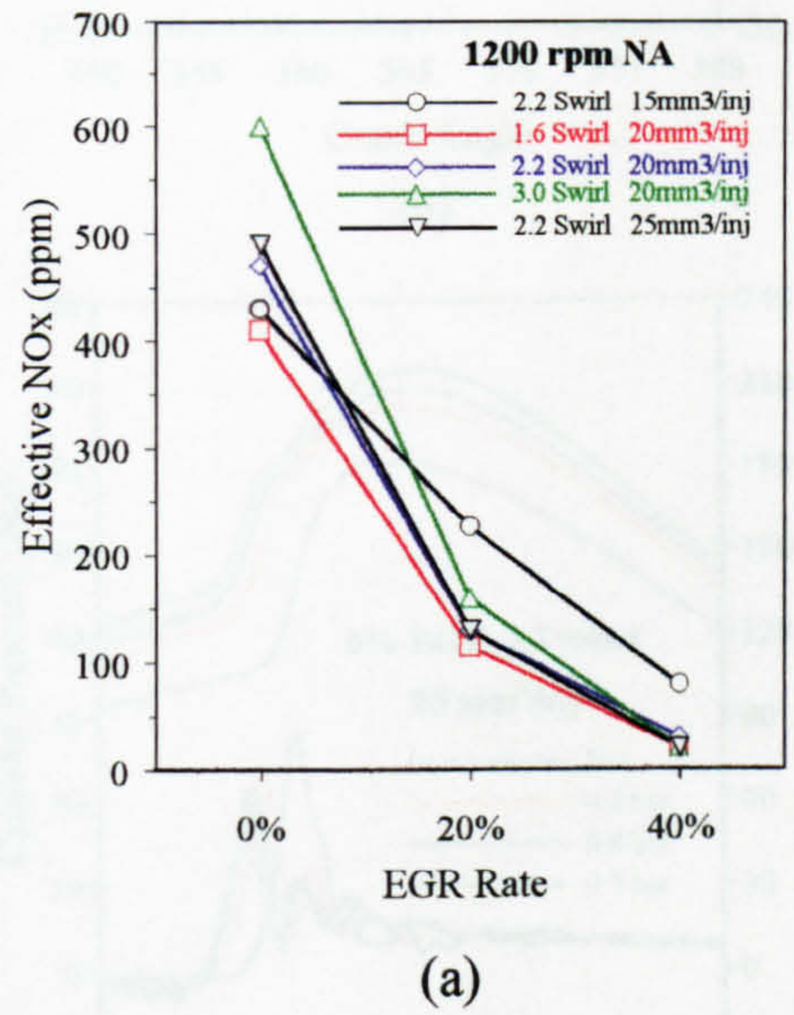


Figure 2.11 IMEP plotted against EGR rate for various fuel deliveries under NA conditions; single-cylinder engine



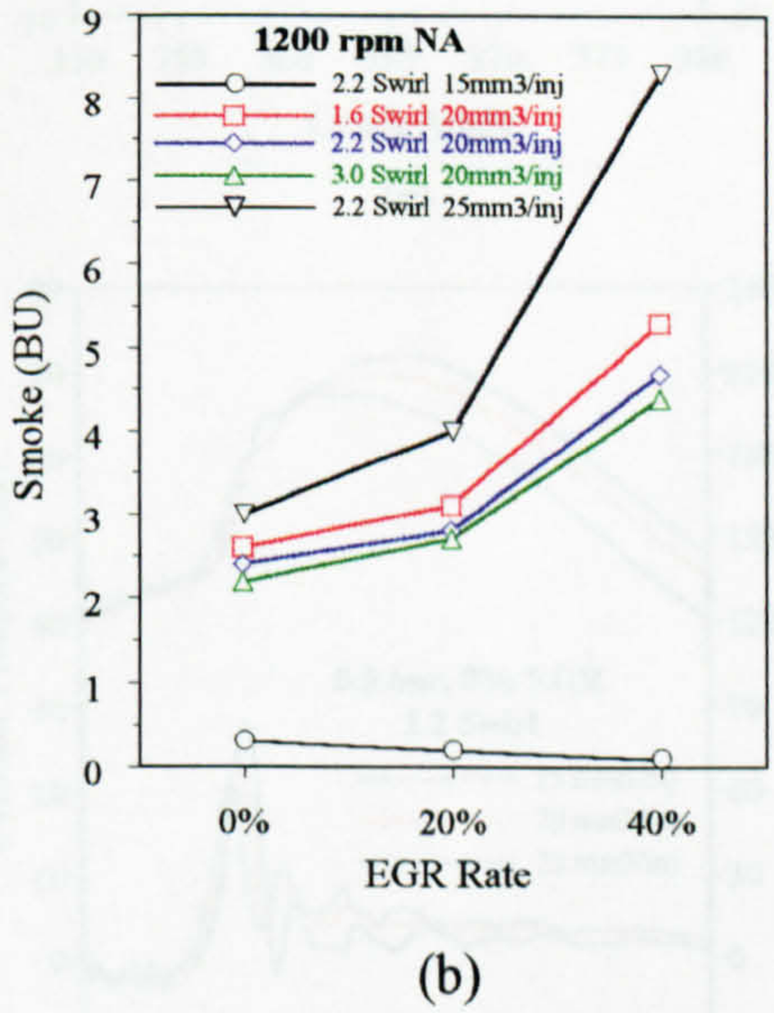


Figure 2.12 Bosch smoke number and NO_x concentrations plotted against EGR rate for fuel deliveries and swirl ratios under NA conditions; single-cylinder engine

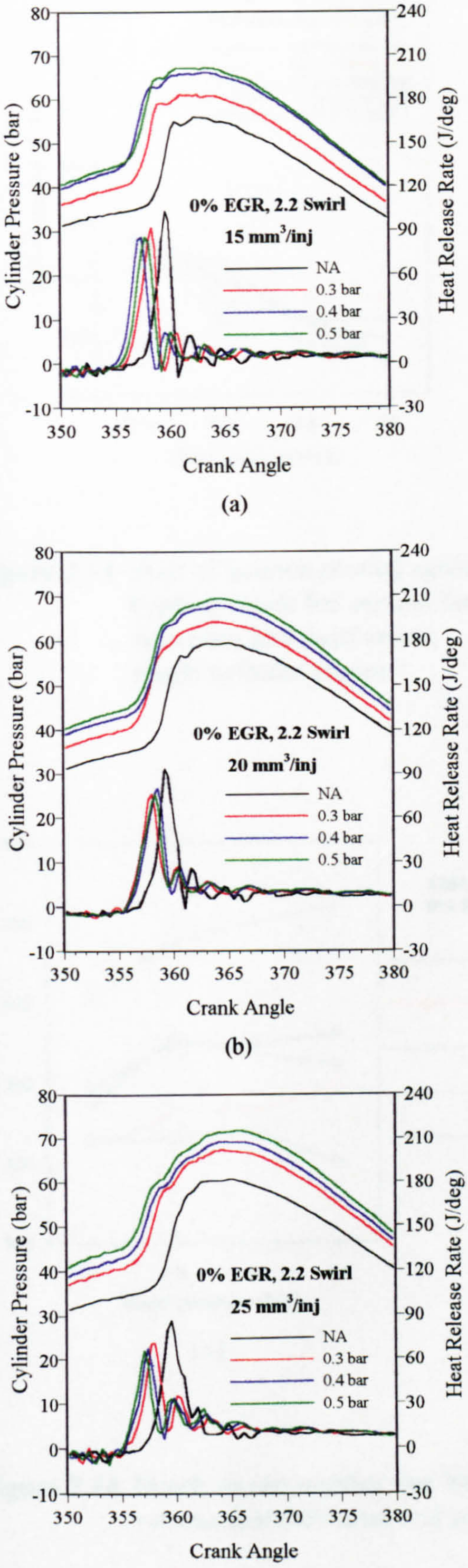


Figure 2.13 Cylinder pressure and heat release rate curves at engine speed of 1200rpm and at various boost pressures and fuel deliveries; single-cylinder engine

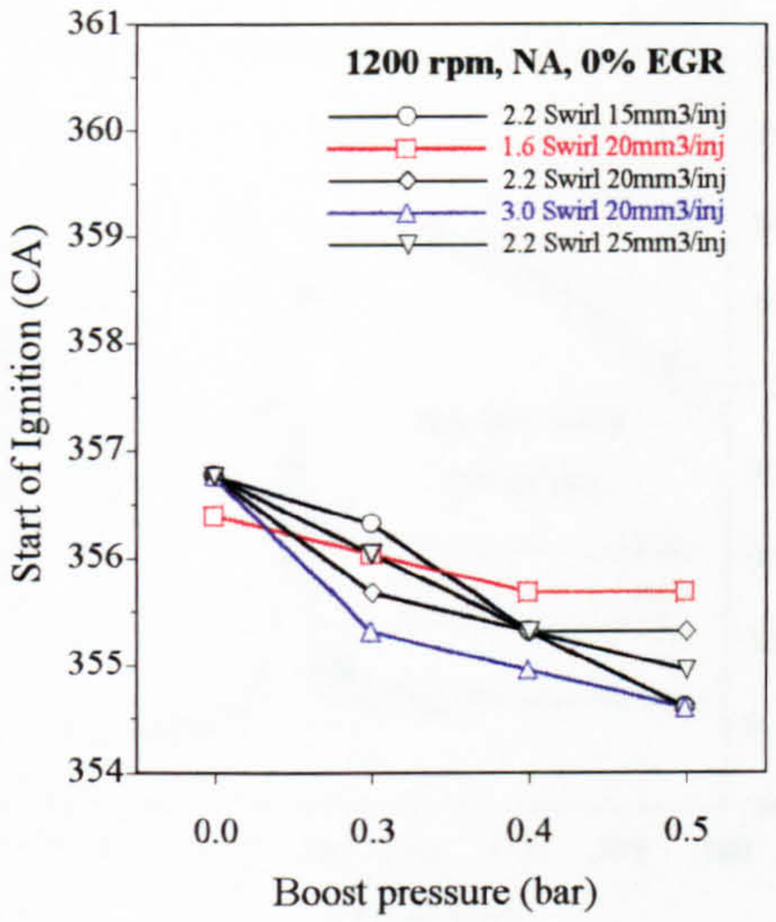


Figure 2.14 Start of ignition plotted against boost pressure for various fuel deliveries and swirl ratios; single-cylinder engine

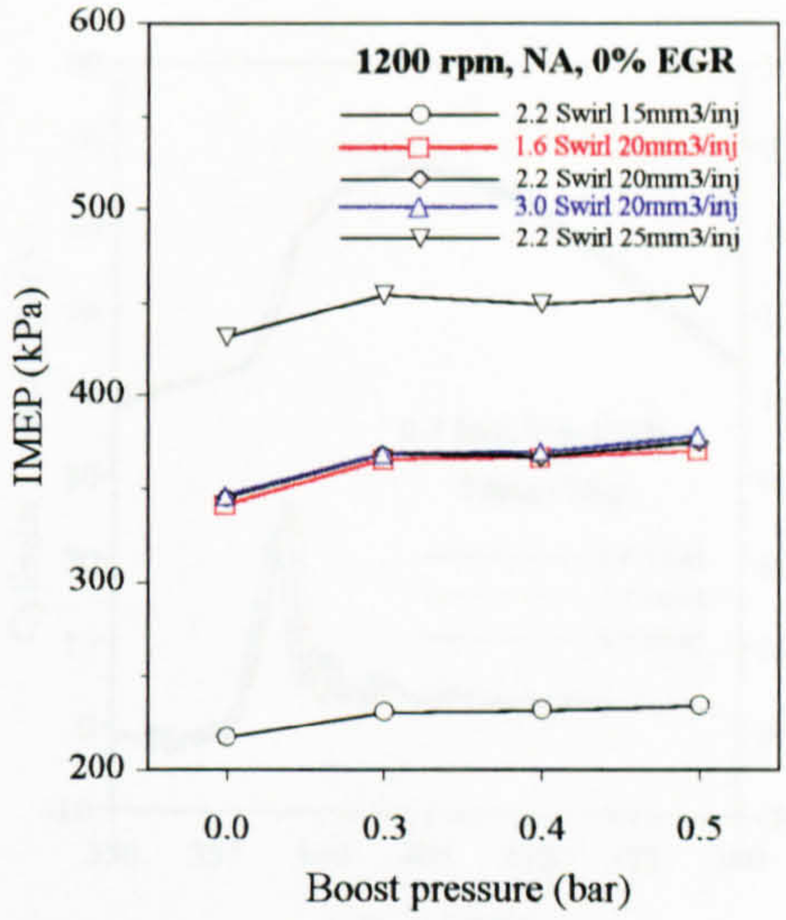


Figure 2.15 IMEP plotted against boost pressure for various fuel deliveries and swirl ratios; single-cylinder engine

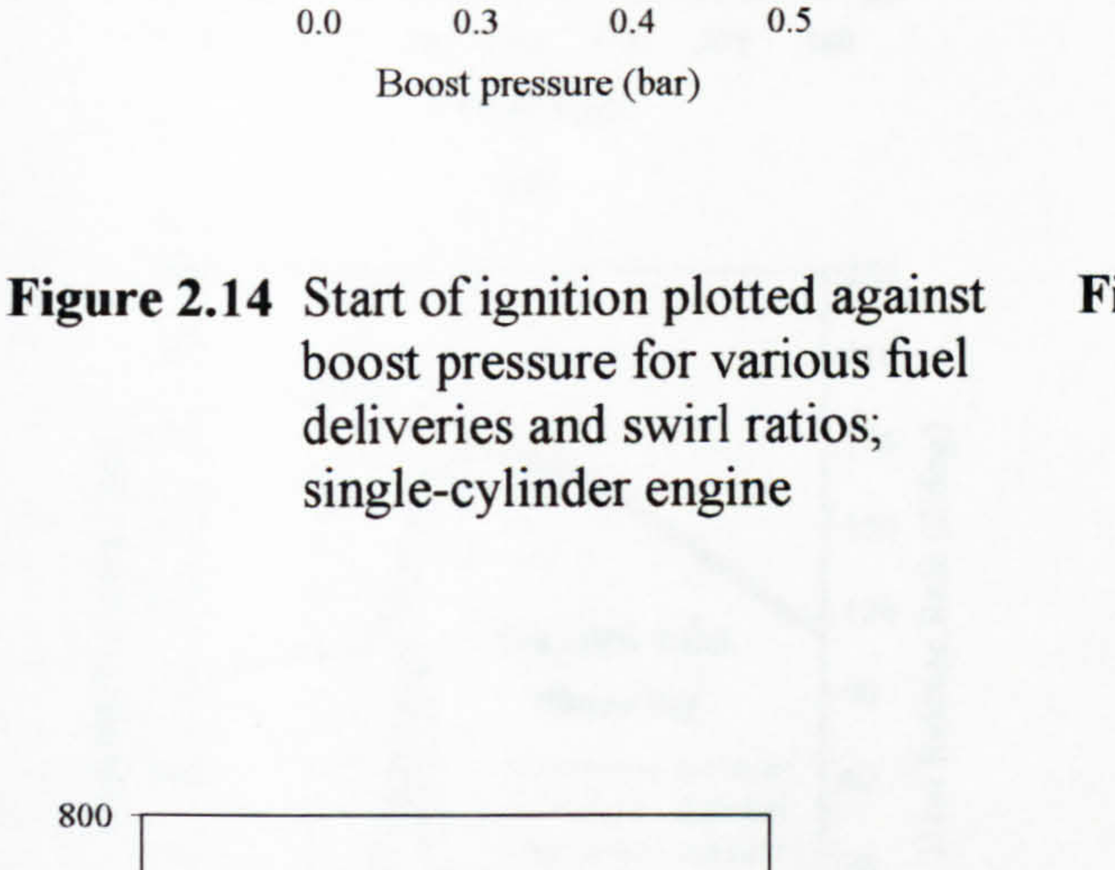


Figure 2.16 Bosch smoke number and NO_x concentrations plotted against boost pressure for various fuel deliveries and swirl ratios; single-cylinder engine

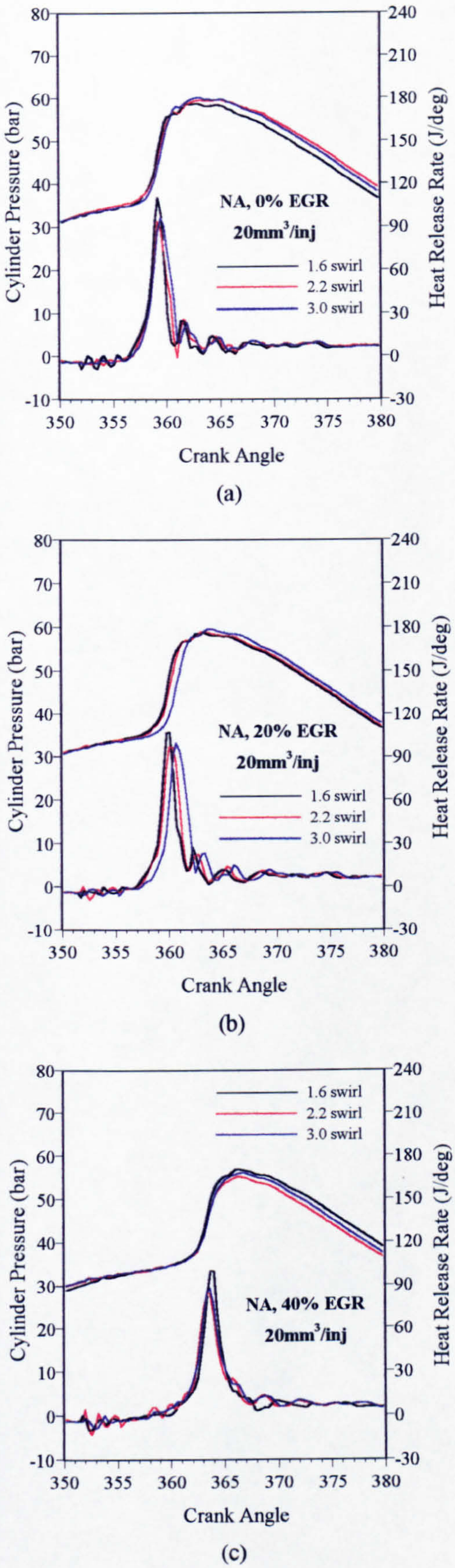


Figure 2.17 Cylinder pressure and heat release rate curves at engine speed of 1200rpm for various swirl ratios; single-cylinder engine

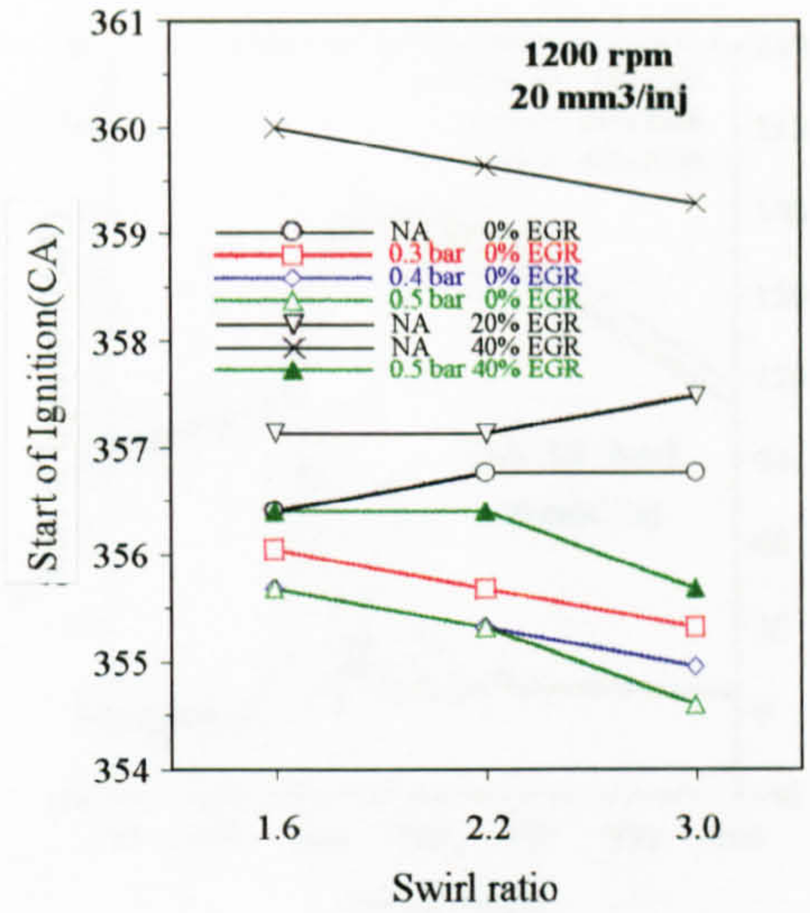


Figure 2.18 Start of ignition plotted against swirl ratio for various EGR rates and boost pressures; single-cylinder engine

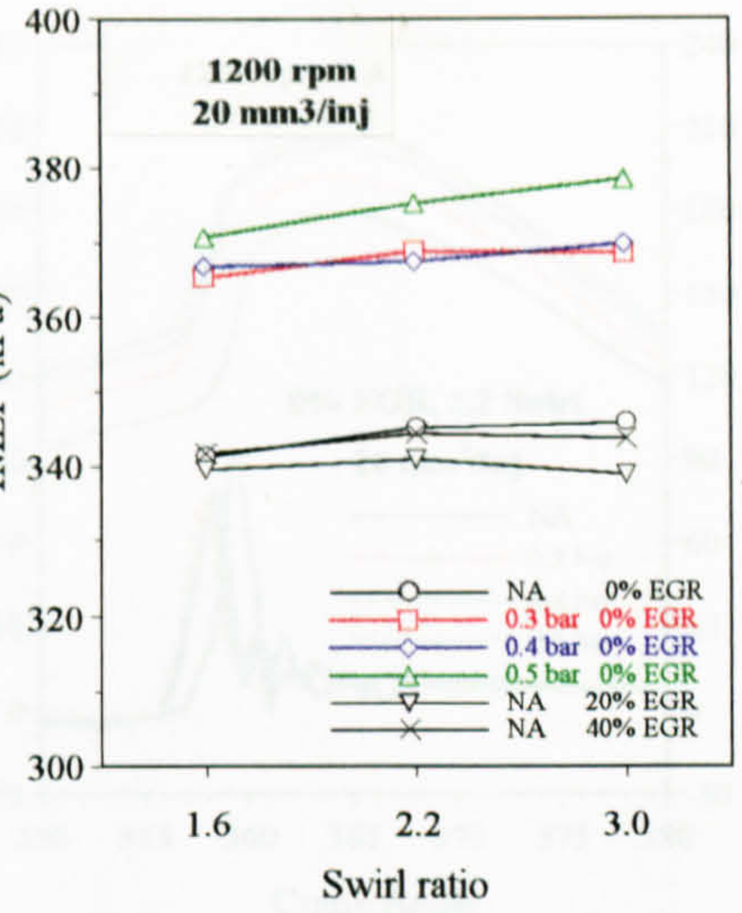
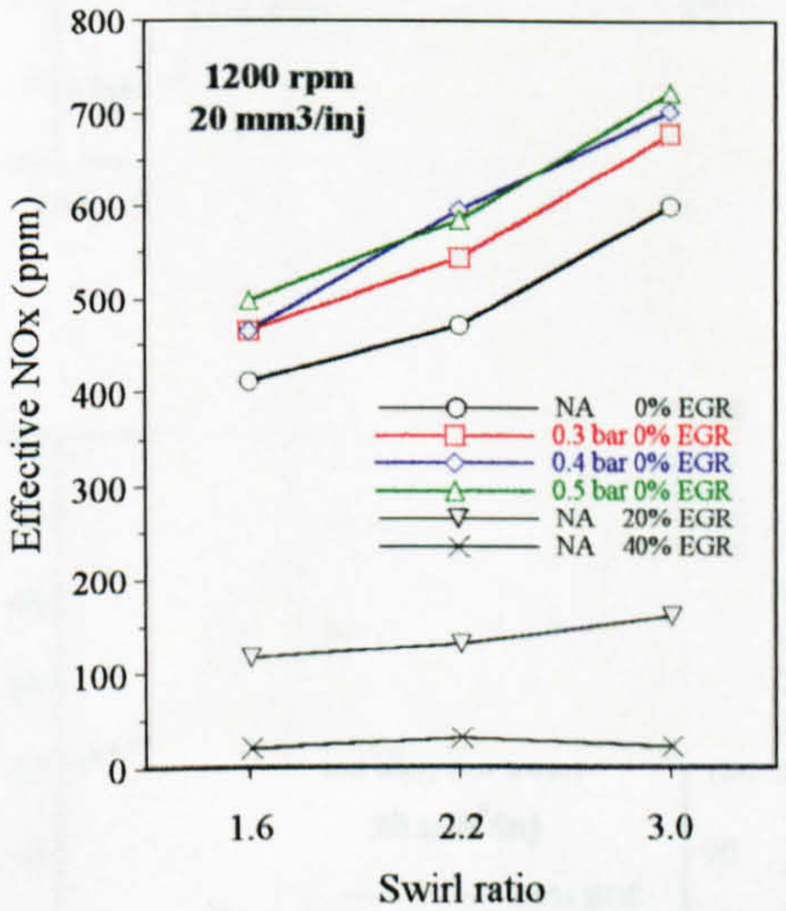


Figure 2.19 IMEP plotted against swirl ratio for various EGR rates and boost pressures; single-cylinder engine



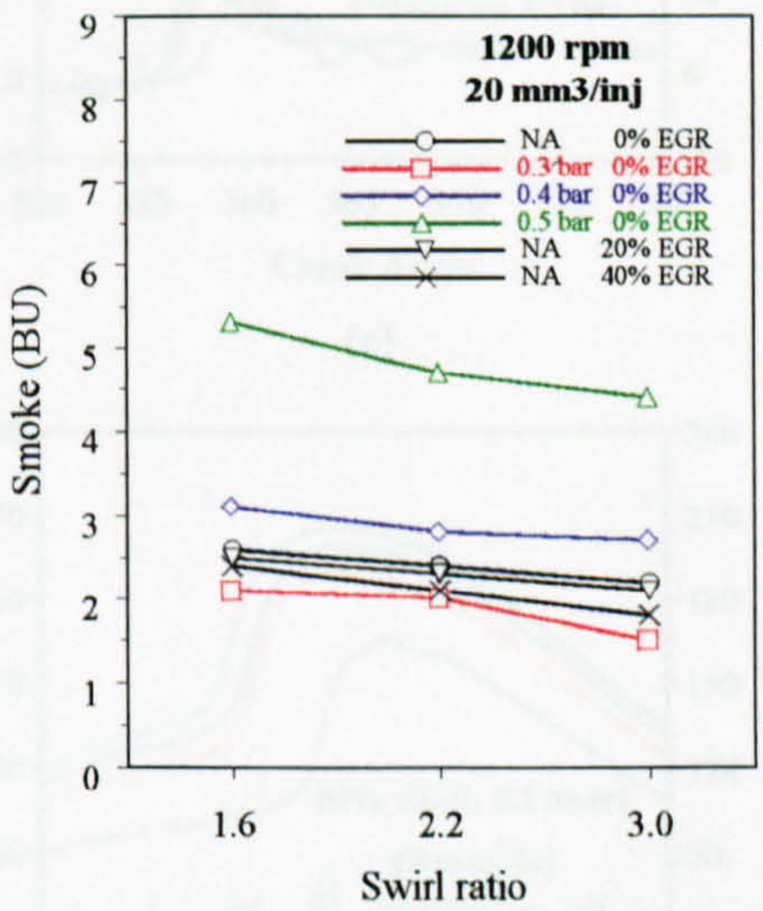


Figure 2.20 Bosch smoke number and NO_x concentrations plotted against swirl ratio for various EGR rates and boost pressures; single-cylinder engine

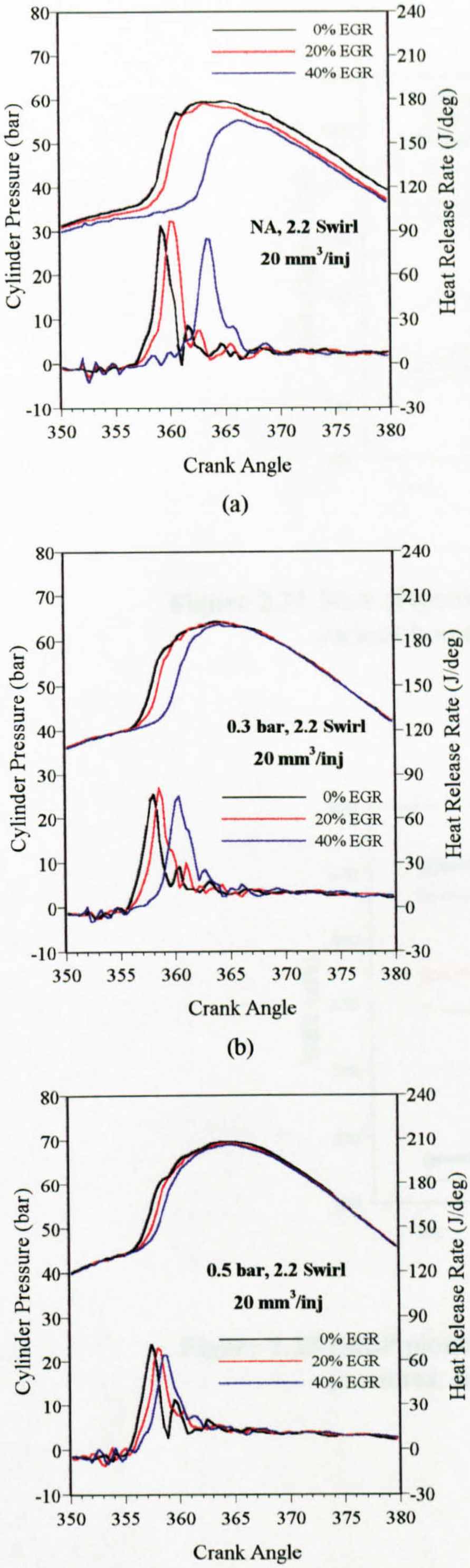


Figure 2.21 Cylinder pressure and heat release rate curves at engine speed of 1200rpm at various EGR rates and boost pressures; single-cylinder engine

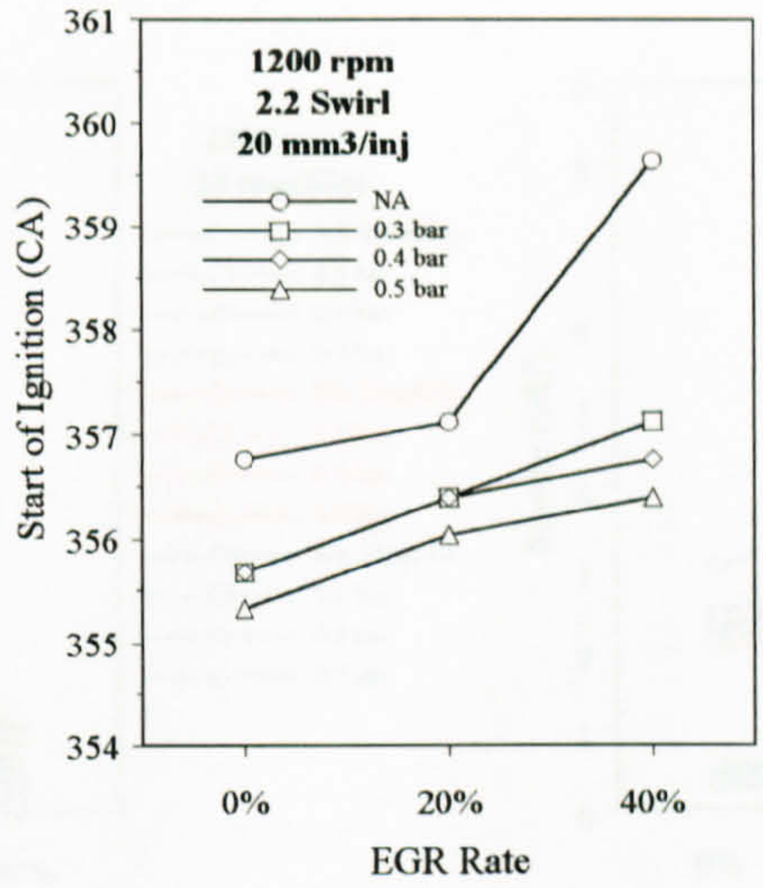


Figure 2.22 Start of ignition plotted against EGR rate for various boost pressures; single-cylinder engine

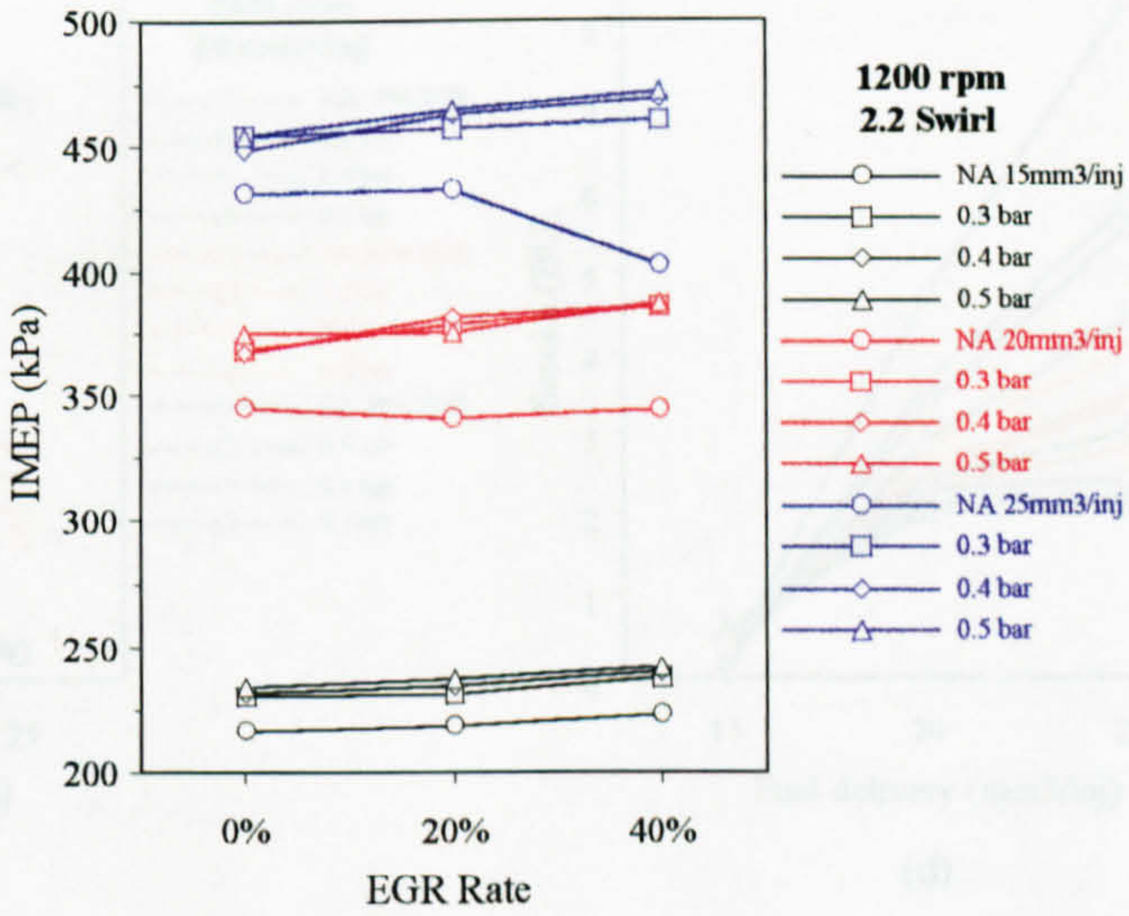
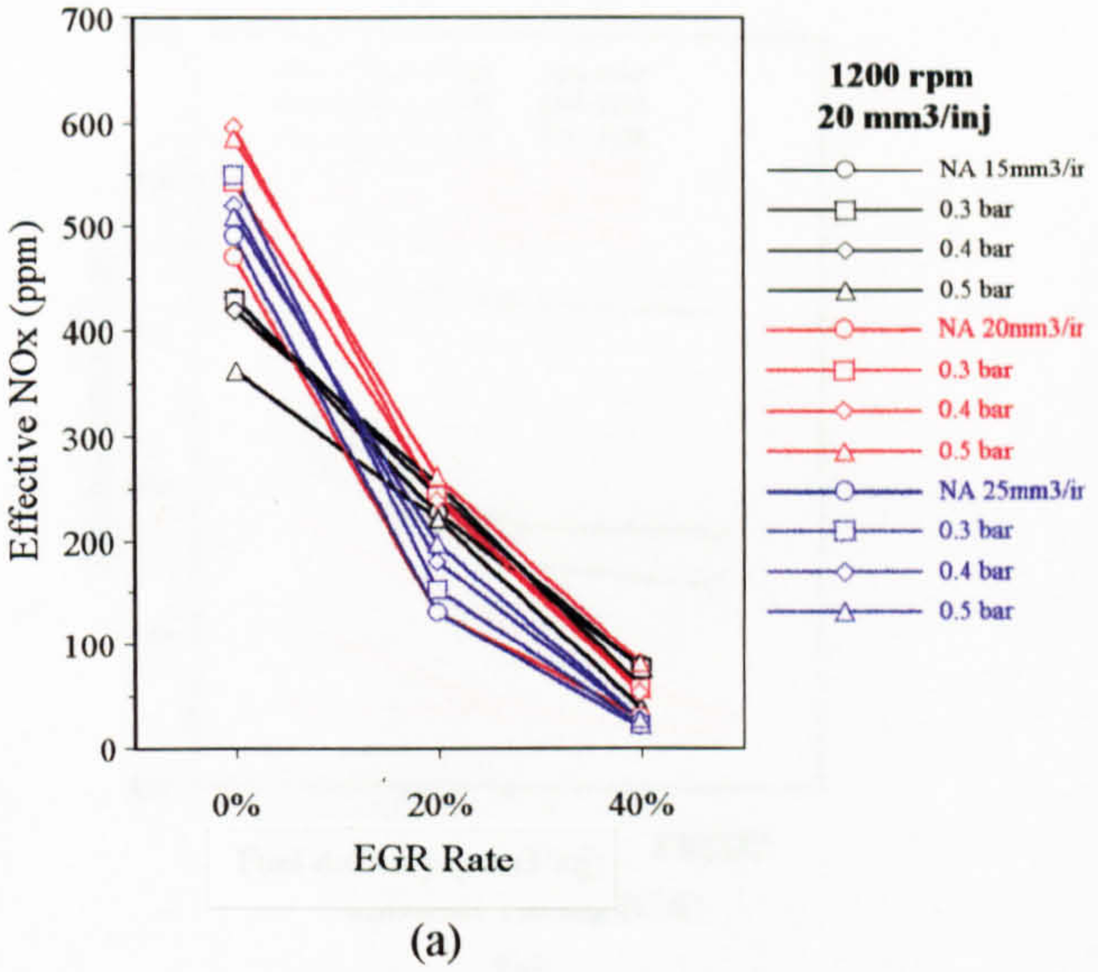
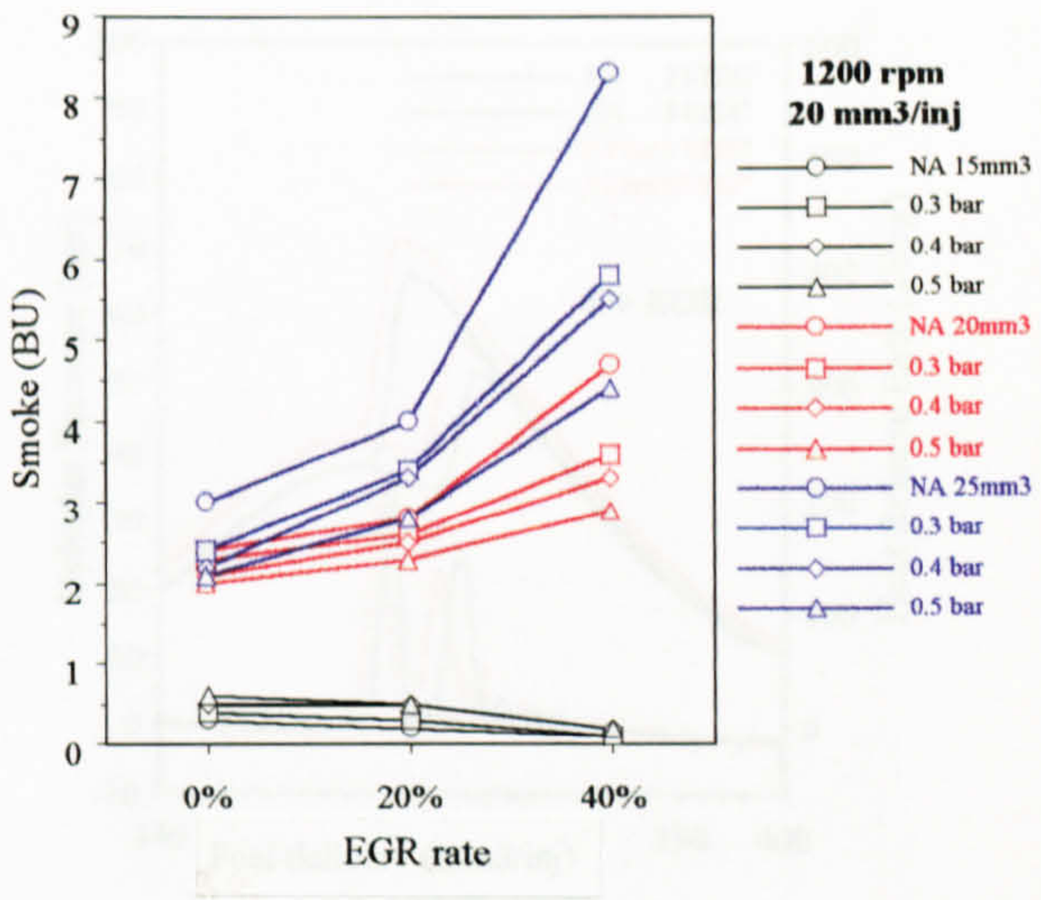


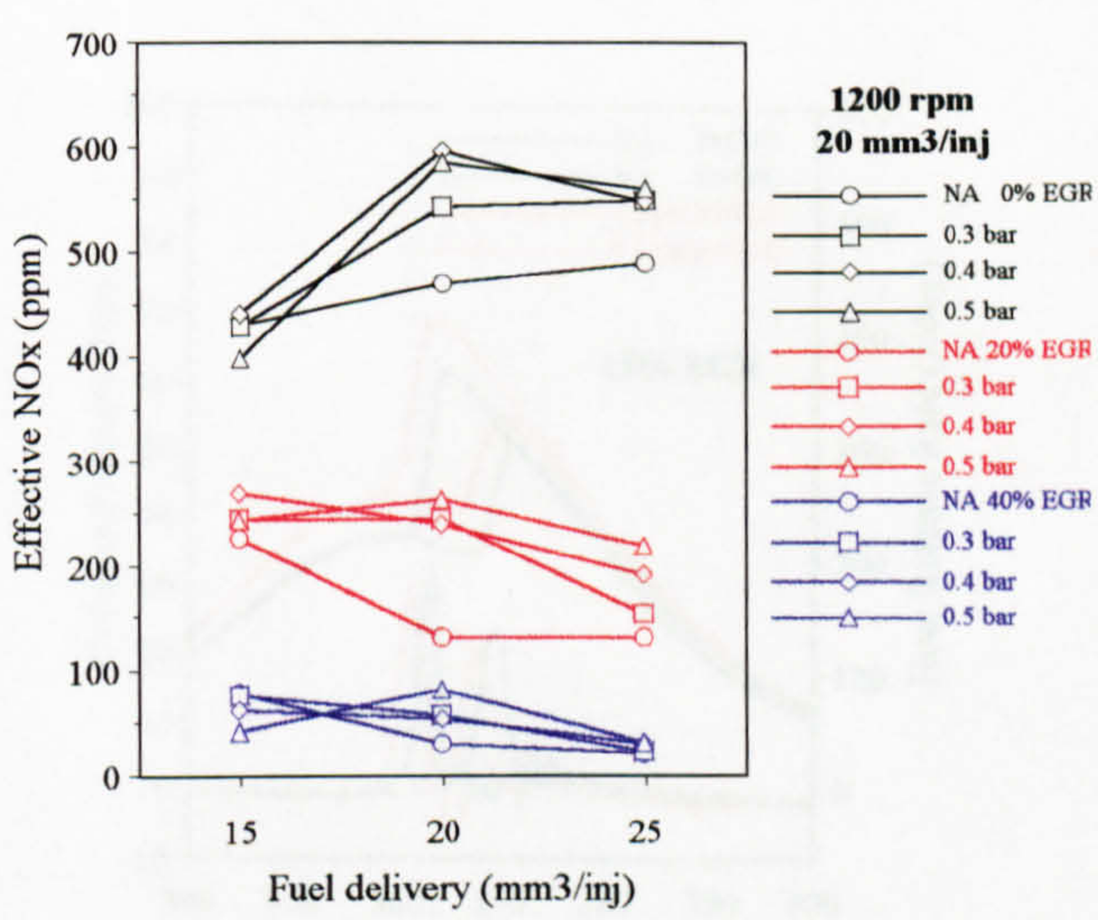
Figure 2.23 IMEP plotted against EGR rate for various boost pressures; single-cylinder engine



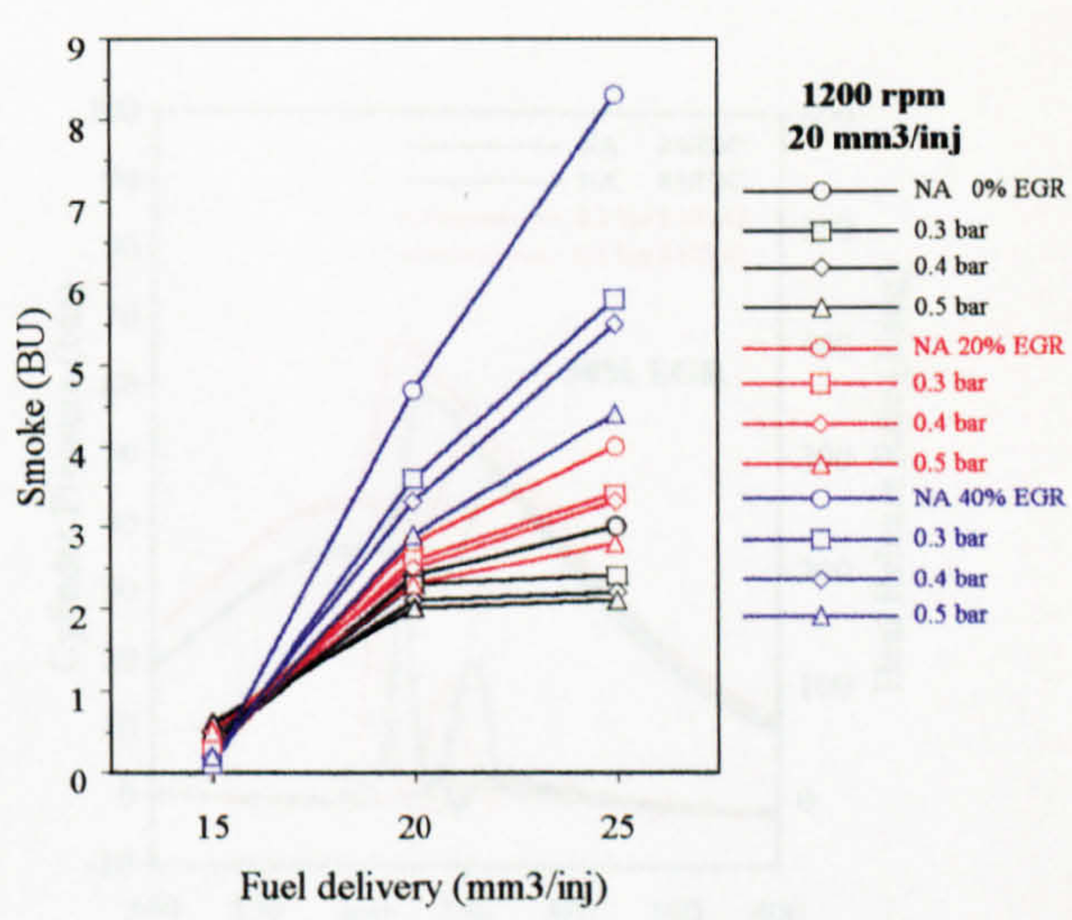
(a)



(b)

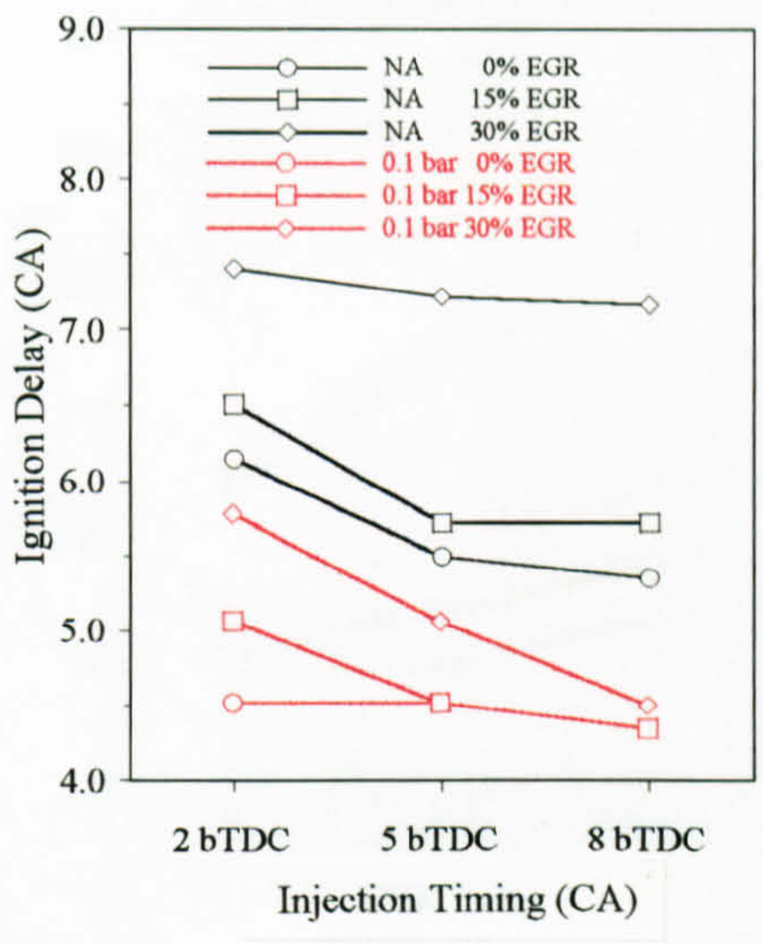


(c)

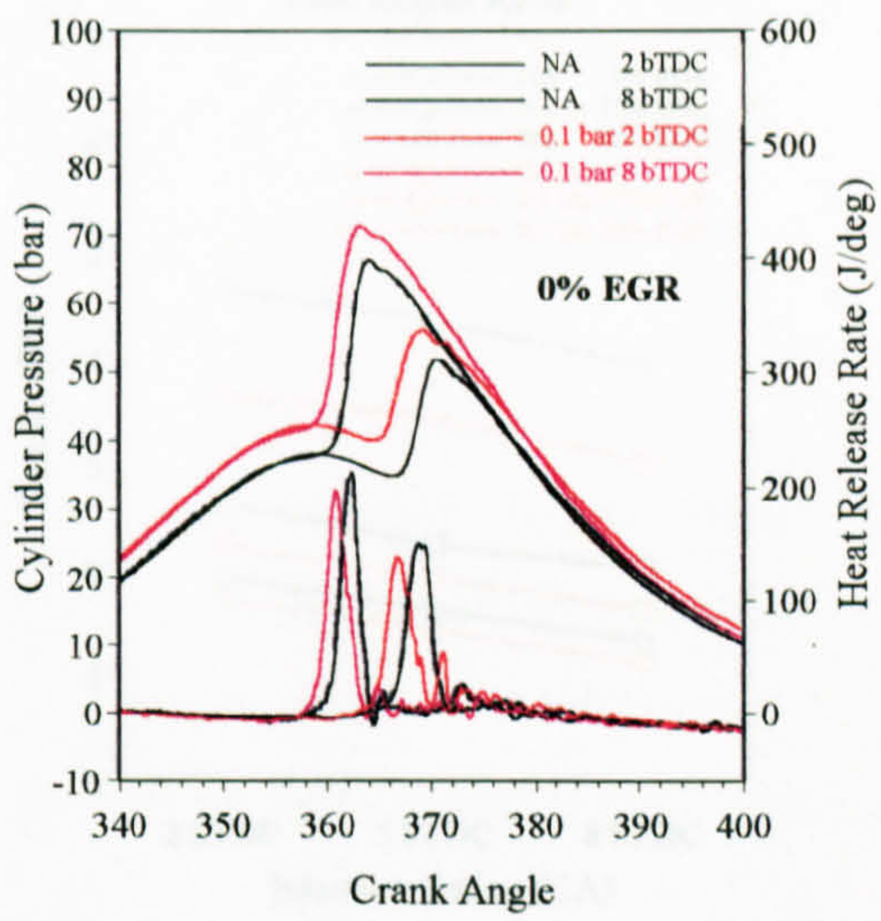


(d)

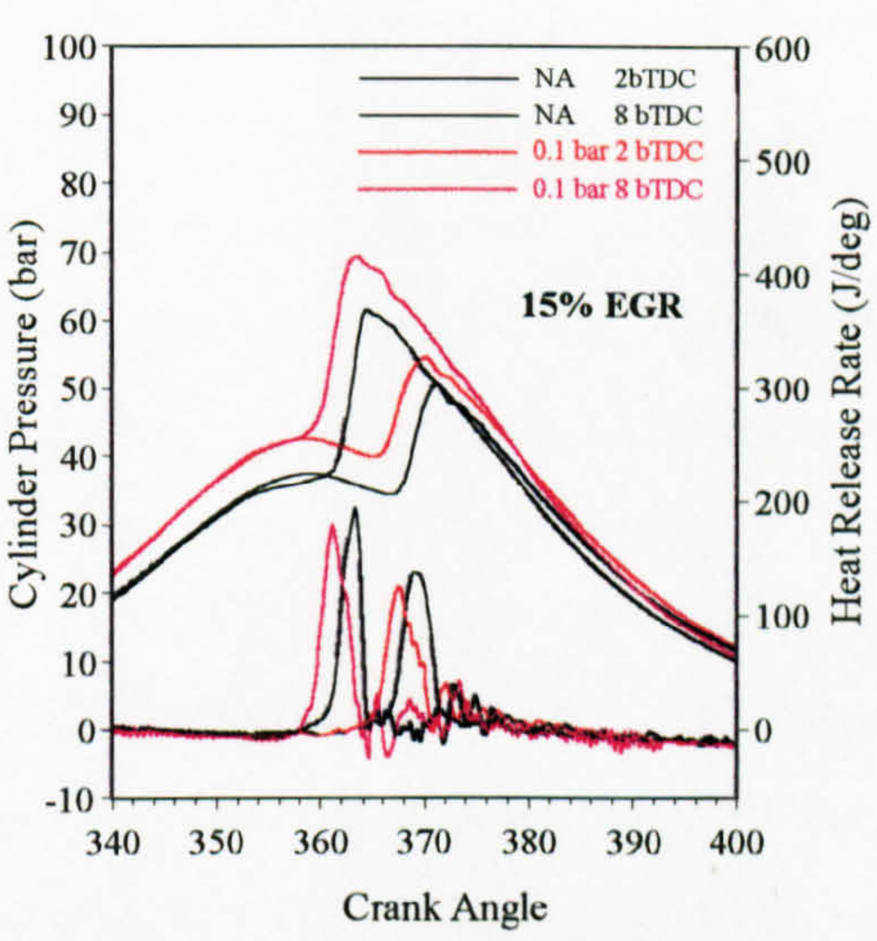
Figure 2.24 Bosch smoke number and NO_x concentrations for various EGR rates and boost pressures; single-cylinder engine



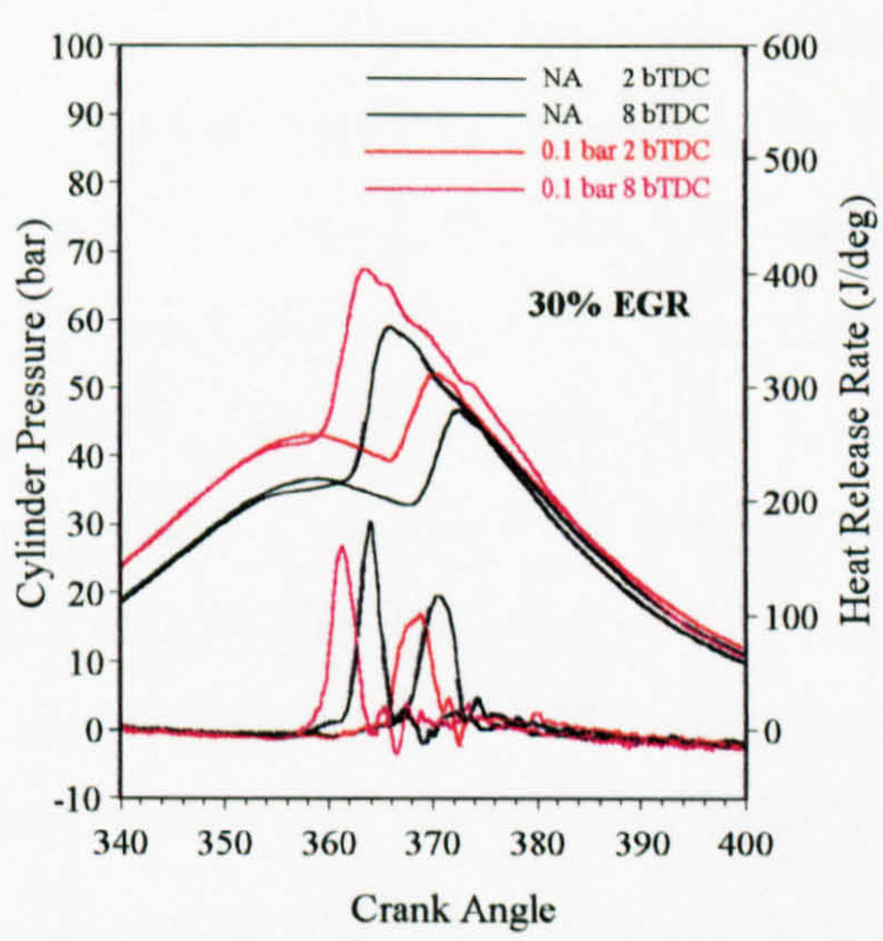
(a)



(b)



(c)



(d)

Figure 2.25 Start of ignition, cylinder pressure and heat release rate curves at engine speed of 1500rpm for various engine operating conditions; four-cylinder engine

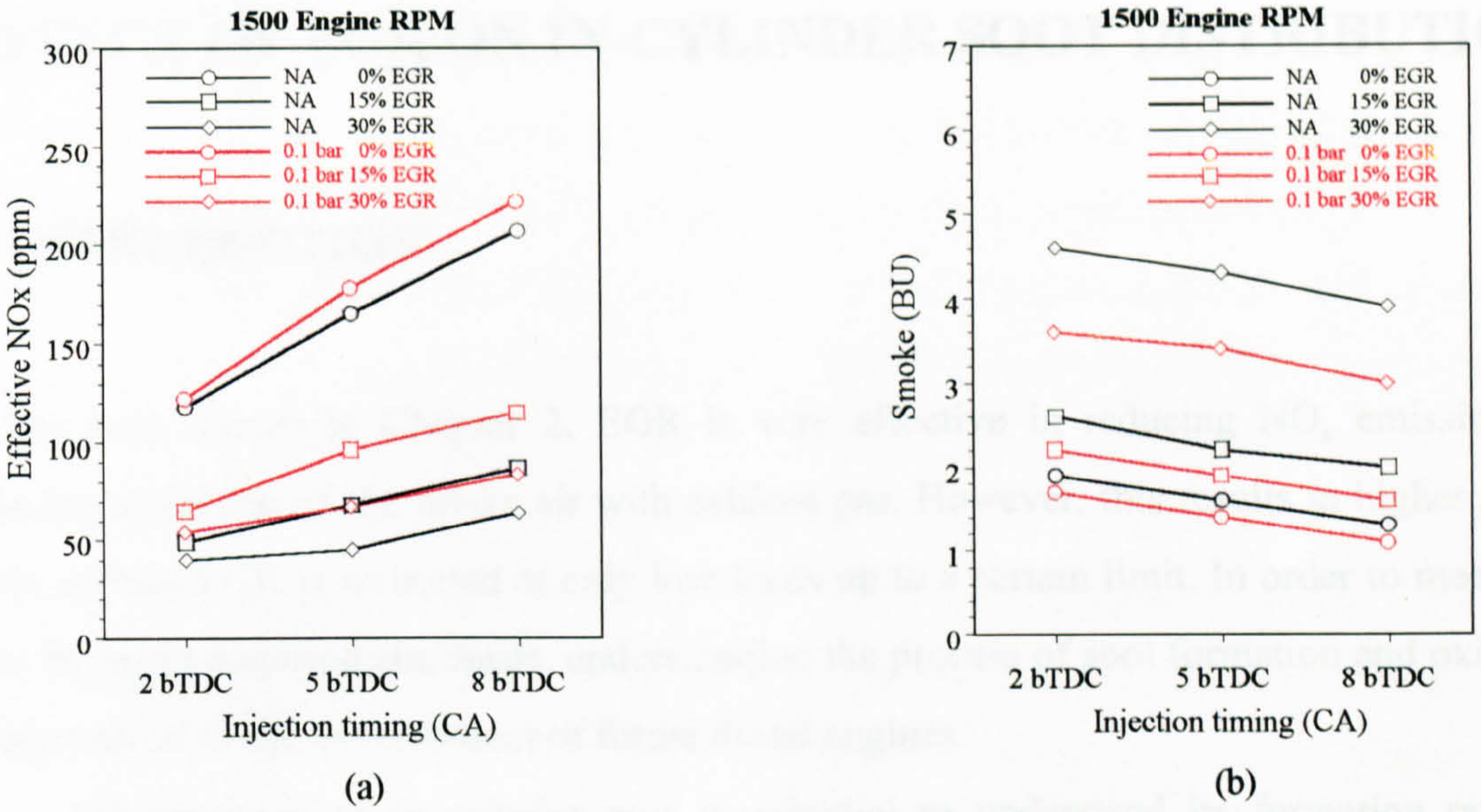


Figure 2.26 Bosch smoke number NO_x concentrations; four-cylinder engine

CHAPTER 3

EFFECT OF EGR ON IN-CYLINDER SOOT DISTRIBUTION

3.1 INTRODUCTION

As has been shown in Chapter 2, EGR is very effective in reducing NO_x emissions by replacing a fraction of the intake air with exhāust gas. However, this results in higher smoke levels, so that EGR is restricted at only low loads up to a certain limit. In order to meet even more stringent emission standards, understanding the process of soot formation and oxidation is very critical to the development of future diesel engines.

Measurement of in-cylinder soot is essential to understand its formation rate and determine effective approaches for soot reduction through oxidation. The measurement of soot particle size and the whole soot formation process in an engine yields information about any similarities between diesel and laboratory diffusion flames. Flame luminance which reflects the presence and position of radiating soot particles has been used extensively in the past to identify the regions of the spray plume which produce soot. Quantitative two-colour pyrometry has also been used to evaluate the flame temperature and soot volume fraction (for example see, Matsui *et al.*, 1982; Arcoumanis *et al.*, 1995b). These measurements are semi-quantitative since they must assume a certain path length and a uniform soot distribution. Thus, there are limitations in measuring soot particle size with this method. Point cylinder sampling (Fujiwara *et al.*, 1984) and total cylinder sampling (Luo *et al.*, 1989) have been utilised to collect soot in the cylinder which was later viewed and characterised using an electron microscope. These methods are aiming to reduce any possibility of altering the size either before or during sampling on the basis that soot reaction rates are quenched.

More recently the application of optical diagnostic techniques in engines has become feasible through better experience in designing optical engines and through the refinement of techniques capable of characterising various vector and scalar quantities inside the engine cylinder. The emerging soot imaging techniques which are superior in term of spatial and temporal resolution to conventional techniques are capable of providing detailed information of the soot concentration distribution in a diesel flame. For example, laser induced

incandescence (LII) has been used to visualise soot in an optically accessible engine (zur Loye *et al.*, 1990, Dec *et al.*, 1991); a laser was used to form a two-dimensional very thin sheet of light which induces an incandescent radiation by the soot particles similar to a black body emitting at 4500K. The radiation signal can then be related to the soot volume fraction, $\pi Nd^3/6$ where N is the number density and d is the particle diameter. Simultaneous measurements by LII and the laser induced scattering (LIS) technique which gives a signal proportional to Nd^6 in the Rayleigh limit, can provide information about the soot particle size and number density. This approach was used to describe qualitative differences in the soot particle sizes at different regions of the spray plume (Dec, 1992). Pinson *et al.* (1993) developed a method to obtain quantitative distributions of the soot particle size and number density by calibrating simultaneous by the LII and LIS imaging techniques. The vertical and the horizontal scattering intensities from the soot particles present along laser sheet area the flame were taken simultaneously to obtain the polarisation ratio, which was employed by Lee *et al.* (1990) to distinguish soot particles from fuel droplets. This method was used to investigate the effect of swirl on soot formation; the study concluded that soot was uniformly distributed in the combustion chamber bowl at the high swirl condition, but in the case of no swirl, soot was mainly observed near the wall and in the top region of the combustion bowl. The light extinction technique was also applied for the analysis of soot formation and oxidation (Nakakita *et al.*, 1990, Wiartalla *et al.*, 1995). Shioji *et al.* (1995) have applied the LIS technique to the visualisation of soot in the cylinder and pointed out that combustion at increased fuel injection pressures and reduced nozzle orifice diameters enhances soot oxidation. Also the LII technique was used to investigate the effect of injection pressure on the relative soot concentration by Dec and Espey(1992). They revealed that in-cylinder soot concentration decreases with increasing injection pressure. Using multiple laser techniques, Dec and Espey (1995) have more recently investigated the ignition and early soot formation process. They indicated that the first soot occurs at random locations, and shortly thereafter, small soot particles are developed throughout the cross section of the leading portion of the flame, which arise from the fuel rich premixed burn. They also showed that significantly larger soot particles appear around the periphery of the jet, presumably associated with the initial diffusion phase of combustion.

Two optical techniques were used simultaneously by Tree and Foster (1994) involving light scattering, extinction and radiation to measure soot particle size and number density at various engine speeds and overall equivalence ratios. They revealed that the peak soot

diameters were in the range of 30~50 nm and the peak soot diameter and soot volume fraction appeared to increase with equivalence ratio at the measurement location. Won *et al.* (1992) applied the LII and LIS techniques at the same time using double-pulsed laser sheet during a short time interval to investigate the mechanism of soot formation and the flow pattern in unsteady spray flames. They have found that soot is mainly formed in the periphery of the flame tip where air entrainment is less and flame temperature favours soot formation; it is then conveyed to the flame periphery by large scale vortices formed in the flame head. The LII and LIS techniques were also applied simultaneously to free spray flames in a rapid compression machine, where the 2-D distributions of soot concentration, particle size, and number density along a cross section of the flame were measured by Kosaka (1995).

In the present chapter, the LII and LIS techniques were employed to investigate the effect of EGR on soot formation in the four-cylinder engine. The results of the soot distribution at two different EGR rates and their cycle to cycle variations are presented and discussed below.

3.2 IMAGING DIAGNOSTICS

3.2.1 Laser Induced Incandescence (LII)

The laser induced incandescence images are generated by recording the thermal radiation emitted from soot particles on a CCD sensor when these particles are heated by a sheet of pulsed laser light (Dec and Espey, 1995). Greater than 10^7 W/cm^2 of laser power densities should be employed in order to raise the temperature of soot close to its vaporisation temperature of about 4500K, thus obtaining an LII signal above the background noise level, i.e. above the natural flame luminosity (Melton, 1984). Since non-laser-heated soot has a temperature of around 2200K and can even exceed 2500K (Arcoumanis *et al.*, 1995b), the natural flame luminosity can be removed from the LII images through appropriate spectral filtering and camera gating, since there is a substantial difference between the laser-heated soot particles being at a temperature of about 4500K and the surrounding flame. As a result of this temperature difference, when assuming that the soot behaves like a grey body, the thermal radiation of the laser-heated soot will be much greater than that of the non-laser-heated soot, especially at shorter wavelengths (Dec and Espey, 1995). This effect, however, is counter-balanced by a reduction in the overall intensity of the collected light as the wavelength is

reduced (Dec *et al.*, 1991) and therefore a compromise has to be found for the best cut-off wavelength. According to zur Loye *et al.* (1990), a 450 nm short-wave-pass (SWP) cut-off provided the best rejection of background luminosity while still allowing a sufficiently strong LII signal.

It was shown by Eckbreth (1977) that laser modulated incandescence from soot particles in a flame could easily overwhelm signal from Raman measurement. It was also suggested through theoretical considerations that the laser flux q can be estimated as a function of the particle surface temperature, hence the soot particle luminosity will increase with increasing laser flux due to the increased particle surface temperature according to the grey body assumption. Weeks and Duley (1974) have demonstrated that characteristic particle size information can be obtained from the incandescence radiation.

The LII signal intensity from a distribution of particles was derived numerically based on the Planck's blackbody formula and energy balance equation (Melton, 1984). The differential equations were derived for the time dependence of the temperature (T) and radius (a) of a laser-heated spherical particle by extending Eckbreth's treatment to include heat transfer to the medium as well as radiation. Thus, the Energy Balance equation gives:

$$K_{abs}(a)\pi \cdot a^2 q - \frac{K_a}{a}\frac{(T-T_0)(4\pi a^2)}{(1+GK_n)} + \frac{\Delta H_v}{W_s}\frac{dM}{dt} - \sigma_{sb}(T^4 - T_0^{\,4}) \times (4\pi \cdot a^2)$$

$$-\tfrac{4}{3}\pi \cdot a^3 \rho_s C_s \frac{dT}{dt} = 0 \qquad (3.1)$$

The terms are, respectively, the laser energy absorbed/sec, the rate of heat transfer to the medium (taken to be air at temperature T_0), the energy expended in vaporisation of the carbon particle, the rate of energy loss by blackbody radiation, and the rate of internal energy rise; the symbols are listed in List of symbols. In this equation, the particles are assumed to be small compared to their mean free path. Also it was assumed that the particles have a uniform internal temperature since the laser pulse is much longer than the characteristic time for internal gradient dissipation and the perturbation time scale for heat transfer approximation follows the expression suggested by Eckbreth. Using the continuity equation at the particle surface–gas interface,

$$-\rho_s \frac{da}{dt} = \rho_v U_v \qquad (3.2)$$

where the vapour velocity was assumed to be given by the Langmuir evaporation rate $U_v = (RT/2W_v)^{1/2}$, that the vapour pressure of carbon is given by the Clapeyron equation and that the perfect gas equation holds, the energy balance equation can be simplified by assuming that the typical soot particle size is less than 100 nm, i.e.

$$K_{abs}(a)q - \frac{8K_a(T-T_0)}{G\lambda} - \frac{\Delta H_v}{W_s}\rho_v U_v - 4\sigma_{sb}(T^4 - T_0{}^4)$$

$$-\tfrac{4}{3}\cdot a\rho_s C_s \frac{dT}{dt} = 0 \qquad (3.3)$$

where K_{abs} may be computed from the Mie absorption equation using optical constants for graphite in the 200 to 1500 nm range and assuming spherical particles. Here the refractive index of soot was assumed to follow the measurements by Carter *et al.* (1965) in the ultraviolet range and those of Lee and Tien (1981) in the visible. The incandescence from a distribution of particles can be obtained by integrating the soot particle radiation predicted by Planck's blackbody formula over the whole soot particle cloud by assuming normal soot distribution and using the definition of a response function, R (the incremental incandescent radiation received at time t in a bandwidth $\Delta\lambda$ centered at λ_{em} for excitation of a particle of radius a at wave-length λ_{ex} with a triangular laser pulse of peak intensity, q and 10ns FWHM). Thus, the LII signal intensity J is

$$J(t,q,\lambda_{ex},\lambda_{em},\Delta\lambda) = \int_0^\infty N\cdot P(a)\cdot R(a,t,q,\lambda_{ex},\lambda_{em},\Delta\lambda)da \qquad (3.4)$$

where N is the number density and $P(a)$ is the normalised probability density for a particle of radius a. It was also assumed that the soot size distribution is approximated by the zero-order log-normal distribution.

For small particles with $a<\delta$ where δ is an absorption length parameter, which means that the excitation wavelength λ_{ex} should be large, i.e. in the visible or infra-red region it can be approximated in the limit of high laser power and maximum temperature (assumed 4000K), as

$$J = C_1\int_0^\infty N\cdot P(a)\cdot a^{3+0.154\cdot\lambda_{em}^{-1}}da \qquad (3.5)$$

where C_1 is a constant, and λ_{em} is the observation wavelength which should be large to achieve an exponent of the radius close to 3. From this equation it follows that J is nearly

proportional to the particle radius cubed, which in turn is proportional to the soot volume fractions.

Interpretation of LII images

The qualitative interpretation of the LII images is straightforward under ideal conditions. Areas of high and low image intensity represent regions of high and low soot concentrations, respectively. Melton (1984) predicted that if laser and signal attenuation are negligible in the limit of high laser power, the signal strength from the laser-heated soot cloud should be directly proportional to the local soot volume fraction.

In the LII experiment, it is difficult but very important to reject the natural luminosity and elastic scattering. This can be achieved by selecting appropriate filters, such as a 450 nm short-wave-pass (SWP) edge filter and another 450 nm SWP interference filter and 532 nm laser mirror. Background luminosity can be further suppressed by a short camera exposure time synchronised with the laser pulse (Dec, 1992). Since the laser-heated soot will cool rapidly after the laser pulse (Melton, 1984), maximum suppression of background luminosity could be achieved by limiting the exposure time to be on the order of the laser pulse duration.

For a more precise experiment, the shot-to-shot variations in the laser sheet power and the non-uniformity of laser power in sheet width and thickness should be minimised. The shot-to-shot variations can be estimated by measuring the laser power for each pulse and then normalising the images accordingly. Spatial non-uniformities can be estimated by using a 1-D array of photo-diodes or a CCD camera sensor to image the laser sheet and normalise the LII images on a pixel-line by pixel-line basis. Also, clipping the edges of the laser sheet prevents edge effects from influencing the images. In the experiment of Kosaka *et al.* (1995), the part of laser sheet which is divided by a beam splitter is measured in its longitudinal intensity distribution using a photodiode array.

Also the effect of non-grey body type radiation on the LII signal should be considered. Dec (1992) has obtained an LII emission spectrum and confirmed that its general shape is very much like the grey body spectrum, particularly in the 400 to 450 nm range, and that it does not contain spectral lines or typical bands of molecular emissions. He thus considered that the only significant source of the LII emission is grey body radiation from the soot cloud illuminated by the laser sheet.

Additionally, it is necessary to examine the assumption for the reduction effect in the soot particles size by means of vaporisation during laser sheet exposure and the effect of the

different temperatures of soot particles. The LII technique is partially intrusive, because some of the soot is vaporised. The particles decrease in size due to this vaporisation, while the particle number density remains constant. The diameter of the particles was found to decay exponentially from the original diameter with increasing laser flux (Dasch, 1984). Since a small particle may be completely vaporised during the laser pulse, this could present a problem in an experiment where images are acquired in quick succession. However, the effect can be negligible if only one LII image is taken in a particular engine cycle, and furthermore the smallest particles contribute the least to the volume fraction measurement.

As predicted by Melton (1984) and experimentally verified by Quay *et al.* (1994) and Tait *et al.* (1992), a laser flux exceeding $3x10^7$ W/cm^2 causes vaporisation which dominates heat losses from the particle. However, the effect of different temperatures of soot particles can usually be minimised by increasing the laser power well above the minimum threshold necessary for heating the particles to the same degree.

In order to derive semi-quantitative or even quantitative information about the soot particle distribution and size from the LII images, it is essential to take into account the effect of attenuation by taking care of the facts mentioned above and by establishing relevant calibration methods.

As with most laser-based planar imaging techniques applied to particle fields in flows, interpretation of the LII images can be complicated by the effect of attenuation of the laser sheet power and the LII signal. As the laser sheet traverses the image plane, attenuation by the soot cloud will reduce the amount of laser power available for heating. This could reduce the temperature and/or vary the rate of vaporisation of some of the laser-heated soot (Dec *et al.*, 1991). The transmittance of radiation through the media, T, can be calculated using Beers law given by $T = e^{-\int k_{ext} ds}$, where k_{ext} is the extinction coefficient and s is the path length. From this equation, it can be estimated that signal attenuation is slightly worse for the shorter wavelength and becomes significant for soot fraction above 10^{-6} (Pinson *et al.*, 1993). Also attenuation of the LII signal by soot or liquid fuel droplets between the laser sheet and the camera could result in a low image intensity in regions of high soot concentration. The effect of this attenuation can be estimated by obtaining calibration images using a homogeneous mixture of soot particles in the combustion chamber, which can then be used to normalise the experimental images. For generating a homogeneous mixture of particles, a smoke generator or previously collected soot particles can be used. The effect of laser power attenuation can be

minimised by using laser power high enough above the minimum threshold for heating the soot particles, which leads to higher total signal strength.

Dec (1992) has reported that varying the laser power by about ±20% was found to have no significant effect on the intensity distribution of the LII images at typical conditions; however, non-uniform attenuation of the LII signal by the soot cloud between the image plane and the camera may have an effect. Using low sooting fuels can reduce the attenuation of the laser sheet and the LII signal either alternatively or additionally. An investigation into the attenuation of the incident laser sheet by soot particles and non-uniform density gradients as well as the attenuation of LII images by soot particles was performed by Won *et al.* (1991) and the extinction of the incident laser light was considered and compensated in their analysis.

In order to obtain information which can be used to quantify the LII signal obtained from the diesel engine experiment, an absolute calibration of LII signals must be performed through an idealised experiment. Although many possibilities exist for the quantification of light scattering signals, the LII signal must be calibrated against a soot field of known concentration and size distribution. The well established soot field of a laminar diffusion flame should be chosen as the LII calibration source. An experiment of this type has been described by Pinson *et al.* (1993), where an ethylene diffusion flame from an axial burner was used to obtain a calibration curve for the LII signal which was in reasonable agreement with the results of Santoro *et al.* (1983). Also Quay *et al.* (1994) carried out calibration of the observed LII signal by equating the LII signal at a single spatial point where the peak soot volume fraction occurs with the known value of the soot volume fraction at this location from the laser scattering/extinction measurements. All other LII data can be converted to absolute soot volume fraction based on this single point calibration procedure.

3.2.2 Laser Induced Scattering (LIS)

As a laser sheet passes through the combustion chamber of a diesel engine, some of the light will be elastically scattered from fuel droplets, fuel vapour and soot particles in its path; this scattered light can be imaged and interpreted on the basis of the Mie theory of light scattering. The elastic scatter signal intensity is strongly dependent on the particle size. For small particle sizes like typical soot (Rayleigh limit), the elastic scatter signal is proportional to the particle diameter raised to the sixth power (Kerker, 1969). Because of this dependence on particle size, the elastic scatter images can provide a qualitative picture of where soot and/or liquid

fuel droplets are located. However, it is difficult to interpret the images if soot and liquid fuel droplets coexist in the same area although the difference in the polarisation ratio between liquid fuel droplets and soot has been used to distinguish them (Lee *et al.*, 1990). On the other hand, flame luminosity and LII can be easily suppressed using a narrow band pass filter and a short exposure time.

Due to the computationally intensive nature of the full Mie expressions, simplifying assumptions are often employed. When the particles are small compared to the wavelength of the incident light, the contribution of scattering to extinction is small and the Mie relationship can be simplified to the Rayleigh approximation (Kosaka *et al.*, 1995; Pinson *et al.*, 1993). The intensity scattered from an isolated spherical particle illuminated by a parallel beam at a distance r was derived by Kerker (1969) as

$$I_U = \frac{8\pi^4 a^6}{r^2 \lambda^4}\left(\frac{n^2-1}{n^2+2}\right)^2\left(1+\cos^2\theta\right) \tag{3.6}$$

where N is the number of particles per unit volume, I_u is the intensity scattered per particle, a is the particle radius, r is the distance to the particle, λ is the wavelength in the medium, n is the relative refractive index, i.e. the ratio $n1/n2$, and θ is the angle of observation. The basic premise is that the instantaneous field which the particle experiences due to the electromagnetic wave is uniform over its extent because the particle is small compared to the wavelength. Also it is assumed that the incident field oscillates harmonically. Thus, in a random array of identical particles, the scattering is incoherent, so that the intensity scattered per unit volume of the medium is the sum of the effect from each individual particle. Using the particle volume V instead of the radius a, the intensity scattered per unit volume is

$$N \cdot I_u = \frac{9 \cdot \pi^2 \cdot N \cdot V^2}{2 \cdot r^2 \cdot \lambda^4} \cdot \left(\frac{n^2-1}{n^2+2}\right)^2 \cdot \left(1+\cos\theta\right) \tag{3.7}$$

Accordingly, the intensity scattered by a given volume of scattering material, NV, dispersed as small particles, is directly proportional to the volume of the individual particles; the larger these are, the more intense is the scattering. The upper limit of particle radius for which the Rayleigh equation is presumed to be valid is generally set at $a/\lambda \leq 0.05$. For the incident wavelength of 532nm the particle size should hence be less or equal to 26.6 nm which is very close to the size of the carbon core of a soot particle.

Interpretation of LIS images

As mentioned above, the qualitative interpretation of the LIS images is straightforward under ideal conditions, since the scattered intensity is directly proportional to the volume of the individual particles. Areas of high and low image intensity represent regions of high and low soot concentrations, respectively. However, as already mentioned, it is difficult to interpret the images if soot and liquid fuel coexist in the same area unless there is a way to measure the difference in the polarisation ratio between them (Lee *et al.*, 1990).

Flame luminosity and LII can be easily suppressed using a narrow band pass filter at 532 nm with FWHM of 10 nm, and a short exposure time of about 1μs around the laser pulse of about 7ns duration (Dec and Espey, 1995). Although flame luminosity and LII were adequately rejected, laser light elastically scattered from the cylinder surfaces cannot be eliminated easily due to the strength of this signal. Similarly to the LII experiment, the scattering images may be obscured by the effect of light attenuation by the soot particles especially when the soot concentration in the flame becomes too high. A low sooting fuel is preferable for better interpretation of the measured LIS images (Won *et al.*, 1992).

3.3 EXPERIMENTAL SYSTEM

3.3.1 Test Engine and Test Conditions

Figure 3.1 shows the optical engine four-cylinder with the EGR system, which was the same engine used in Chapter 2; EGR rate was controlled by two valves installed on the exhaust pipe. Details of the engine configuration were given in Chapter 2.2.1.1 and Table 2.1; the combustion chamber having optical access through quartz side windows, a piston window and additional sandwich-type windows in the piston is presented in Figure 3.2 with the image of the cylinder head shown in Figure 3.3. The extended pistons in the test engine are hollow, having thus enough room to position mirrors at 45° to the cylinder axis while allowing optical access into the combustion chamber through a 25mm thick quartz window positioned in the bottom of the piston-bowl. The other two square windows of 20mm in length were located in the extended cylinder liner at 90° to each other in three directions to allow further optical access into one of the four cylinders in the engine. In addition, two sandwich-type windows of 3mm in thickness, having a hole shaped the same as the cross section of the bowl in the middle plane, are positioned in the side of the piston and in the upper part of the piston,

respectively. These two sandwich-type windows allow additional optical access during the part of the combustion cycle when they are aligned with the side window in the cylinder liner. In these experiments, only one of the four cylinders was used for visualisation into the combustion chamber through a piston window and a mirror which was supported independently from the engine test bed to isolate it from engine vibrations.

Since both the piston and the cylinder liner were extended by the same length, the optically accessible engine kept a high geometric compression ratio of about 19.5, which is only a slight reduction from the 20.5 of the corresponding production engine as a result of the flat piston window. Also the original combustion chamber geometry was retained except for the removal of the 'pip' in the bowl bottom; this is expected to provide more realistic test results whereas other optical accessible engines had more significant modifications made to the combustion chamber geometry (open instead of re-entrant) in order to increase the optical access into the piston-bowl.

The inlet valve, exhaust valve, cold start glow plug and the injector tip are shown in Figure 3.3. The maximum diameter of the bowl is 40.8mm and its depth is 16.1mm as shown in Table 2.1. The re-entrant diameter is slightly smaller than the diameter at the bottom of the bowl, hence the optical access is restricted by the re-entrant diameter of 37mm.

Since the fuel temperature could not be controlled, it was considered to be equal to the ambient room temperature of about 20° C during the experiments. The amount of fuel injected was kept the same for all test conditions by maintaining the same throttle lever position in the fuel injection pump, whereas the start of injection was independently adjusted by a micrometer fitted on the cam movement device of the fuel injection pump, with confirmation of the start of injection provided by needle lift signal on the oscilloscope obtained using a needle lift sensor.

All the tests were conducted at idle condition at 1000rpm to prevent fast window fouling by soot and minimise the effect of attenuation, instead of using a low sooting fuel. To investigate the effect of EGR rate on soot formation, the EGR rate was varied between 0% and 50%; Table 3.1 provides a summary of the test conditions.

The temperature of the engine oil and cooling water was maintained at a constant level of 85°C during the experiments by means of an automatic temperature control system. Due to this engine constant temperature of 85°C the intake air temperature measured near to the cylinder liner remained at about 55°C provided there is sufficient cooling period after the previous engine firing, until it reaches temperatures less than 30°C by the introduction of fresh

air during motoring conditions. "SHELL Gas Oil SH" was used as fuel for all the experiments.

The EGR rate has been defined here as the percentage of exhaust gas mass present in the inlet charge, similarly to the definition given in Chapter 2, i.e.

$$EGR \text{ rate} = (1 - F / I_o) \times 100$$

The airflow meter used to monitor the flow of fresh air charge was first calibrated on a steady-flow rig prior to its connection during the experiments to the inlet of a surge tank attached to the engine intake. The EGR rate was controlled by adjusting a mechanical throttle (Figure 3.1) until the intake mass of fresh air was reduced to the flow rate desired. To achieve high EGR rates an additional throttle was placed in the exhaust pipe to increase the back pressure when desired; this was only used for the 50% EGR test case. An alternative to this second throttle would be to pass the exhaust gas through the turbine of a turbocharger in order to increase the back pressure (Hentschel and Röpke, 1993). This increase of the exhaust back pressure above normal operating conditions has two main effects on the engine characteristics according to Montgomery and Reitz (1996): firstly, the exhaust gas residuals are increased as more mass is trapped in the cylinder at exhaust valve opening due to the increase of the back pressure and also exhaust gases are backwashed into the intake manifold during valve overlap as the exhaust back pressure is higher than the intake pressure. The same authors describe as the second major effect of an increased exhaust back pressure the reduction in power output since the pumping work required during the exhaust stroke increases due to the increased back pressure.

Concerning the optical system, the images were saved either through video recording or through real-time 'grabbing' to the hard disk of a PC. For simultaneous imaging applications, however, only two cameras are generally connected to the computer as the maximum number of frames possible to 'grab' is 24, which means two cameras obtaining 12 frames each or even three cameras of 8 frames each.

3.3.2 Laser Sheet and Optical Set-Up

For obtaining good images of LII, LIS and flame luminosity simultaneously, various combinations of spectral filtering, relevant laser power and sheet thickness and camera exposure time have been attempted following suggestions of several investigators, which are

summarised below, based on their experiments on diesel engines using the LII and the LIS technique.

Investigators	Laser sheet	Optical set-up
zur Loye *et al.* (1990)	500μm thick and 50mm wide, 300mJ per pulse, 8ns pulse	2 x 450nm SWP interference filter, BG39 Schottglass glass filter, camera intensifier gate 80ns, 532nm laser-line mirror
Dec *et al.* (1991)	300μm thick and 50mm wide, 200mJ per pulse	2 x 450nm SWP interference filter, BG39 Schott-glass filter, 532nm laser line mirror, camera intensifier gate 80ns
Dec (1992)	300μm thick and 50mm wide, 200mJ per pulse, 8ns pulse	2 x 450nm SWP interference filter, BG39 Schott-glass filter, 532nm laser-line mirror, camera intensifier gate 70ns
Dec and Espey (1992)	250μm thick and 50mm wide, 200mJ per pulse	450nm SWP, camera intensifier gate 70ns, 532nm laser-line mirror
Won *et al.* (1992)	LII: 1064nm laser wavelength, 260mJ per pulse LIS: 150μm thick and 40mm wide, 20mJ per pulse	LII: 400nm SWP and UV mirror, 50ns gate time LIS: 532nm±4nm, camera intensifier gate for 500ns
Alatas *et al.* (1993)	200μm thick and 20mm wide, 200mJ per pulse, 10ns pulse	400nm interference filter with band-width of 70nm, camera intensifier gate 50ns, 532nm laser-line mirror
Espey and Dec (1993)	300μm thick and 30mm wide, 180mJ per pulse, 8ns pulse	450nm SWP interference filter, camera intensifier gate 25ns, 532nm laser-line mirror
Pinson *et al.* (1993)	300μm thick and 60mm wide sheet	400nm±12nm, camera intensifier gate 50ns, dichroic beam split at 532nm
Dec and Espey (1995)	300μm thick and 25mm wide, 80mJ per pulse, 7ns pulse	105mm focal length, 450nm SWP, reflection of 475nm edge filter, colour glass filter, camera intensifier gate 50ns, 532nm laser-line mirror

In these experiments, a frequency doubled (532 nm) Nd:YAG laser was used for the LII and LIS imaging studies. The laser beam of 8mm in diameter was formed into a horizontal sheet using a combination of cylindrical and spherical lenses. The optical set up used for this experiment is shown in Figure 3.4 and Figure 3.5. The laser power was set to 200 mJ for the LII images which resulted in a theoretical laser power density of 6.3×10^8 W/cm^2; however, due to the eight optical elements in the path of the laser beam (four coated and four uncoated)

the laser power density is estimated to be reduced by about 61% to just $3.9x10^8$ W/cm^2 when reaching the inside of the piston-bowl. The LIS experiment employed a laser power of 100mJ resulting in an estimated effective laser power density of $1.9x10^8$ W/cm^2.

The selection of lenses has provided an estimated laser sheet at a wavelength of 532nm of about 300μm thickness and up to 25mm width. The beam waist is located at a distance of 1345mm from the last lens. All lenses, beam splitters and prisms are custom-coated with a broadband anti-reflective coating to decrease the reflection losses per surface by 50% to the current 2%. Beam positioning is performed through two reflection prisms, with micrometer adjustment of the top prism in rotation as well as in height. The use of prisms instead of laser-line mirrors allows multi-wavelength use, which could be important for simultaneous application of LII and LIS. To improve the LIS signal it may be useful to polarise the laser light in the horizontal direction so as to obtain the maximum scattering intensity at the 90° imaging plane.

The laser sheet passes through a square liner window into the cylinder, where an optional sandwich window in the piston allows imaging inside the combustion bowl at engine timings around TDC (Figure 3.6). The field of view, however, is severely restricted by the limited optical access obtainable because of material constraints and because of the demand for keeping the design close to that of the production engine.

It is important to use the appropriate spectral filtering and exposure time of the camera in order to suppress the background luminosity while keeping the LII and LIS signals sufficiently strong. The selection of the filter, exposure time, lens aperture and intensifier for flame, LIS and LII imaging should be made with the goal to improve the signal-to-noise ratio and to allow simultaneous imaging of LII, LIS and the flame. It should be considered that each filter not only has the desired effect of filtering certain wavelengths but also reduces the overall transmitted light (maximum transmittance can be as low as 50%). Therefore it is necessary to minimise the number of filters. Since some filters are used not only to image the transmitted light but also the reflected one, the selected filters have the desired specifications with respect to both transmission and reflection.

Based on these considerations, the combination of spectral filtering for each image was decided as follows:

Flame imaging

a broadband (300nm~700nm) beamsplitter, which has at a 45° incidence angle a 9% reflectance and 80% transmittance, was used to reflect a relatively small amount of light into the lens (f/75mm) of an intensified CCD camera (with an exposure time of 1μs and a lens aperture of f/1.8).

LII imaging

the reflected light from a 500 nm LWP filter was subsequently passed through a BG39 colour glass filter and a 450nm SWP filter. Ideally this third filter should have transmission from 300nm to about 380 nm; however, off-the-shelf SWP filters usually transmit only down to about 415 nm with the selected one having the lowest possible cut-off at 400 nm. The exposure time has to be very short (here 25ns) as the LII signal takes about 8 ns to reach a maximum and then decays almost exponentially. Longer exposure times would allow the natural broadband flame luminosity to be considered as background noise.

LIS imaging

the transmitted light from a 500 nm LWP was subsequently passed through a 532nm interference filter (FWHM of 10 nm) to isolate the laser scattered light from the background flame luminosity. However, since the exposure time could not be reduced below 1μs, two neutral density filters (50/50 and ND1) were added to the optical path and the aperture decreased to f/22.

The specification curves of the standard off-the-shelf filters are shown in Figure 3.7.

3.3.3 Timing, Triggering

Eckbreth (1977) has shown experimentally that the temporally-resolved laser-modulated particle incandescence at 684 nm as a function of the laser focal flux has an initial spike due to its temperature rise up to the vaporisation temperature followed by a decay that reflects the exponential decrease in the particle's size (diameter) with time. This can help in setting the optimum exposure time of the CCD sensor with respect to the laser pulse. In this respect, Kittelson *et al.* (1988) have found a time lag between the start of combustion and the start of significant soot formation to increase with load and to vary between 0.2 and 1.0ms.

The main triggering requirements of the experimental set-up are governed by the need on the one hand to synchronise the engine and the Nd:Yag laser and on the other hand to provide the appropriate frequency to the laser for accurate timing of the CCD camera in relation to the laser pulse.

A personal computer with some hardware circuitry and an oscilloscope/delay-generator provide the laser and the cameras with the triggering pulses required. The computer incorporates a timer card (CIO-CTR 10 card) which uses the shaft-encoder signal as an input to generate a 16.67 Hz signal, to delay this signal by a variable time and to check the engine speed. Should the engine speed drift outside the tolerances of the laser (16.67 Hz±10%), then an independent frequency generator provides the required signal to the laser. The computer, hence, provides always a 16.67 Hz signal to the laser lamps; this signal is synchronised to the engine whenever it is possible otherwise it is externally generated. The delay between the laser lamp and Q-switch was set internally on the laser control using the laser lamp synchronised output and the adjustable Q-switch delay was used for triggering the oscilloscope/delay-generator and the LII or LIS camera. For future simultaneous imaging the oscilloscope output could be used to trigger the LIS camera while the flame camera could be triggered by a delayed shaft-encoder pulse; this would result in three images of the same cycle with the flame image being taken about 60μs before the other two images. To avoid triggering of the cameras during the warm-up period of the engine and laser and during motoring conditions, a circuit was designed which coupled the camera triggering to an increase in the injection line pressure signal.

3.3.4 Image Processing

The public-domain software "Khoros", which provides a visual programming interface for image processing was used for the image processing. This programme performs a number of tasks in order to obtain soot concentration images from the original CCD pictures. At first, the images recorded on the SVHS video tape were grabbed into the hard disc of a personal computer (486DX) using a purpose written software through 'grabbing' card (Matrox Image LC) and the images were stored in the bmp-file format. Then the bmp-image files were transferred to a workstation (DEC 5000) which was in turn connected to a Silicon Graphics (IRIX) machine. These bmp-image files were converted to viff-type files of which format can be read by Khoros. A floor was set of 30 grey level intensity (GLI) in order to eliminate most

low intensity of background noise which consists of both white noise of the sensor and spurious illumination of the bowl due to reflections of the laser sheet. The image showing the piston-bowl boundary, which was taken without firing, was used to identify corresponding points in all images in order to extract the images precisely for subsequent comparison between the flame development and soot concentration. To ease the interpretation, a piston-bowl with the outline of the crossing laser sheet was superimposed on the images and the 0 to 255 grey levels were translated to a 10 banded colour scheme which gave clearer areas and boundaries of the signal intensities; Figure 3.8 provides an example of the processed image relative to the unmodified one.

3.3.5 Uncertainties

The results presented in this thesis are qualitative only, mainly because no calibration of the experimental system was performed using a known soot source due to time limitations. The errors involved are hence caused by the engine experiment itself and are summarised below:

1. Shot-to-shot repeatability of laser power: the variation in laser power is estimated to be less than ±5% and is not compensated during the image processing since the effect of this variation on the grey level intensity cannot be quantified without experiments using a calibration flame.
2. Uniformity of the laser power along the length, width and thickness of the laser sheet: variation along the length of the laser sheet is estimated to be about 5% while across the width it was not noticeable in the images since the sheet was clipped at the edges by an iris; the power distribution across the thickness was considered negligible.
3. Effect of natural flame luminosity on LII image: due to the strength of this background noise, the light levels reaching the camera had to be severely reduced. Of the three options to reduce the light levels, the most advantageous is to decrease the exposure time since only the noise is reduced but not the short duration signal of interest.
4. Effect of non-grey body type luminosity on LII signal: no noise could be detected from the experimental set-up employed.
5. Effect of laser sheet on soot particles of different initial size and temperature: this effect is especially important for diesel engines incorporating EGR since different soot particle sizes are expected which could bias the signal. In order to decrease the bias caused by varying size and temperature, it was decided to increase the laser power above the

minimum threshold; however, this effect has to be taken into account when interpreting the images.

6. Attenuation of the laser sheet as it travels through the combustion chamber: this effect is considered to be negligible since the light distribution of the laser sheet before entering and after exiting the combustion chamber showed little difference due to the high laser power used. Further, no decrease in laser power could be detected from the images as the laser traversed the combustion chamber.
7. Attenuation of the LII signal as it travels through the combustion chamber: this effect is not negligible, especially at the load conditions with high fuelling. However, it could be negligible in this experiment since all the tests were intentionally performed at very low load conditions.
8. Calibration of the LII signal: no calibration was performed as this would have required a calibrated flame with an associated substantial investment of time.

Analysing an unmodified LIS image (Figure 3.8) two types of noise can be distinguished in the part of the piston-bowl which is not directly illuminated by the laser sheet: (i) a low light level, corresponding to homogenous noise of about 25 grey levels intensity which can be eliminated through appropriate image processing and (ii) a very localised and bright noise of grey levels similar to the actual signal. The existence of this latter form of noise means that a high grey level intensity signal does not necessarily result from a soot particle being heated within the laser sheet but possibly from soot particles heated outside, i.e. above or below the laser sheet due to especially strong reflections or the presence of large soot particles. However, this effect has to be assumed negligible for any interpretation of the images to be valid.

3.4 RESULTS AND DISCUSSION

The original attempts in this experiment were to examine the possibility to get the LII, LIS and natural flame images simultaneously in the four-cylinder diesel engine whose size is relatively small compared to engines used in previous LII experiments. The experimental set-up, especially optical set-up put together in this experiment might be applied to further investigations of the soot behaviour using the LII and LIS techniques. It should be noted that up to date, none of the experiments using LII and/or LIS techniques (or LIF) for better

understanding of soot formation and oxidation (or NO, OH radicals formation) has been conducted in such a small size four-cylinder engine of production geometry other than in relatively large size single-cylinder engines or in special purpose-built machines simulating diesel-like combustion, where it is easier to employ laser techniques due to the use of larger windows. A typical heavy-duty sized diesel engine with several modifications not only on the piston but also on the cylinder wall and cylinder head to provide suitable optical access for laser sheet passage has been used for the application of 2-dimensional laser imaging techniques (Dec *et al.* 1991, 1992, 1995). Two windows for optical access were utilised in their test engines; one is a piston-crown window on a classic extended piston which permits viewing of the whole combustion bowl but not the squish region, and another one fitted at the position of one of the exhaust valves on the cylinder head, which provides simultaneous view of the outer portion of the combustion bowl and the squish region with minimum visual obstruction by soot deposition on the window due to its special position. Additional windows located around the top of the cylinder liner provide the orthogonal optical access required for two-dimensional laser imaging diagnostics, thus allowing the laser sheet to enter and exit the cylinder after passing through the combustion chamber. In addition to the above modifications, one of the valves on the piston crown was cut out to permit the laser sheet to pass the piston bowl near the top dead centre (TDC), resulting in reduction of the compression ratio and some effect on the combustion behaviour. A rapid compression machine having a large sized combustion chamber with two very wide optical windows has also been used to simulate diesel combustion in experiments using 2-dimensional laser techniques (Won *et al.*, 1992; Alatas, 1993). The windows in this machine were located vertically so that quick contamination by soot could be minimised. In both cases, the LII and LIS techniques could be applied even at high load engine test conditions due to the relatively small window fouling by soot deposition experienced in this configuration.

In the present experiment, all tests were conducted at idle conditions to minimise laser power attenuation during passage across the combustion chamber and early deposition of soot on the piston window resulting in attenuation of the image collected. The LII and LIS signals obtained under this test condition over the whole range of crank angles, however, were very weak so that the effect of EGR rate on soot formation was not very clear. Also it should be noted that since there were some difficulties in obtaining the LII, LIS and the natural flame luminosity images simultaneously, each image was obtained separately using different laser power while the engine operating condition was kept the same. Since only one CCD camera

capable of adjusting the exposure time less than 1μs was available for the LII imaging, when the same laser power of 200 mJ was employed for both LII and LIS images simultaneously, the LIS images obtained had much higher intensity compared to the LII images, despite adding two neutral density filters (50/50 and ND1) due to the longer camera exposure time of 1μs. Therefore, a lower laser power of 100 mJ was applied in the case of LIS experiment while the LII experiment was conducted with 200 mJ. It was also very difficult to reject the scattered light from the in-cylinder surfaces and injector tip completely, which caused some noise problems for the LIS images, mainly as a result of some scattered light from the injector tip being superimposed on the presented LIS images. It should be mentioned that the laser sheet entered the piston-bowl always from the bottom of the images shown in this chapter.

The presented images have been selected subjectively from a batch of about 20 images to represent individual crank angles. Even though the in-cylinder pressure and flame images do not show large cycle-to-cycle variations, applying planar laser techniques at the selected test point of 1000rpm/idle does indicate the presence of large fluctuations and selection is necessarily subjective. Averaging techniques can be applied in future analysis but due to the large spatial variations a very large number of images would have to be obtained, processed and finally averaged.

A temporal sequence of spray images obtained with a high speed CCD camera (IMACON 468, which was described in Chapter 2.3.3.1) at 1000rpm, no load condition with 0% EGR rate are shown in Figure 3.9. Two flash lights which are synchronised with the camera were used for illumination. Each six-images of two batches was obtained sequentially from one cycle with a time resolution of 0.4°CA. No clear influence of EGR rate to the spray behaviour was found in the spray images (not shown here) with 50% EGR rate. A temporal sequence of natural flame images, obtained through the piston window in order to estimate the soot distribution from the LII and LIS images, is shown in Figure 3.10, which presents six single-shot-per-cycle images of combustion after the onset of auto-ignition just before 362.88°CA until 373.68°CA for the cases of 0% EGR rate and 50% EGR rate. The flame seems to gradually envelop the region previously occupied by the five spray plumes, with the luminous area gaining in size until 367.20°CA at a faster rate than can be observed during the subsequent relatively slow decrease in luminosity. Concerning the self-illuminated flame images, these are generated when the soot formed during combustion reaches a temperature high enough to emit grey body radiation in the visible part of the spectrum. The lower luminosity in the case of the 50% EGR rate indicates that the temperature does not reach as

high levels as in the case of 0% EGR rate due to the lack of oxygen. This can be interpreted as the soot formation being the dominant mechanism up to 367°CA regardless of the EGR rate, since the largest area of the flame is observed at this crank angle (Figure 3.10). Swirl is observed to rotate in a clockwise direction and the position of the swirl centre is not in the geometric centre, i.e. at the injector, but has moved towards the inlet valve, with this position remaining constant throughout the observation window. While the six flame images in Figure 3.10 were taken at different crank angles from six engine cycles, i.e. one image per cycle, all six images in Figure 3.11 were obtained subsequently in batches from the same cycle with a time resolution of 0.25°CA to detect the start of auto-ignition using an IMACON 468 camera. As deduced from Figure 3.11, auto-ignition occurred at around 362.5°CA by which time fuel injection was almost completed without any significant differences induced by the EGR rate. However, it is likely that ignition timing happened earlier than this crank angle since the chemiluminescence emission which is too weak to be captured with the low intensified camera exists throughout the leading portion of the spray jet prior to the much brighter soot luminosity, according to Dec and Espey (1995).

As already mentioned, the intensity of the LII images is proportional to the soot volume fraction ($\pi Nd^3/6$), while the LIS signal is proportional to the product of the number density N and the sixth power of the particle diameter *d*. Thus the LIS images are expected to have a much greater contrast in intensity than the LII images when a range of soot particle sizes is present, while direct comparison of the two images allows both the relative soot concentration and the soot particle size distribution to be determined. The LII and LIS images (Figures 3.12 ~ Figure 3.15) during the main combustion phase (364.04°CA to 373.68°CA) show parts of the soot cloud passing through the measurement plane at 12.7mm below the cylinder head. The LIS images during the main combustion period show the injector tip roughly in the centre of the piston-bowl with some noise present around the far end of the chamber. Since the pulsed laser was used as the light source, only one LII or LIS image can be obtained for each combustion event. To examine the cycle-to-cycle variations of the soot images, three images taken from different runs have been selected for analysis. The soot distribution and concentration differ a little but in general resemble each other. Overall it can be said that this engine operating condition results in little soot formation and hence the signal is rather weak. As a result, the flame-like shaped images cannot be obtained as would be expected by LII and LIS although the usual problems of laser and signal attenuation due to the presence of dense soot clouds are not important here. At 364.04°CA in the LII images, little

soot was detected around the leading portion of the flame jet which does not coincide exactly with the sooting regions seen in the LIS images, where soot is present at the upstream side of the flame as well as at the edges of the flame. It has been reported by Won *et al.* (1992) that soot is mainly formed in the periphery of the flame tip. Since the LII and LIS images for 50% EGR rates show relatively similar soot distribution pattern but higher soot concentrations than for the 0% EGR rates over the whole period, the soot formation and oxidation seem to be little influenced by EGR despite the reduction in the oxygen concentration at this engine condition. At 367.20°CA, at which the natural flame luminosity images show the largest area of the flame, soot concentration increases as would be expected. In the images at the following crank angles (369.36°CA and 373.68°CA) the flame area is reduced but the soot concentration increases slightly for both LII and LIS; this increase is more pronounced at the 50% EGR rate than at 0% which could be the result of reduced soot oxidation rate expected at 50% EGR. Also the soot distribution tends to move towards the centre of the flame, especially in the LIS images. The LII and LIS images indicating the changes in soot concentration after the main combustion period at 0% and 50% EGR rates are shown in Figures 3.16 and 3.17, respectively. It should be noted that the LII and LIS images after main combustion were obtained at different test conditions from the previous one; fuel delivery was doubled to 12mm^3/st, since the LII and LIS signals were too weak to be visualised due to the very low soot concentration on the measurement plane. Similarly to the main combustion period, higher soot concentration, but not much higher, is observed for 50% EGR than for 0% EGR. At 490°CA when the combustion phase is completed and no more soot oxidation occurs, it is considered that the remaining in-cylinder soot concentration has a close correspondence with the level of exhaust smoke or particulates. Hiroyasu *et al.* (1980) have argued that the exhaust smoke level is mainly determined by the concentration of soot in the cylinder at the time of exhaust valve opening. The correlation between the in-cylinder effects of EGR and the exhaust gas concentration has been investigated by Shimazaki *et al.* (1996) by comparing in-cylinder gas sampling with exhaust gas measurements; during the main combustion phase the in-cylinder soot concentration was not found to represent the trends expected with increasing EGR at the engine exhaust but after 12°CA aTDC the soot levels started showing similar trends to the exhaust particulate emissions, i.e. increasing Bosch smoke number with increasing EGR rates; the in-cylinder NO_x concentration was found to be at similar levels for 0% to 23% EGR rates until about 9°CA aTDC after which the NO_x concentration increased for 0% and 11% EGR rates but remained relatively constant for the 23% EGR rate, showing

similar trend to the exhaust NO_x measurements. In general, it seems that the emission trends caused by EGR at the engine exhaust are linked to the in-cylinder emission concentration but only after about 12°CA aTDC, while Li and Wallace (1995b) have showed that the exhaust levels are reached at about 50°CA aTDC following the formation of a rather homogenous gas mixture in the combustion chamber at about 30°CA aTDC ~ 35°CA aTDC. In the present experiment, any significant differences, however, between two different EGR rates can not be observed due to the low soot concentration at idle conditions and the reduction in soot density resulting from the increase of the cylinder volume during the expansion stroke. It is considered that a certain level of soot concentration is required for the investigation of the temporal and spatial variation of the soot formation and oxidation using planar laser diagnostics such as LII and LIS; thus at least partial load test conditions should have been employed for better results. Alatas *et al.* (1993) have concluded that no soot images can be obtained by the laser induced incandescence or Mie scattering method before 20 degrees aTDC since the soot concentration is rather low. On the other hand, in order to use the LII and LIS techniques at higher loads, any windows should be positioned either vertically against the combustion chamber or above the combustion chamber in order to prevent fast window fouling by the relatively high concentration of soot particles under these engine conditions.

3.5 SUMMARY

The objective of this experiment was to investigate the effect of EGR on soot formation and oxidation by applying the LII and LIS techniques to the four-cylinder diesel engine. These techniques required a lot of care in setting up the experimental system, especially in the optical configuration for transforming the laser beam into a very thin but well distributed flat sheet and for receiving the very weak LII and relatively strong LIS signals. Considerable attention was also required to exclude electrical noise and the natural flame luminosity from the LII signal and rejecting the elastic scattered light, from in-cylinder surfaces and injector tip, from the LIS images. It also proved difficult to achieve synchronisation in the timing of the camera and the laser with the engine, since the laser sheet had to be transmitted through the very thin, 3mm in thickness, sandwich-type window inserted in the piston while the detectable LII signal lasted only for about 10ns. As a result, the LII/LIS images obtained under idle conditions have provided relatively limited information concerning the overall

effect of EGR on soot formation/oxidation. The main conclusions can be summarised as follows;

1. The soot formation and oxidation seem to be little influenced by EGR during the main combustion phase under idle conditions despite the reduction in the oxygen concentration.
2. The maximum soot concentration in the LII and LIS images was observed later than the time of maximum flame area development (367.20°CA).
3. Similarly to the main combustion period, the soot concentration was slightly higher at 50% EGR than at 0% EGR at the end of combustion phase (490°CA).

Description	Test Conditions
Engine speed [rpm]	1000
Load (BMEP) [bar]	idle
Fuel injected / per cylinder [mm³|mg]	6 | 5
Injection Frequency [Hz]	8.3
Start of injection, average [°CA]	357.68
End of injection, average [CA]	362.13
Injection duration, average [ms|°CA]	0.74 | 4.45
Swirl ratio	3.9
EGR rate	0% 30% 50%
Intake mass flow rate of air [kg/h]	55 | 39 | 28

Table 3.1 Test conditions for LII and LIS experiment

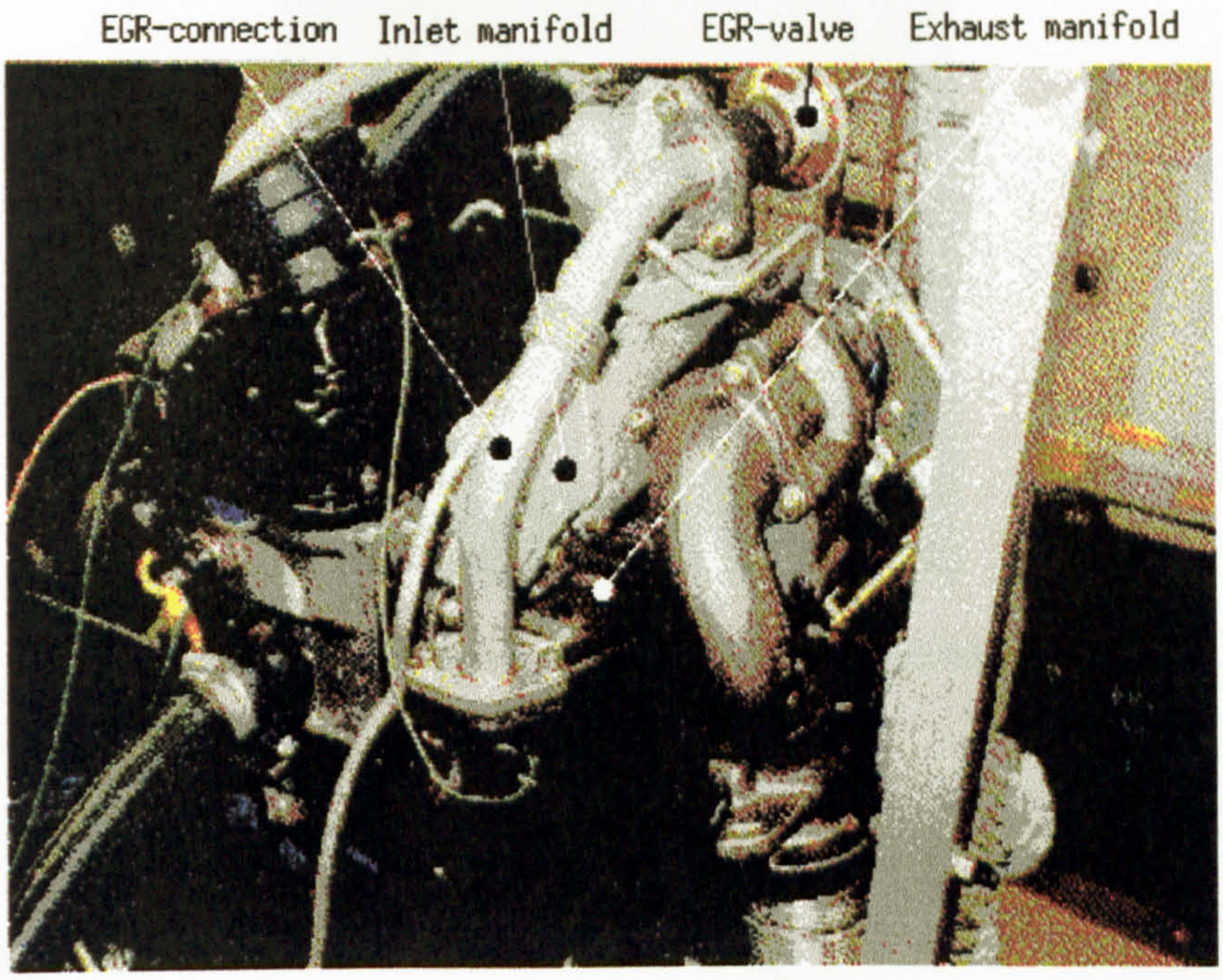


Figure 3.1 Photograph of the exhaust gas recirculation system in VW 1.9L HSDI diesel engine

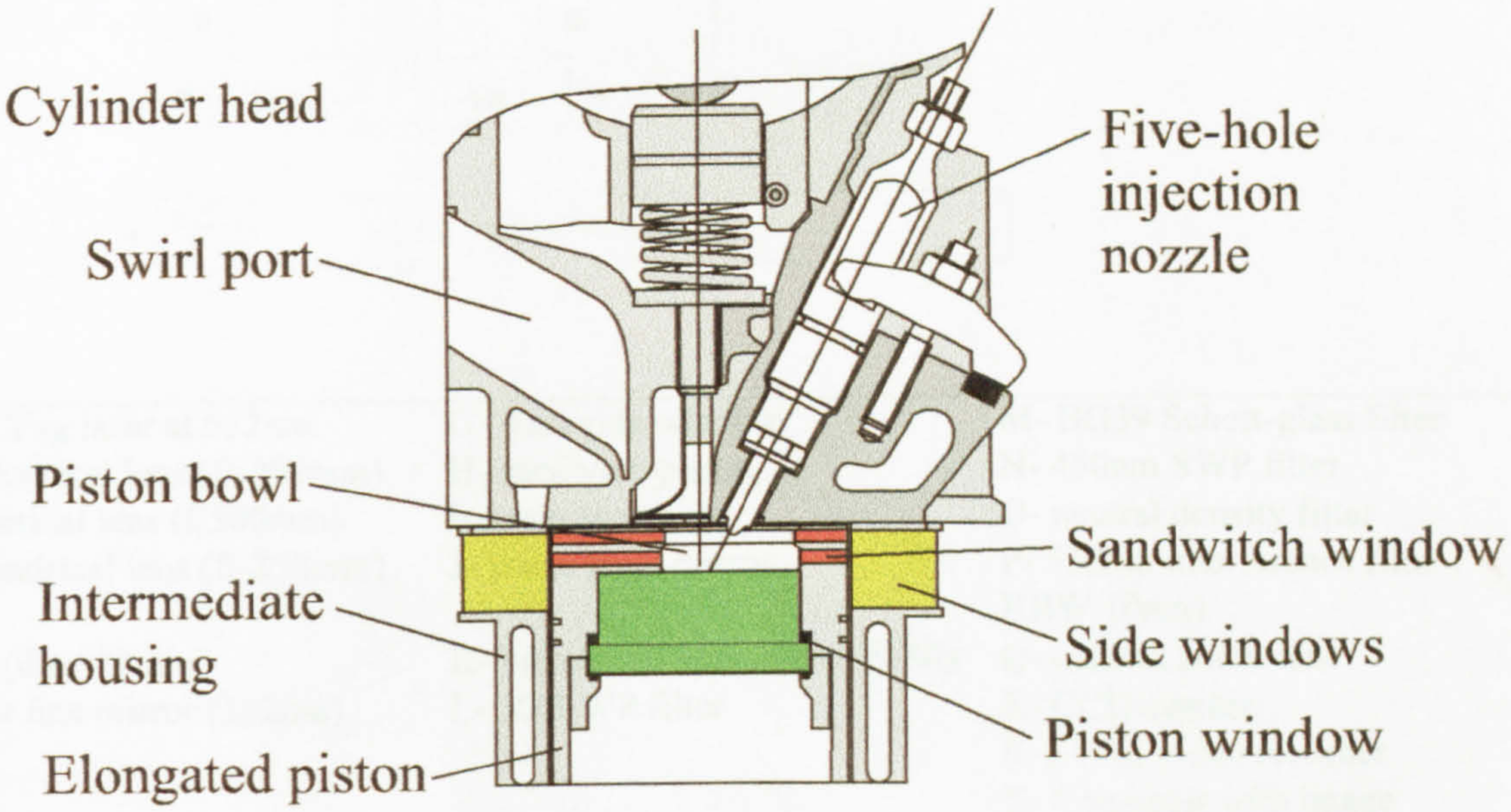


Figure 3.2 Cylinder head and piston-bowl geometry of VW 1.9L HSDI diesel engine: optical access through quartz side-window in the liner and a pair of quartz plates in the piston-bowl side wall

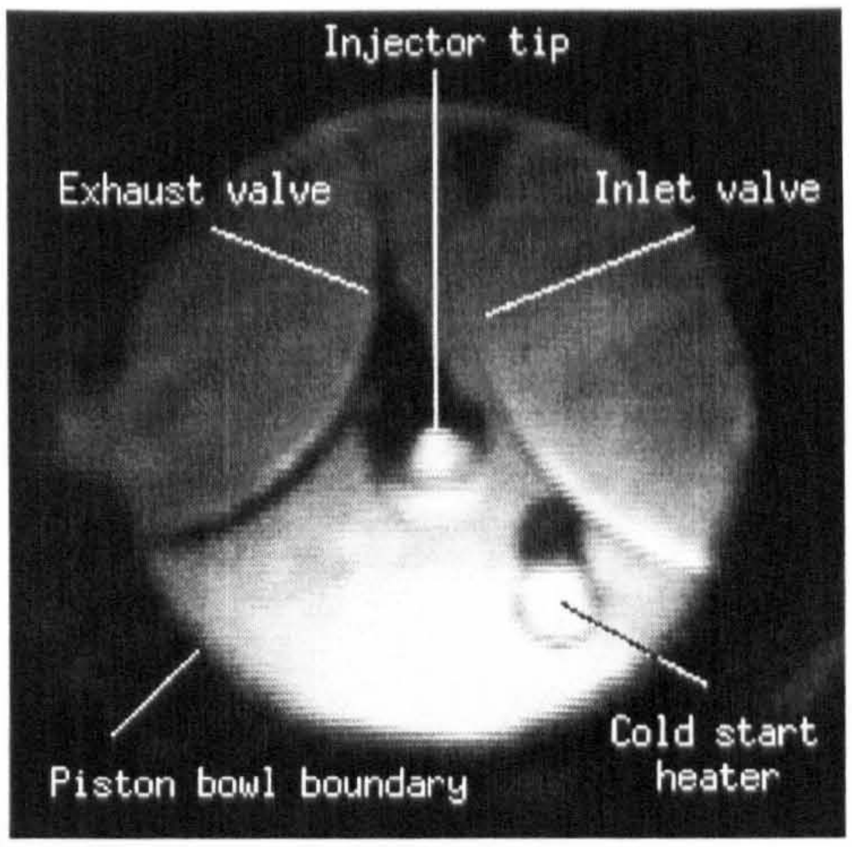
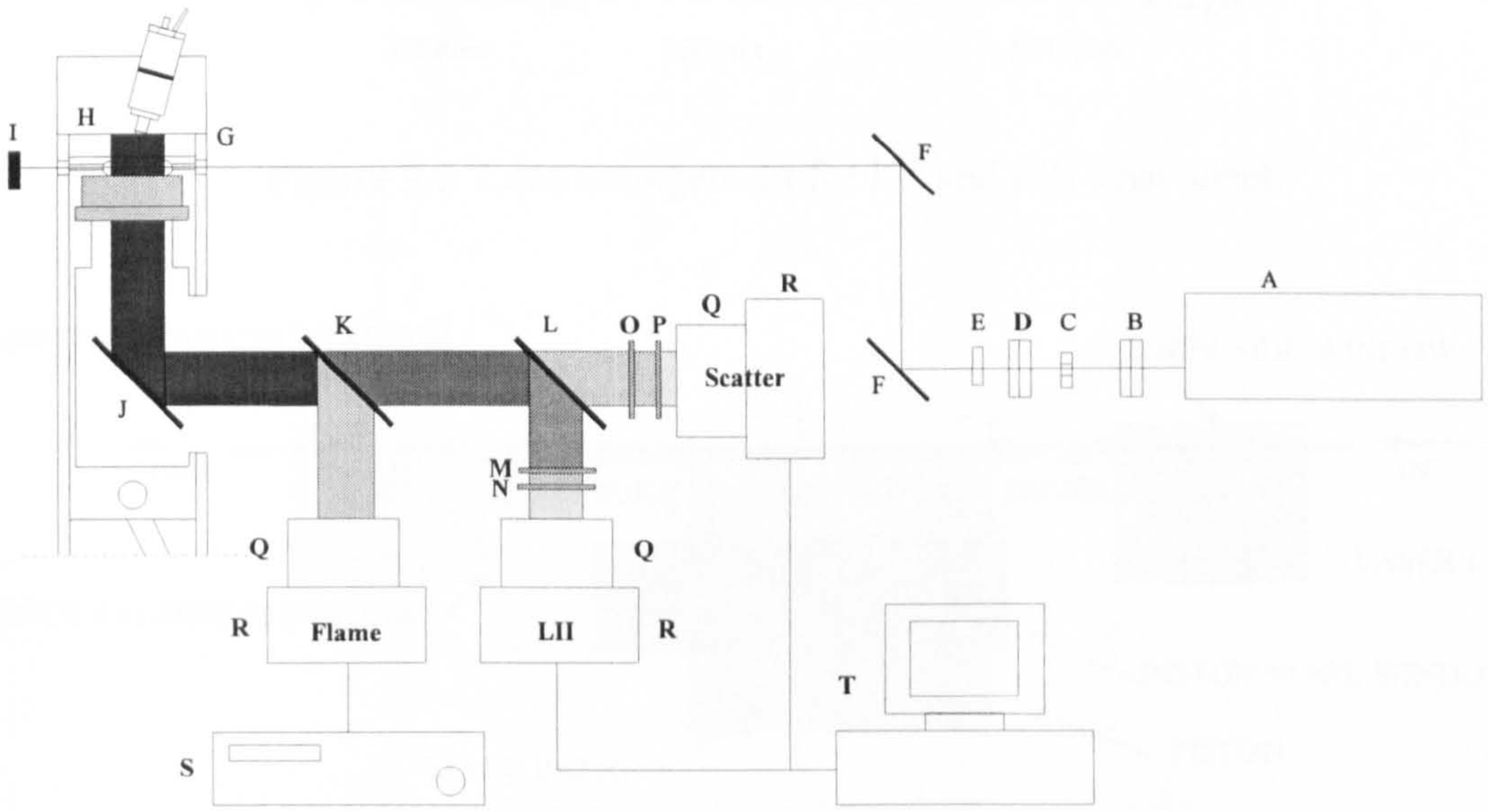


Figure 3.3 Piston-bowl image with identified landmarks.



A- Nd:Yag laser at 532nm	G- liner side window	M- BG39 Schott-glass filter
B- cylindrical lens (f/-200mm)	H- sandwich piston	N- 450nm SWP filter
C- spherical lens (f/500mm)	I- beam stop	O- neutral density filter
D- cylindrical lens (f/-250mm)	J- broad band mirror	P- 532nm interference filter (HBW 10nm)
E- iris (dia.: 20mm)	K- broadband beamsplit (20/80)	Q- camera zoom lens
F- laser line mirror (532nm)	L- 500LWP filter	R- CCD camera
		S- SVHS video recorder
		T- Computer with image acquisition system

Figure 3.4 Experimental set-up for the LII and LIS experiment

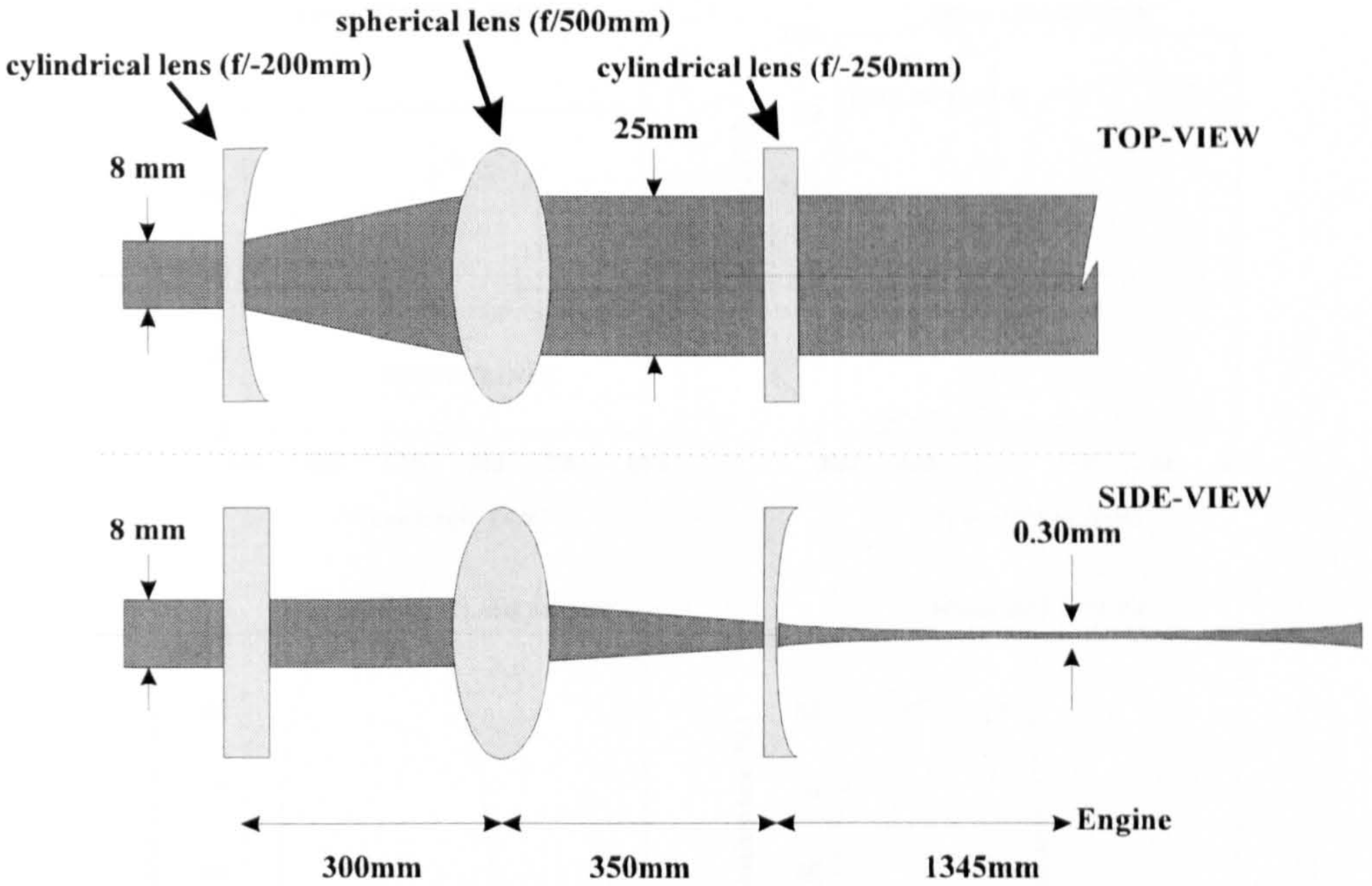


Figure 3.5 Lens arrangement for LII and LIS laser sheet.

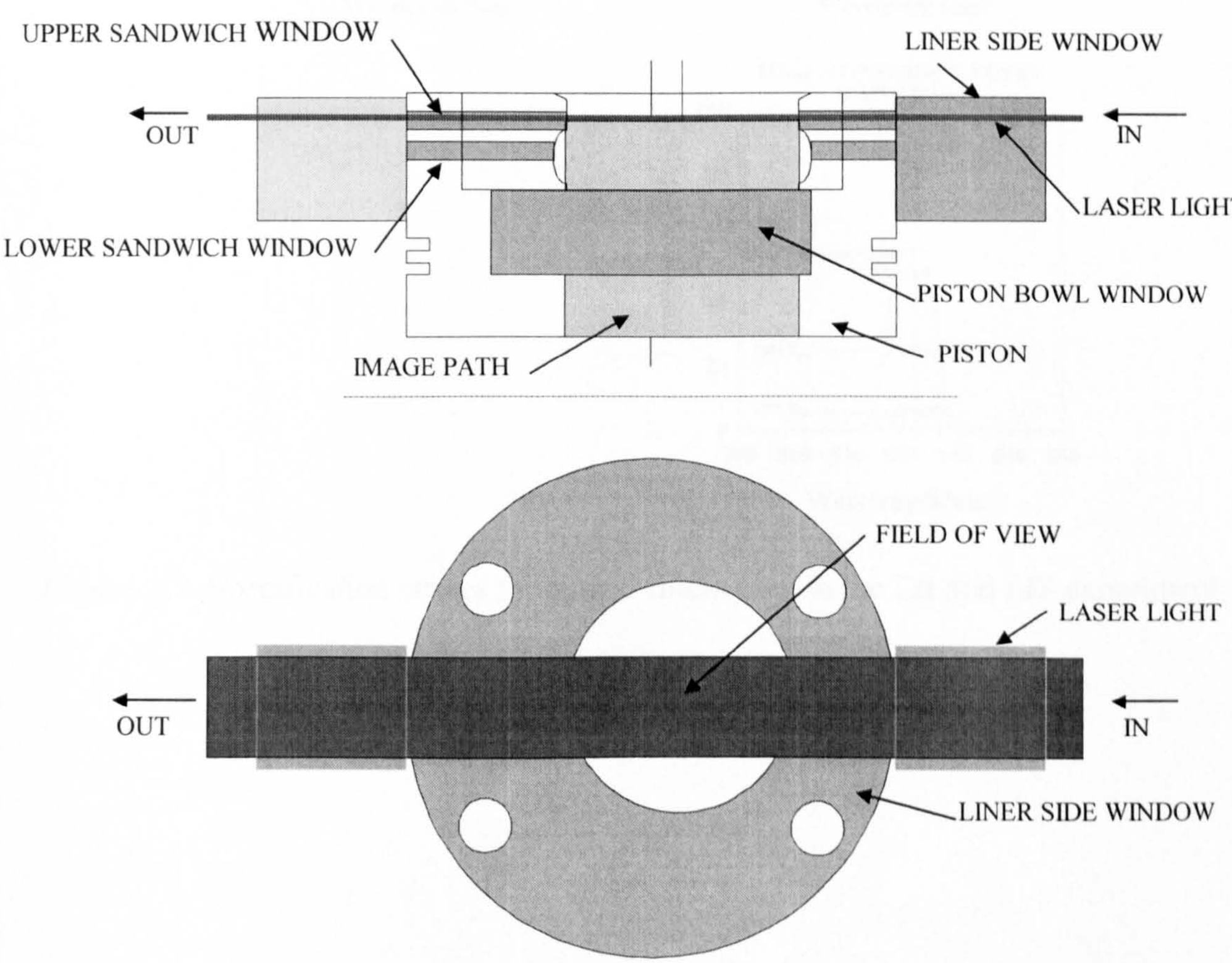


Figure 3.6 Optical access into the test engine.

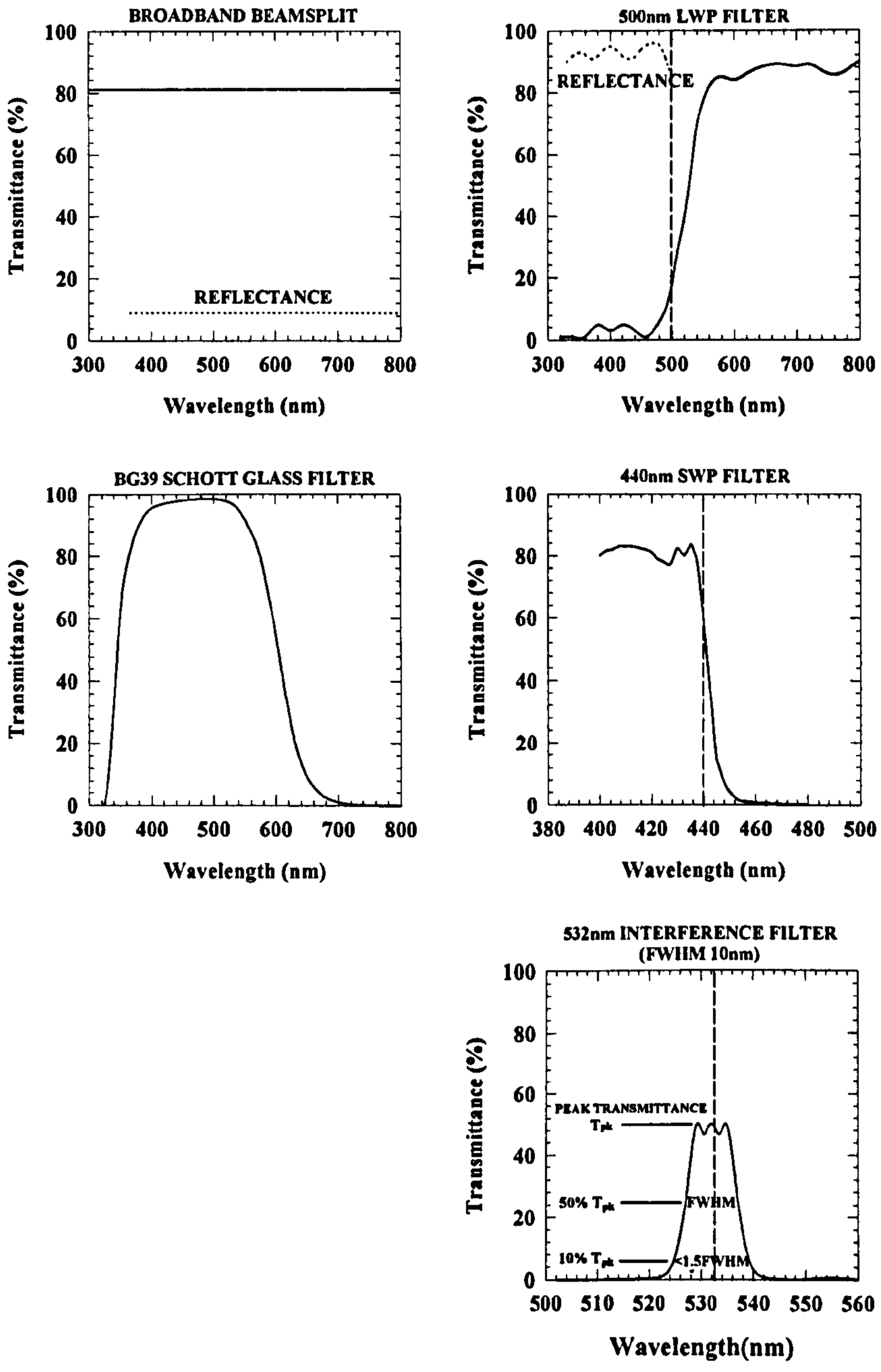


Figure 3.7 Specification curves for optical filters used in the LII and LIS experiment.



Figure 3.8 Unmodified (left) and processed (right) LIS image.

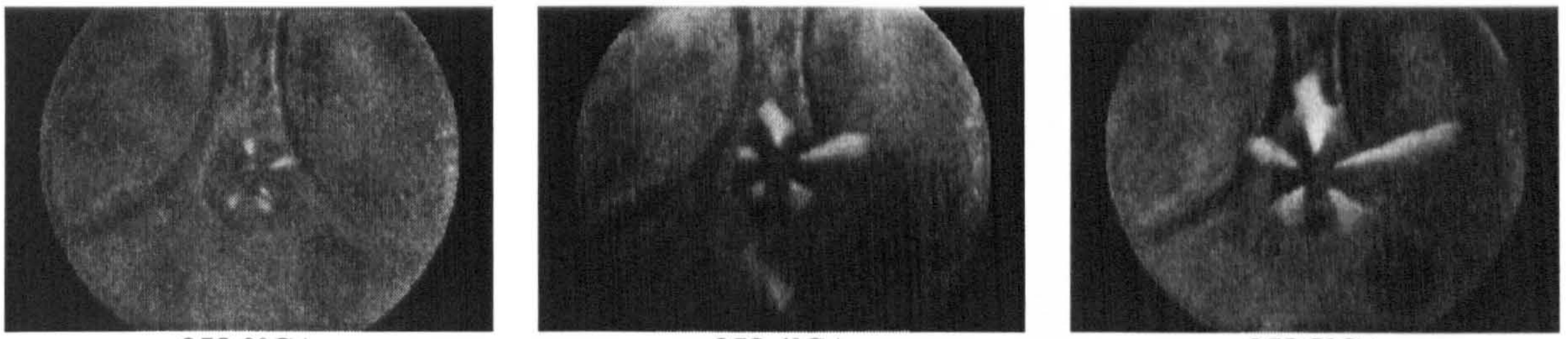
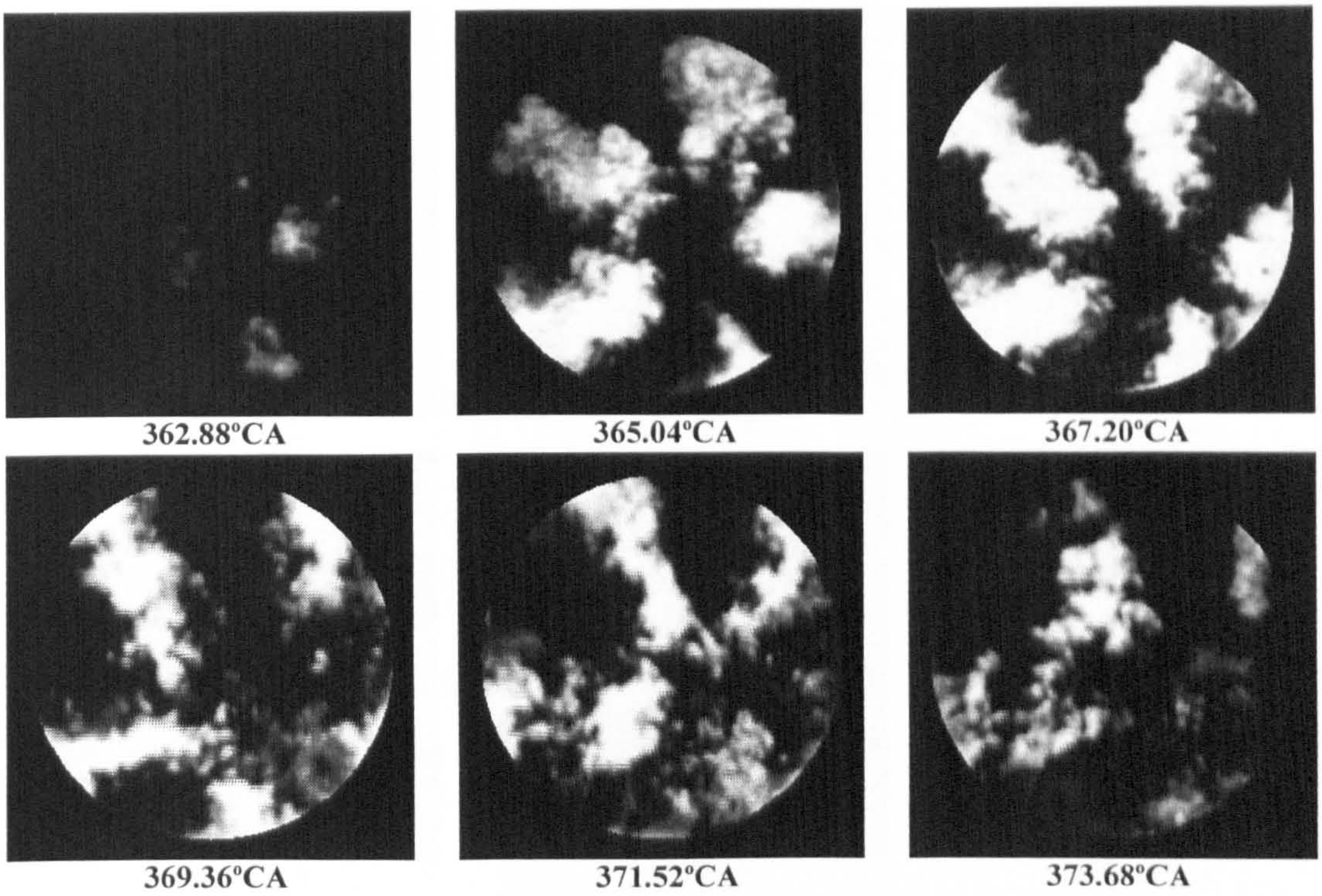


Figure 3.9 Spray images obtained with high-speed CCD camera (IMACON 468) at 1000rpm with 0% EGR rate

0% EGR



50% EGR

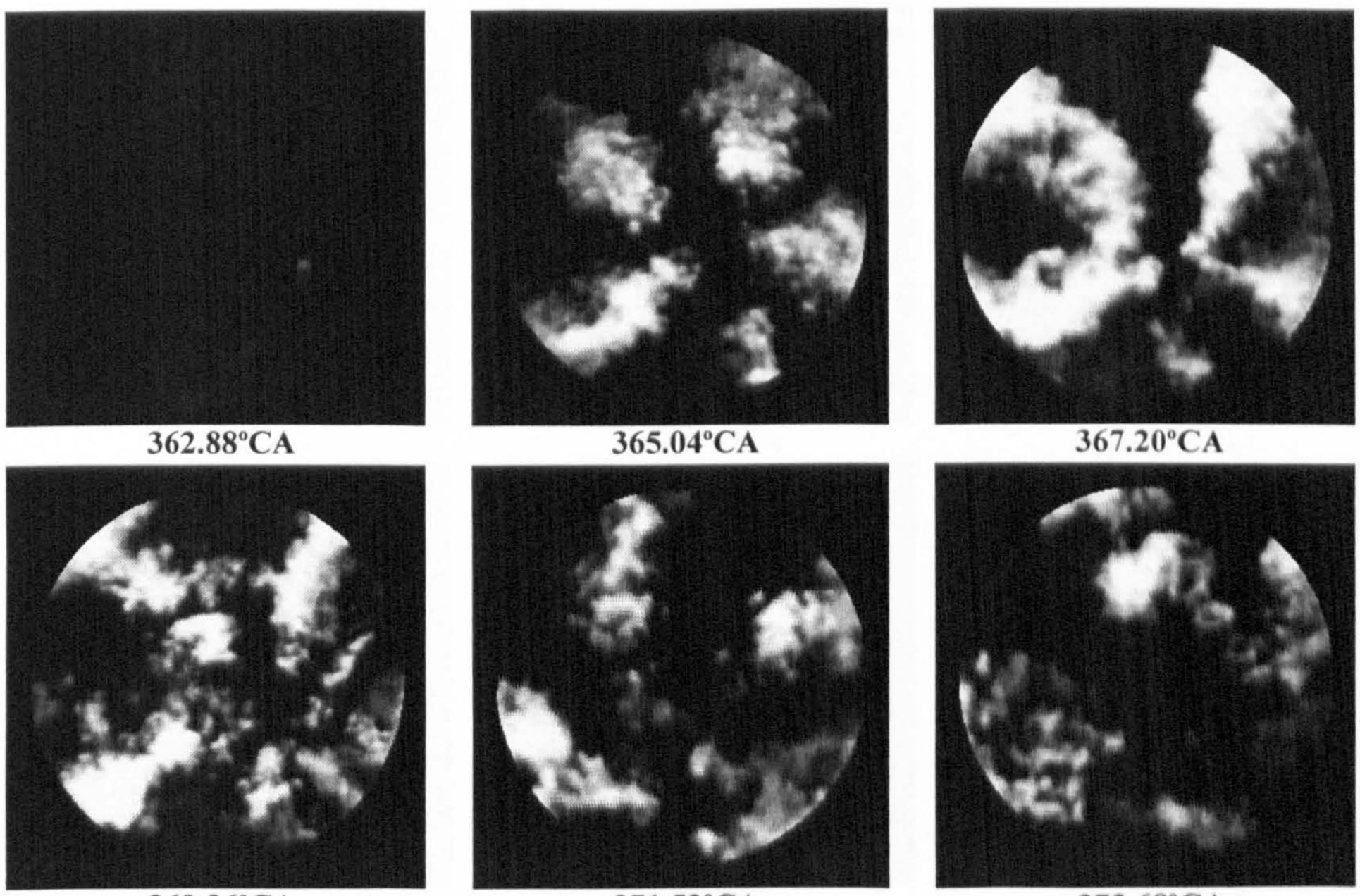


Figure 3.10 Flame images obtained with high-speed CCD camera at 1000rpm

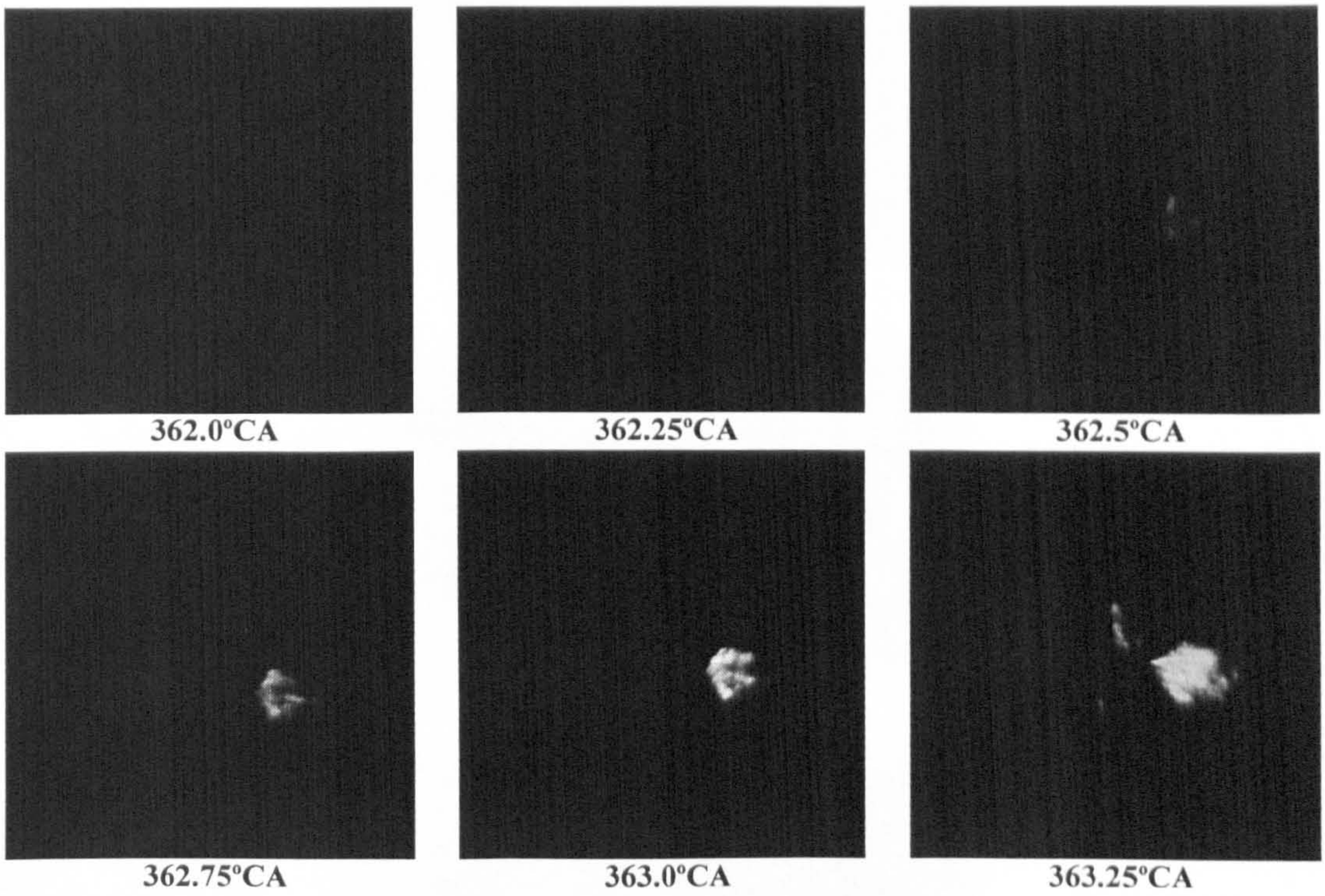
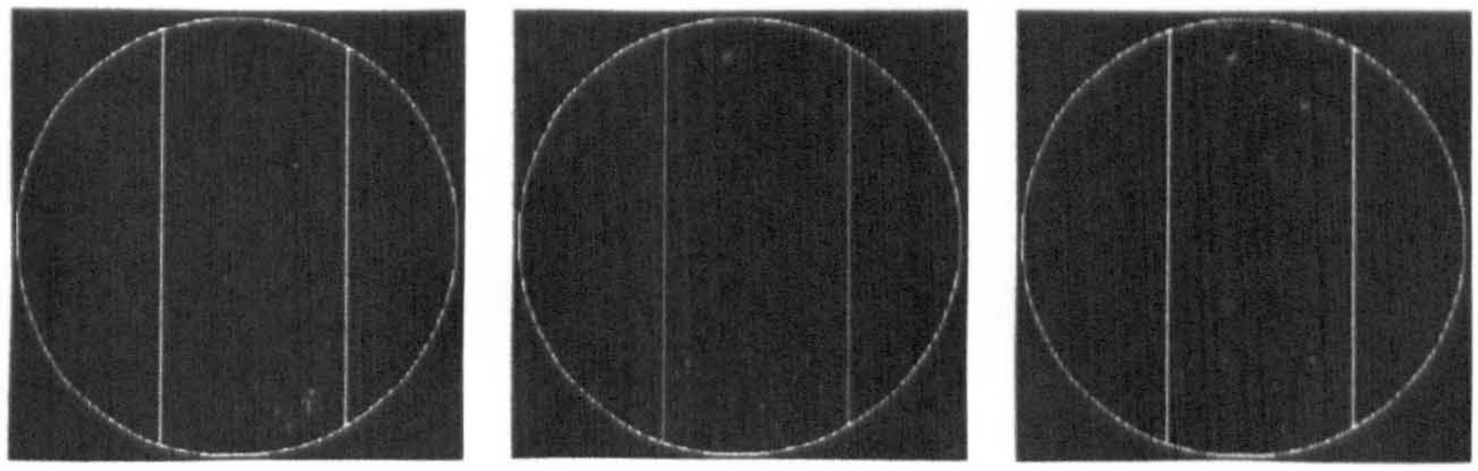
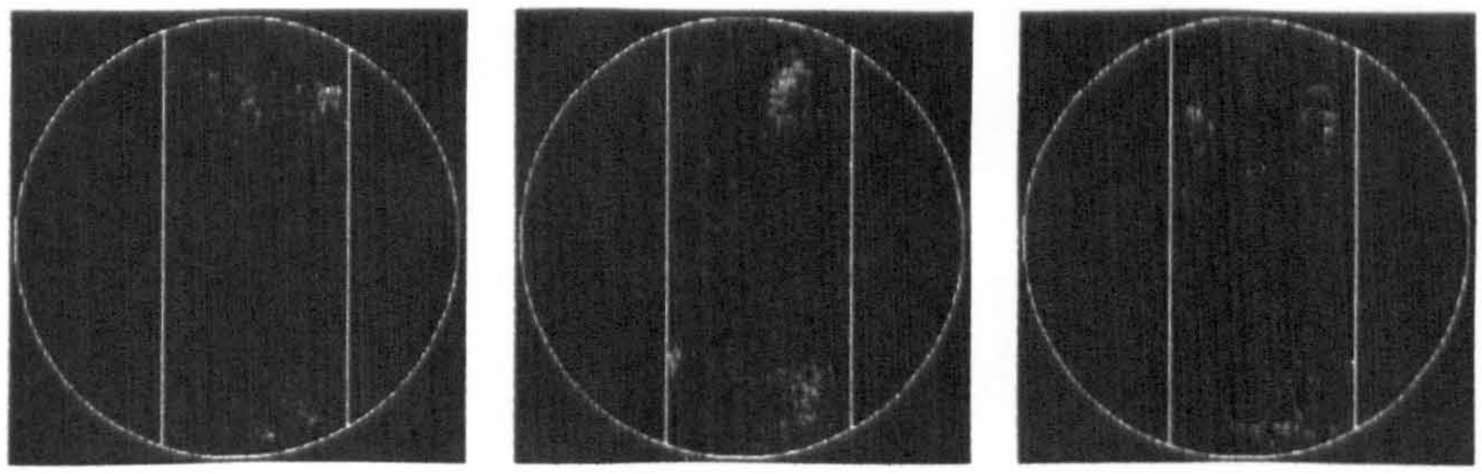


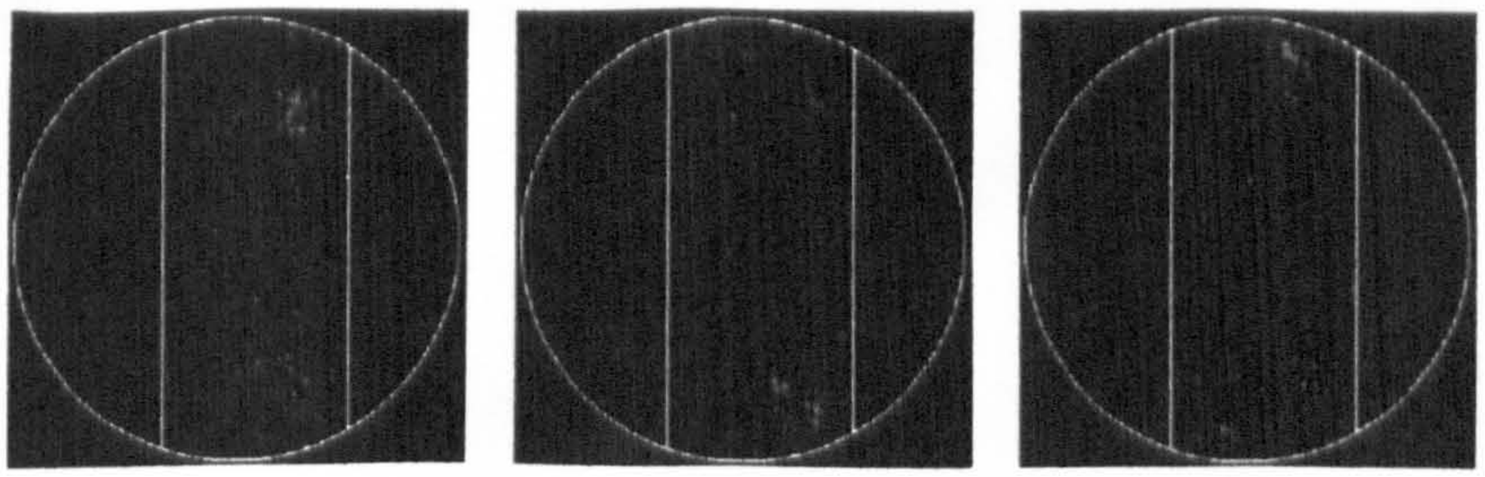
Figure 3.11 Flame images obtained with high-speed CCD camera (IMACON 468) at 1000rpm with time resolution of 0.25°CA



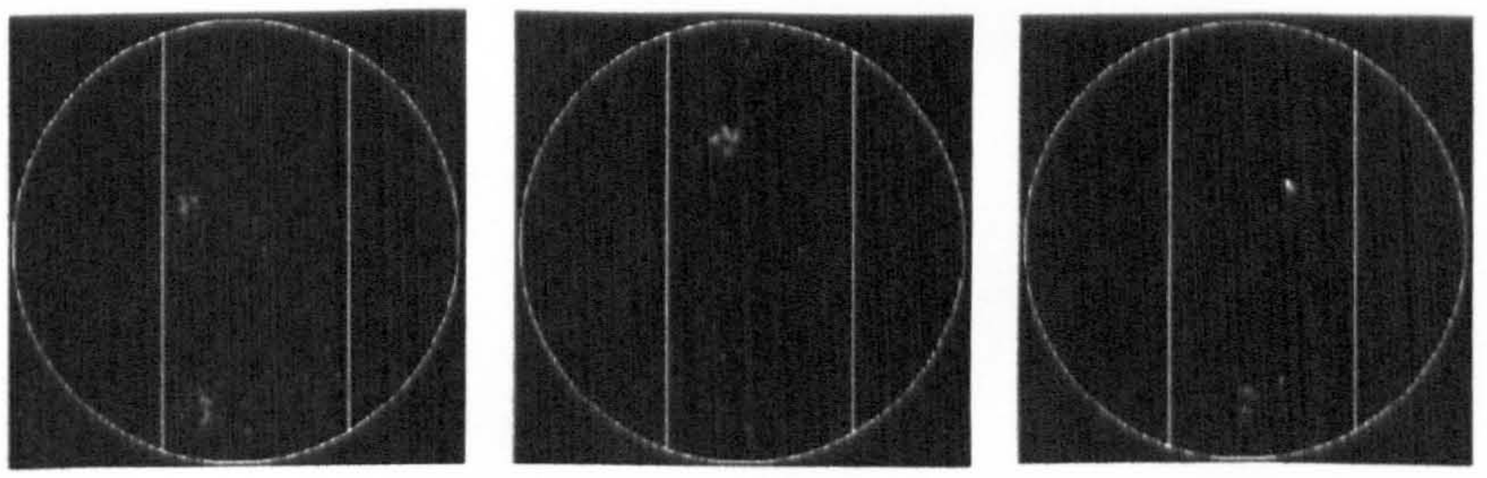
364.04°CA



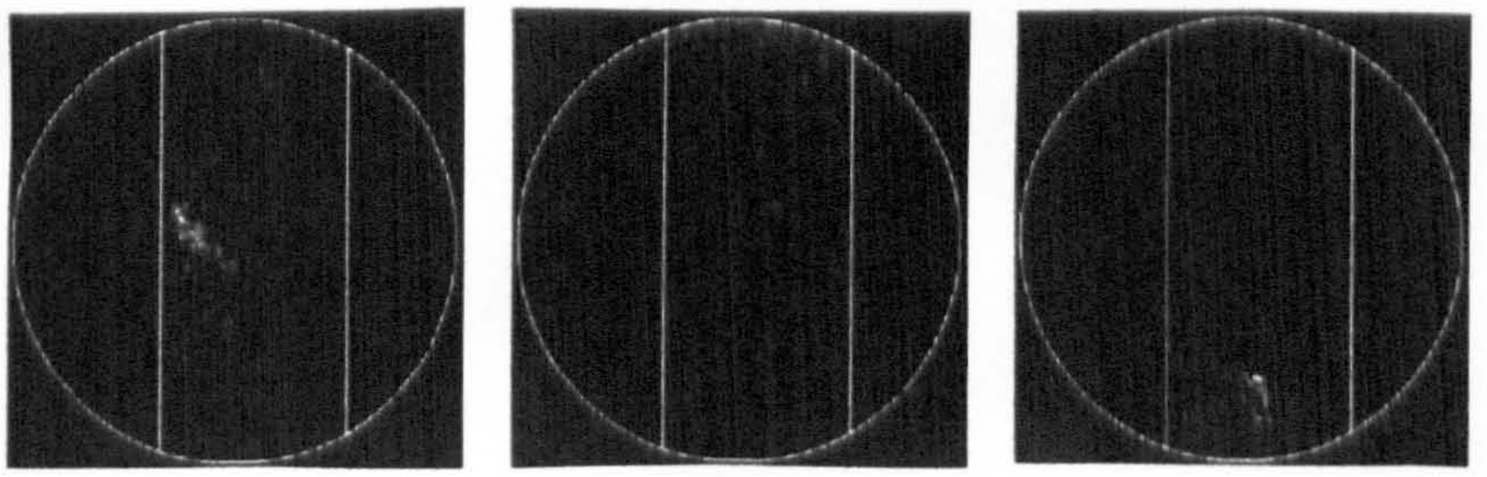
367.20°CA



369.36°CA

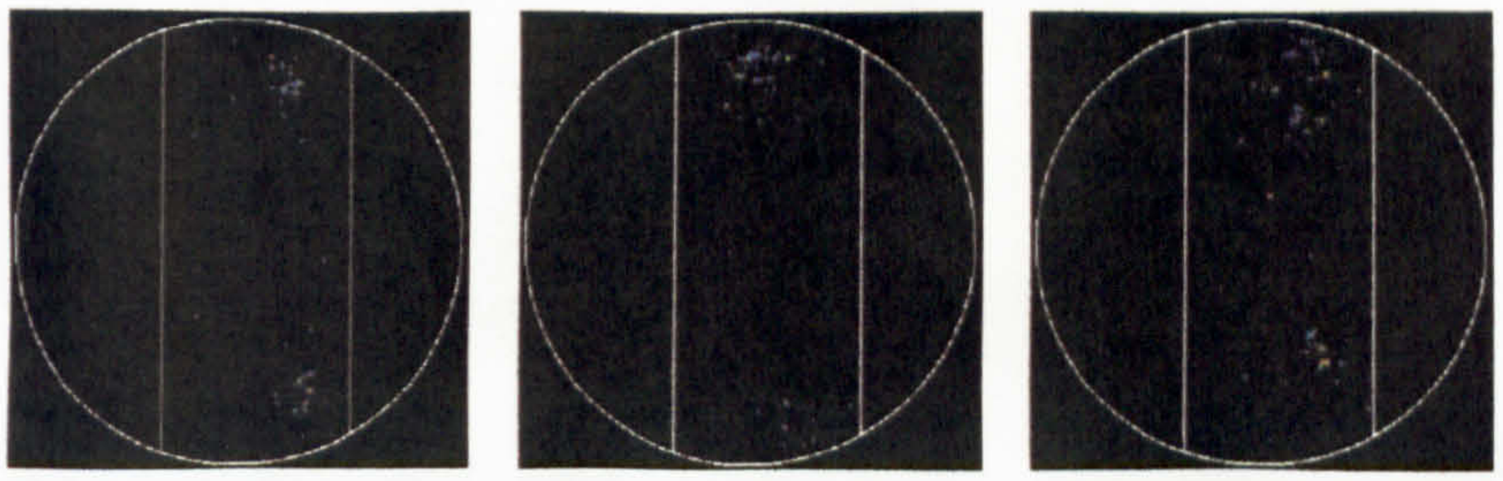


371.52°CA

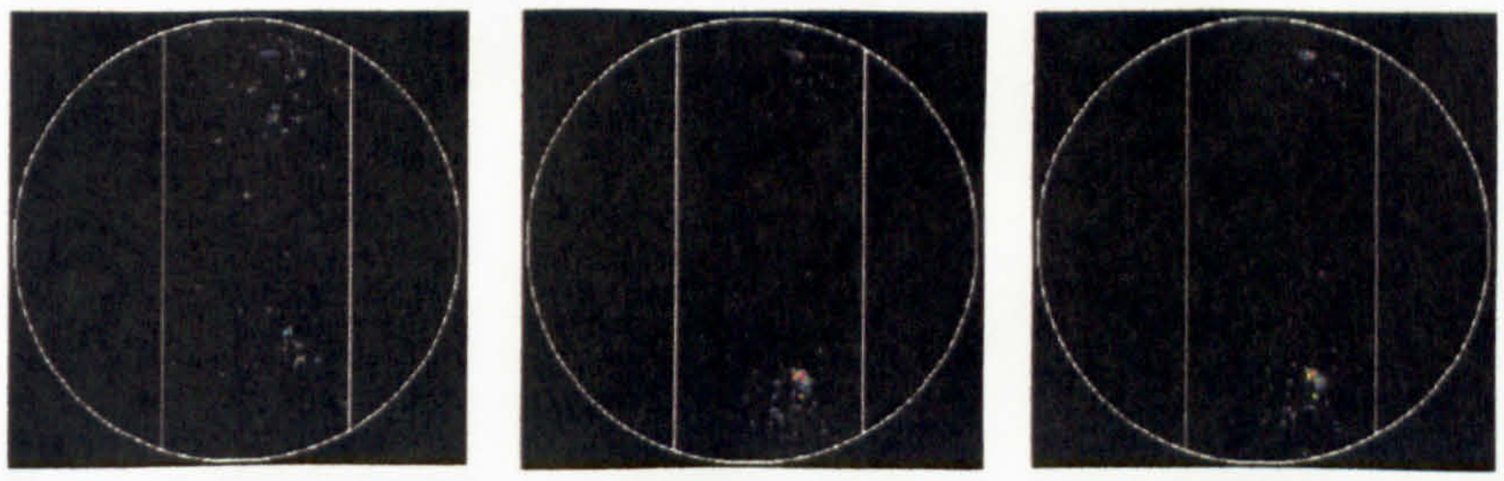


373.68°CA

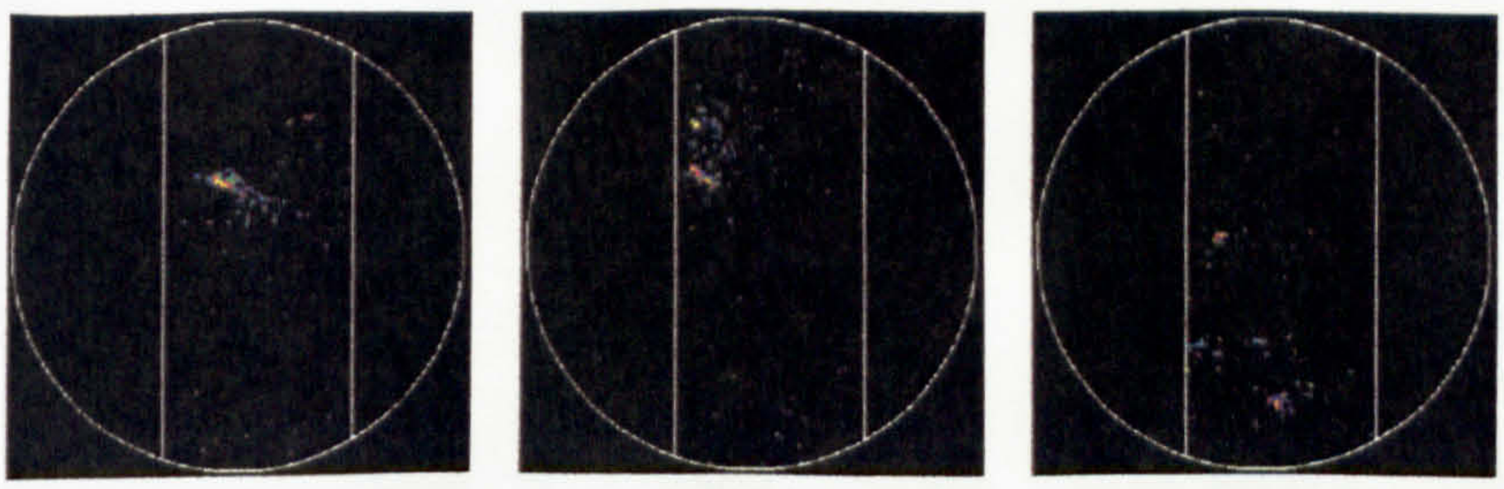
Figure 3.12 Cycle-to-cycle variation of LII images at 1000rpm with 0% EGR rate during main combustion period



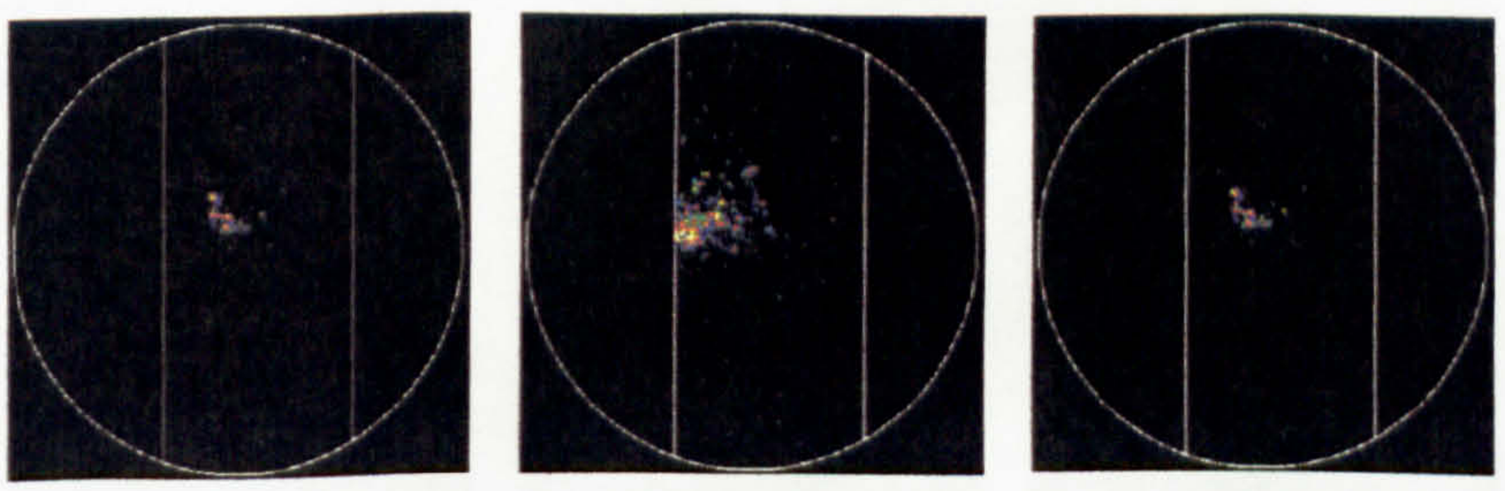
364.04°CA



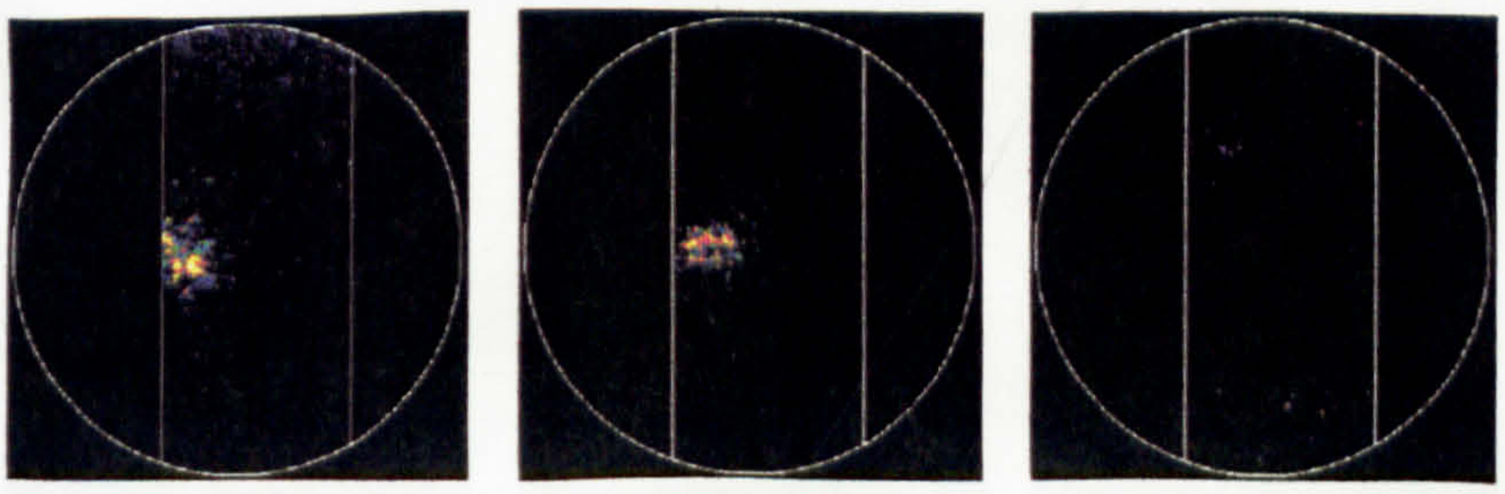
367.20°CA



369.36°CA

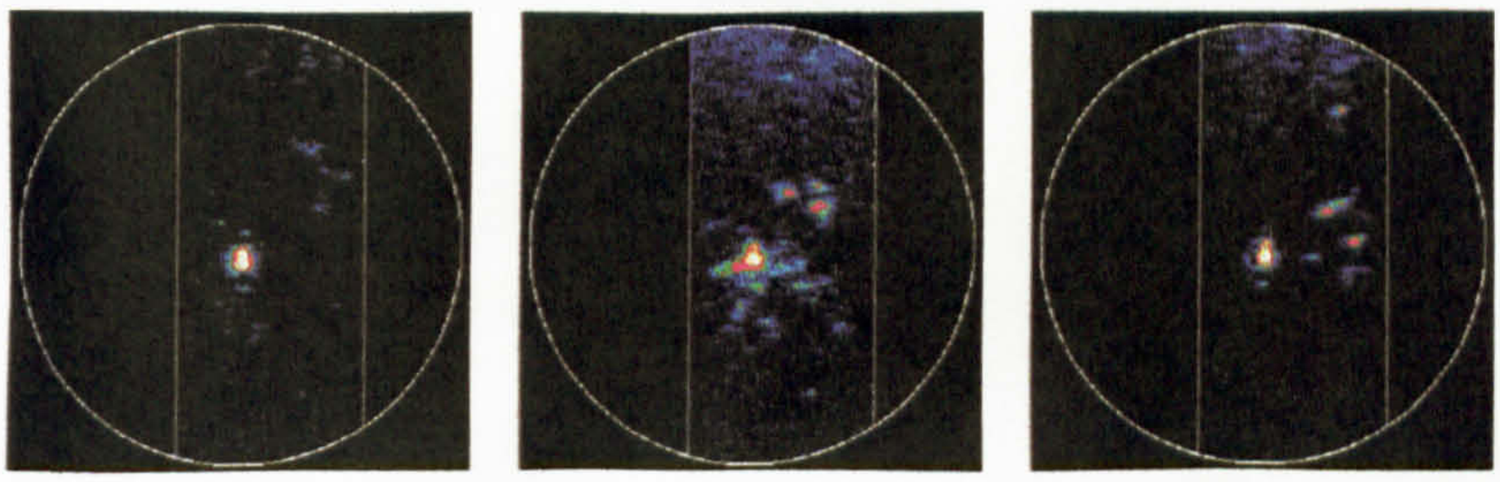


371.52°CA



373.68°CA

Figure 3.13 Cycle-to-cycle variation of LII images at 1000rpm with 50% EGR rate during main combustion period



365.04°CA

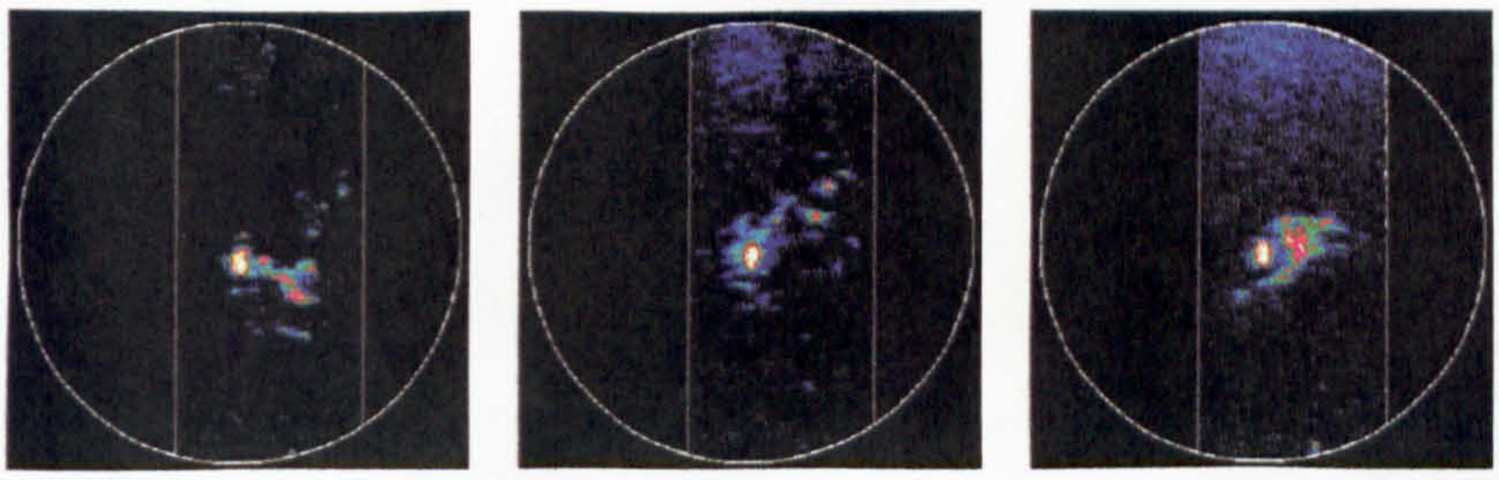
367.20°CA

369.36°CA

371.52°CA

373.68°CA

Figure 3.14 Cycle-to-cycle variation of LIS images at 1000rpm with 0% EGR rate during main combustion period



365.04°CA

367.20°CA

369.36°CA

371.52°CA

373.68°CA

Figure 3.15 Cycle-to-cycle variation of LIS images at 1000rpm with 50% EGR rate during main combustion period

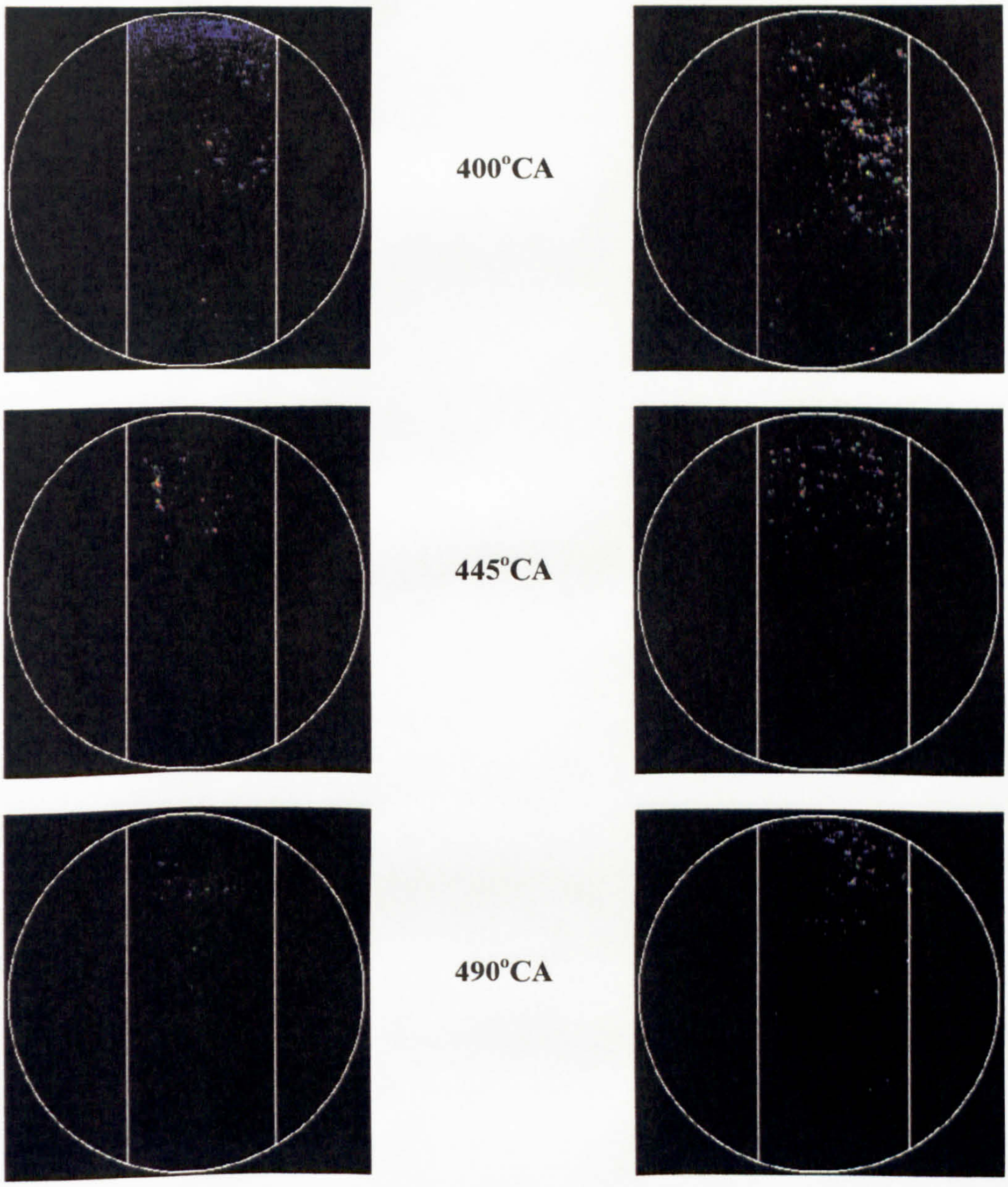


Figure 3.16 LII images at 1000rpm with 12mm^3/st of fuel delivery after main combustion

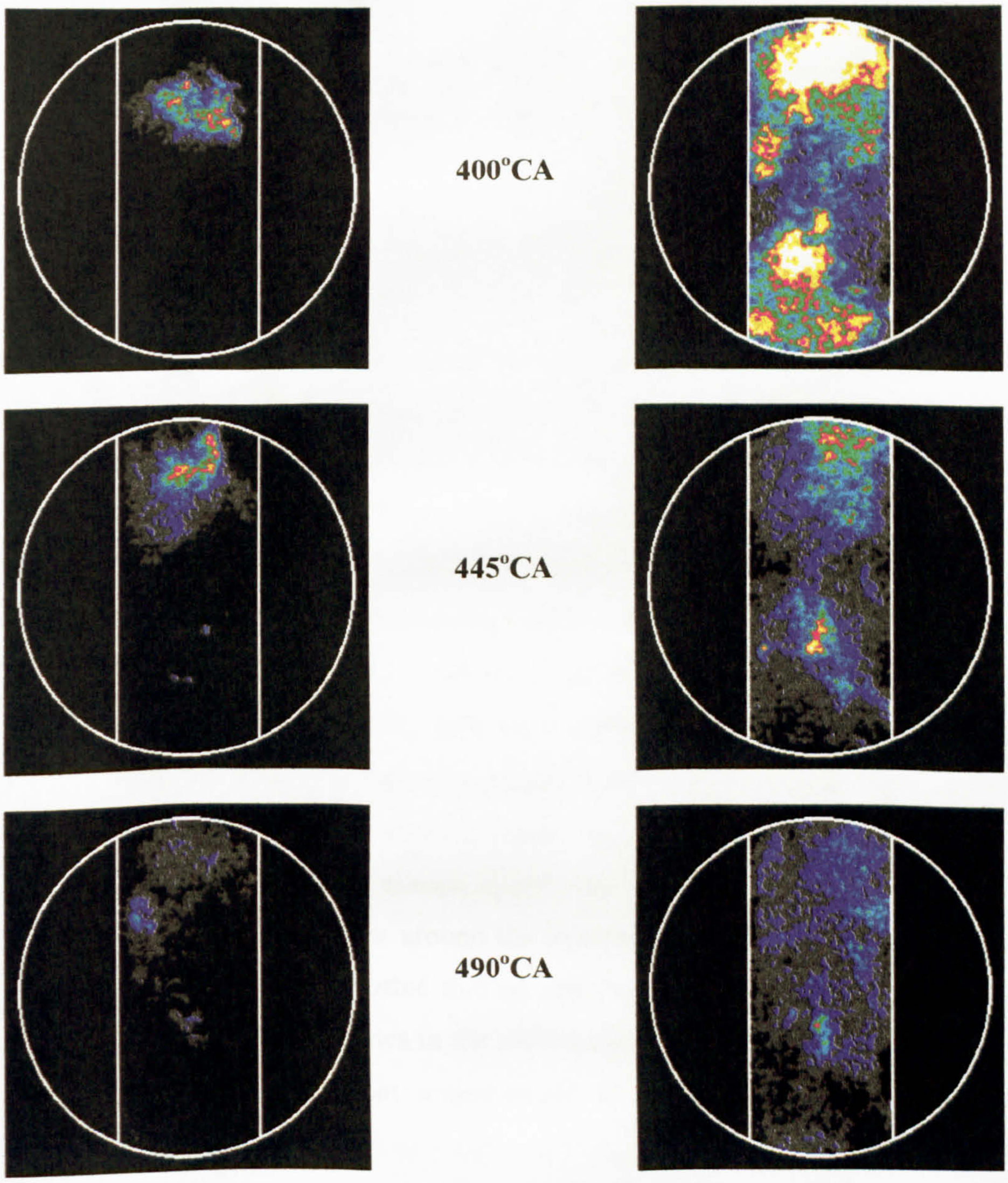


Figure 3.17 LIS images at 1000rpm with 12mm^3/st of fuel delivery after main combustion

CHAPTER 4

THE ROLE OF FUEL INJECTION PARAMETERS IN DIRECT-INJECTION DIESEL ENGINES

4.1 INTRODUCTION

Over the last few years, most investigations on diesel engines have focused on ways to reduce particulate and NO_x emissions without any deterioration in fuel economy. As a result, a new engine configuration for future emission regulations has been suggested involving turbocharging and intercooling, sophisticated EGR control and a passive De-NO_x catalyst and based on a 4-valve cylinder head with central vertical injector connected to an electronically controlled high pressure injection system. It is well known that EGR is effective in reducing NO_x emissions, but the problems of EGR are increased particulate emissions, reliability of engine parts due to increased wear, and difficulty of using high EGR ratios in turbocharged engines (Vaert *et al.*, 1996). There is also evidence that supercharging is effective in increasing engine power without deterioration in particulate and NO_x exhaust emissions.

The 4-valve cylinder head allows larger valve annular area than 2-valve heads and improved cooling in the central area around the injector, which leads to higher specific power output. Herrmann *et al.* (1995) reported that an improvement in volumetric efficiency of up to 8% can be achieved in 4-valve engines in the medium and high speed range. They also observed that this contributed to a significant improvement in engine performance, of up to 25% at constant smoke levels in comparison to 2-valve engines, and that this could be further improved with an advanced fuel injection system. Since the combustion piston bowl is located centrally in 4-valve engines, due to the symmetrical squish area the flow field is more regular in the axisymmetric piston bowl than in the eccentric piston bowl of 2-valve engines which reduces the requirement for high intake swirl levels. This implies that each spray from the multi-hole nozzle has similar interaction with the air motion giving rise to symmetrical air entrainment. In addition, since a symmetrical combustion chamber layout can be achieved with a truly vertical and central injector, the penalty associated with inclination of the injector can be eliminated. All fuel sprays from a vertical injector installed at the centre of the cylinder are expected to have similar development and the corresponding air-fuel mixing rates to be also similar. This improved fuel distribution leads to a nearly optimal mixture formation and combustion with lower smoke levels

and better fuel consumption. This more uniform combustion can be achieved without local hot spots while keeping the mean flame temperature similar, thus contributing to reduction of NO_x emissions (Shiozaki *et al.*, 1998). There are three possible geometric arrangements of the gas exchange ports in a 4-valve engine; twin, tandem and twisted design, which depend on the valve position relative to the crank shaft axis and the arrangement of the ports. Different arrangement provides different swirl levels and air flow efficiency, which both affect engine performance and exhaust emissions.

Soot and NO_x formation along with engine noise are highly dependent on the combustion process. Therefore, precise control over the fuel injection and spray formation is essential in making improvements to the combustion process. Raising the injection pressure and optimising the nozzle hole diameter have proven to be an effective strategy to reduce particulate emissions due to improved atomisation of the fuel and enhanced air fuel mixing.

Spray characteristics such as droplet size, spray cone angle, spray penetration, and liquid exit velocity are the most important parameters affecting atomization and air fuel mixing. The fuel droplet size and velocity in diesel sprays has been measured (Hardalupas *et al.*, 1992) and its effect on combustion and exhaust emissions has been investigated. Higher injection pressure has been demonstrated to produce sprays with smaller overall droplet sizes (Su *et al.*, 1995; Su and Farrell, 1998). Verhoeven *et al.* (1998), Naber and Sieber (1996), and Farrell *et al.* (1996) have investigated the effects of injection pressure on spray characteristics and found that liquid phase spray angle decreases with increasing injection pressure at high temperatures, while vapour phase spray angle is not affected by injection pressure. They also found that liquid and vapour penetration were affected little by injection pressure, while the liquid and vapour penetration rate increases with increasing injection pressure. Karasawa *et al.* (1991), and Su *et al.* (1995) found that a sharp edge-nozzle inlet gives smaller droplet sizes, longer spray tip penetration, and a narrower spray cone angle than a rounded inlet nozzle for the same mean injection velocity. Any changes in the spray characteristics affect the ignition and combustion process, thus controlling particulates and NO_x emissions. Sundoh *et al.* (1992) reported that high pressure injection resulted in shortened ignition delay but its contribution to NO_x reduction was very small at the usual injection timing, while it was more effective, as a result of reduction in the premixed combustion phase, at considerably retarded injection timing. Verhoeven et al. (1998) found that the position of the first visible emission from the combusting spray is further away from the injector at higher injection pressures, i.e., near or even beyond the tip of the liquid part of the spray. Since smaller spray droplet sizes are resulting from high pressure injection, the enhanced air/fuel mixing process contributes to a reduction in particulates but at the expense of increased

NO_x emissions (Su *et al.*, 1998). These higher NO_x levels are believed to be due to locally higher temperatures and oxygen rich regions at the beginning of the combustion process. In order to improve the particulates-NO_x trade off without sacrificing fuel consumption, it is important to understand the relationships between the various injection parameters and the resulting spray characteristics and combustion process. Therefore, in most diesel engines, combustion timing retardation is employed as the standard method for improving the trade off between particulate and NO_x emissions (Sundoh *et al.*, 1991). Retarding injection timing to reduce peak cylinder temperatures and pressures slows down the rate of NO_x formation. This, however, is not an efficient energy process and increases fuel consumption. Pierpont *et al.* (1995) have reported that there is a large decrease in particulates at higher injection pressures, but the injection timing must be retarded in order to maintain constant NO_x levels. They found that this injection retard results in 1~3% increase in BSFC. In addition, since the driving torque required by the fuel system increases with increased injection pressure, an additional loss in BSFC is expected. In order to reduce NO_x emissions without injection timing retard, many researchers are presently investigating EGR, pilot injection, multiple injections, premixed compression ignition, and after treatment technologies including de-NO_x catalytic and storage catalysts. It is well known that pilot injection is effective in shortening ignition delay of the main injection (Yokota *et al.*, 1997). Especially when the main injection is considerably retarded, pilot injection suppresses any increases in NO_x emissions, and also suppresses possible misfire of the main injection, but achieves only a minor improvement in the trade off between NO_x emissions and fuel consumption. Pierpont *et al.* (1995) and Montgomery *et al.* (1996) have reported that while NO_x is reduced by EGR and particulates are reduced by multiple high pressure injection, the latter itself doesn't seem to be effective as NO_x suppressant.

Three broad types of the electronically controlled high pressure injection system are now available. Rotary distributor-type pumps can provide up to 1500 bar, electronic unit injectors up to 2000 bar and common rail systems at present up to 1400 bar but with promise to reach 2000 bar; it should be noted that their pressure is largely independent of engine speed, which is their main advantage, although production systems are still far from perfect.

It is thus important to have better understanding of the influence of high injection pressure to spray characteristics, air entrainment, spray/wall interaction, ignition, combustion development, exhaust emissions and engine performance. In this experiment, the visualisation of spray and combustion development with various injection parameters was carried out in a single cylinder engine having a 4-valve cylinder head with central and vertical injector. A new rotary distributor-type pump was used to generate high injection pressure while the injection timing and

duration were controlled electronically. Fuel injection pressure was varied up to 1200 bar by changing the pump speed with halved gear ratio, while the engine speed was kept constant. This investigation is complemented by measurements or calculations of the cylinder pressure, heat release rate, IMEP, ignition delay and exhaust emissions.

4.2 EXPERIMENTAL SYSTEM

4.2.1 Engine and Fuel Injection System

The test engine used for this experiment was a modified version of the Hydra single-cylinder engine presented in Chapter 2; its 2-valve cylinder head incorporating an old version of Lucas EUI 50 was replaced with a 4-valve head having a centrally positioned vertical injector and incorporating a Bosch VP44 injection pump. The cylinder bore, piston and compression ratio remained the same as in the base Hydra engine, but the bowl shape has been modified into an axisymmetric re-entrant geometry in both the metal piston used for the engine performance tests and the optical piston. Since the high-pressure injection pump requires a higher driving force, the existing belt-driven system for the EUI was converted to a chain-driven system; details of the new engine are given in Table 4.1.

The new fuel injection system consists of a Bosch pump (VP44) which is a rotary type injection pump, electronically-controlled, and capable of generating high-pressures up to around 1500 bar, an electronic control unit (ECU) and conventional 17mm injectors. The ring-type cam used in this new injection pump allows much higher injection pressures than conventional rotary pumps having a disc-type cam. In this experiment, the engine control and monitoring system GREDI that has been developed as an engine development tool was installed in between the injection pump and the ECU; it allows control of injection timing, fuel delivery and other parameters directly without having to modify control maps already programmed in the ECU.

The injection pressure of jerk type pumps, such as the conventional rotary pump, in-line pump and EUI, increases with increasing pump speed or fuel delivery unlike the common rail system. For investigating the effects of high injection pressure on sprays, combustion and emissions, it was required to increase the pump speed while the engine speed and fuel delivery were kept constant. This can be achieved by doubling the pump speed and by changing the gear ratio between the engine crank shaft and pump shaft, i.e. 1:2. However, the pump speed can be increased by either two or three times while the injection timing should be kept at around the top dead center (TDC) at every engine cycle. In this experiment, the doubled pump speed was

selected because the injection pressure at that speed is high enough for these tests. Since doubling the pump speed results, in principle, in injecting twice during each engine cycle, one of the two injection shots during an engine cycle should be skipped. Skipping one injection at every cycle can be achieved by adding a Solid State Relay (SSR) which is an electronic switch on the circuit between the solenoid valve and the control circuit of the pump, that controls a spill valve inside the pump determining the amount of fuel injected. SSR only allows the command signal to be transferred to the solenoid valve for fuel injection to commence when a high voltage is supplied to SSR through a pulse generator adjusting the triggered pulse per cycle from the encoder installed on the valve camshaft. A diagram of the set-up is shown in Figure 4.1.

Two separate injectors were used in this study having a different nozzle hole size, 0.158mm (S nozzle) and 0.172mm (L nozzle) with flow rates of 760 and 880 cm^3/min at 100 bar, respectively. Both injectors are two-stage injectors containing two springs so that the first nozzle opening pressure is 220 bar for an initial lift of 0.03mm and the second one is 420 bar for the maximum lift of 0.2mm, the same number of holes (6), and a spray cone angle of 158°. The injectors were instrumented with a needle lift sensor and two piezoresistive pressure transducers were installed in the high pressure pipe which is 510mm long and 1.2mm in diameter; one is installed 30mm downstream from the outlet of the pump end (PE) and the other is installed 30mm upstream from the injector end (NE).

Prior to the engine tests, the mass injection rate was measured using a Ono Sokki rate-of-injection meter and the command values of GREDI corresponding to fuel deliveries (20, 25mm3/inj) and injection timings (12° bTDC to 3° aTDC) at each pump speed tested in the engine (600, 750, 900, 1200, 1500, 1800rpm) were obtained during tests in the pump test rig (Hartridge 1100).

A piezoelectric pressure transducer was installed into the cylinder head to measure the combustion chamber pressure. A probe was fitted to the exhaust system at a position 250mm downstream of the exhaust valves, to allow samples of the exhaust gas to be analysed. A new fast chemiluminescence analyser (Cambustion DCS 400) provided information about the NO_x concentration in ppm while smoke was measured using a Bosch smoke meter positioned 1500mm from the exhaust valve. For each test case, the data from the pressure transducers, shaft encoder and NO_x analyser were digitised and transferred to a personal computer using a data acquisition card.

The temperatures of the engine oil and cooling water during all the tests was maintained constant at 85°C, while that of the fuel (SHELL Gas Oil SH) was kept at 60°C.

4.2.2 Optical System

Visualisation of the six sprays exiting from the nozzle under different injection pressures was performed by employing a Drum Camera (Oxford Lasers) to obtain 35mm spray images prior to the start of combustion. Illumination of the spray was provided by a Copper-Vapour pulsed laser (Oxford Lasers CU15) at a frequency of 10 kHz, which provides 0.1ms in time resolution (corresponding to 0.72CAat 1200rpm engine speed). The laser light was directed towards the piston bowl, through the quartz window in the piston base, using an optical fibre which was positioned to scatter the light off the fuel spray. More details of this system were given in Chapter 2.

Flame visualisation was performed by using a high-speed colour digital camcorder (Kodak EktraPro RO Imager), which is capable of capturing 2000 frames per second (fps). Since the rate of 2000fps is not adequate to obtain consecutive flame images from one engine cycle during the early combustion phase, images captured at different timings from different engine cycles were combined in order to compare the flame development under different injection pressures, while images of late combustion were obtained from a single engine cycle.

4.2.3 Test Conditions

A series of engine experiments was performed to examine the effects of injection pressure and nozzle configuration on sprays, combustion and emissions; engine test conditions are described in Table 4.2. Two injection pressures corresponding to normal and doubled pump speed (same as engine speed) were tested at three different engine speeds for two different fuel deliveries and three different nozzle protrusions into the chamber. In all test cases, the cylinder pressures, NO_x and smoke emissions were measured at 5~6 different injection timings between 12° bTDC and 3° aTDC.

Visualisation of the sprays was performed for two different injection pressures and nozzle configurations at 1200rpm engine speed with a fuel delivery of 20mm3/inj. Flame images were also obtained at the two different injection pressures and 1200rpm engine speed.

NOMENCLATURE – The following convention will be used to describe the pump speed, nozzle configuration, fuel delivery and injection timing used for each test. For example,

600S/L+20+6bTDC+L/M/H

where; Pump speed (rpm) ; 600, 750, 900, 1200, 1500, 1800

Nozzle configuration ; S =ø 0.158mm hole, L =ø 0.172mm

Fuel delivery (mm^3/inj) ; 20, 25

Injection timing ; 3° aTDC and 0°, 3°, 6°, 9°, 12° bTDC

Nozzle protrusion into cylinder ; L = 1.7mm, M = 1.2mm, H = 0.7mm

4.3 RESULTS AND DISCUSSION

Prior to the engine tests, measurements of injection rate, injection pressure and needle lift at six different pump speeds, which correspond to six different injection pressures, combined with two nozzle configurations and different fuel deliveries, were obtained in the injection pump test rig. For the engine tests, it was necessary to optimise each engine operating condition, since the engine used was newly assembled with a 4-valve cylinder head, a piston having a central bowl and an electronically controlled fuel injection system with a centrally located and vertical injector. As a first step, engine performance tests were conducted to decide the optimum protrusion of the nozzle into the cylinder chamber at 1200rpm engine speed, and then three different shims of different thickness were used for adjusting nozzle protrusion.

Next, engine performance tests and measurements of exhaust emissions were conducted at three different engine speeds with two different injection pressures, three different nozzle protrusions and two different nozzle hole sizes. For the purpose of investigating the combustion characteristics, engine performance was estimated in terms of cylinder pressure and IMEP, in conjunction with exhaust emissions of NO_x and smoke. Heat release analysis of the cylinder pressure is performed to allow further understanding of combustion. Spray and flame images were obtained at two different injection pressures to determine the effect of injection pressure on spray characteristics and combustion. The injection timing and the amount of fuel were kept constant at the various injection pressures in order to facilitate direct comparison of the results. Measurements of the spray tip penetration, spray angle and spray impingement against the wall for different injection pressures are presented in the next section.

4.3.1 Measurement of Injection Parameters

The fuel injection pressure at the end of the high-pressure pipe, the needle lift and the rate of injection, obtained in the pump test rig, are shown as a function of time in Figures 4.2~4.4. These

tests were performed at six different pump speeds with two nozzles having hole sizes of 0.158mm (S nozzle) and 0.172mm (L nozzle), and two different fuel deliveries of 20mm^3/inj and 25mm^3/inj; injection timing, in all cases, was kept constant. In general, the injection rate correlates well with injection pressure as it should be. The peak of injection pressure increased with doubled pump speed, reduced nozzle size and increased fuel delivery. For example, doubling the pump speed with the large hole nozzle and 20mm^3/inj of fuel, increased the peak injection pressure to 721, 848, 946 bar from 523, 582, 642 bar for normal pump speed at equivalent 1200, 1500, 1800rpm engine speed, respectively. Injection rates were also higher for the doubled pump speed, which indicates that the exit velocity of the fuel injected through the nozzle was higher than at the normal pump speed.

On the other hand, the total injection duration was reduced at higher injection pressures in absolute time from 1.05, 0.95, 0.85ms to 0.80, 0.70, 0.60ms, respectively, which corresponds in CAD to a reduction from 7.56, 8.55, 9.18°CA to 5.56, 6.3, 6.48°CA, respectively. As explained in a previous section, the injector used for these experiments is a two-stage injector employing two springs for controlling the initial injection rate and reducing the premixed combustion phase that affects noise and NO_x emissions. It is very clear from Figure 4.2 for the case of 600rpm pump speed that the pre-needle lift, which was very small (0.03mm), lasted for 0.35ms (corresponding to 2.52°CA) before reaching its maximum lift of 0.25mm. It is interesting to note that the behaviour of the needle lift changed with increasing injection pressure. It appears that the duration of maximum lift remained almost constant at 0.70ms with increasing pump speed while the duration of the pre-needle lift was reduced to 0.1ms at 1200rpm of pump speed. The needle lift reached immediately its maximum value without a pre-lift stage when the pump speed was above 1500rpm. This shortened pre-needle lift duration resulted in rapid rise of the injection rate just after the start of injection so that the advantage of the two-stage injector becomes minimal and implies that it is more effective in reducing noise and NO_x emissions at low speeds, by suppressing the initial injection rate. This change in the needle lift pattern also affects combustion and exhaust emissions due to an increase in the premixed burn fraction. As shown in Figure 4.3, the injection pressures, injection rates and injection duration all increased with increasing fuel delivery, but these increases were relatively small compared to the increases associated with higher pump speeds. When the injected fuel quantity increased from 20 to 25mm^3/inj, the injection pressures increased by 35~95 bar and the total duration of injection by 0.1~0.158ms; however, the initial injection rates and the duration of pre-lifts remained unchanged.

Reducing the size of the nozzle hole resulted in a slight decrease in the injection rate but an increase in injection pressure when pump speeds and fuel deliveries were kept constant, as shown in Figure 4.4. In particular, when the diameter of the nozzle hole was reduced from 0.172 to 0.158mm, peak injection pressures increased by 17~38% (100~200 bar) and injection rates increased by about 10% (3~5mm^3/ms). It should be noted that the initial injection rate also increased at low speeds unlike the case of increasing fuel delivery. The higher injection pressure resulted in improved fuel atomisation, which could lead to a reduction in smoke levels. In general, higher injection pressures are combined with nozzles having a smaller hole size. Otherwise, the higher velocity of the spray and the longer spray tip penetration can result in impingement of the fuel on the wall, which may offset the reduction in smoke associated with the improved atomisation induced by the higher injection pressure.

4.3.2 Spray and Early Flame Development

The drum camera equipped with a 105mm lens provided visualisation of the six sprays exiting the vertical injector, up to the point of wall impingement, in a sequence of approximately 12 images with a time resolution of 0.1ms (0.72 CAD at 1200rpm) for two pump speeds (two injection pressures) and two nozzle configurations. Images of the sprays with varying fuel delivery are not presented here since the previous investigation described in Chapter 2 has revealed that the quantity of fuel injected has only a negligible effect upon the spray tip penetration.

Spray images arranged sequentially after the start of injection are shown in Figure 4.5a and 4.5b for 600rpm/1200rpm of the pump speed and 0.158mm/0.172mm of nozzle hole at an engine speed of 1200rpm. The fuel delivery and injection timing remained constant at 20mm^3/inj and 3° bTDC, respectively. Each series of images started to be shown at a slightly different timing after start of injection (SOI) but with the same time interval; this is due to the uncontrollable delay time in the controller of the camera shutter and the pulsed laser. Since the injector was positioned vertically in the center of the cylinder head, it was expected that the development of all six sprays would be symmetric. However, some differences between sprays were noticeable according to Figure 4.5, which could be the result of variations in the injection hole geometry.

Overall, the six sprays were distributed evenly and wall jets were observed to form along-the piston-bowl wall after spray impingement on it. Wall jets from adjacent sprays impinged on each other somewhere in the middle of their distance and started moving towards the center of

the cylinder. This indicates that the air-fuel mixing process was performed very evenly over the whole circumference, which contributes to the reduction of NO_x emissions by preventing the formation of local hot zones unlike the inclined injector which resulted in uneven distribution of the fuel droplets. From these images, only a minor effect of swirl on spray penetration was observed. There seems to be no influence of swirl on the spray before impingement on the wall, but there was in the case of the normal pump speed some movement of the wall jet after impingement towards the counter clockwise direction, which disappeared in the case of the doubled pump speed probably as a result of the higher speed of the wall jet.

The spray development in terms of the tip penetration, estimated from the images of Figure 4.5, is shown in Figure 4.6. Figure 4.6a presents the tip penetration of sprays injected from the nozzle having holes of 0.158mm in diameter at two different pump speeds, the normal pump speed of 600rpm and the doubled pump speed of 1200rpm. Figure 4.6b presents results for the nozzle with the larger holes of 0.172mm in diameter. In both cases, the normal pump speed resulted in the typical spray tip penetration, fast at the early stage of injection and slower later as the spray tip is penetrating far from the injector. However, the doubled pump speed produced much faster penetration than the normal pump speed, with its initial penetration speed remaining almost constant until spray impingement on the wall. This is attributed to the increased by about 40% injection pressure in the case of the 1200rpm engine speed. This is in agreement with recent investigations by Su and Farrell (1998) and Verhoeven *et al* (1998) who showed that higher injection pressures result in higher tip penetration speed, narrower spray angle and a small increase in the penetration length. Unfortunately the penetration lengths could not be compared in the present images since the sprays impinged on the piston bowl of 46mm diameter before they reached their maximum penetration. In the study by Verhoeven *et al* (1998), it was observed that the liquid penetration changed only by about 15% as injection pressure was increased from 40 to 150 MPa while Kamimoto *et al.* (1987) reported that liquid penetration remained approximately constant for injection pressures between 26 and 110 MPa. Their study also showed that the liquid penetration length could be between 20 and 30mm for the test conditions used in this experiment, where air density and temperature were around 18 kg/m^3 and 800° K, respectively.

The higher penetration speed due to the higher injection pressure results in earlier impingement of the fuel on the wall. This earlier impingement gives rise to earlier dispersion of the fuel droplets along the piston-bowl wall and might lead to enhanced air-fuel mixing with associated reduction in ignition delay. However, this decrease in ignition delay will not contribute to significantly reduced NO_x emissions because the amount of fuel injected during the

ignition delay period will not be reduced as much as the ignition delay decrease, as a result of the increased injection rate by the higher injection pressure. On the other hand, the higher penetration speed would result in higher concentration of fuel droplets near the wall due to the reduced time available for air entrainment into the spray and fuel vaporisation. This may result locally in hot spots that contribute to increased NO_x emissions. In addition, at higher pump speeds more fuel can wet the wall due to its higher speed at impingement which may cause higher hydrocarbon emissions due to the late vaporisation of the impinging fuel.

The comparisons of spray tip penetration between the two different nozzle configurations are presented in Figure 4.6c; penetration can not be compared directly spray by spray because of the difference in the injection hole geometry. Overall, when the doubled pump speed was applied, penetration was faster with the S nozzle than with the L nozzle, but there were no differences between them when the normal pump speed was applied. It is considered that this is the result of the differences in droplet size and injection pressure. The size of the fuel droplets injected through the S nozzle is smaller and their initial speeds are higher due to the higher injection pressure relative to those through the L nozzle. Therefore, the fuel droplets injected through the small hole will exit with higher momentum and this results in higher initial penetration speed. However, these smaller droplets will loose their momentum earlier, after passing through the dense air in the cylinder, than the larger size droplets and their speed will decrease at a faster rate. By the same reason, in the case of the normal pump speed the overall penetration speed was similar between the S and L nozzle.

The influence of the injection pressure on flame development was investigated through flame images obtained by using a high speed colour digital camcorder (Kodak EktraPro RO Imager). The sequences of the flame images for two injection pressures are presented in Figure 4.7. These images were obtained at an engine speed of 1200rpm with the S nozzle while the fuel delivery and injection timing were kept constant at $20mm^3$/inj and 3° bTDC. It should be noted that the first four images having a time interval of 0.9 CAD were obtained from four different engine cycles because of the insufficient time resolution of the camera, but the rest were obtained from the same engine cycle as the first one.

Figure 4.7 shows that combustion at the normal pump speed lasted longer than with the doubled pump speed; this is attributed to the longer injection duration for the same fuel delivery at the lower injection pressure. The flame was also found to propagate further with the normal pump speed. This implies that more fuel droplets were dispersed and vaporised before impingement on the wall, since there was more time until impingement due to their lower penetration speed. On the other hand, in the case of the doubled pump speed, the flame was

concentrated near the point of wall impingement and the intensity of the images was stronger than that in the case of the normal pump speed, which indicates that an insufficient air-fuel mixing may offset the effect of fine atomisation on the reduction of smoke emissions while the presence of local hot spot may result in increased NO_x emissions.

The combustion images also show that the first visible flame was observed at about two-thirds along the way of the spray axis when the normal pump speed was applied, while it was found on the surface of the piston bowl wall in the case of the doubled pump speed. This clearly indicates that the higher injection pressure pushes the fuel droplets further away delaying their mixing with the surrounding air. This is in agreement with the investigation by Verhoeven *et al.* (1998) who found that the first observable flame luminosity was closer to the injection tip in the case of the lower injection pressure.

4.3.3 Combustion and Emissions

4.3.3.1. Effect of injection pressure

The cylinder pressure and heat release rate are presented for two injection pressures (normal and doubled pump speeds), three engine speeds and two different nozzle configurations in Figure 4.8. Overall, the doubled pump speed resulted in reduced ignition delay and a rapid rise in heat release rate. Especially this shorter ignition delay became more obvious at the late injection timing, which may be attributed to the faster vaporisation of the smaller spray droplet sizes generated by the higher injection pressure. As Sundoh *et al.* (1992) reported, the higher injection pressure generates smaller droplets and improves the air-fuel mixing process through enhanced air entrainment which results in favourable conditions for auto-ignition. This reduction in ignition delay brought combustion closer to TDC giving rise to higher temperatures in the cylinder and increased NO_x emissions. In addition, higher NO_x levels can be predicted from the rapid rise of heat release rate as a result of the increased premixed burn fraction due to the higher injection rate in spite of the shortened ignition delay. As a result of the significant difference in the ignition delay at the late injection timing, combustion was very unstable at the normal pump speed and 3° aTDC injection timing, while it was relatively stable at the doubled pump speed and the same injection timing due to the shortened ignition delay.

The results of NO_x emissions, measured for various injection timings at each engine speed with different injection pressures and fuel deliveries, are shown in Figure 4.9. The doubled pump speed resulted in higher NO_x emissions than the normal pump speed for all engine speeds

tested. As mentioned above, this is attributed, on the one hand, to the enhanced air-fuel mixing as a result of the smaller spray droplets due to the increased injection pressure and on the other to an increase in the premixed burn fraction due to the increased injection rate, especially due to the shortened duration of the pre-needle lift. As expected, NO_x emissions decreased with retarded injection timing, but the trend started reversing when injection timing was retarded beyond TDC due to the very long ignition delay, which caused a significant increase in the premixed burn fraction and led to higher NO_x emissions.

An interesting phenomenon was encountered in Figure 4.9 where NO_x emissions for 25mm3/inj of fuel delivery were lower at the advanced injection timing despite the higher peak of injection pressure and injection rate, but similar at retarded injection timings to those for 20mm3/inj. Since increased fuel delivery has no influence on the initial injection rate as shown in Figure 4.3, it is hard to explain the above trend in terms of the injection rate. A possible explanation is that the fuel injected after the start of combustion cools down the in-cylinder gases due to the latent heat of vaporisation, which, in turn, suppresses NO_x formation. Thus, the more fuel is injected the more heat is absorbed which results in lower NO_x levels for constant initial injection rate and ignition delay. On the other hand, since the ignition delay becomes longer when the injection timing is retarded, the premixed burn fraction increases and the amount of fuel injected after the start of combustion is reduced which suppresses the cooling effect and leads to rather small differences in NO_x emissions at late injection timings.

The results of the smoke measurements are shown in Figure 4.10. Overall, the smoke levels were lower for the doubled pump speed over all engine speeds tested than for the normal pump speed. This is attributed to better fuel atomisation due to the higher injection pressure despite the shortened ignition delay and the higher injection rate. The shortened ignition delay, high injection rate and fine atomisation affect smoke emissions in different ways. The shortened ignition delay results in an increase in smoke due to the reduced time for air-fuel mixing before combustion. On the other hand, the high injection rate indicates an increase in the premixed burn fraction, which allows more fuel to be mixed with air before combustion so that smoke decreases. The high injection pressure also contributes to a reduction in particulates but at the expense of increased NO_x emissions since the smaller spray droplets created by the high injection pressure enhance the air-fuel mixing process. Therefore, the effects of the high injection pressure on smoke will vary depending on which of these counterbalancing effects becomes dominant on smoke formation under certain test conditions. As shown in Figure 4.10, the smoke emissions increase when retarding the injection timing from 12° bTDC to 3° bTDC but decrease at further retarded injection timings beyond 3° bTDC. Under heavy load conditions,

smoke increases significantly at very retarded injection timings since the later part of the diffusion combustion phase is frozen as the cylinder pressure drops. At the light load conditions used in this study, however, it rather decreases since the diffusion combustion phase finishes before reaching the limit of soot oxidation freezing temperature, and instead, the prolonged ignition delay allows more fuel to be mixed with air before the start of combustion. Since the ignition delay with the doubled pump speed was shorter than with the normal pump speed according to Figure 4.8, the turning points in the reduction of smoke emissions against injection timing appeared later for the cases of the doubled pump speeds than those of the normal pump speeds.

Smoke emissions plotted against NO_x are presented in Figure 4.11 for normal and doubled pump speeds at three different engine speeds and two different fuel deliveries. The corrected NO_x emissions shown in Figure 4.11 were obtained by dividing the measured NO_x by the IMEP calculated from the cylinder pressure data at each injection timing. The results show the typical smoke vs. NO_x trade-off curve existing between 12° bTDC to 3° bTDC, and confirm the characteristic decrease in smoke and flattening with advancing injection timing. However, there is no evidence of the typical shape at late injection timings; this is due to the variation of smoke emissions with injection timing towards late injection timings at low load conditions. Pierpont and Reitz (1995) have confirmed the traditional particulates vs. NO_x trade-off trend at 75% loads and different injection pressures but not at 25% load.

Overall, since lower smoke but higher NO_x emissions resulted from the doubled pump speed (higher injection pressure), the smoke-NO_x trade-off curves for the doubled pump speed were shifted rightwards and downwards. In the case of 20mm^3/inj of fuel delivery, there was no improvement in the smoke-NO_x trade-off curve but a small improvement was observed in the case of 25mm^3/inj. As shown in Figure 4.9, NO_x emissions increased with advanced injection timing, but the increase rate was lower for higher fuel deliveries than for lower fuel deliveries. Therefore, it is expected that further improvement in the smoke-NO_x trade-off curve can be achieved at higher load conditions.

Injection timing must be retarded in order to maintain the same NO_x levels, when raising the injection pressure. This is attributed to an increase in the injection rate and premixed burn fraction, which contribute to an increase in NO_x emissions. Unfortunately, any injection retard implies a loss in engine power in addition to the power loss caused by the higher driving torque required for higher injection pressure. It is shown in Figure 4.12 that the doubled pump speed improved IMEP by 10 – 15%, however the actual improvement in engine torque will be smaller than this because the additional driving torque was not involved in the IMEP calculation. For

example, the additional driving torque required to raise pump speed from 600rpm to 1200rpm is 0.9 N·m, which corresponds to about 20kPa in terms of IMEP. Shimada *et al.* (1989) have reported that there was a 1.3% increase in BSFC by the driving torque required to increase the injection pressure (hydraulically operated EUI) from 72 to 160 MPa.

4.3.3.2 Effect of nozzle hole size

The injection pressures and injection rates measured in the pump test rig were presented in Figure 4.4 for the cases of the S and L nozzles operating at different pump speeds and fuel deliveries. Reducing the nozzle hole size resulted in an increase in the injection pressure but a slight decrease in the peak injection rate. Employing the S nozzle increased the injection pressure at the normal pump speed and 20mm^3/inj from 523, 582, 642 bar to 698, 808, 868 bar at 1200, 1500 and 1800rpm of engine speed, respectively. In the case of the doubled pump speed, the relative increases for reducing the nozzle hole size were from 721, 848, 964 bar to 928, 1016, 1131 bar, while increasing fuel delivery made further increases possible up to 1204 bar at 1800rpm. Since the initial injection rate was reduced despite the insignificant change in the peak injection rate, this may have an effect in suppressing any increases of NO_x.

The cylinder pressures and heat release rates are presented for two nozzle configurations, three engine speeds and two different pump speeds in Figure 4.13. Overall, the S nozzle resulted in a slight decrease in ignition delay which is attributed to the higher injection pressure resulting in smaller spray droplets sizes. However, the heat release rates remained almost the same since the effect of improved atomisation on heat release was offset by the reduction of the premixed burn fraction due to the shorter ignition delay. Figures 4.14~4.16 show NO_x and smoke emissions against injection timing as well as smoke-NO_x trade–off curves for different nozzle configurations at three engine speeds and two pump speeds. Similarly to the case of increasing injection pressure, reducing nozzle hole size resulted in lower smoke and higher NO_x emissions, but the rate of decrease in smoke and rate of increase in NO_x was greater than in the case of increased injection pressure. As a result of this, the smoke-NO_x trade-off has improved significantly in both cases of normal and doubled pump speeds unlike the trend observed when raising the injection pressure. It appears that the smaller nozzle hole is more effective in improving the smoke-NO_x trade-off curve than raising the injection pressure for all the conditions tested here. However, this is not the optimum solution since injection duration increases excessively at higher loads when nozzle holes are reduced but without raising the injection pressure. The end result is a significant increase in smoke levels because the soot

formed at the late period of combustion can not be oxidised due to the low cylinder temperatures. Therefore, smaller nozzle holes should be employed in conjunction with higher injection pressures in order to maintain proper injection duration and injection rate.

4.3.3.3 Effect of injection rate

Figure 4.17 shows the comparison of the injection pressure and injection rate profiles for the case of the S nozzle with the normal pump speed and the L nozzle with the doubled speed. The peak injection pressure resulting from the use of the smaller nozzle hole was approximately the same as that when using the doubled the pump speed with the larger nozzle hole at pump speeds corresponding to 1200 and 1500rpm of engine speed but slightly lower at 1800rpm. However, the injection rates, especially the initial injection rates, were very different; the latter case resulted in much higher injection rate and shorter injection period. The cylinder pressure and heat release rates were presented for these cases at three engine speeds in Figure 4.18. There was no difference in ignition delay at the early injection timing between two cases but the case using the doubled pump speed with the L nozzle showed shorter ignition delay at the late injection timing. The heat release rate also showed only a small difference at the early injection timing but a substantial difference at the late injection timing, which indicates that the effect of injection rate on the heat release rate is growing as injection timing is retarded.

Figures 4.19~4.21 present NO_x and smoke emissions against injection timing as well as smoke-NO_x trade–off curves for a range of operating conditions. Even though the peak injection pressures were similar in all these cases, there was a large difference in the level of smoke and NO_x emissions. The cases involving the S nozzle resulted in much lower smoke and NO_x emissions at all engine speeds and fuel deliveries. As a result, the smoke-NO_x trade-off curve shifted downstream relative to that of the L nozzle case which indicates that smoke emissions do not correlate well only with injection pressure. On the other hand, Pierpont *et al.* (1995) have reported that smoke emissions do not correlate equally well with injection rates; based on numerous engine tests focussing on the effect of nozzle configuration on particulate and NO_x emissions. Their results showed, for example, that a higher injection pressure was applied in the case of the sharp-edged inlet nozzle than for the round-edged inlet nozzle in order to maintain the same injection rates. They also showed that the sharp-edged one with the lower discharge coefficient reduced the particulates dramatically despite the similar injection rates with the round-edged one. These results imply that the smaller nozzle hole is producing the smaller spray droplet sizes which give rise to lower smoke and higher NO_x levels either through the higher

injection pressure or through the higher injection rate. They also imply that the spray droplet size correlates well with the injection velocity and, in turn, with smoke emissions, since both the higher injection pressure and the higher injection rate are associated with higher velocity of the liquid fuel exiting the nozzle hole.

From a different perspective, it can be argued that the hole size of the L nozzle was too large to be used with the injection pressure resulting from the doubled pump speed. This possible imbalance between the injection pressure and the nozzle hole size may have resulted in a larger than normal amount of fuel impinging on the wall; this can have a varying effect on emissions. Obviously, this is an area where increased flexibility in controlling the injection pressure can offer significant advantages in improving the optimisation of the injection system for lower exhaust emissions and higher fuel conversion efficiency.

4.3.3.4 Effect of nozzle protrusion

The position of the nozzle in the cylinder head determines the point of impingement of the fuel on the piston-bowl wall. The spray impingement positions vary with injection timing since the position of the piston varies during the injection period. These different positions of impingement will affect the air-fuel mixing process because the behaviour of the spray after impingement, with the secondary droplet formation and, possibly, the liquid film exerts a controlling influence on exhaust emissions. Figure 4.22a and 4.22b present the measurements of NO_x, smoke emissions and the smoke-NO_x trade-off curve for different nozzle protrusions into the cylinder. Figure 4.22a and 4.22b show that higher position of the nozzle hole resulted in lower smoke and higher NO_x levels; overall, the smoke-NO_x trade-off curve was improved with a higher, less protruding, nozzle position. However, it should be noted that this is the case only at low load conditions when injection duration is relatively short. In the case of higher loads and late injection timing, too high position of the nozzle may cause the later part of the spray not to impinge on the piston bowl, but rather to spread on the piston crown which can have disastrous effect on smoke levels and engine performance.

In this experiment, the effect of increasing the injection pressure and reducing nozzle hole size on smoke and NO_x emissions was maintained regardless of the change in the position of the nozzle tip. Independent of the position of the nozzle, smoke emissions were reduced and NO_x emissions were increased with increasing pump speed and reducing nozzle hole size.

4.4 SUMMARY

An experimental investigation was conducted in a single cylinder engine, having a 4-valve cylinder head with central and vertical injector connected to an electronically controlled high-pressure injection system, to examine the influence of various injection parameters on spray characteristics, combustion development, exhaust emissions and engine performance. The main conclusions can be summarised as follows;

1. The higher injection pressure resulted in much faster spray tip penetration, with its initial penetration rate remaining almost constant until spray impingement on the wall. It also resulted in higher NO_x emissions and lower smoke levels, which is attributed to an increase in the pre-mixed burn fraction and the enhanced air-fuel mixing as a result of the improved atomisation. However, no improvement was observed in the smoke-NO_x trade-off curve.
2. Smaller nozzle hole size resulted in higher NO_x emissions and lower smoke levels, but significant improvement in the smoke-NO_x trade-off curve.
3. A lower injection rate at similar injection pressure resulted in lower smoke and NO_x emissions, and improved smoke-NO_x trade-off curve.
4. Overall, the results revealed that when high-pressure injection is employed, reduction of the nozzle hole size should also be considered at the same time in order to jointly maintain an appropriate injection rate and injection duration for improved combustion.

Description	Specification
Stroke	90.54 mm
Bore	93.67 mm
Connecting rod	154 mm
Compression ratio	16.75 (cold)
Swept volume	0.624 litre
Head clearance	1.2 mm
Inlet valve	2 x ϕ32 mm
Exhaust valve	2 x ϕ32 mm
Swirl ratio	2.5
Fuel Injection System	Bosch VP44

Table 4.1 Geometric characteristics of the modified four-valve single-cylinder Hydra engine

1. Engine performance test

Description	Test Conditions
Engine speed	1200, 1500 and 1800 rpm
Pump speed	600 and 1200 rpm at 1200 rpm of engine speed
	750 and 1500 rpm at 1500 rpm of engine speed
	900 and 1800 rpm at 1800 rpm of engine speed
Nozzle hole diameter	0.158 and 0.172 mm
Nozzle protrusion into cylinder	0.7 mm
	1.2 mm
	1.7 mm
Fuel delivery	20 and 25 mm3/inj

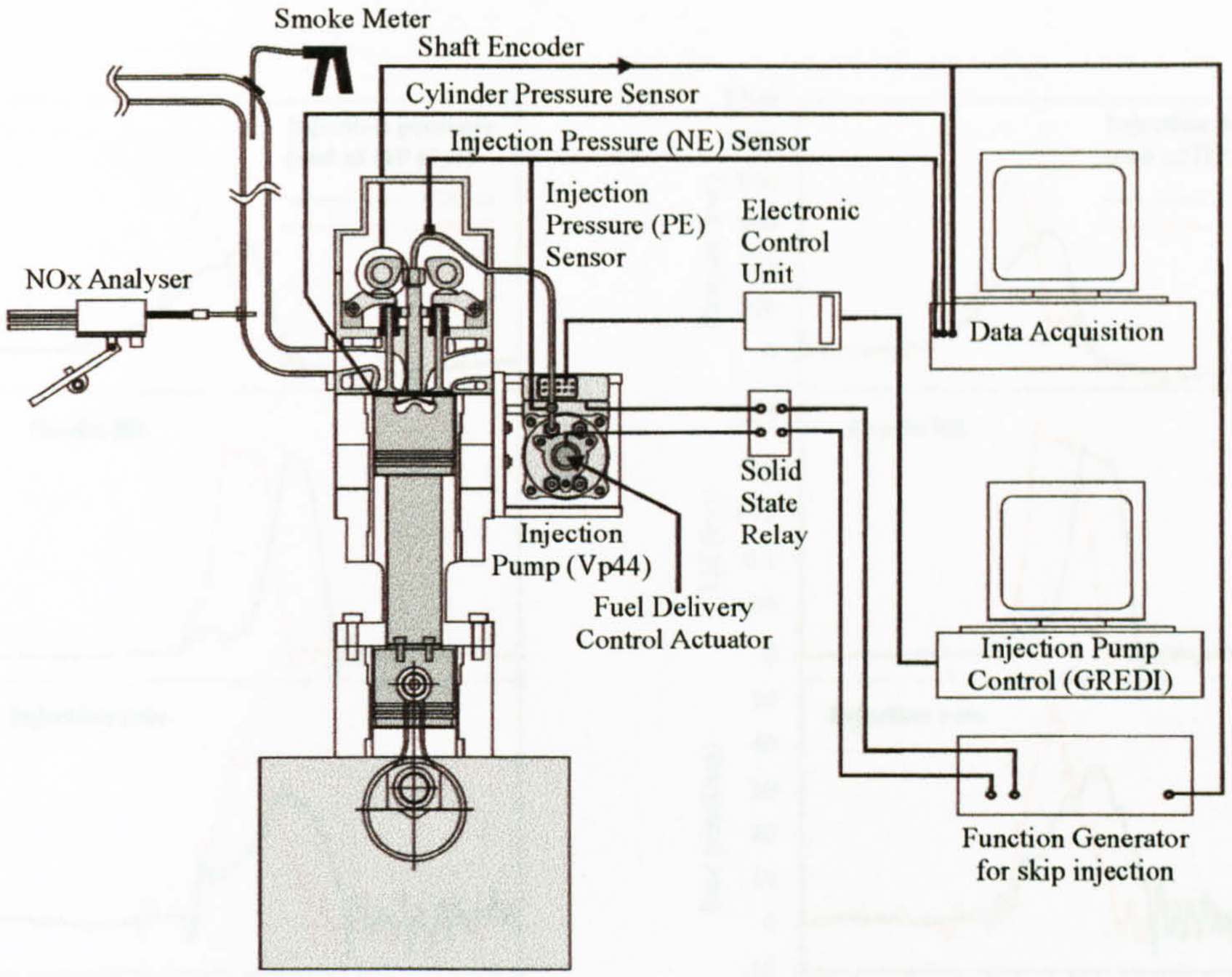
2. Spray visualisation

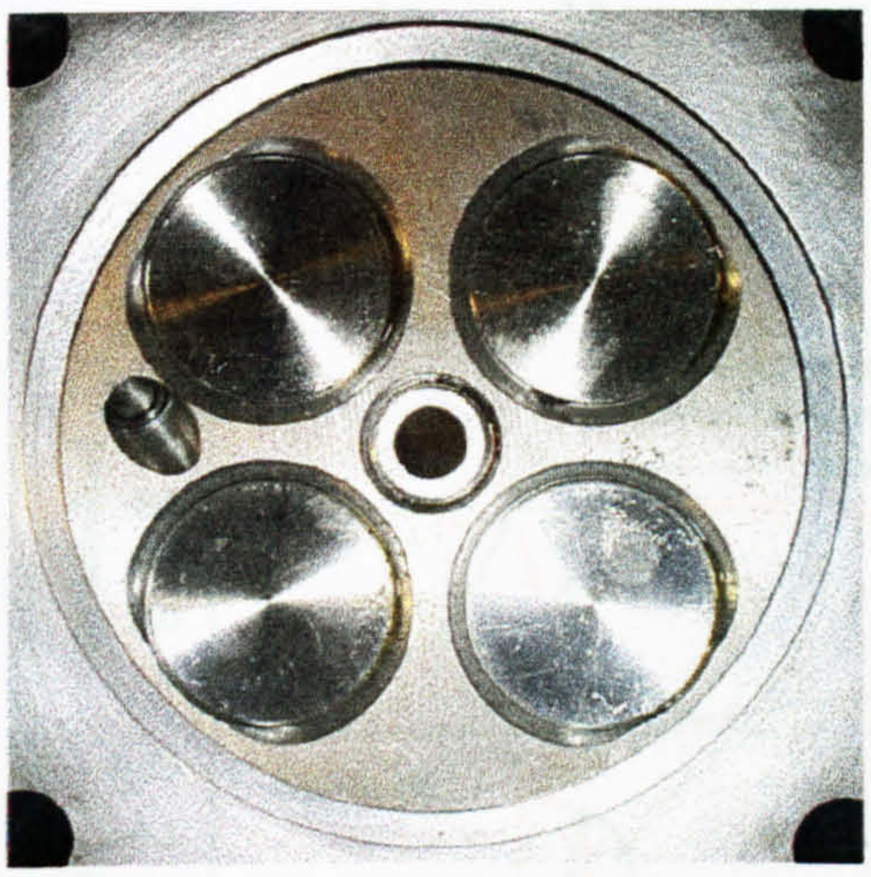
Description	Test Conditions
Engine speed	1200 rpm
Pump speed	600 and 1200 rpm
Nozzle hole diameter	0.158 and 0.172 mm
Nozzle protrusion	3.5mm with washer of 3.0 mm in thickness
Fuel delivery	20 mm3/inj

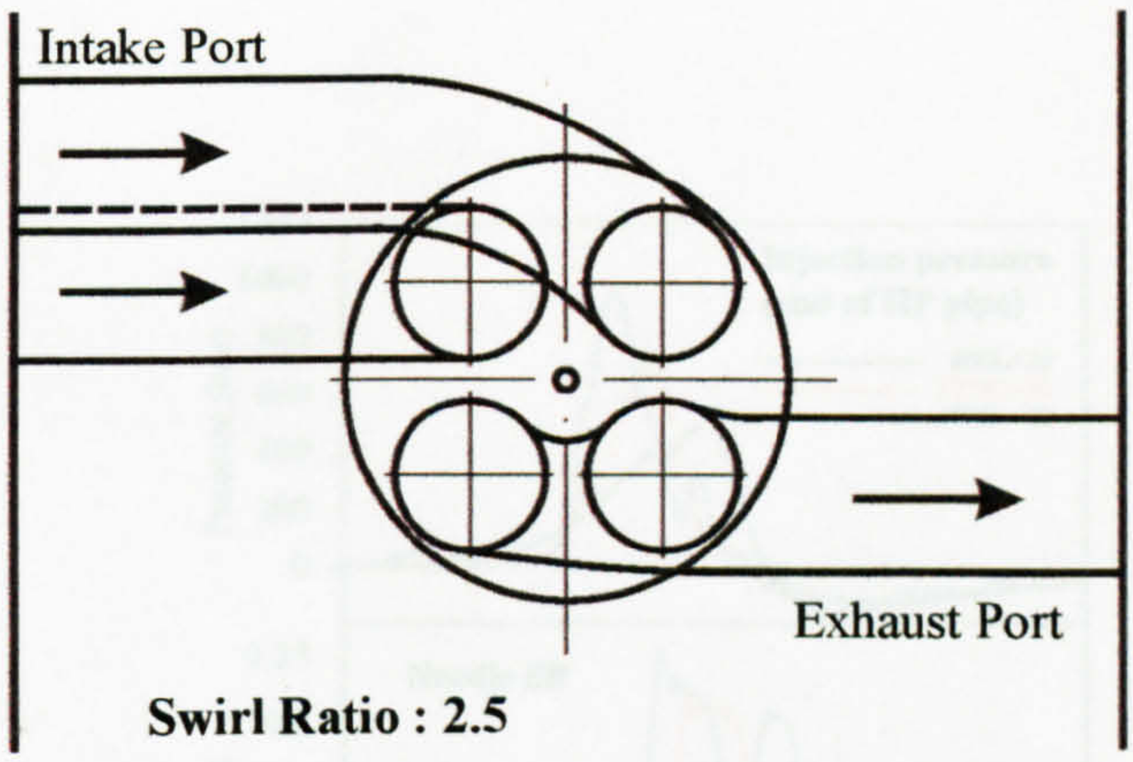
3. Flame visualisation

Description	Test Conditions
Engine speed	1200 rpm
Pump speed	600 and 1200 rpm
Nozzle hole diameter	0.158 mm
Fuel delivery	20 mm3/inj

Table 4.2 Test conditions of the modified Hydra engine









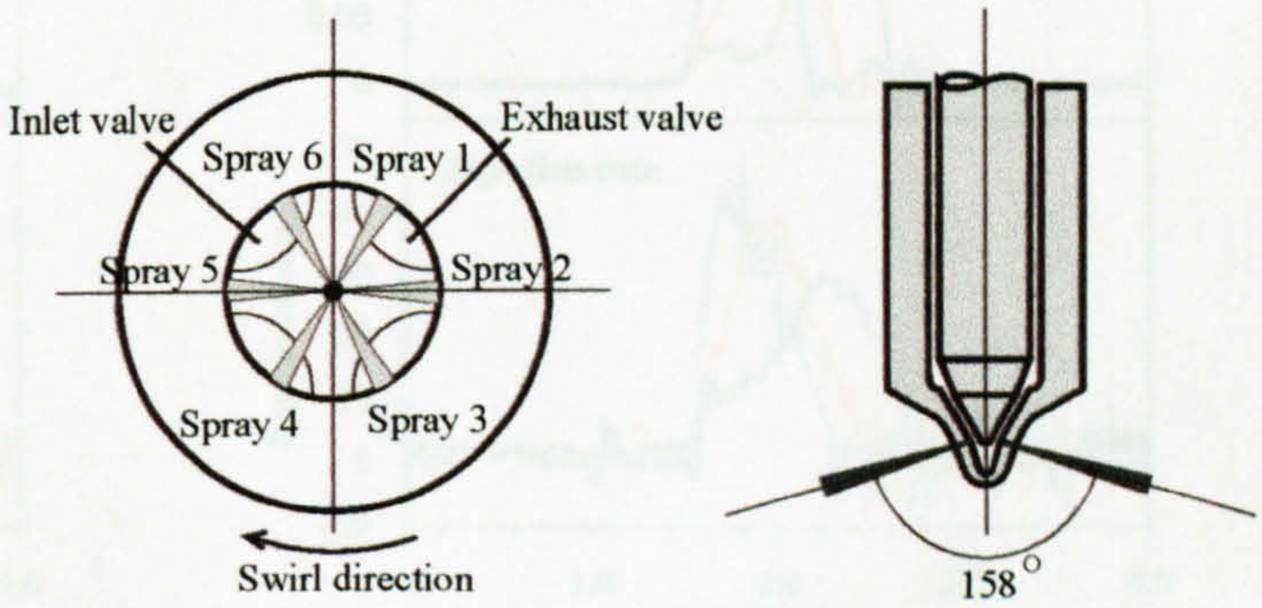
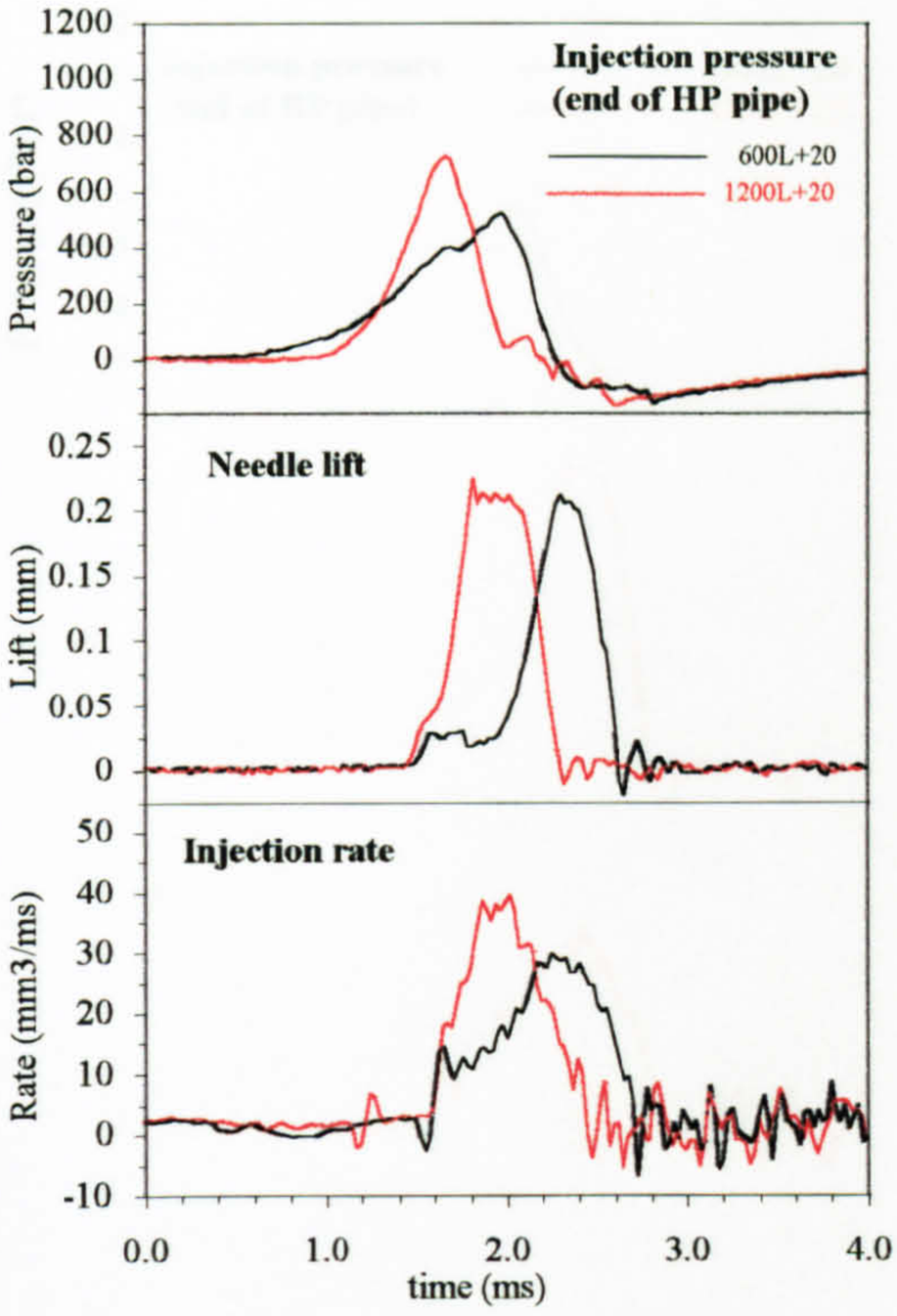
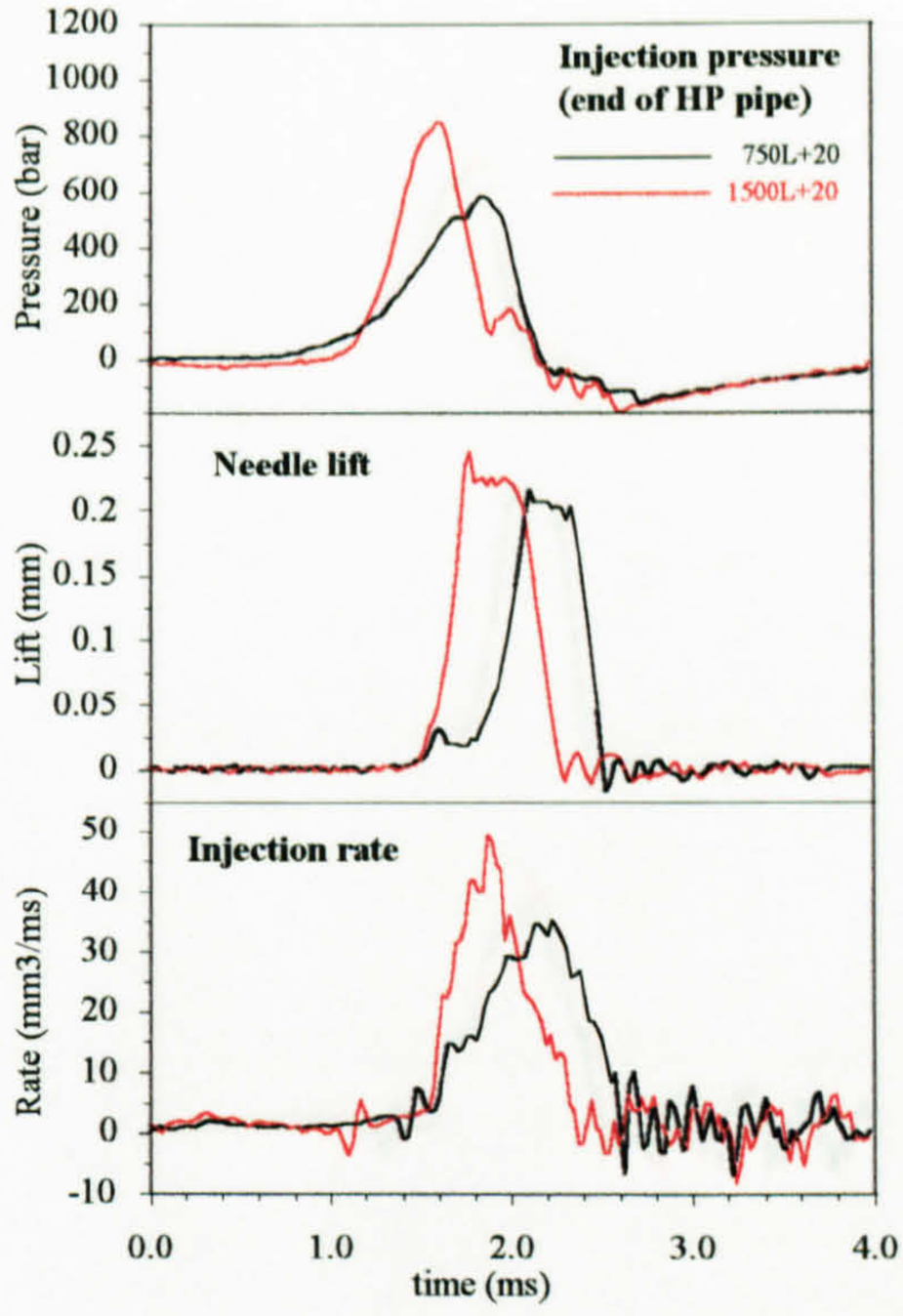
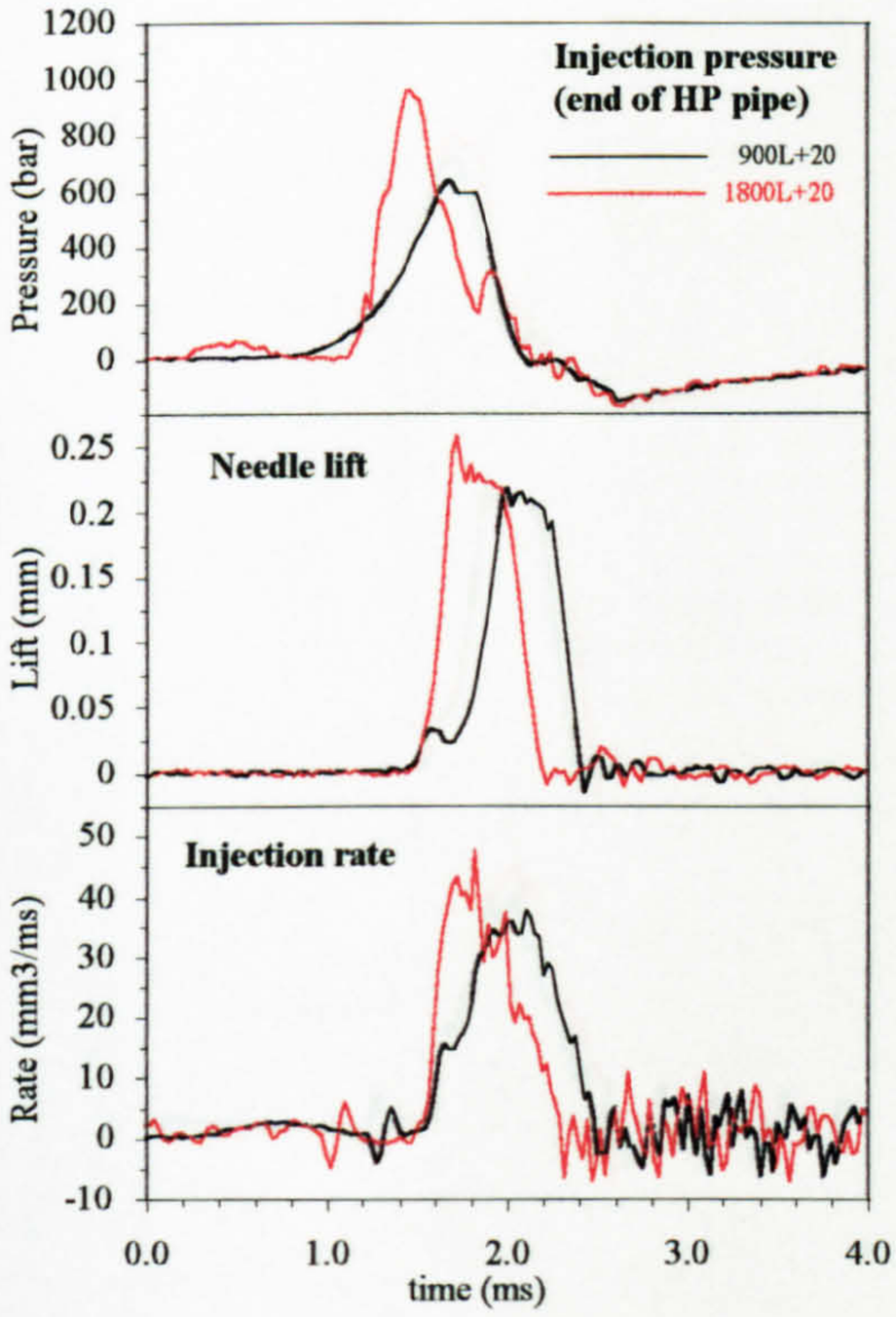


Figure 4.1 Schematic of the four-valve engine incorporating a high pressure injection pump and the orientation of sprays in the cylinder head







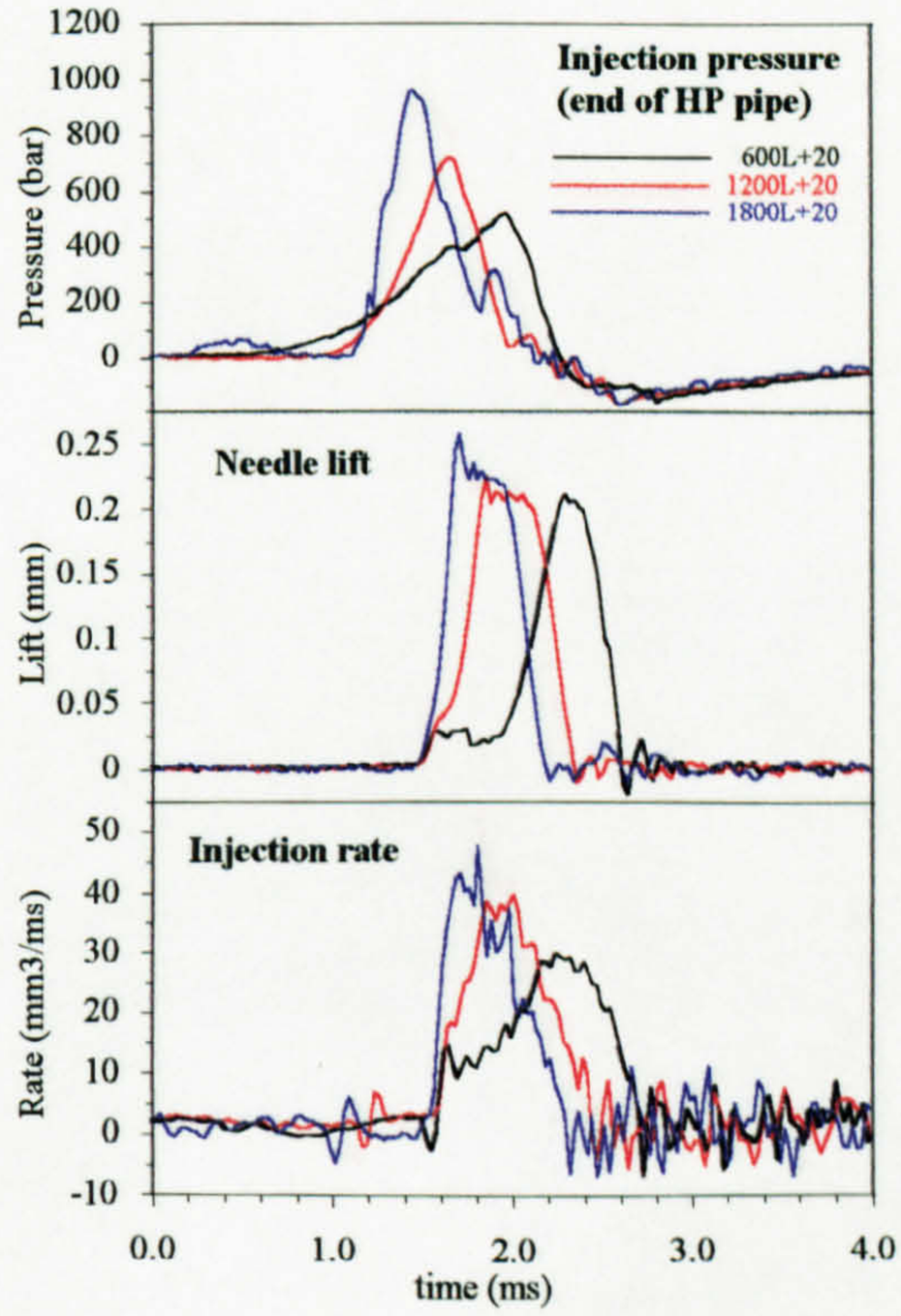
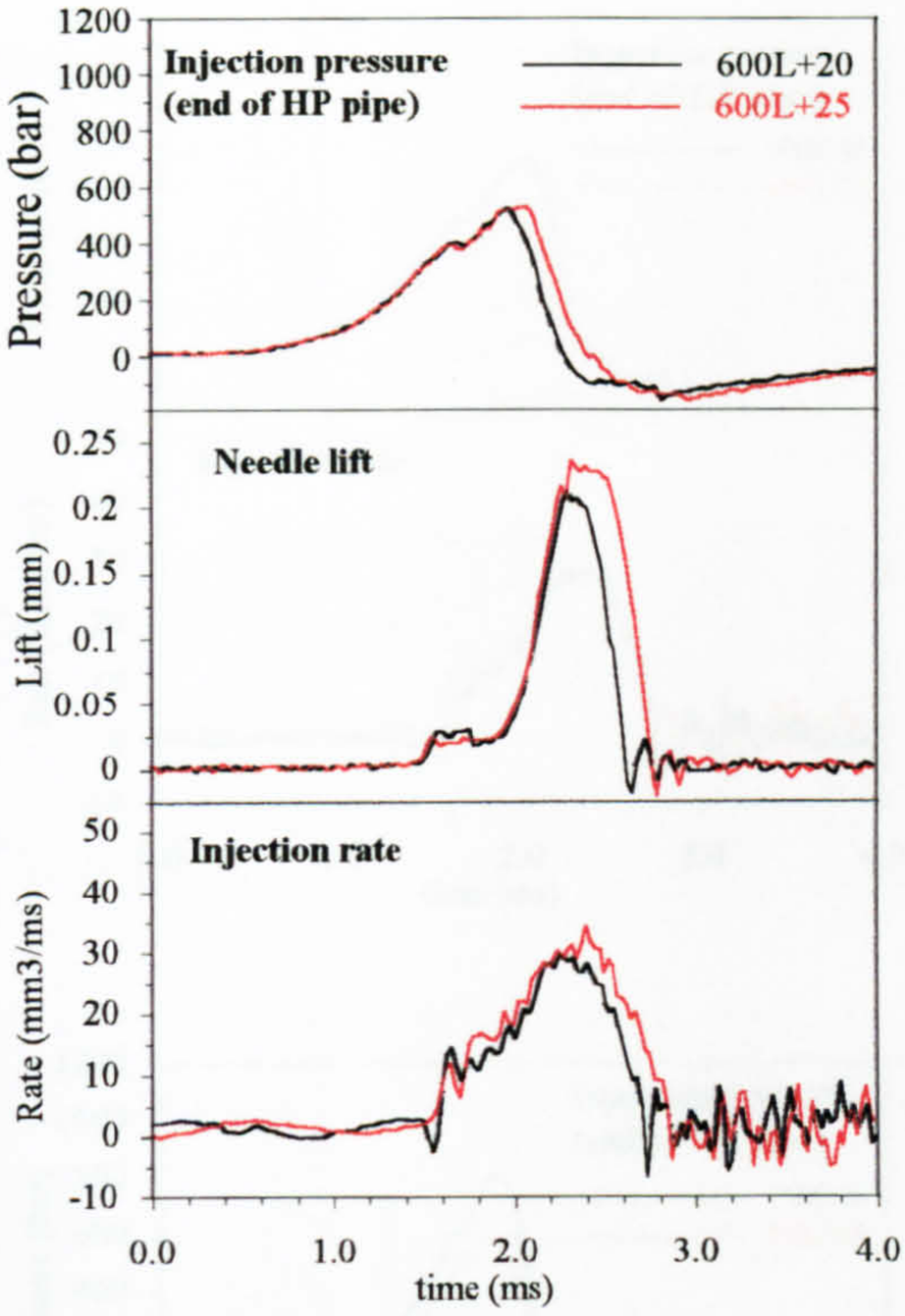
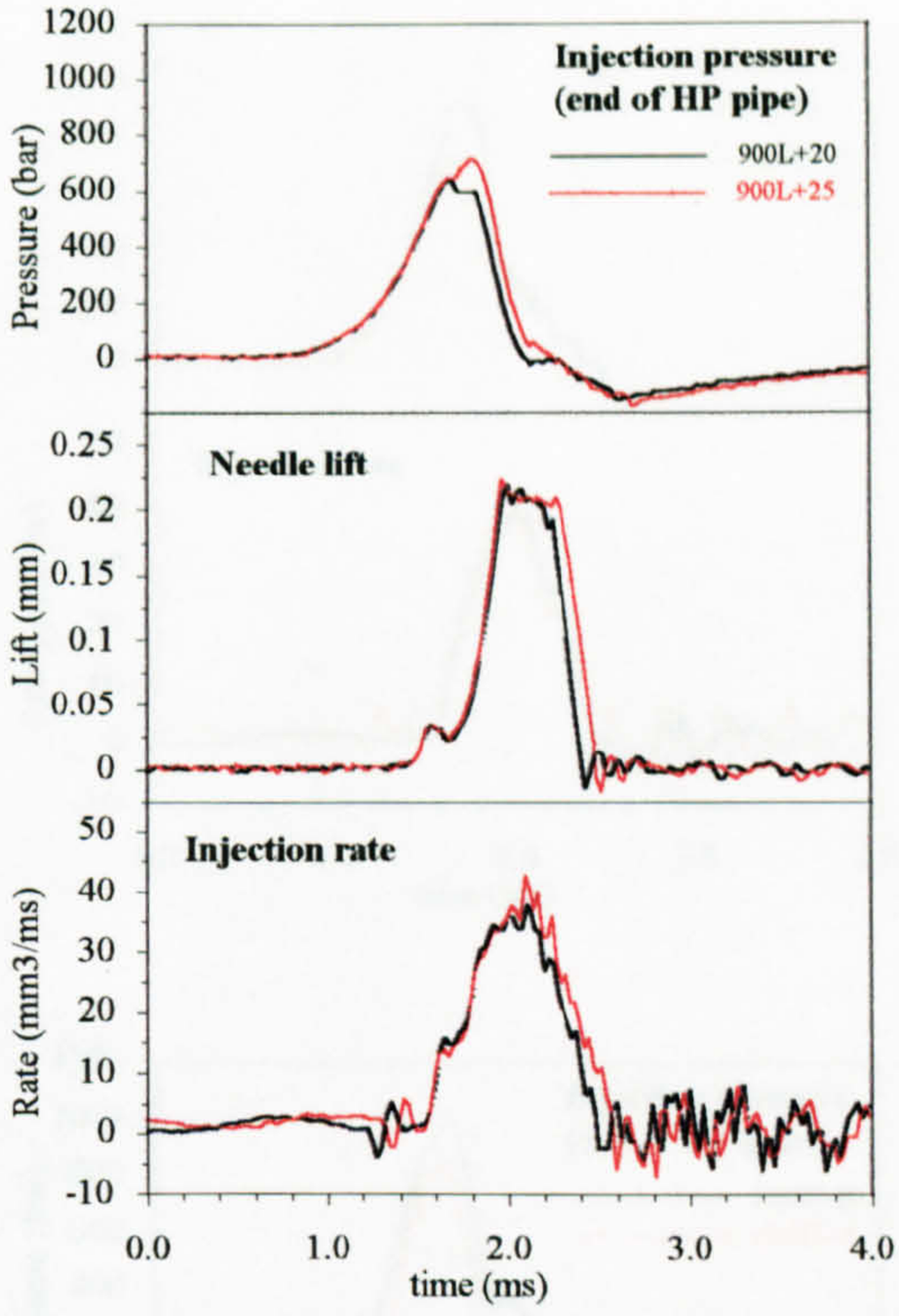
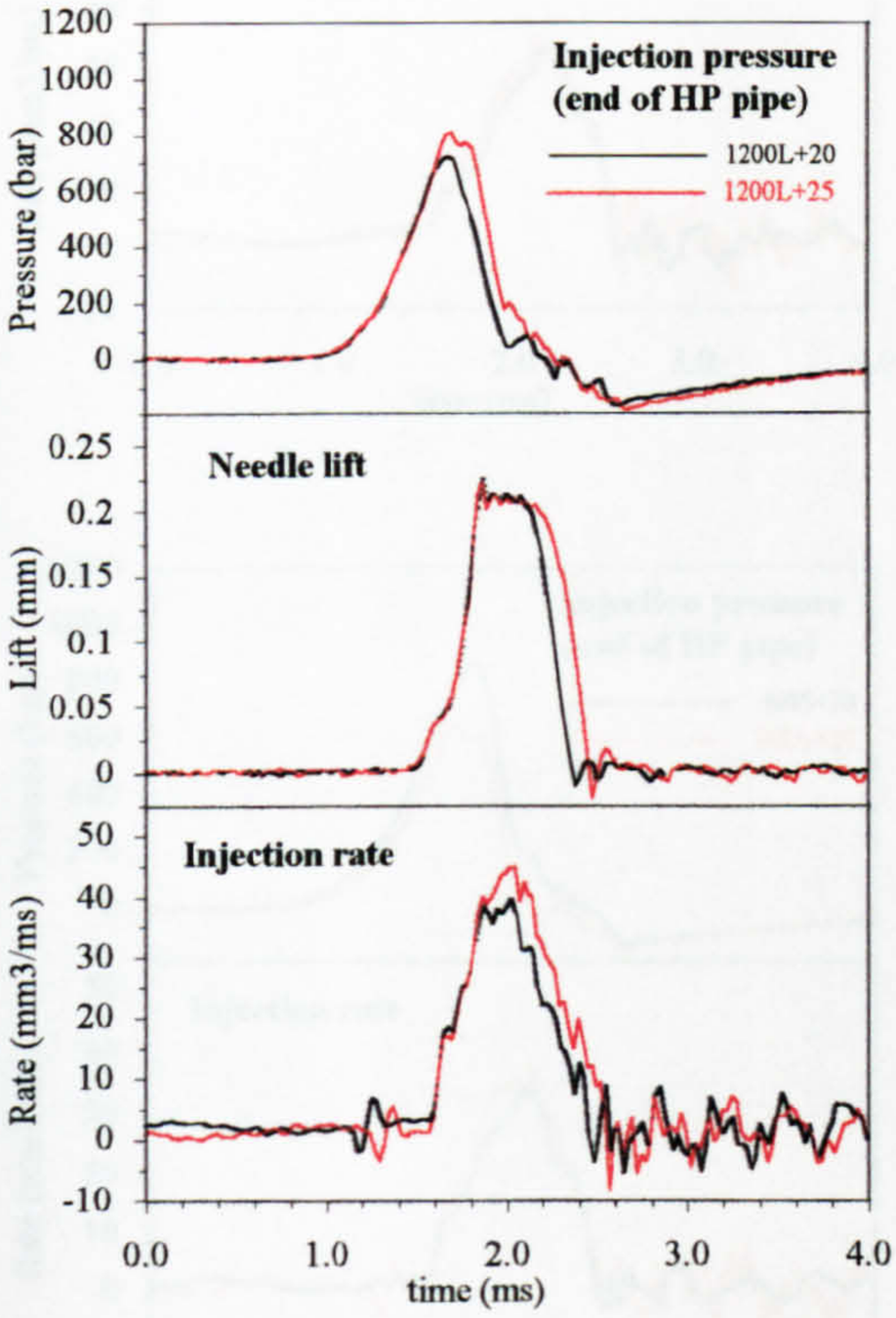


Figure 4.2 Injection pressure, needle lift and injection rate profiles for the normal and doubled pump speeds







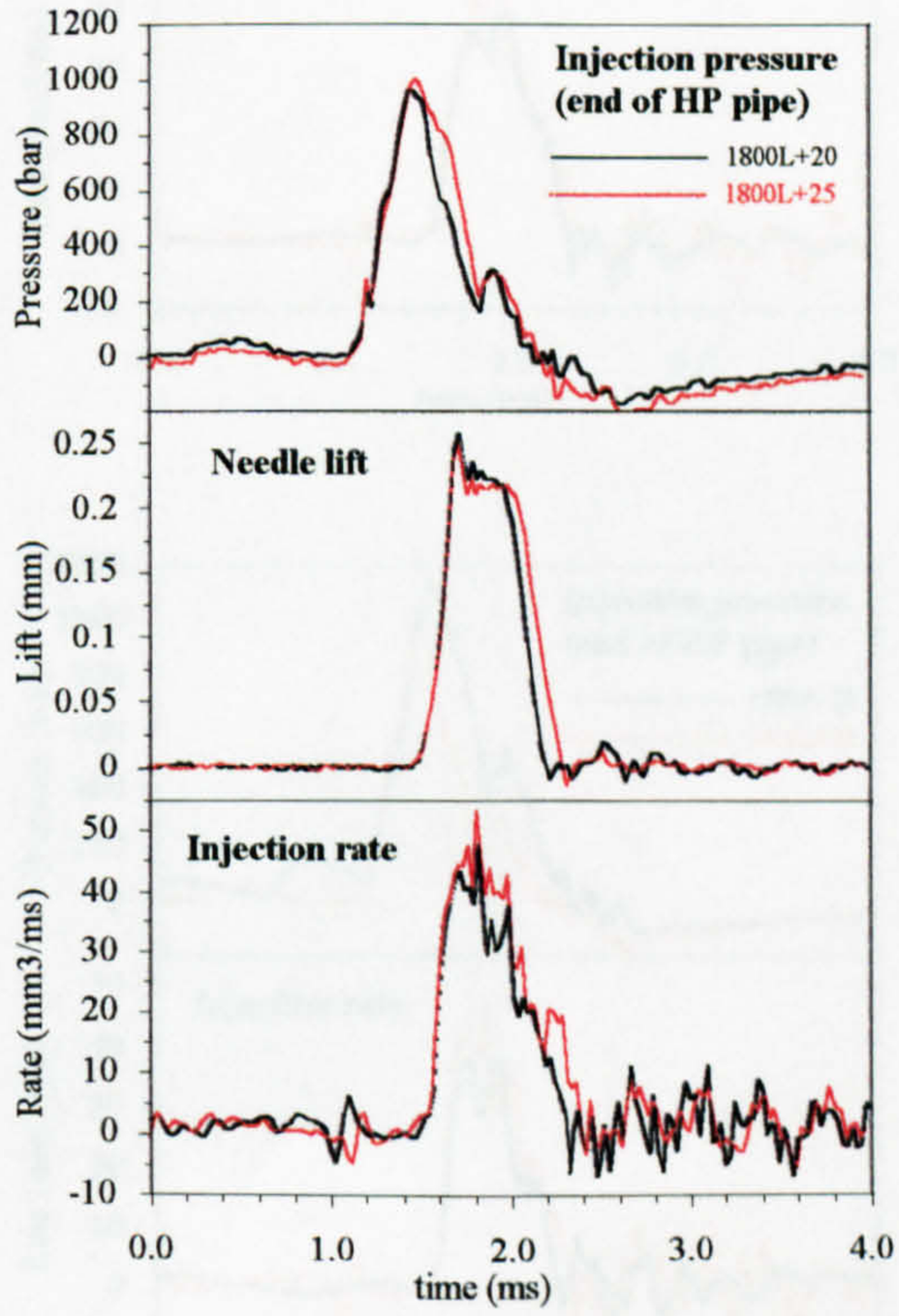
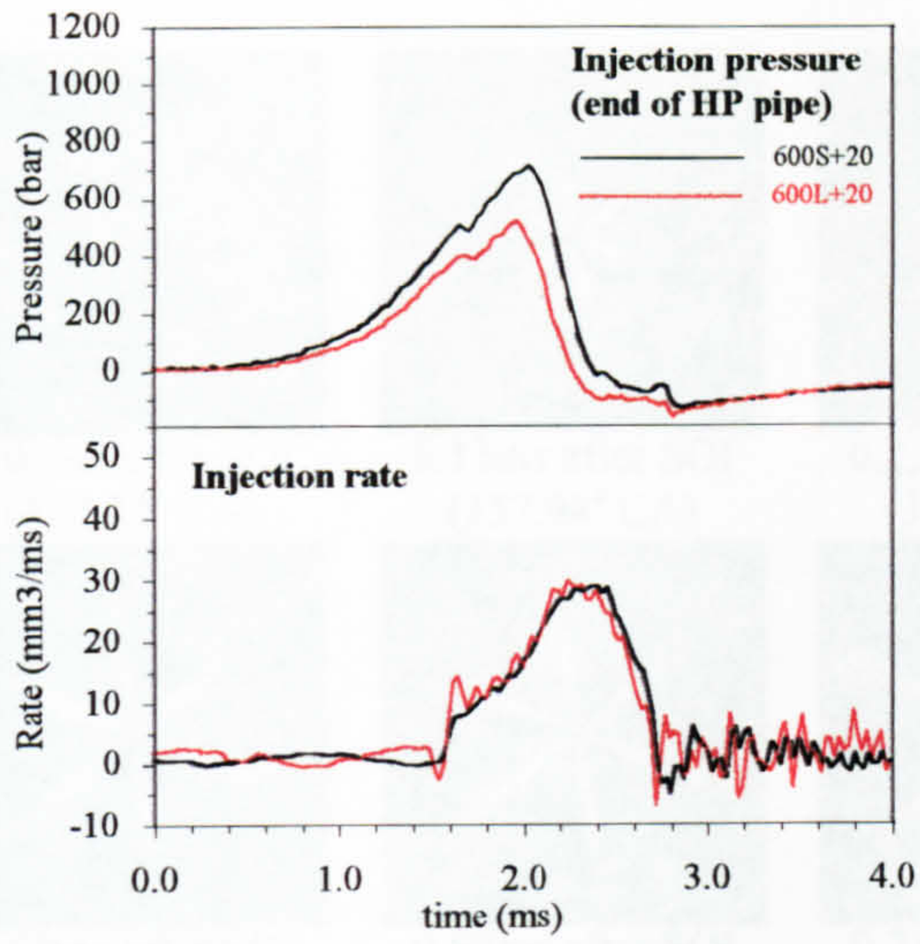
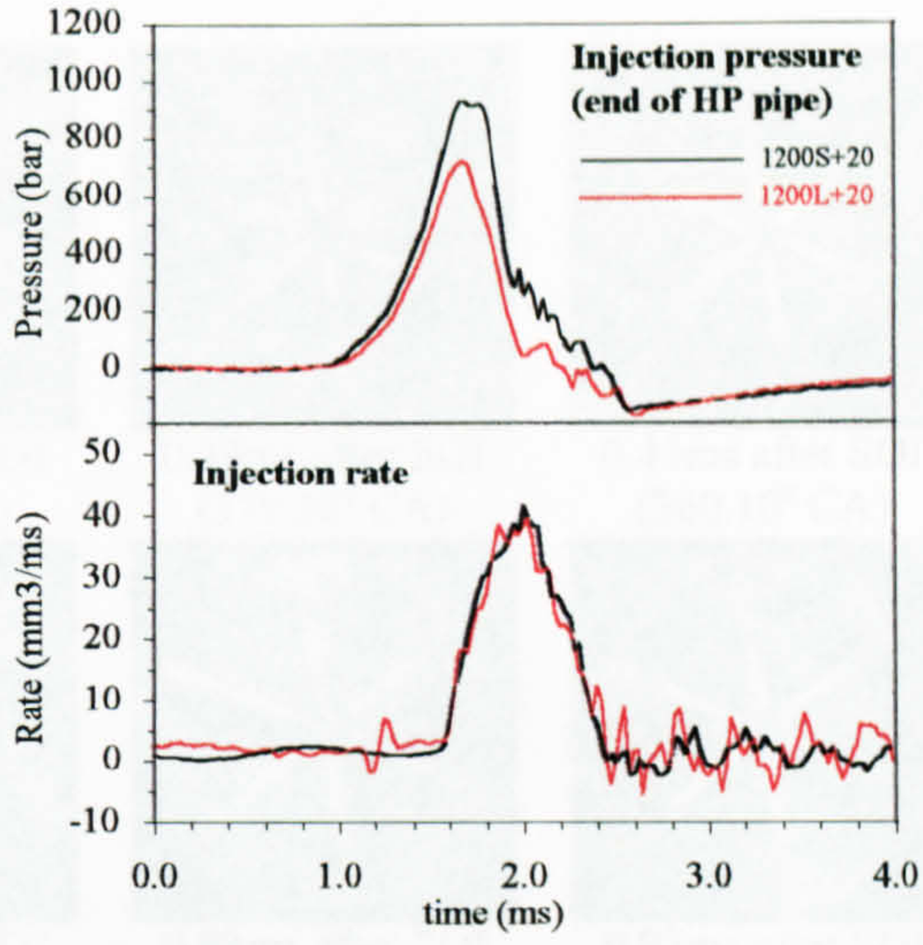
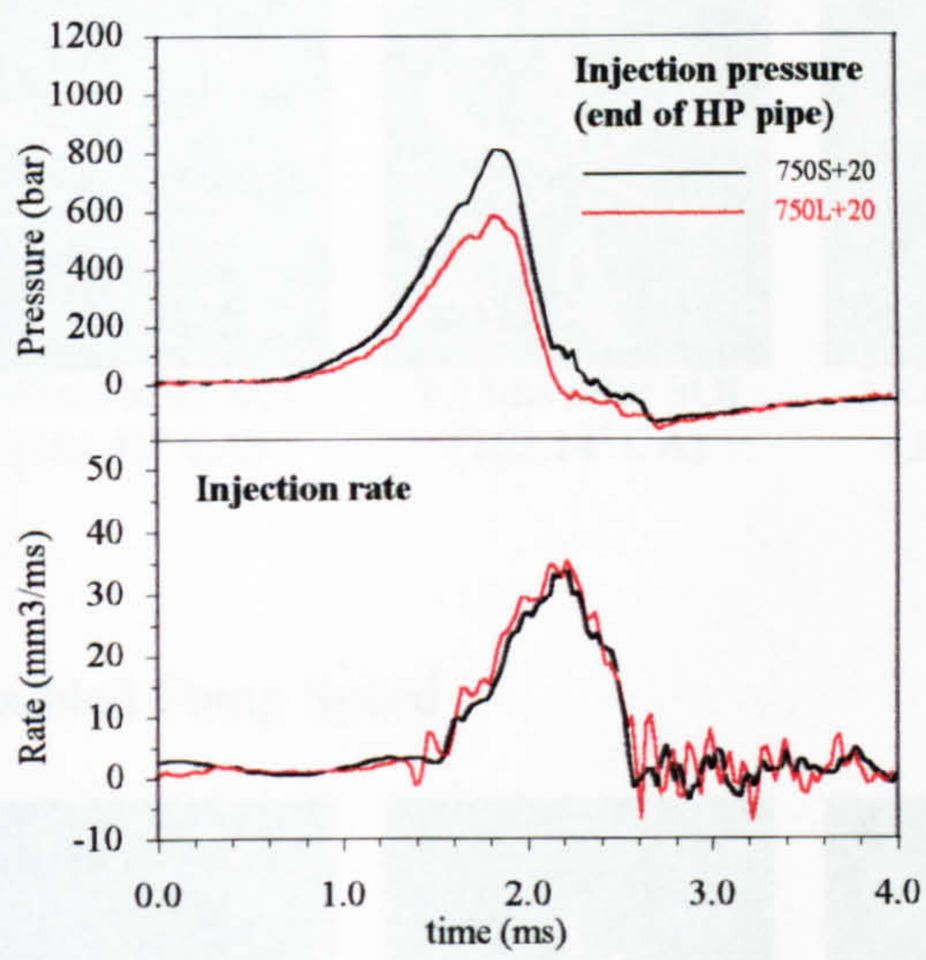
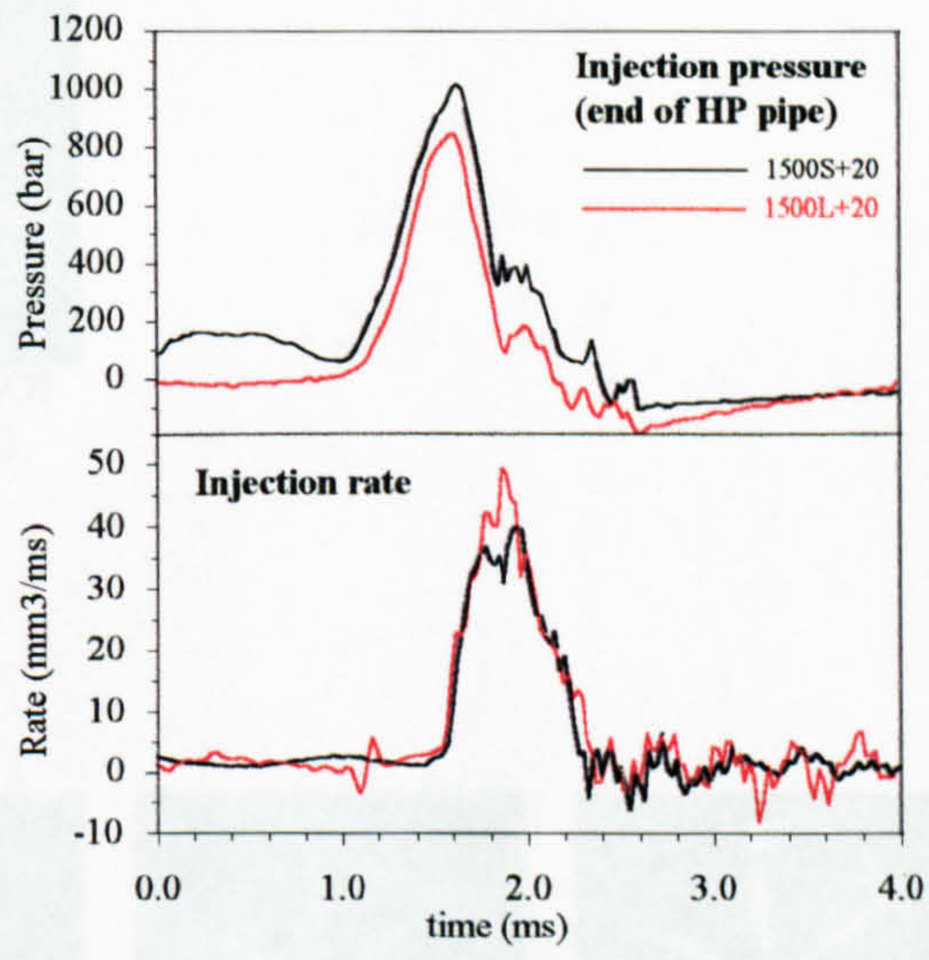


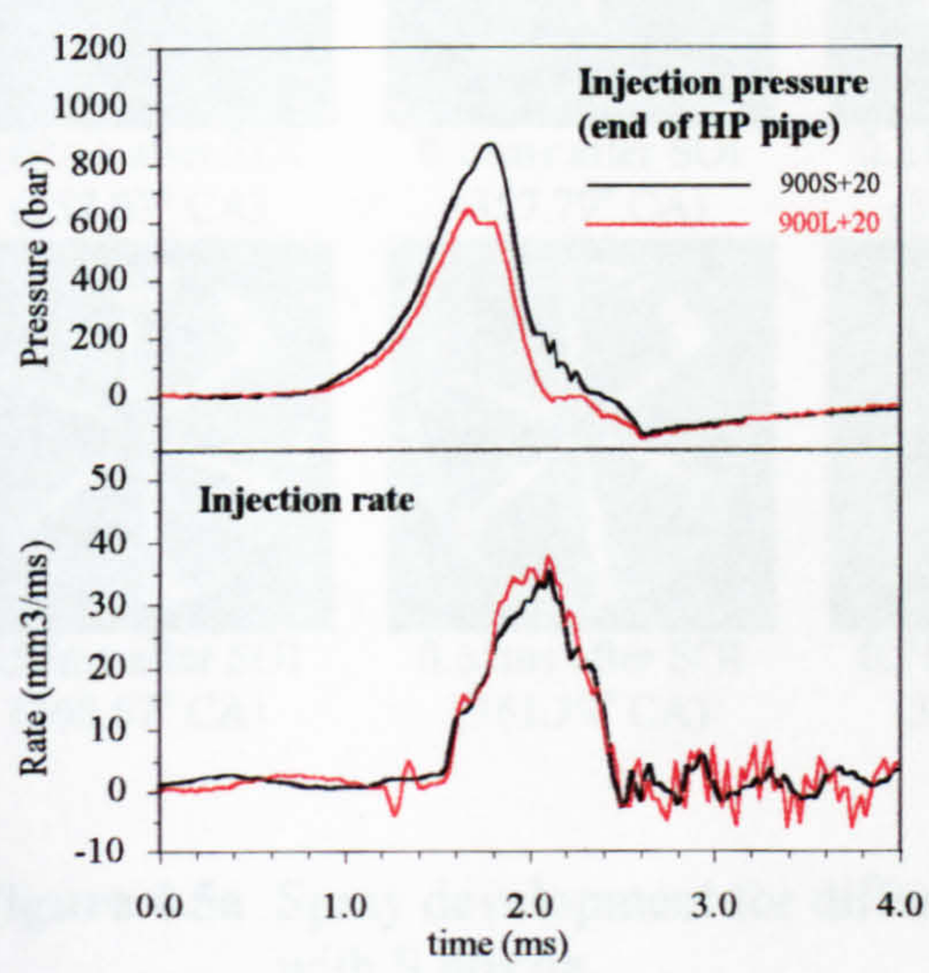
Figure 4.3 Injection pressure, needle lift and injection rate profiles for 20mm^3/inj and 25mm^3/inj of fuel delivery











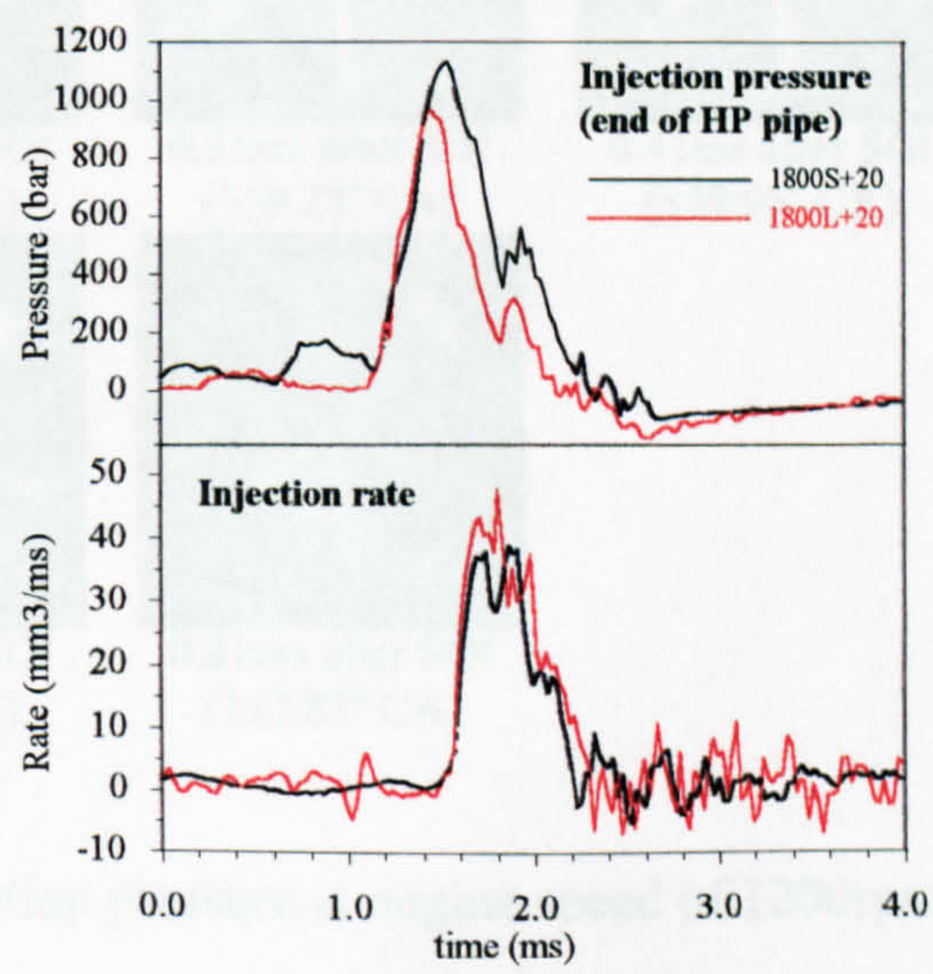
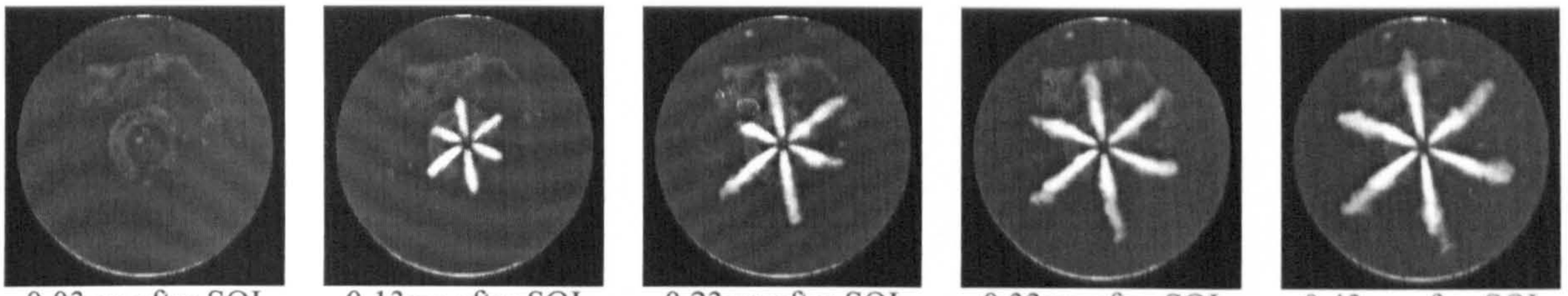


Figure 4.4 Injection pressure and injection rate profiles for the different nozzle configurations

Normal Pump Speed



Doubled Pump Speed

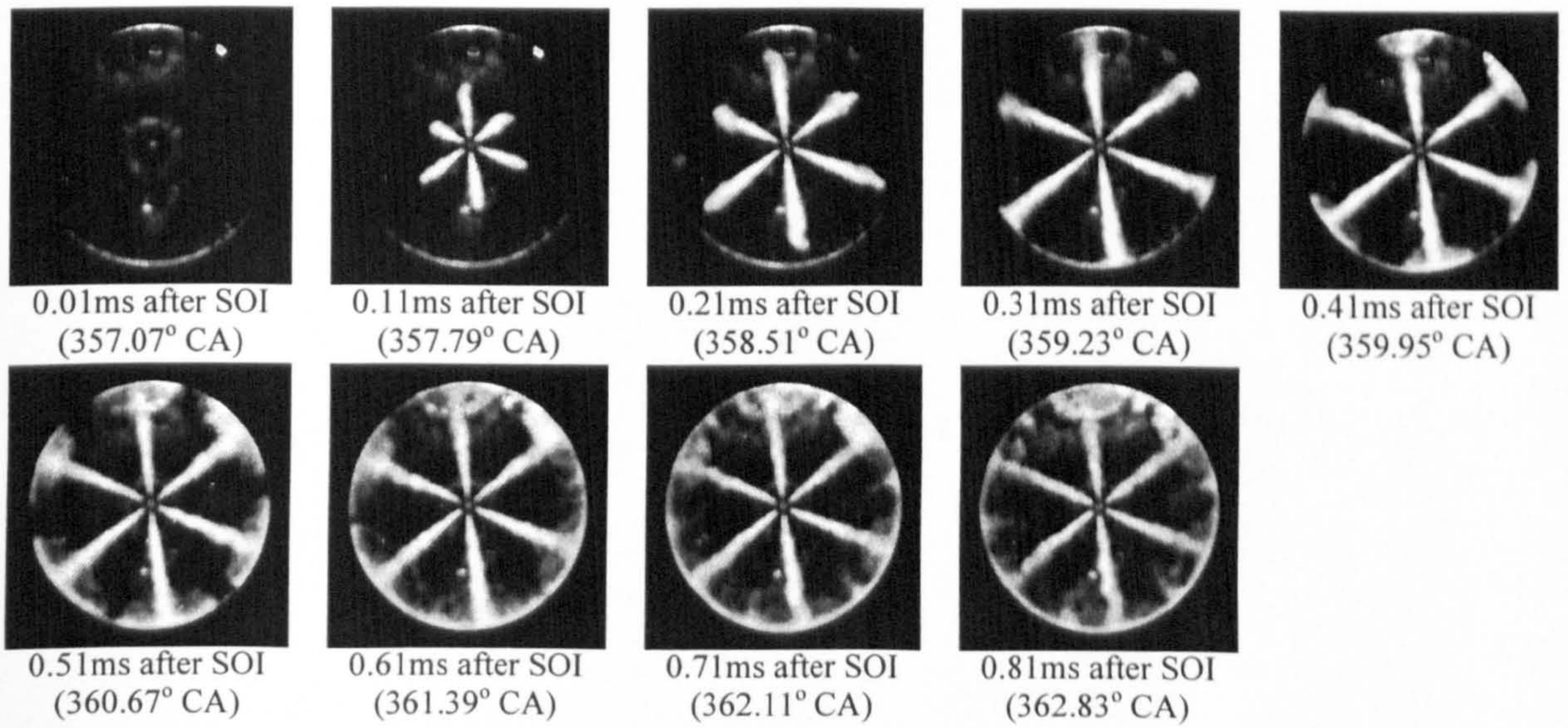
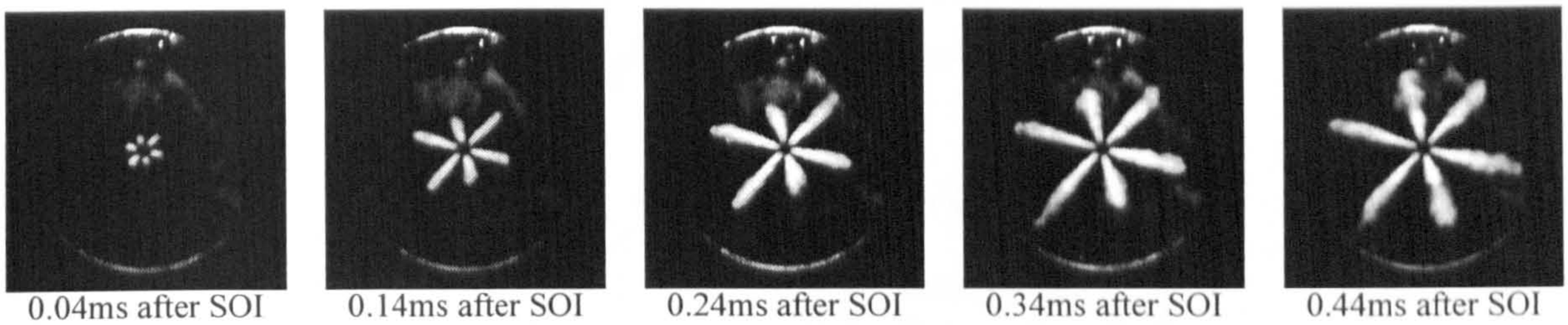


Figure 4.5a Spray development for different injection pressure at engine speed of 1200rpm with S nozzle

Normal Pump Speed



Doubled Pump Speed

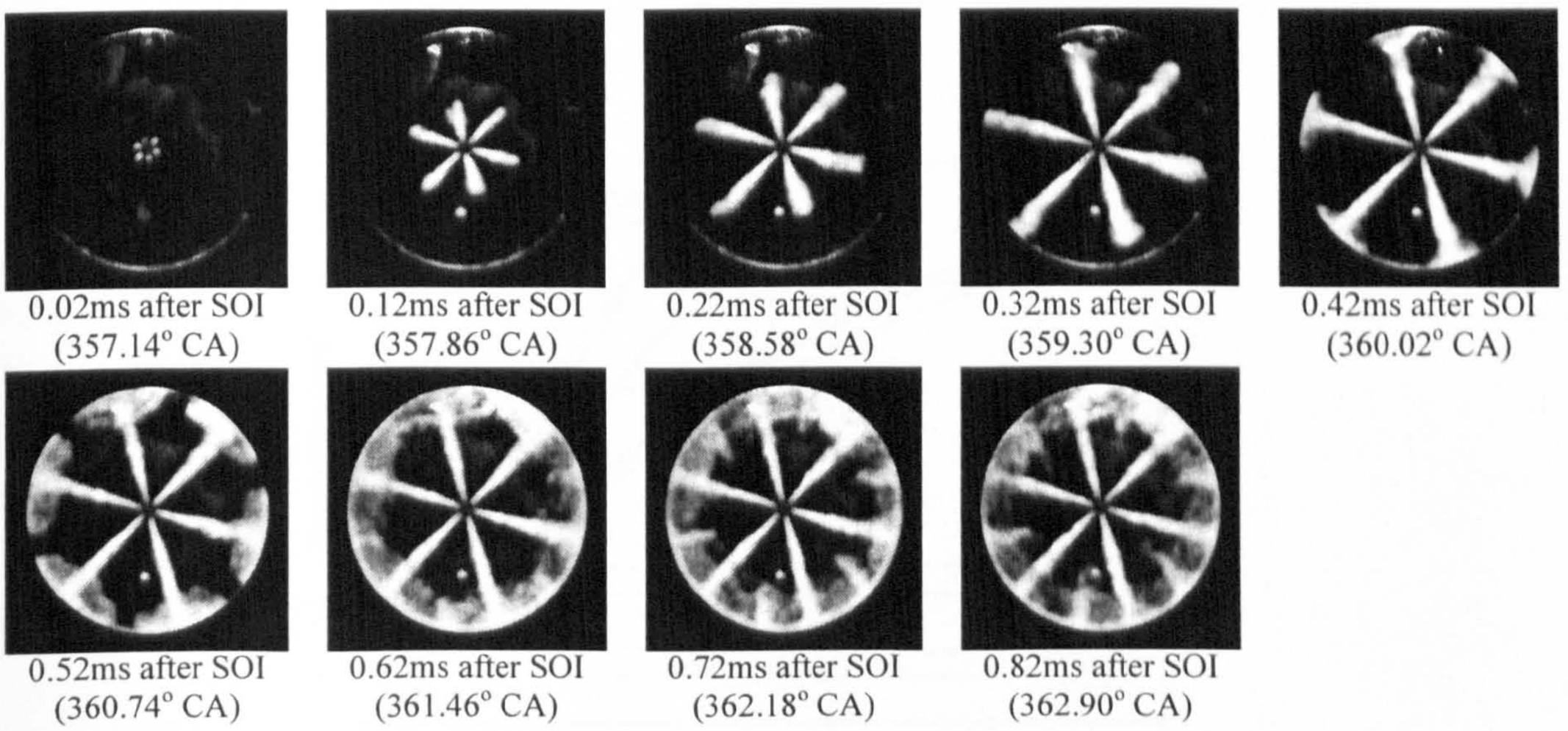
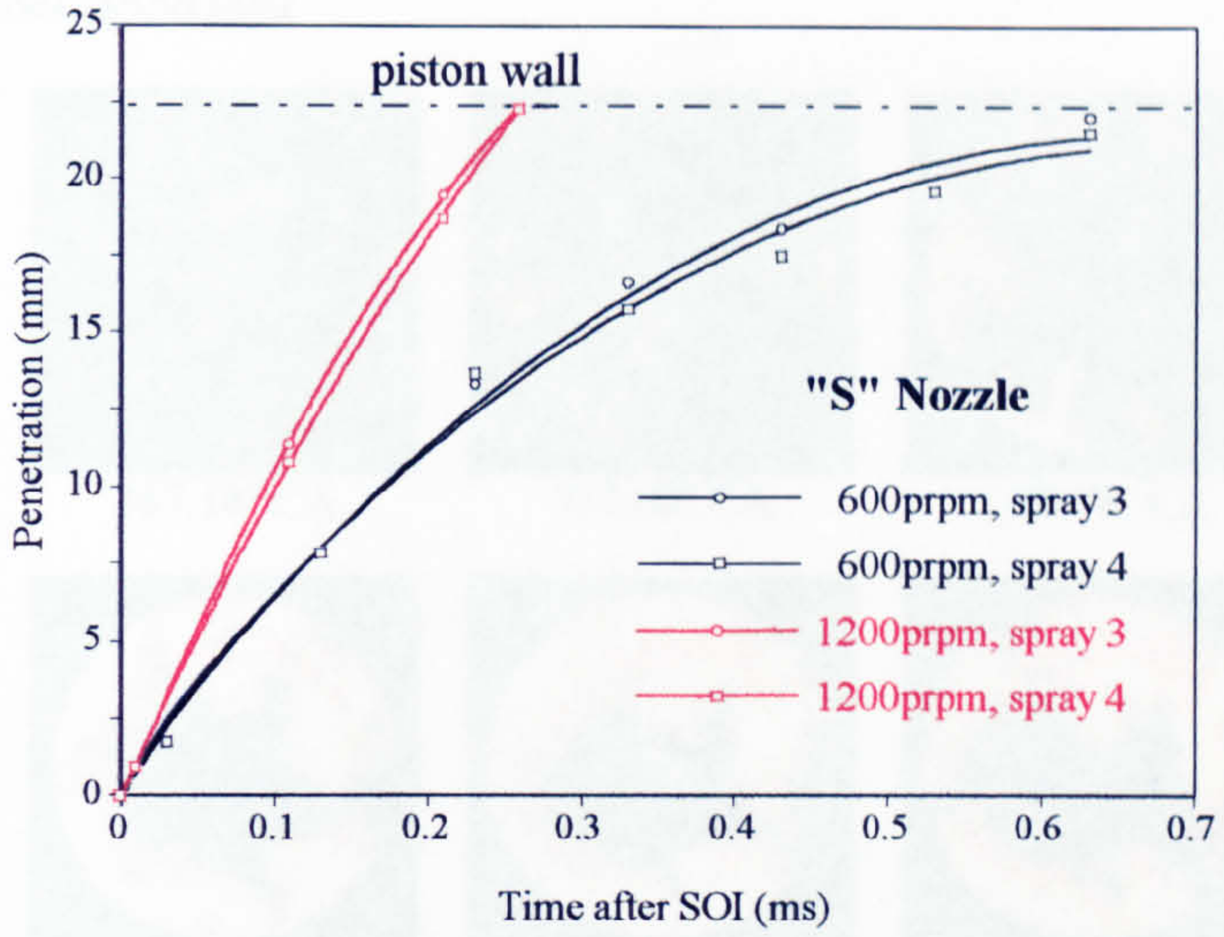
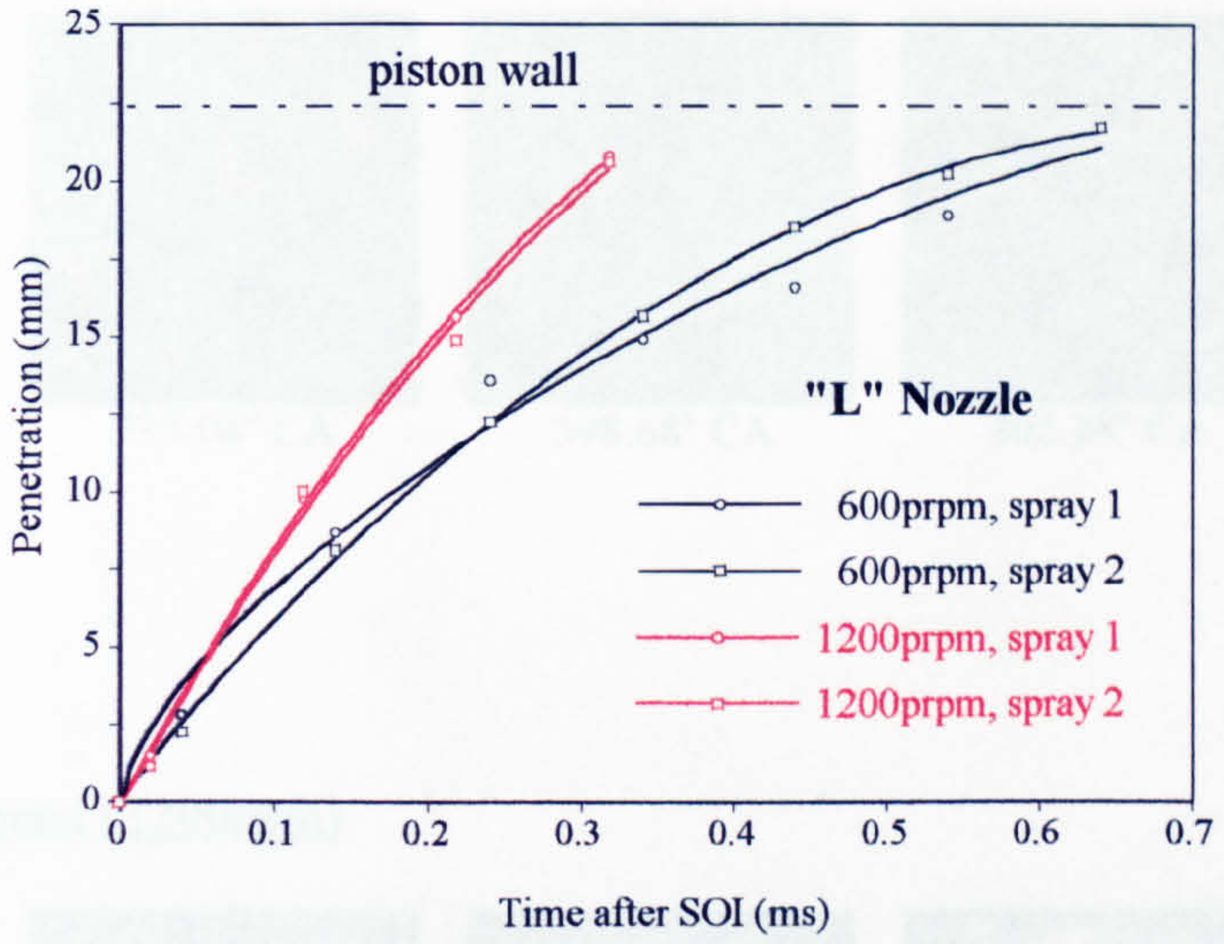


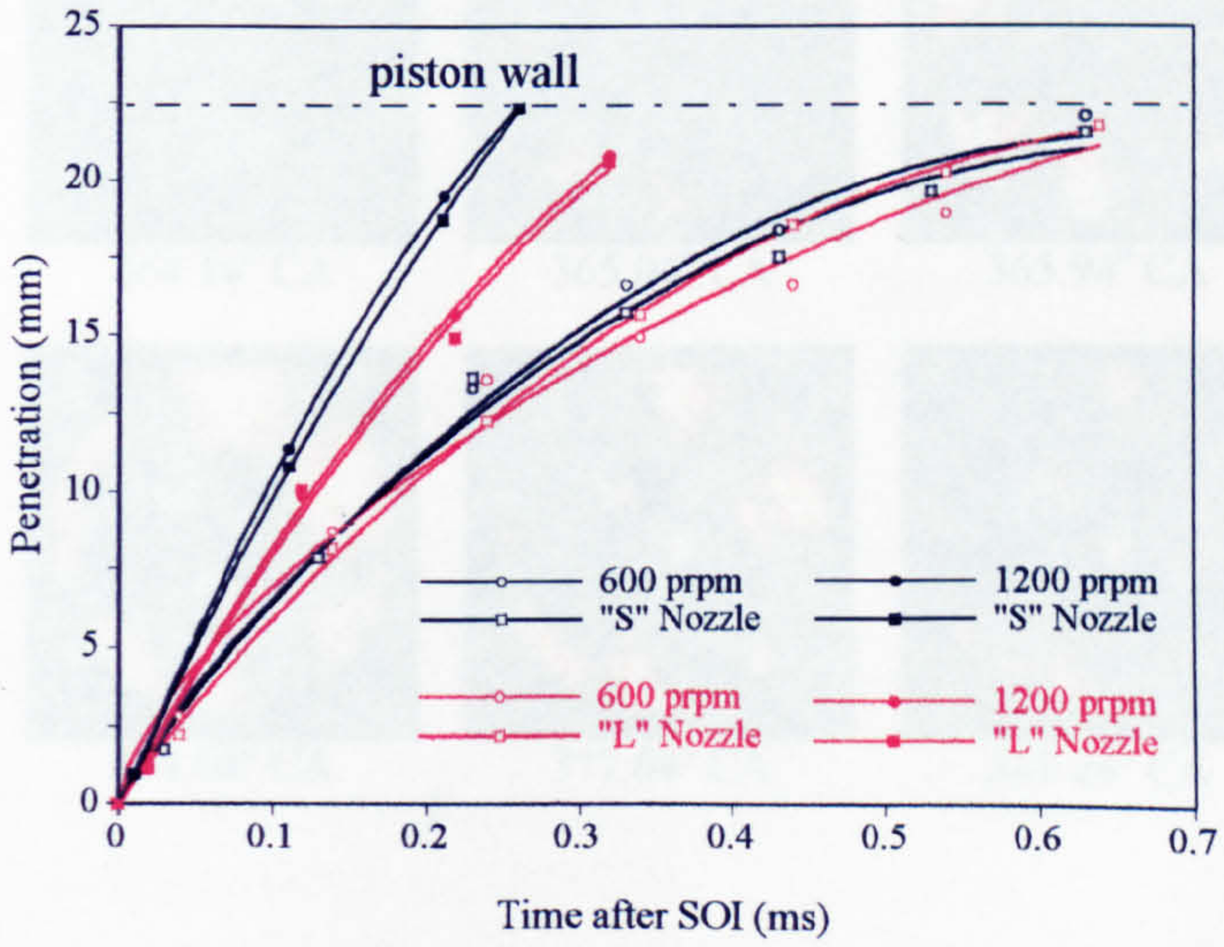
Figure 4.5b Spray development for different injection pressure at engine speed of 1200rpm with L nozzle



(a)



(b)



(c)

Figure 4.6 Spray tip penetration for different injection pressure and nozzle configurations

Normal Pump Speed (600rpm)



Doubled Pump Speed (1200rpm)

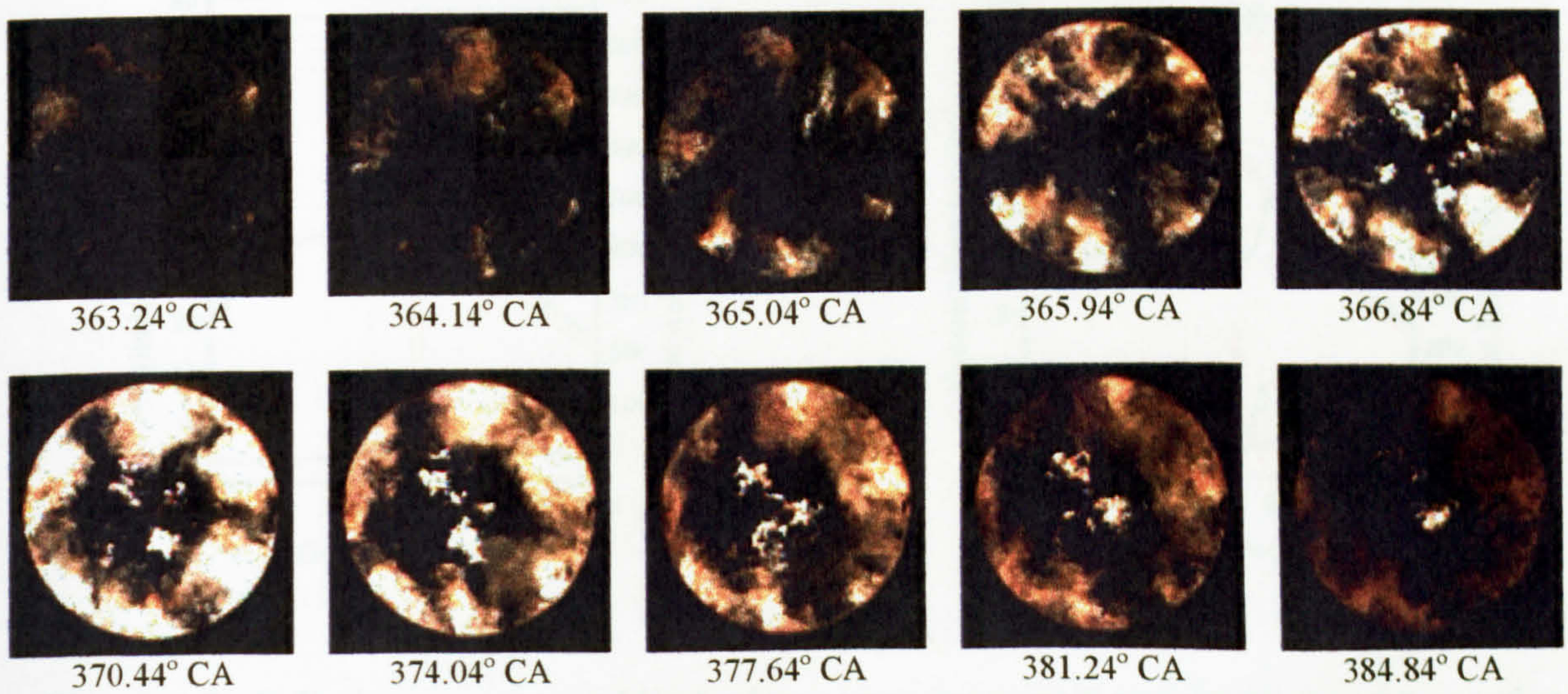
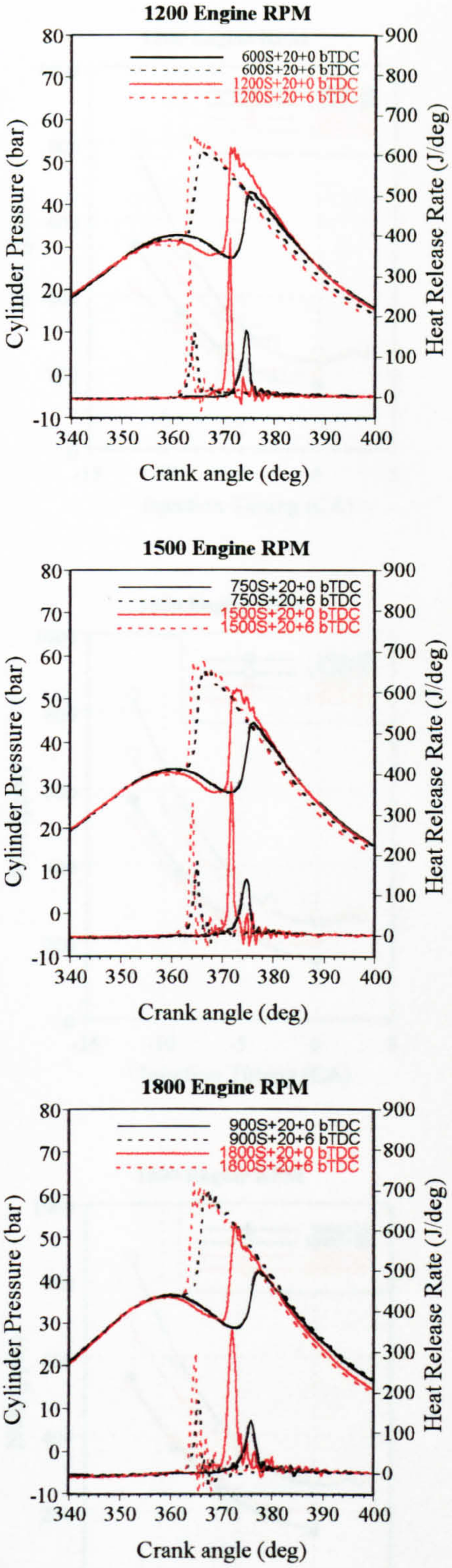


Figure 4.7 Flame development for different injection pressure at engine speed of 1200rpm with S nozzle



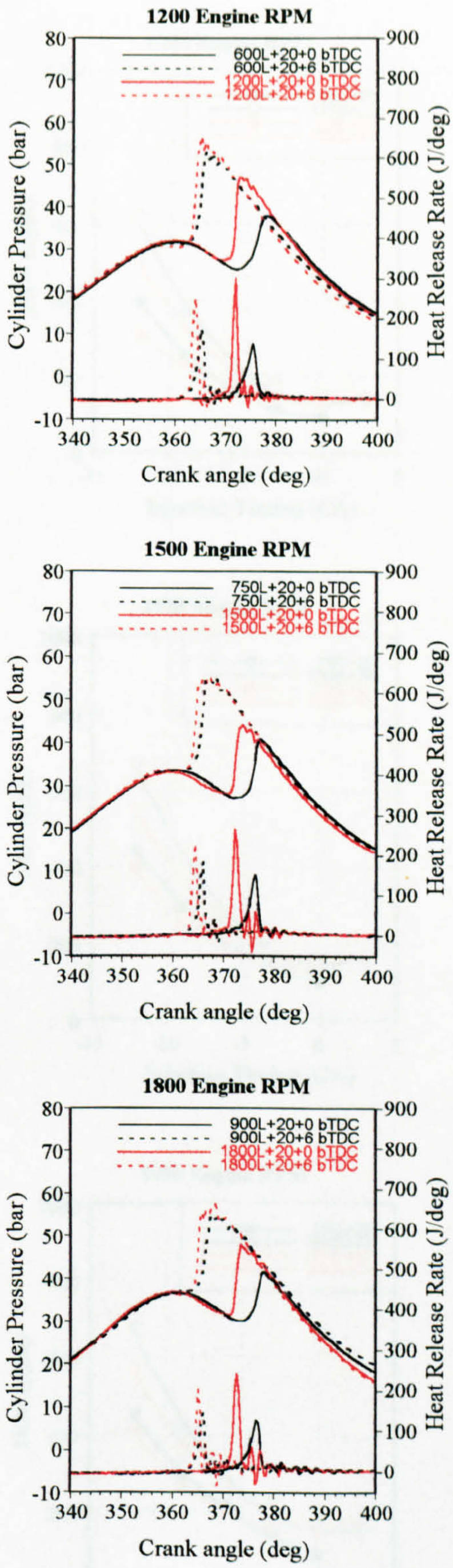
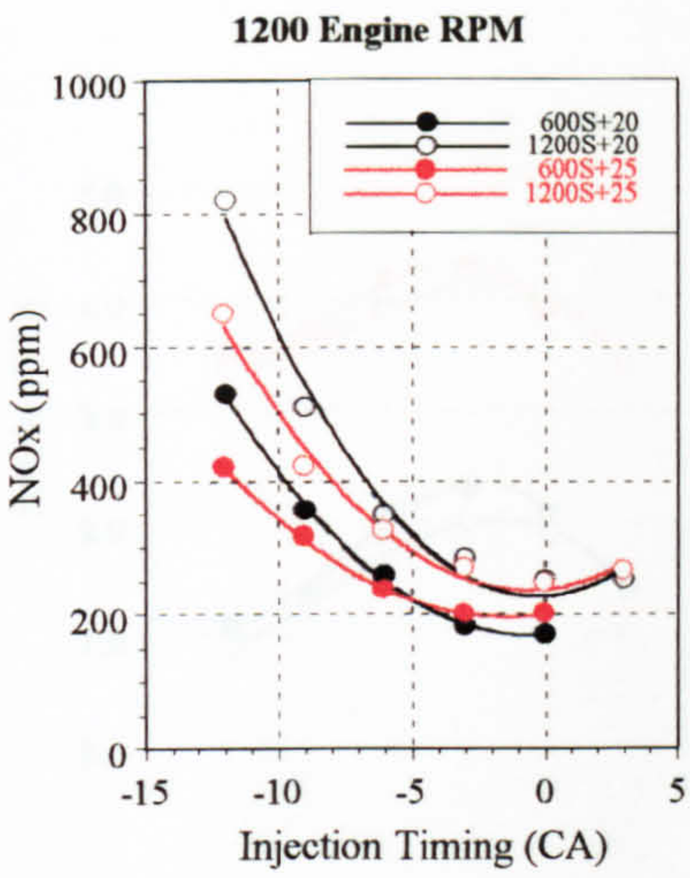
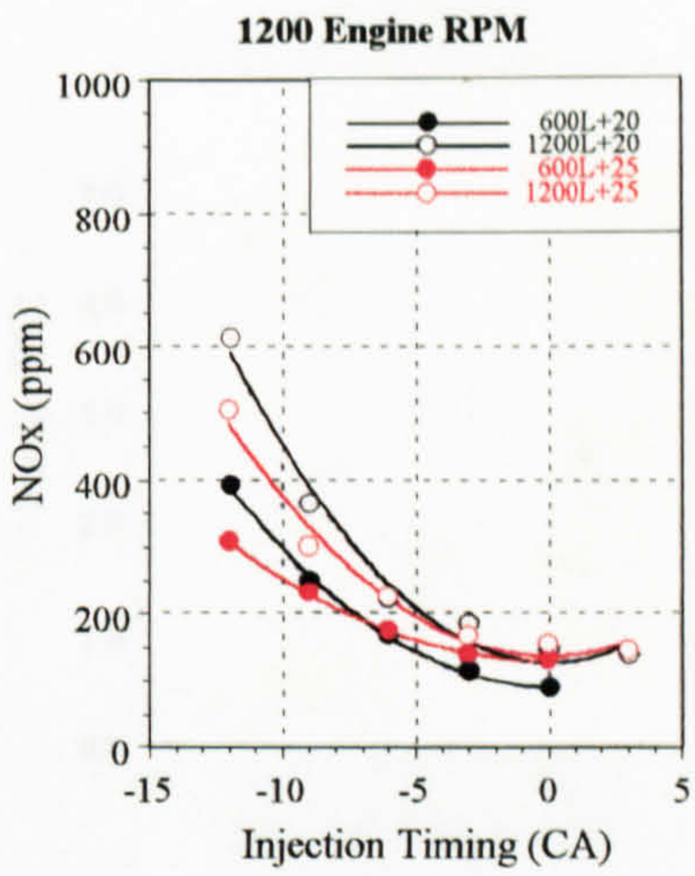
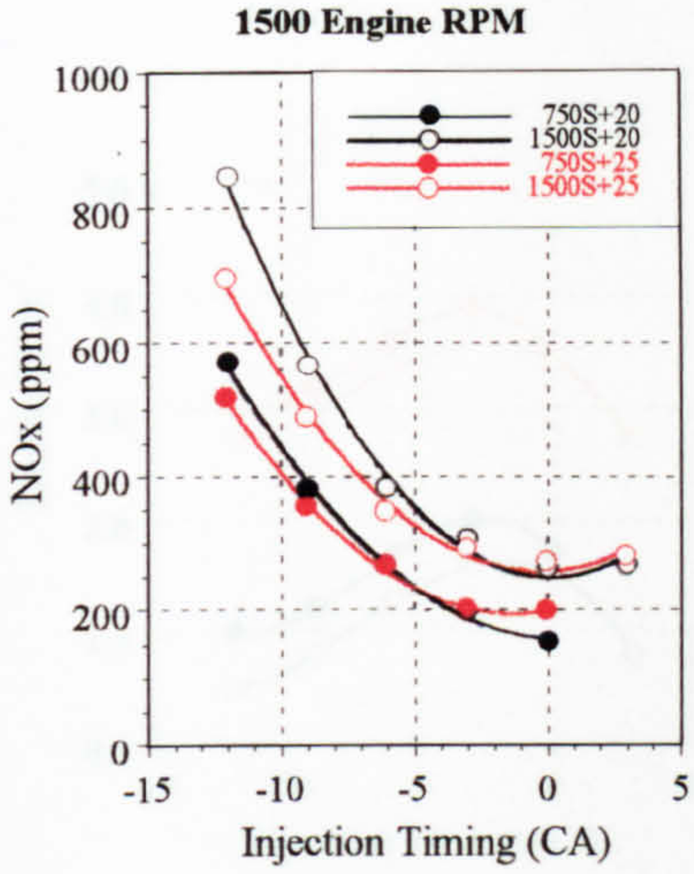
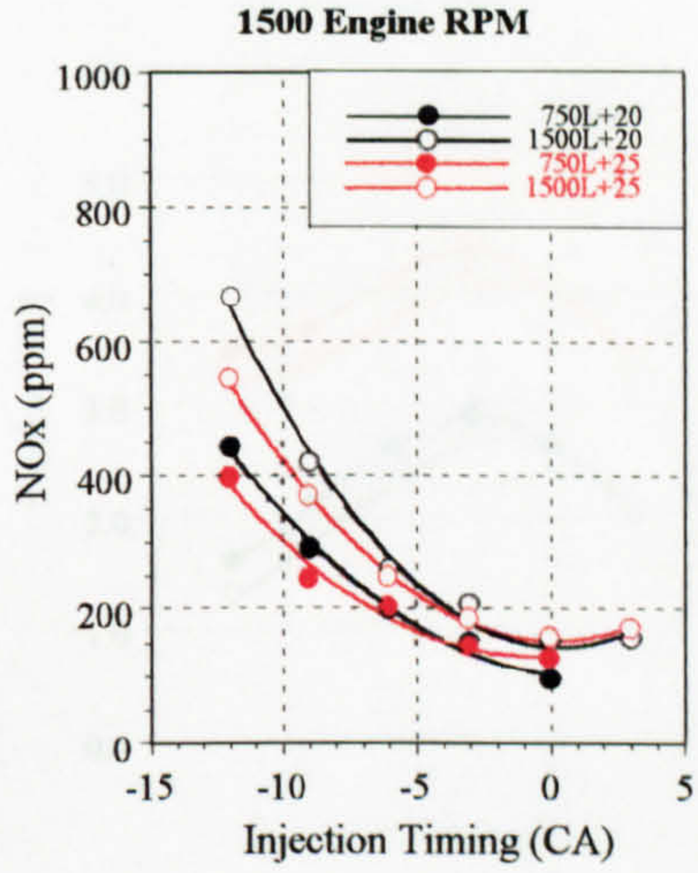


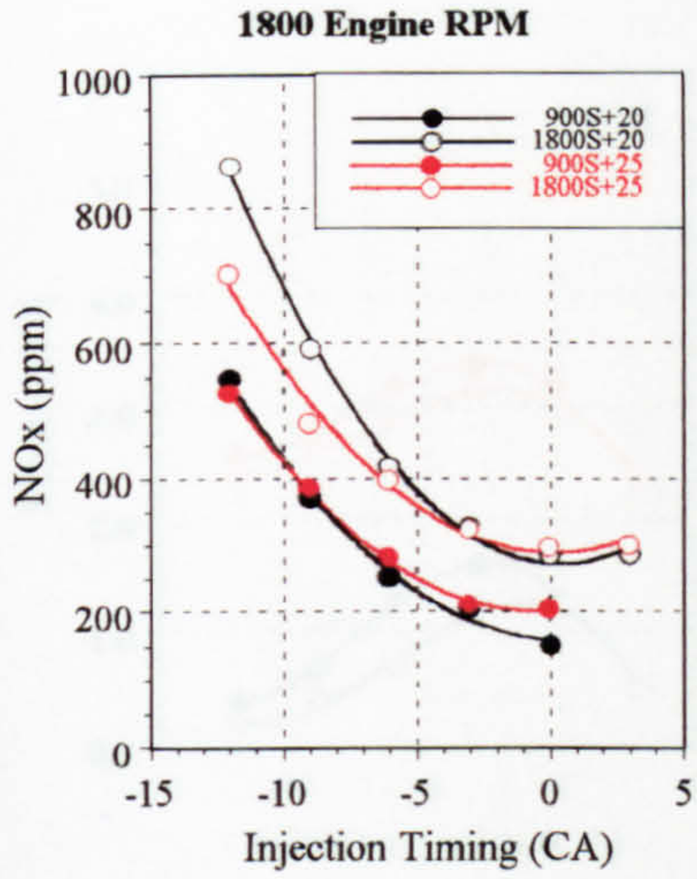
Figure 4.8 Cylinder pressures and heat release rates for normal and doubled pump speed at various engine operating conditions











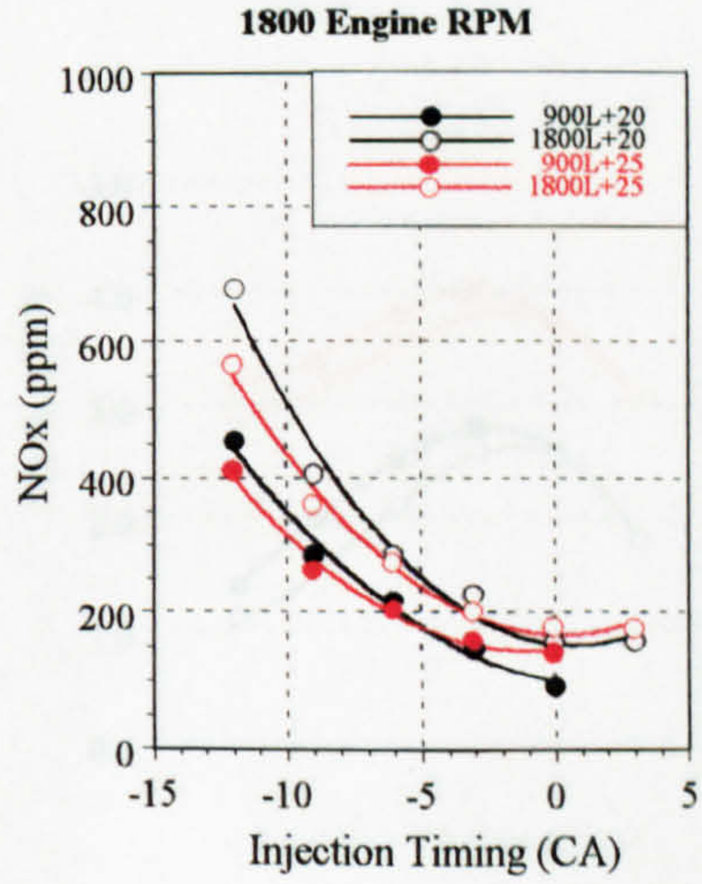
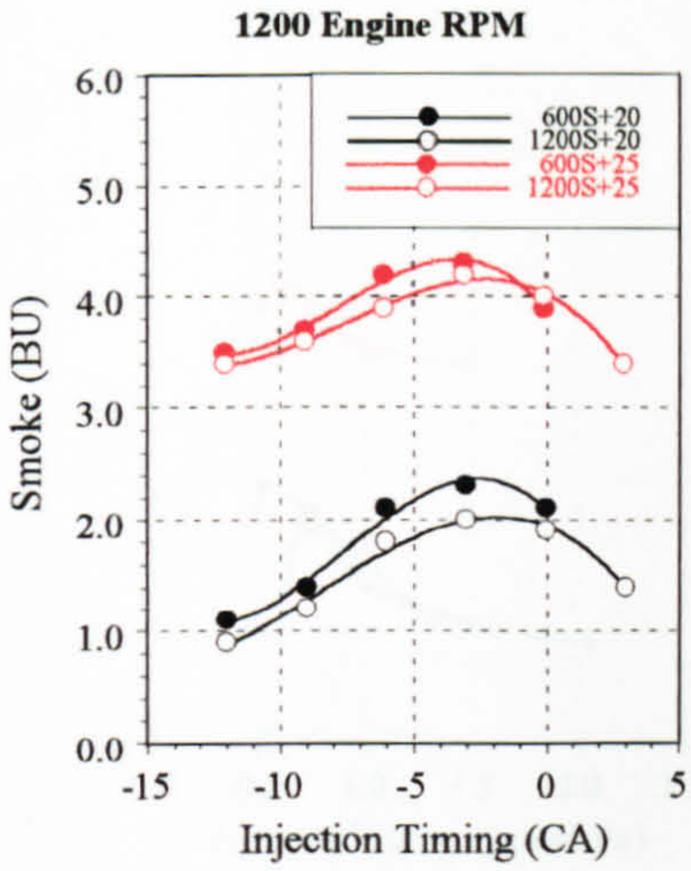
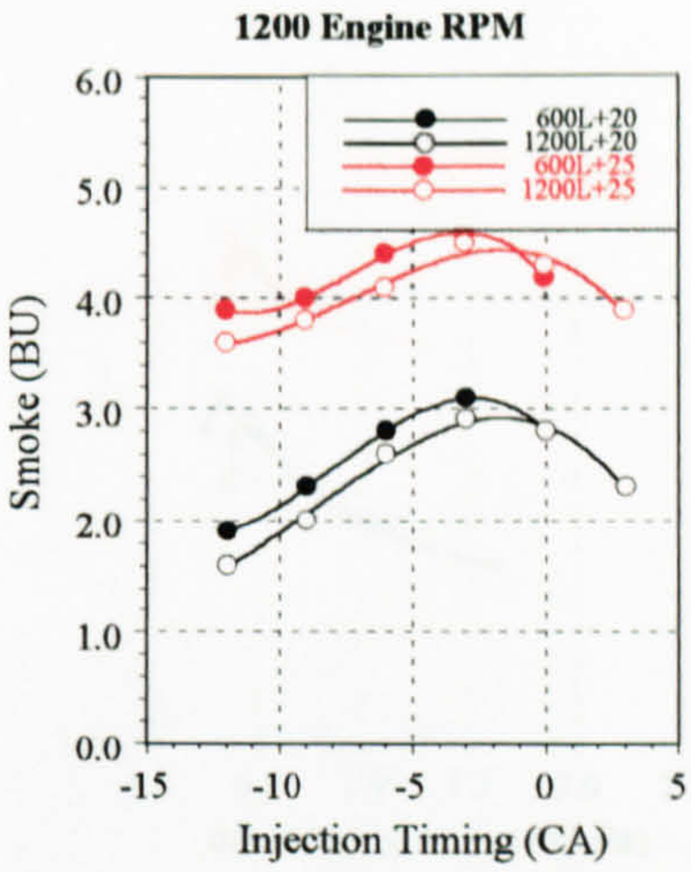
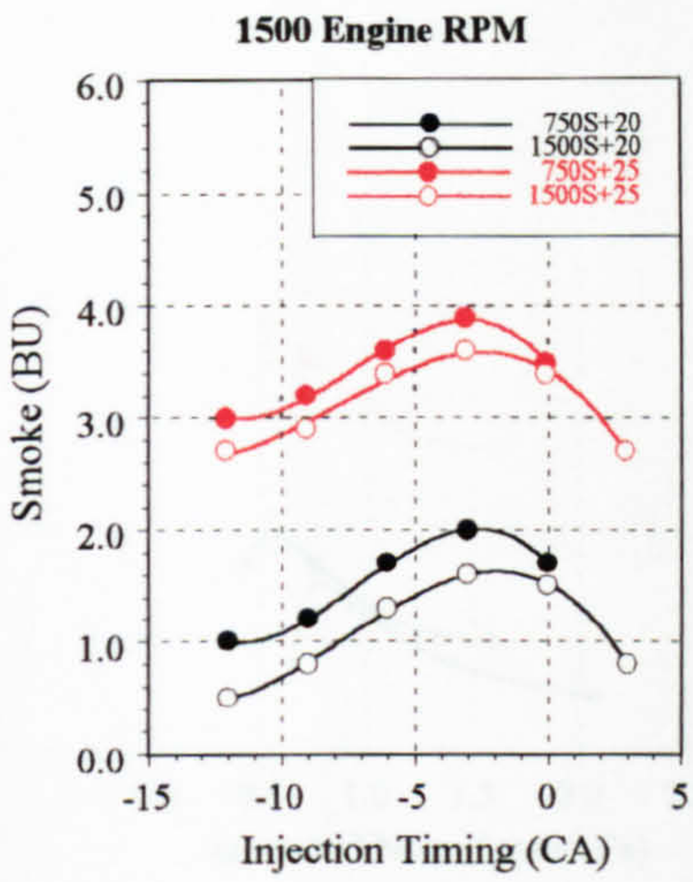
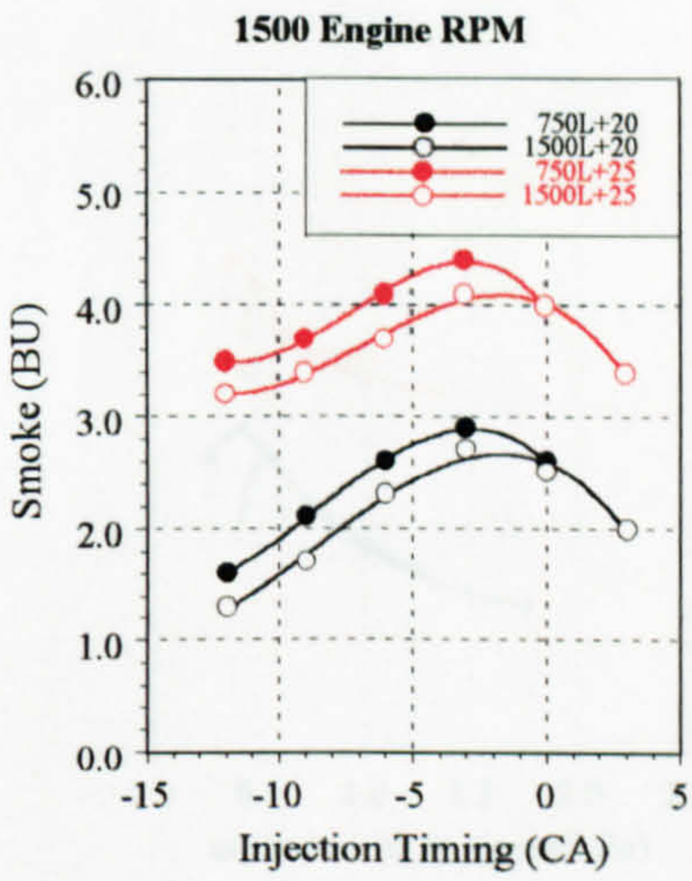


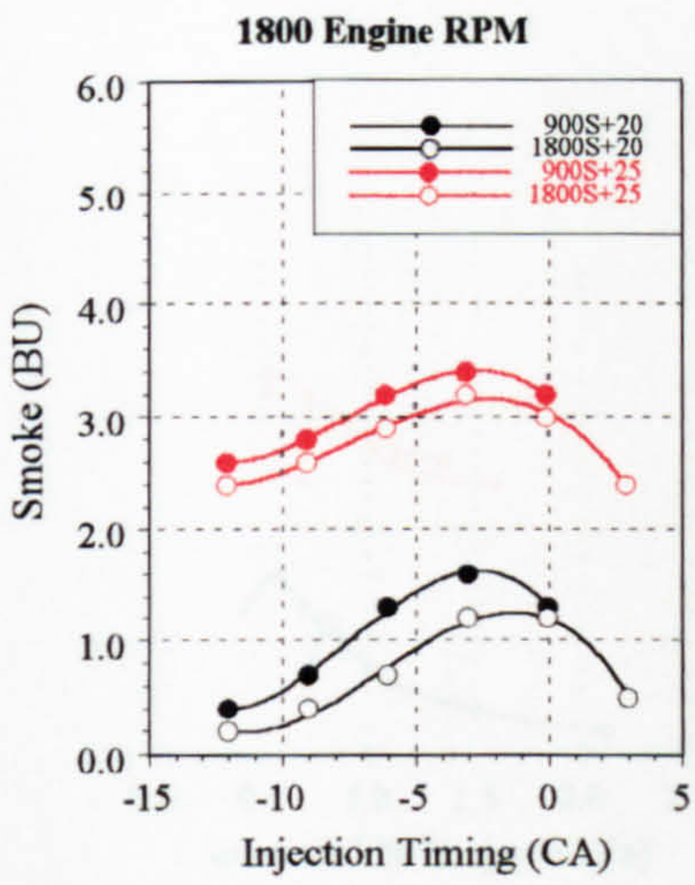
Figure 4.9 Effects of injection pressure on NO_x emissions at various engine operating conditions











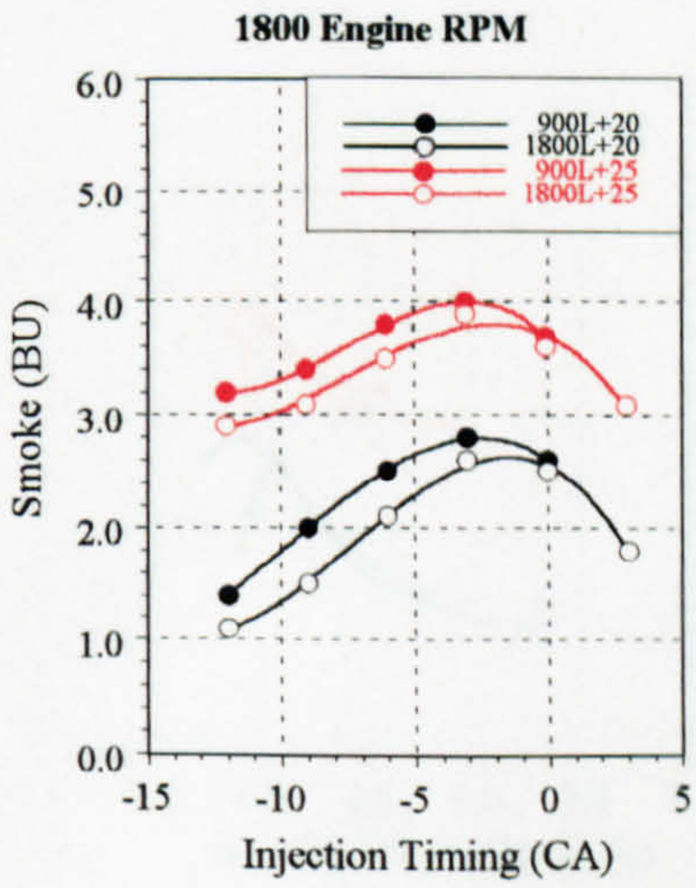
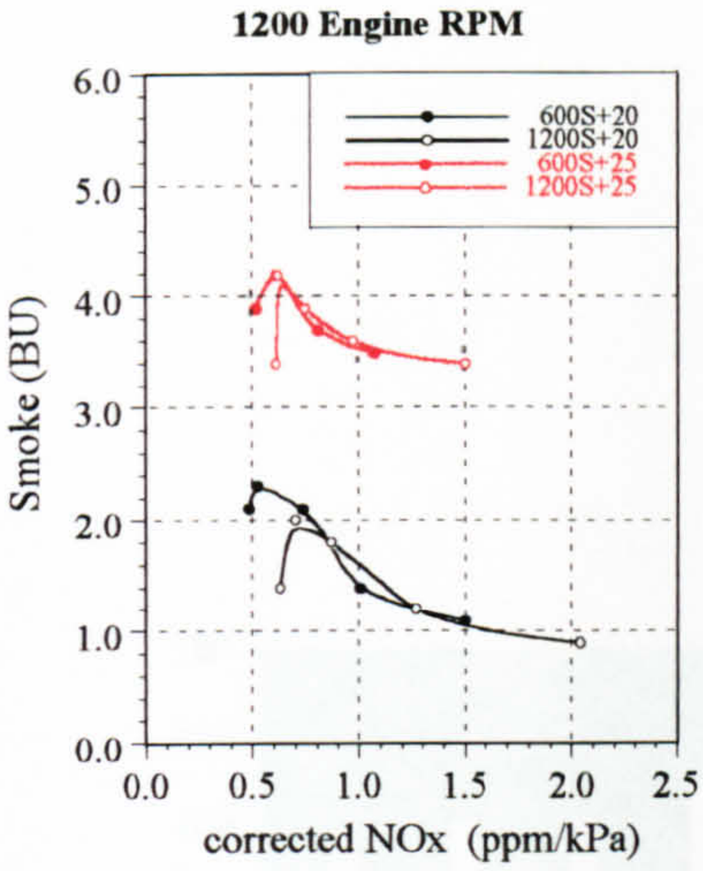
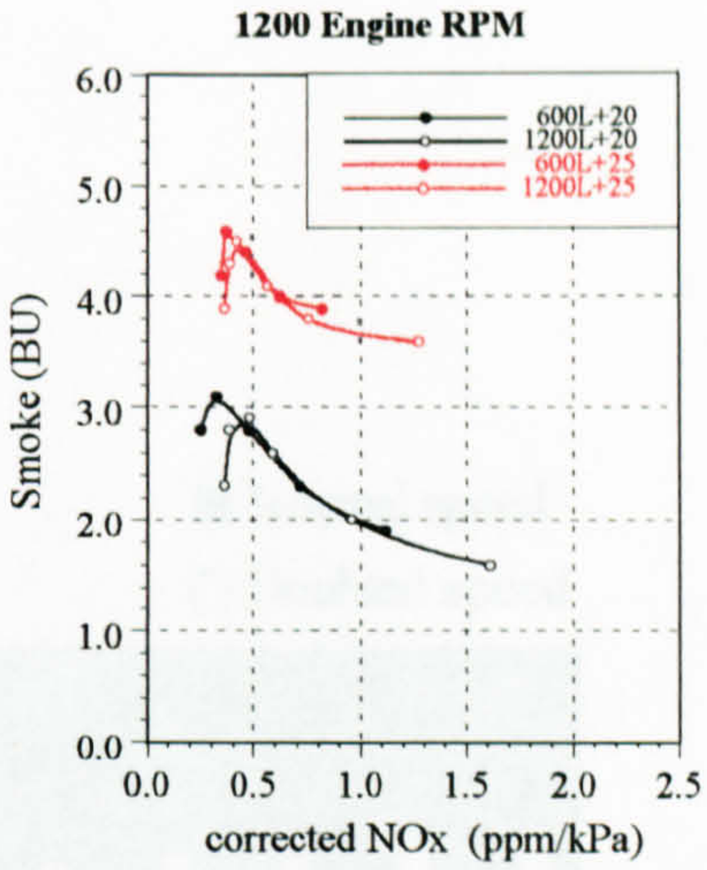
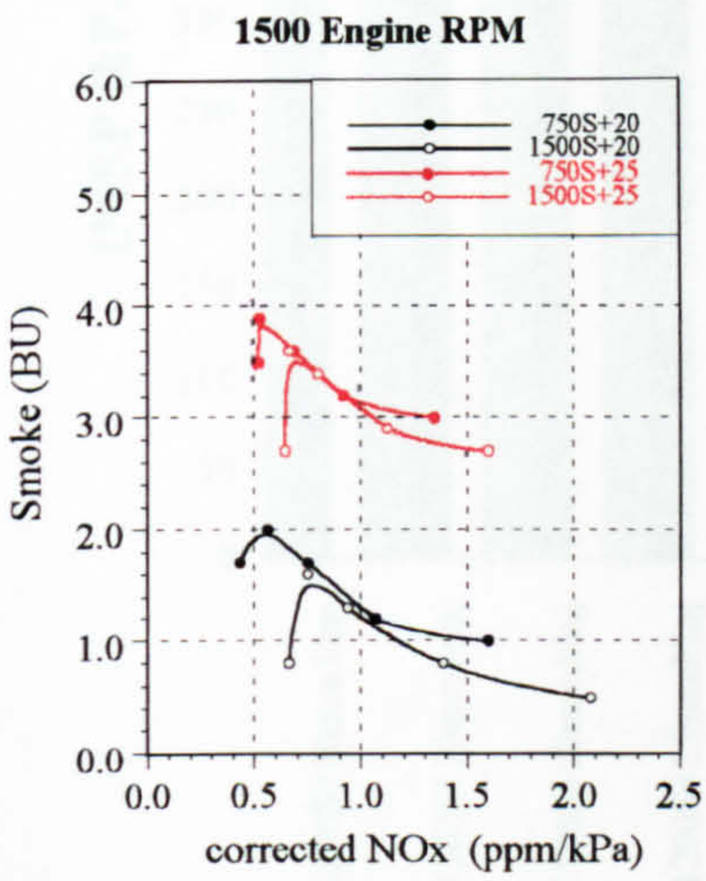
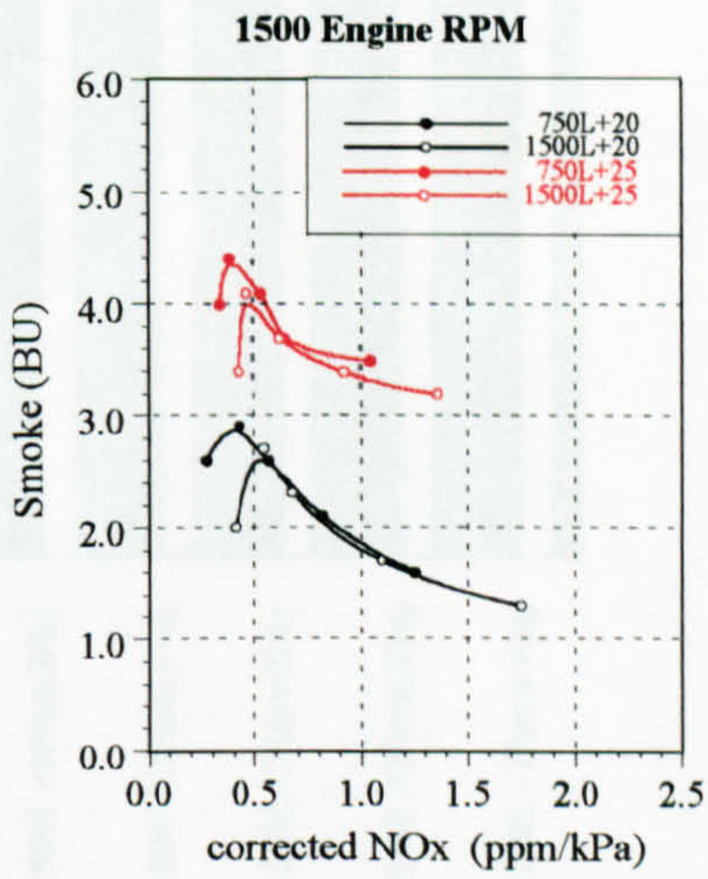


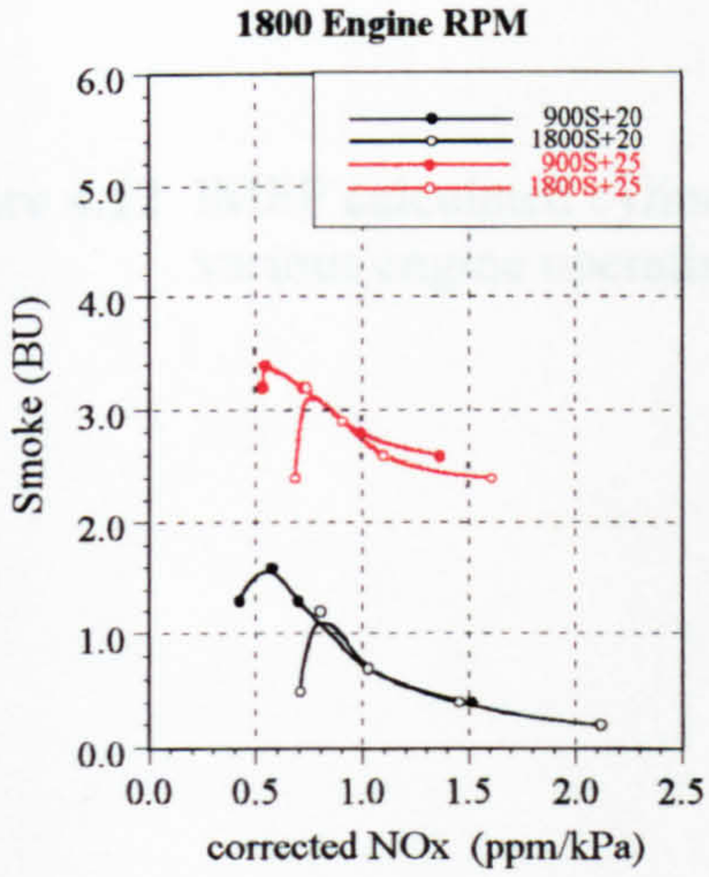
Figure 4.10 Effects of injection pressure on smoke emissions at various engine operating conditions











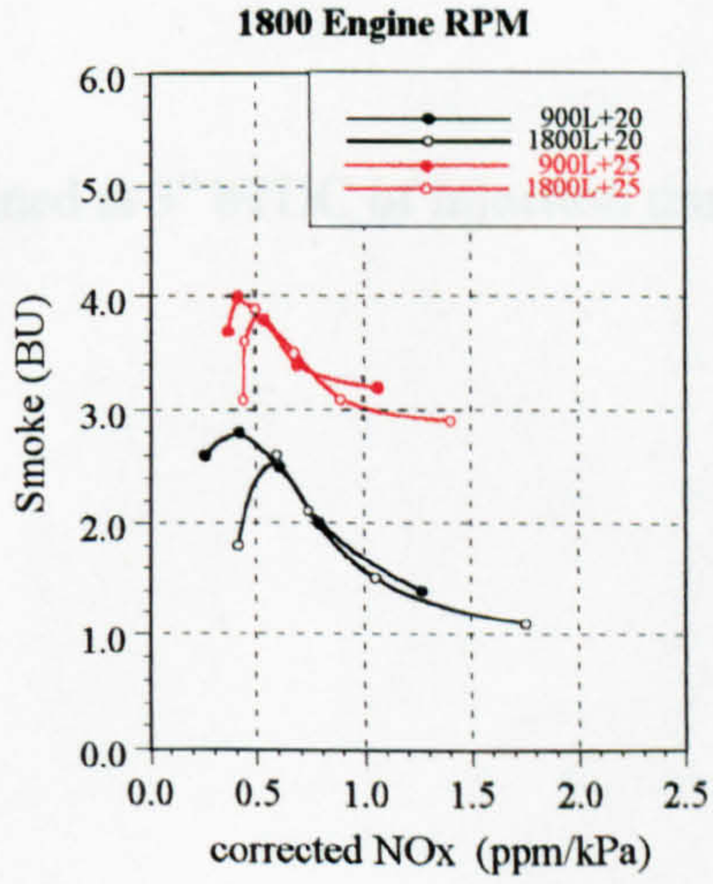


Figure 4.11 Effects of injection pressure on smoke-NO_x trade-off curves at various engine operating conditions

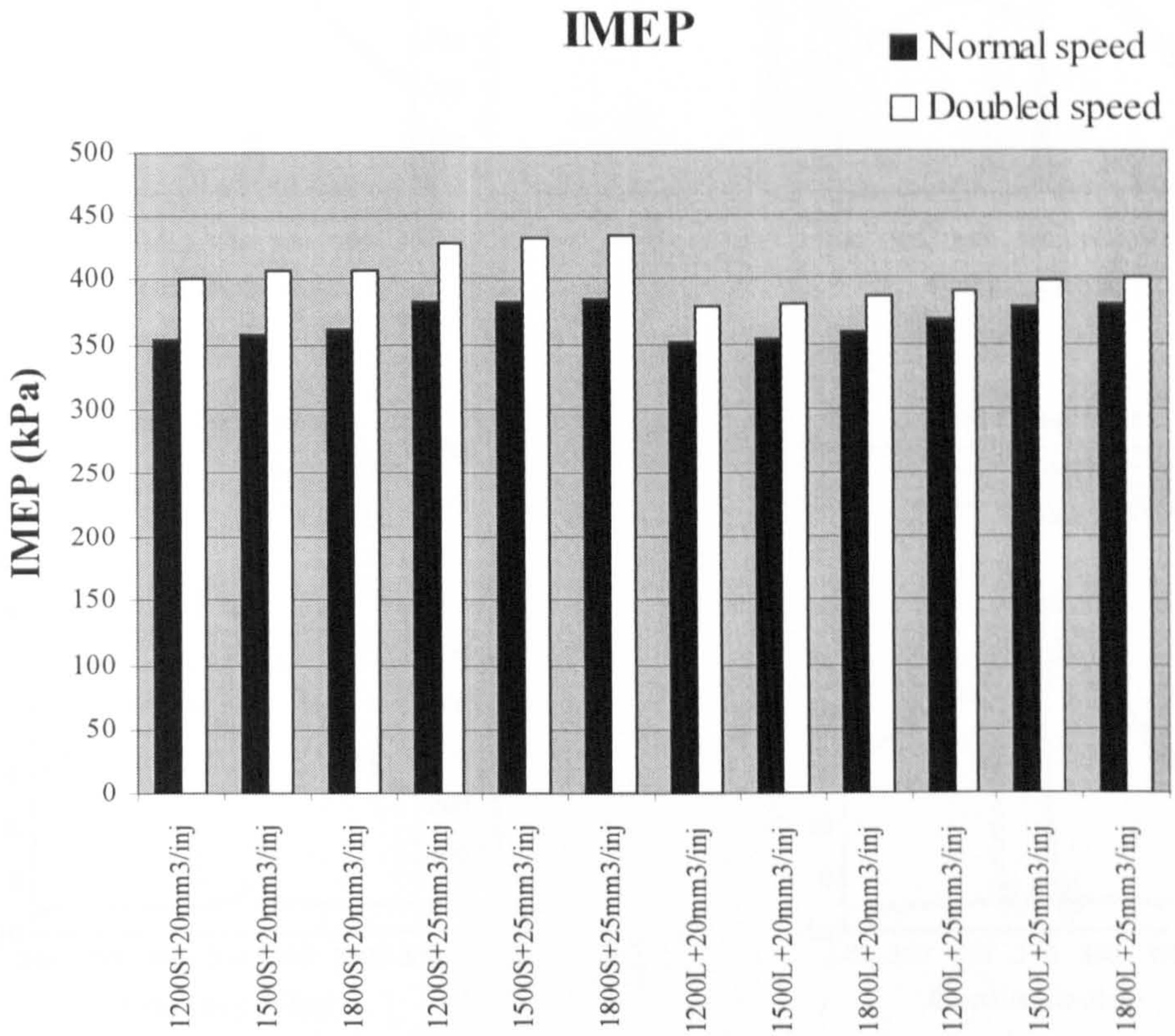


Figure 4.12 IMEP calculated cylinder pressures obtained at 3° bTDC of injection timing for various engine operating conditions

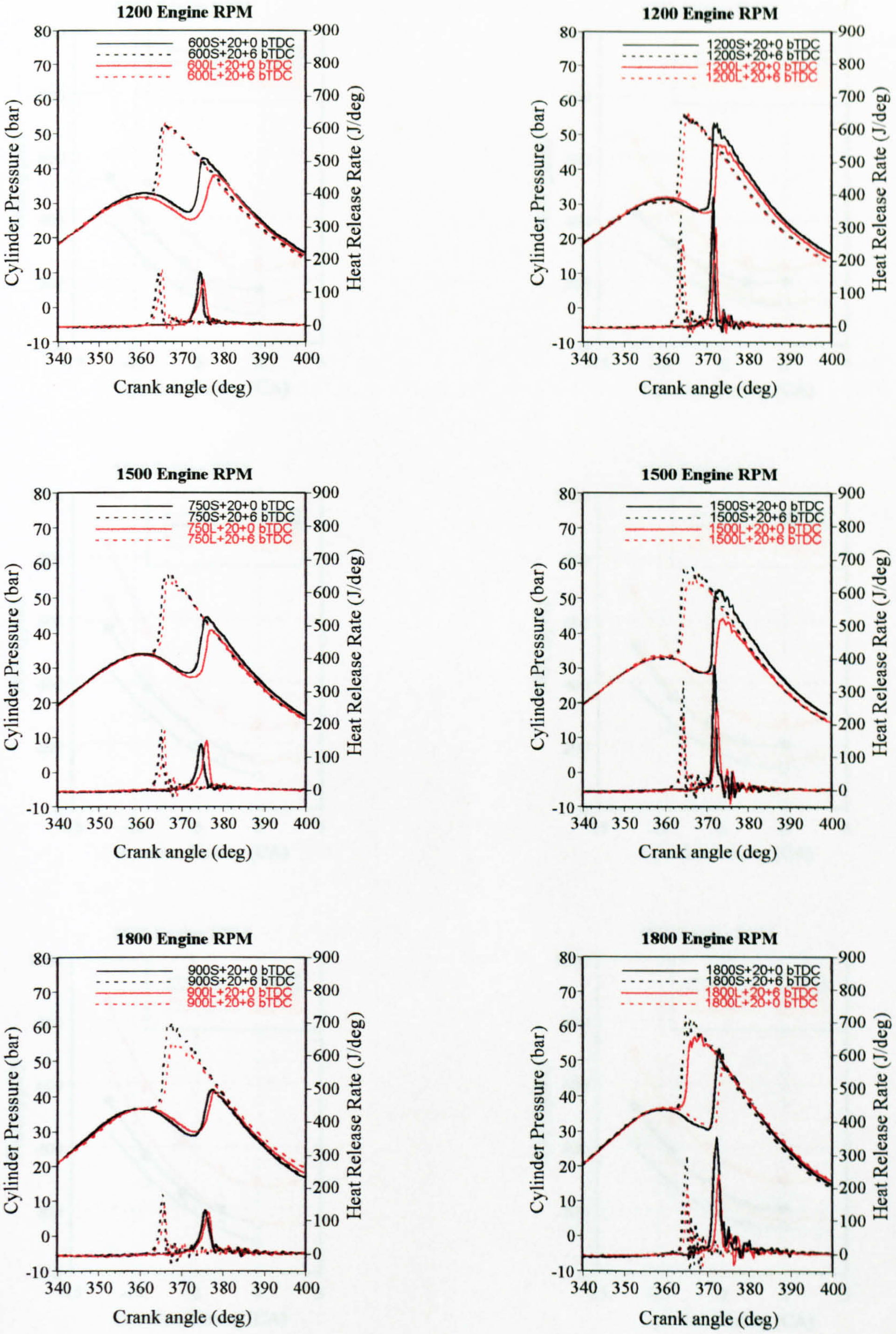
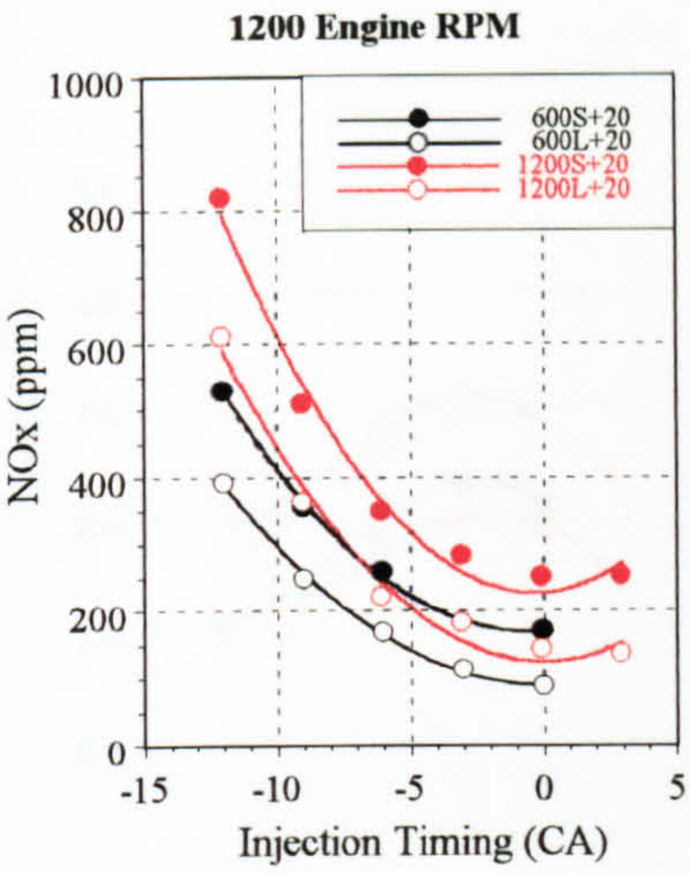
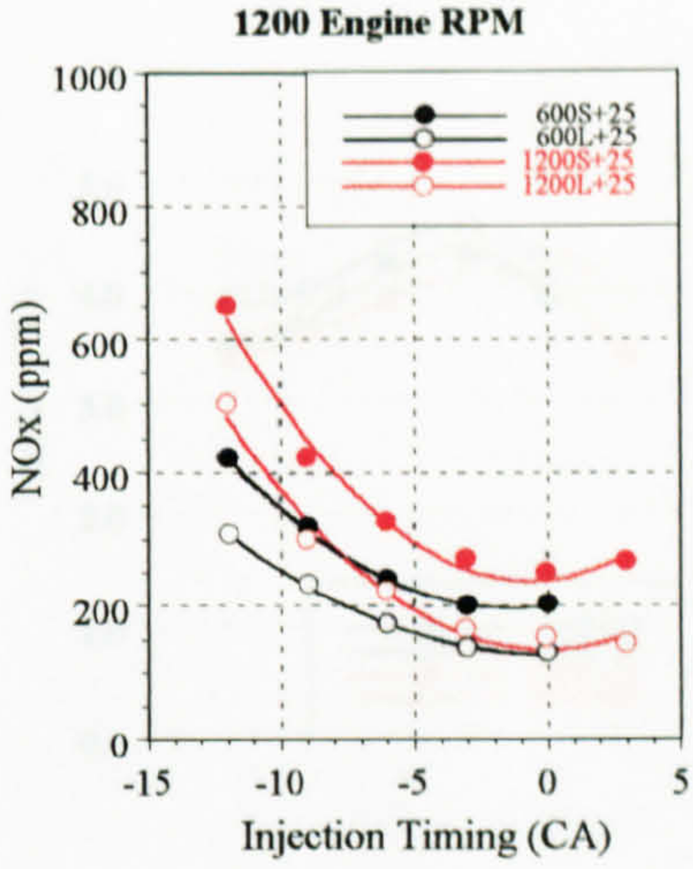
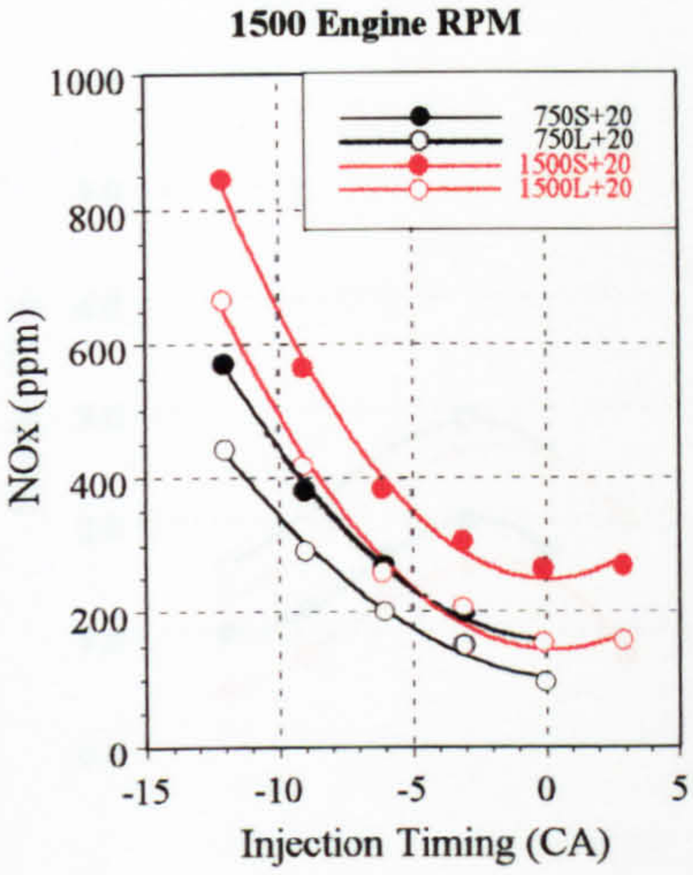
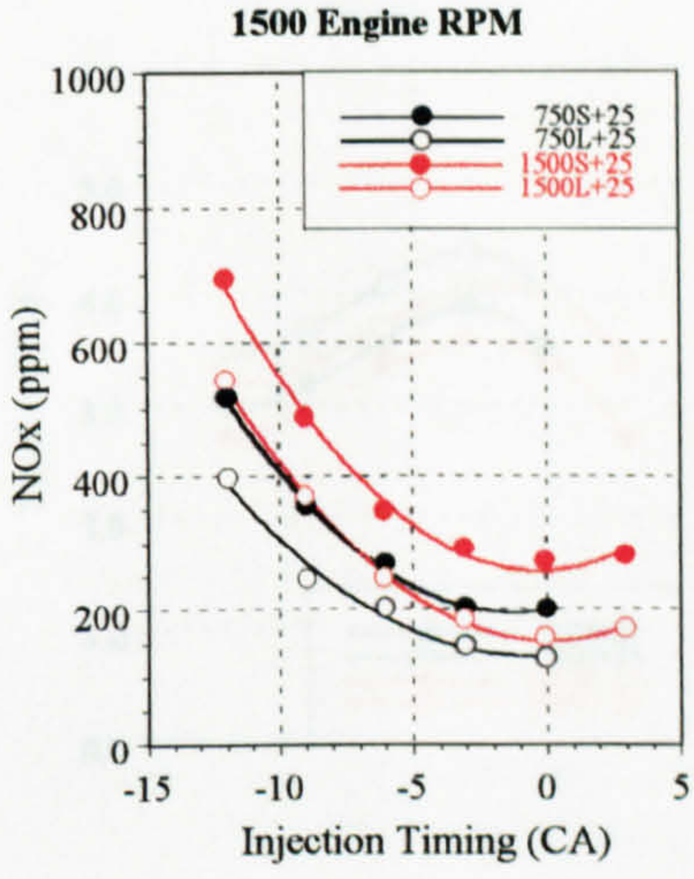


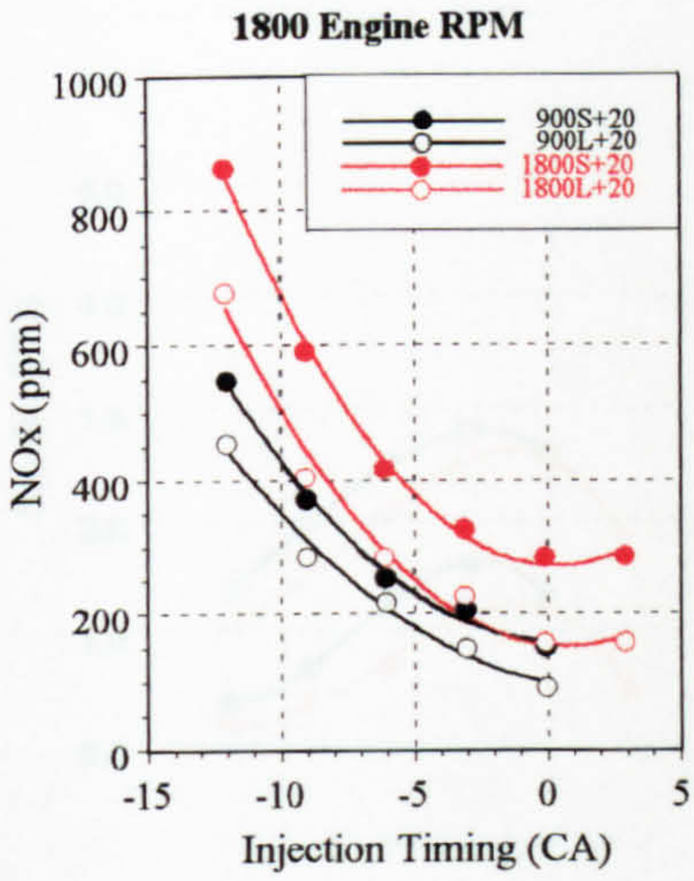
Figure 4.13 Cylinder pressures and heat release rates for different nozzle configurations at various engine operating conditions











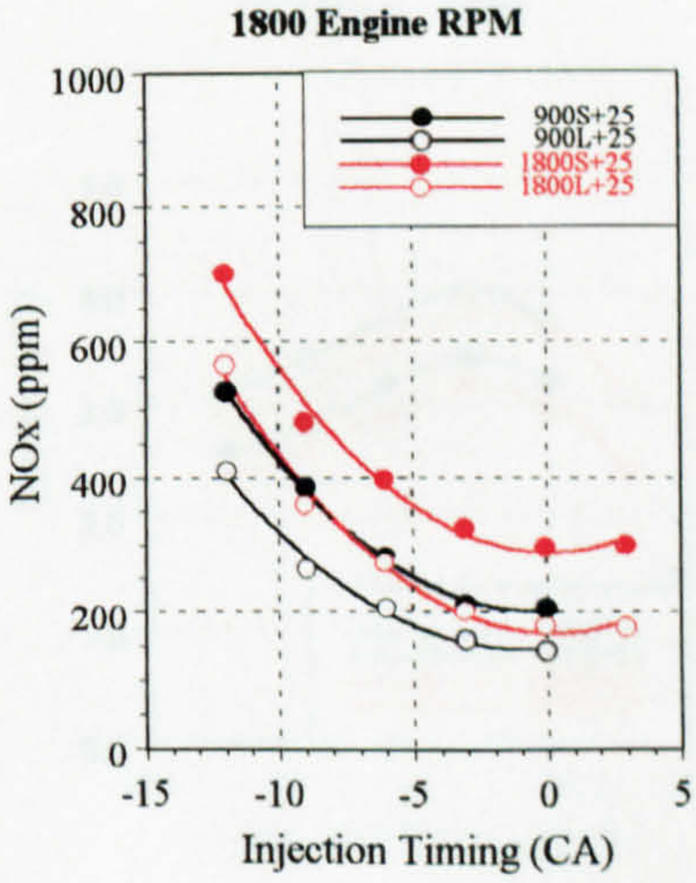
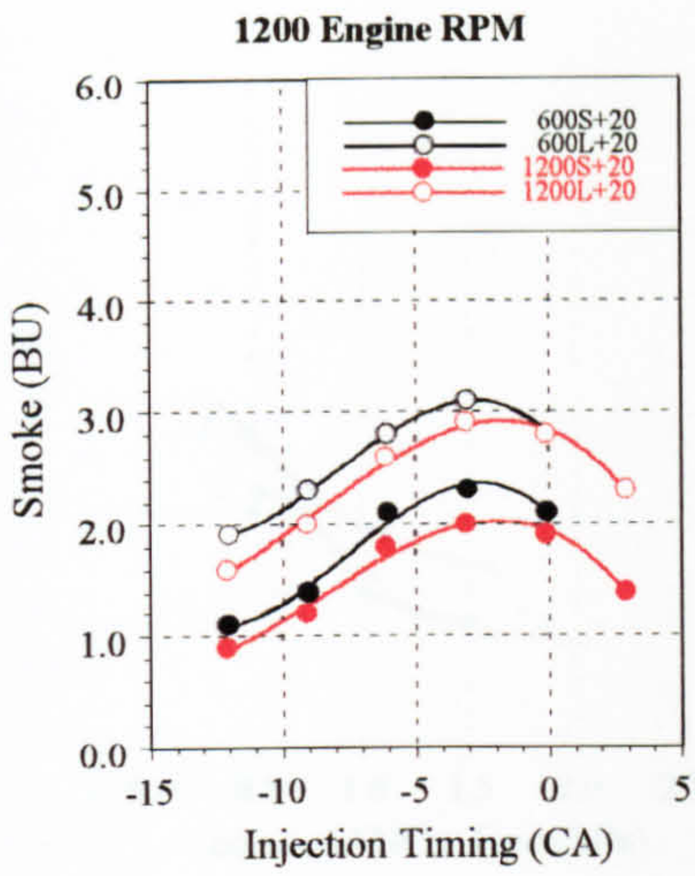
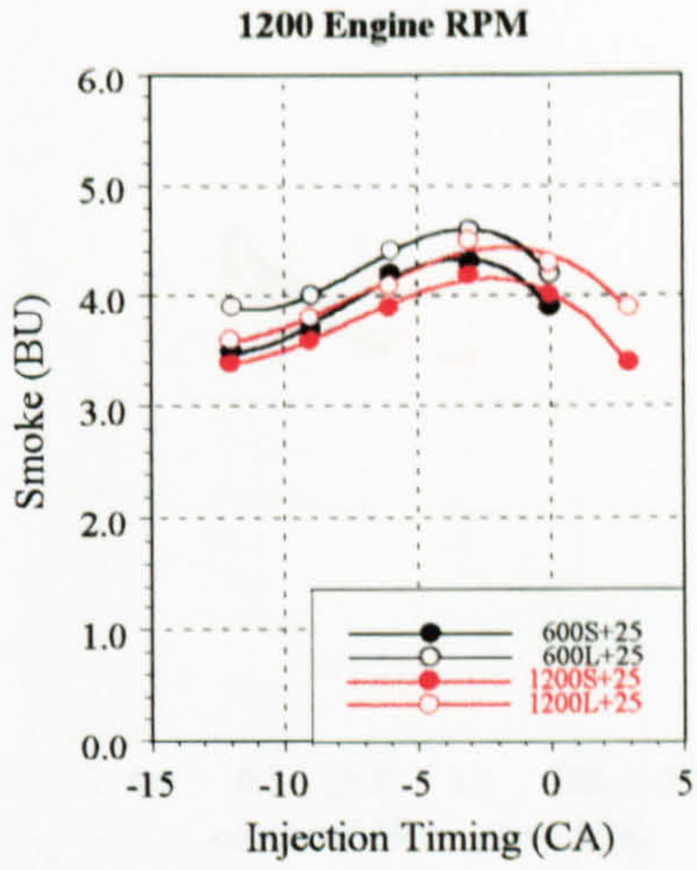
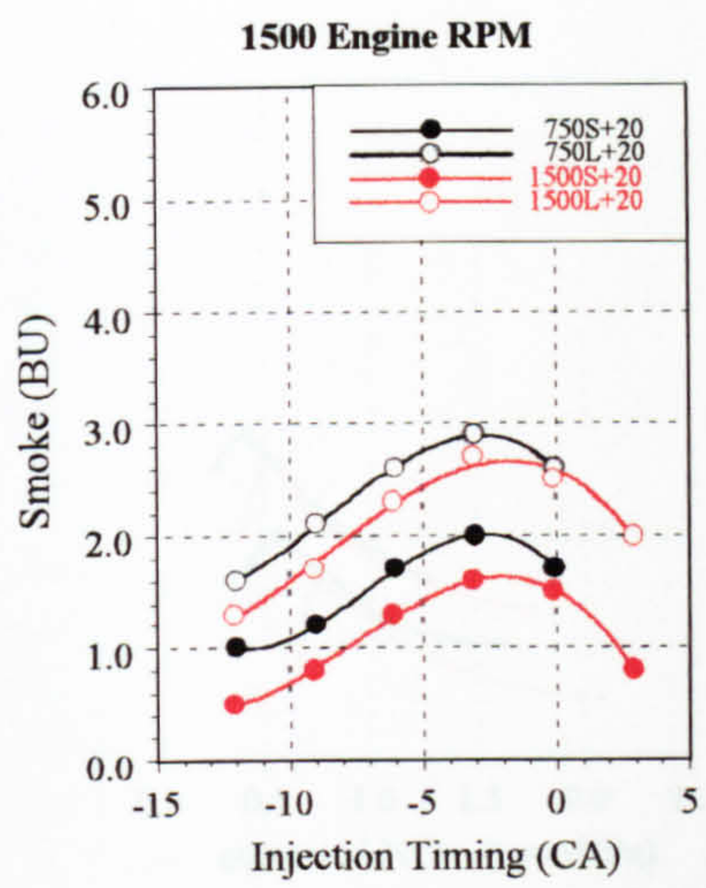
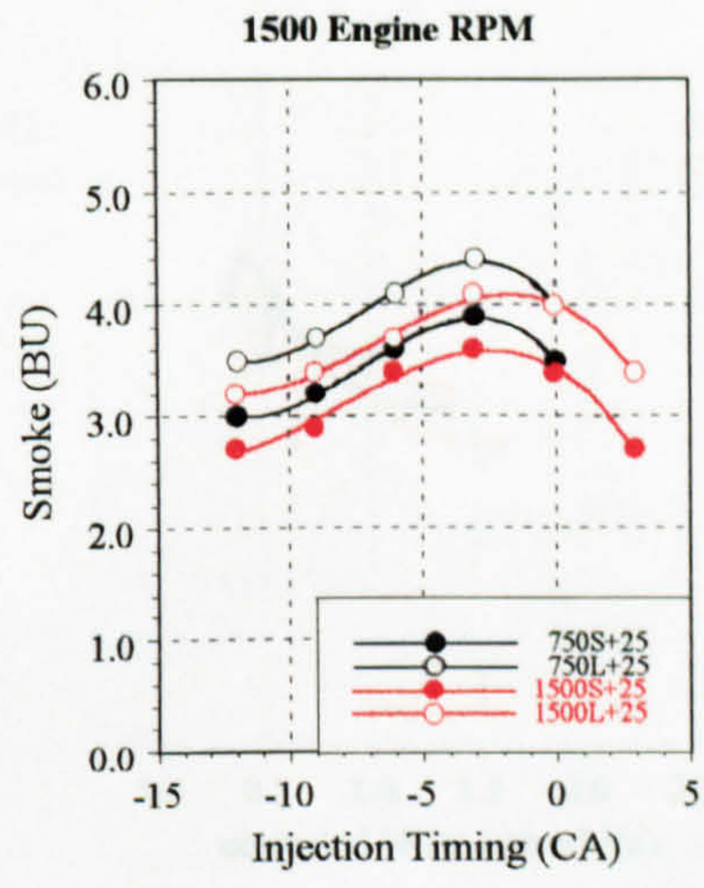


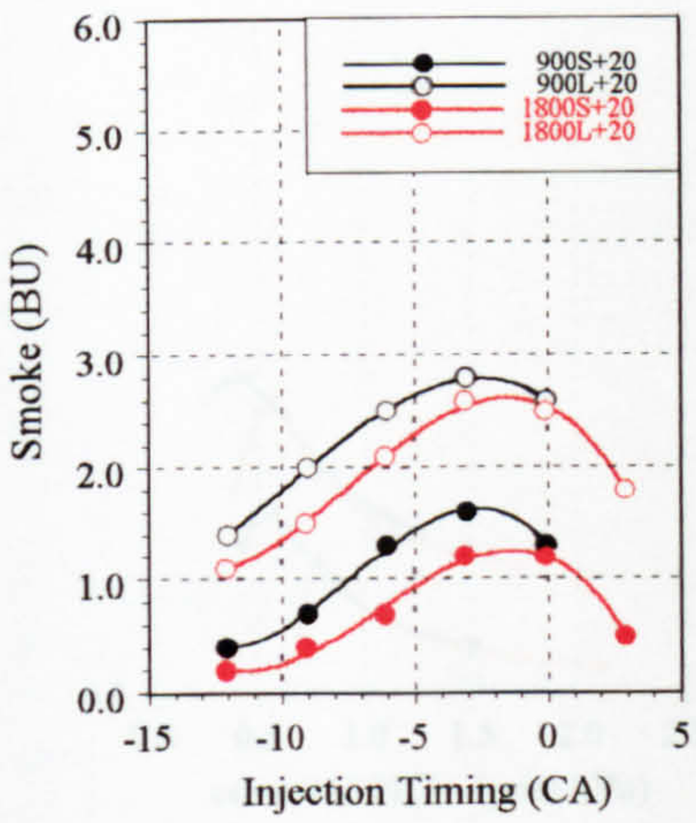
Figure 4.14 Effects of nozzle configuration on NO_x emissions at various engine operating conditions











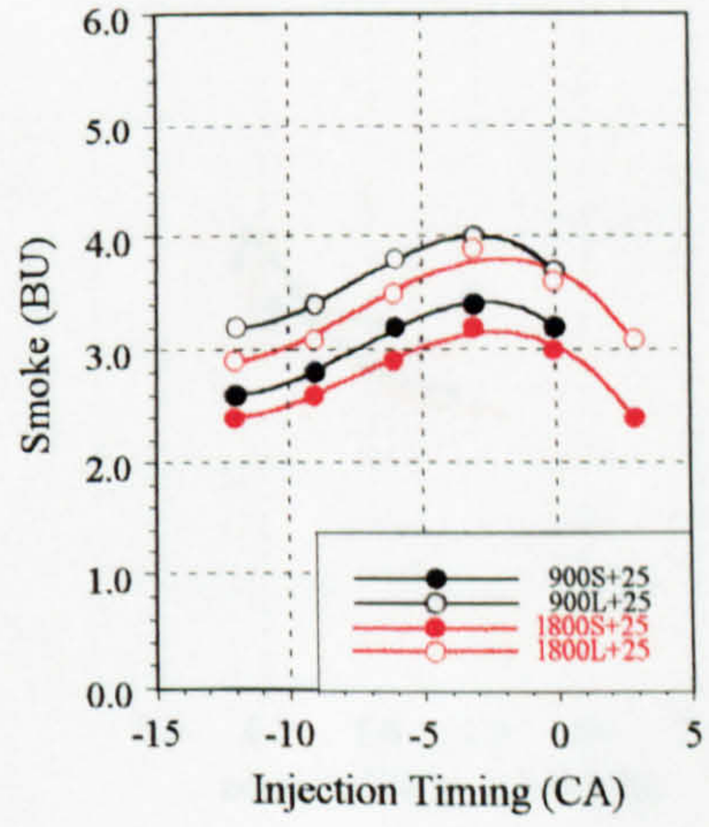
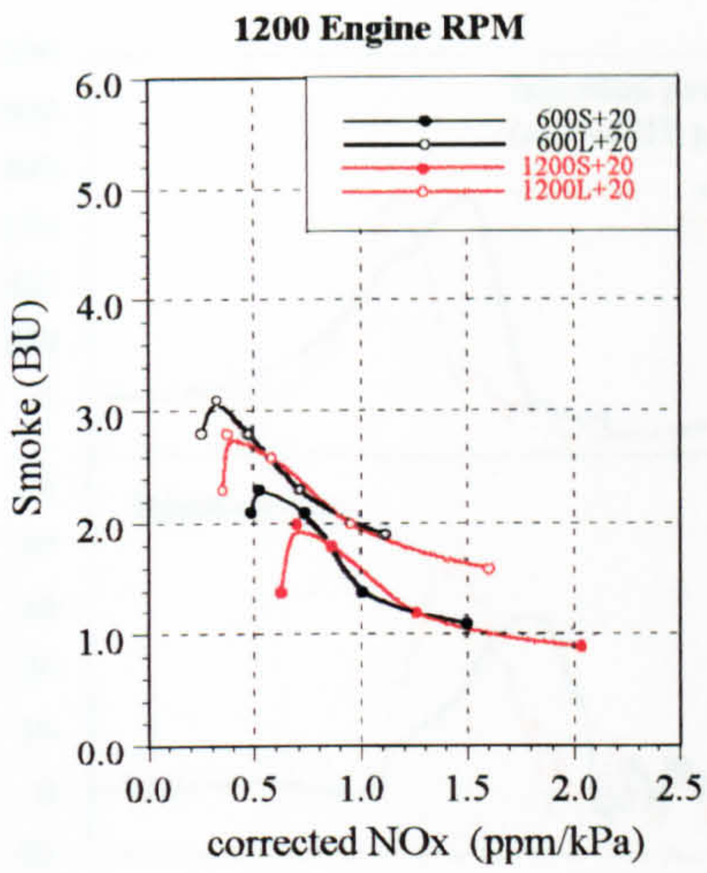
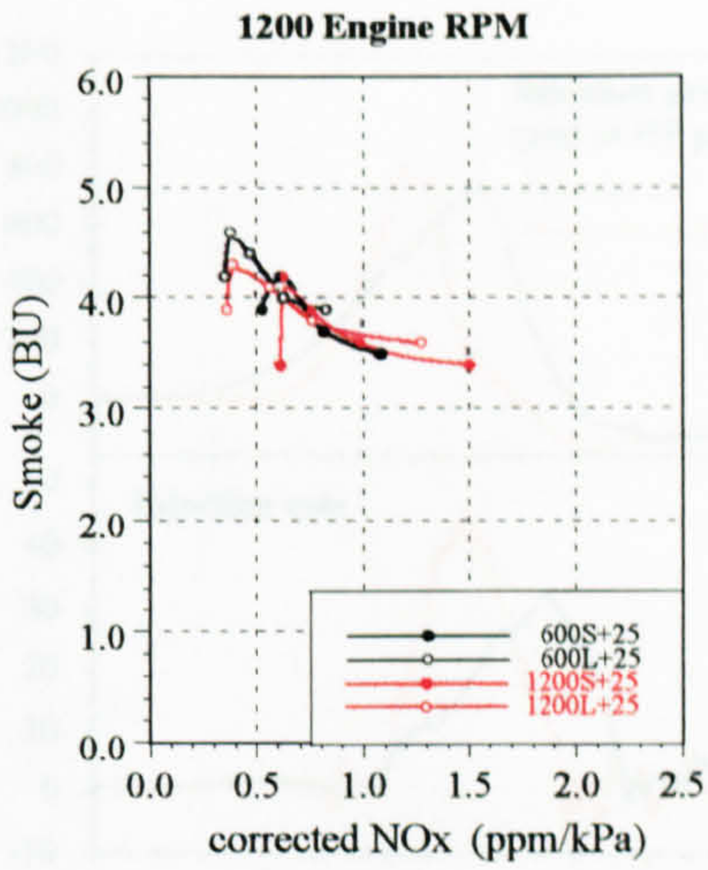
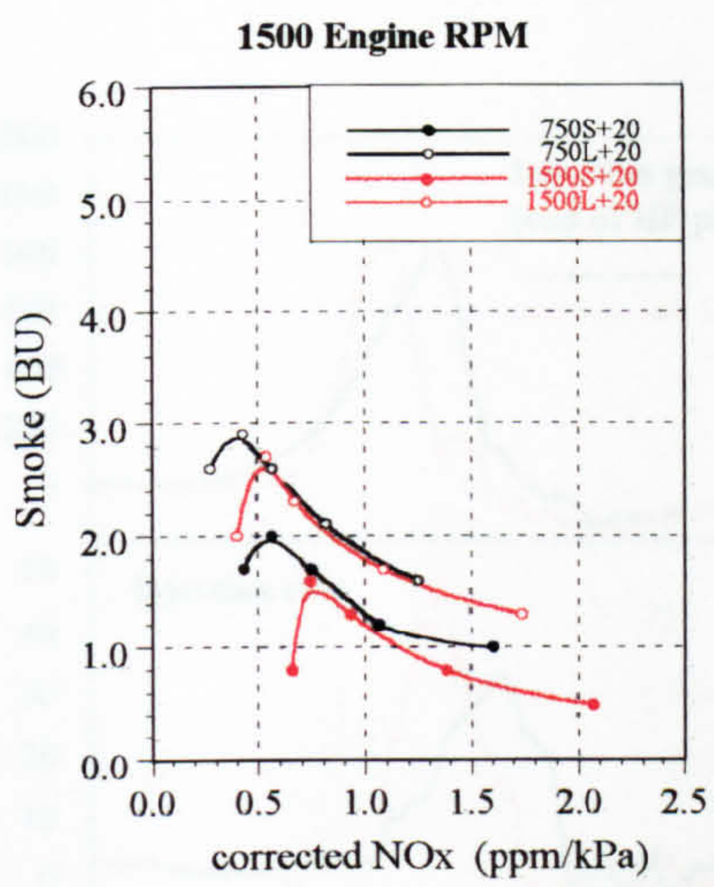
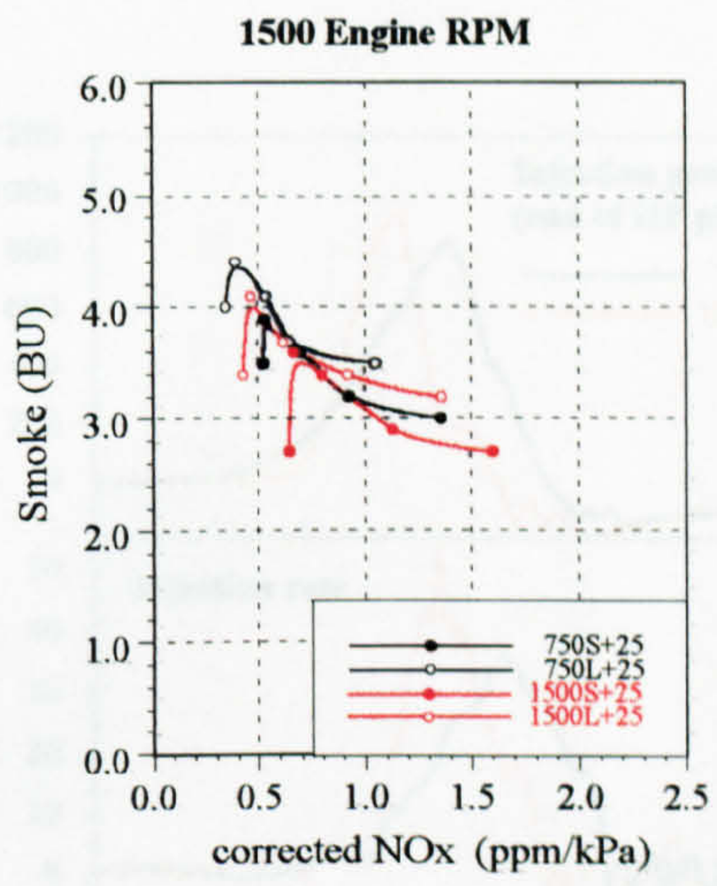


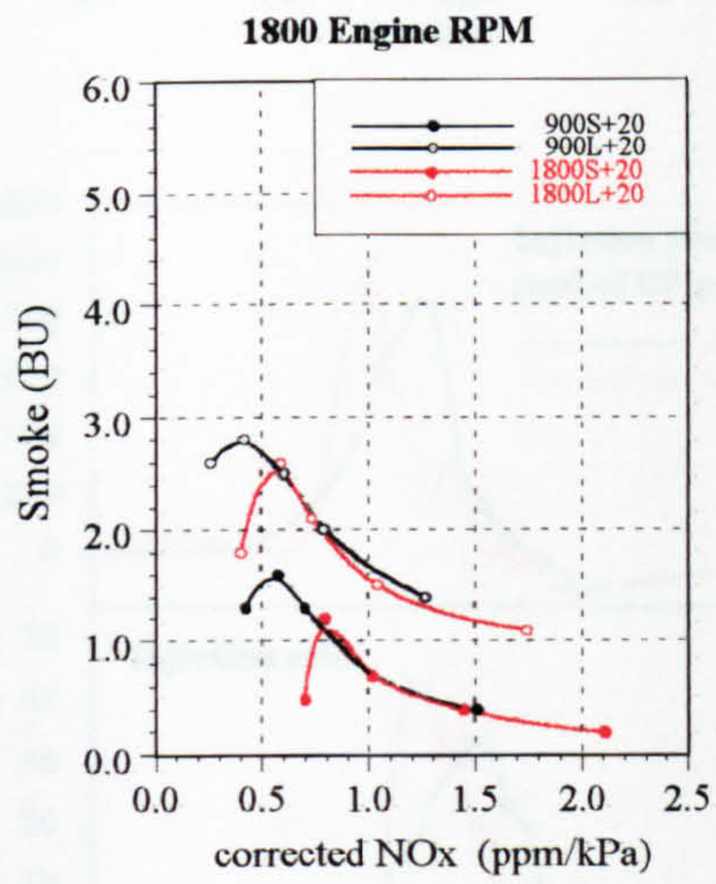
Figure 4.15 Effects of nozzle configuration on smoke emissions at various engine operating conditions











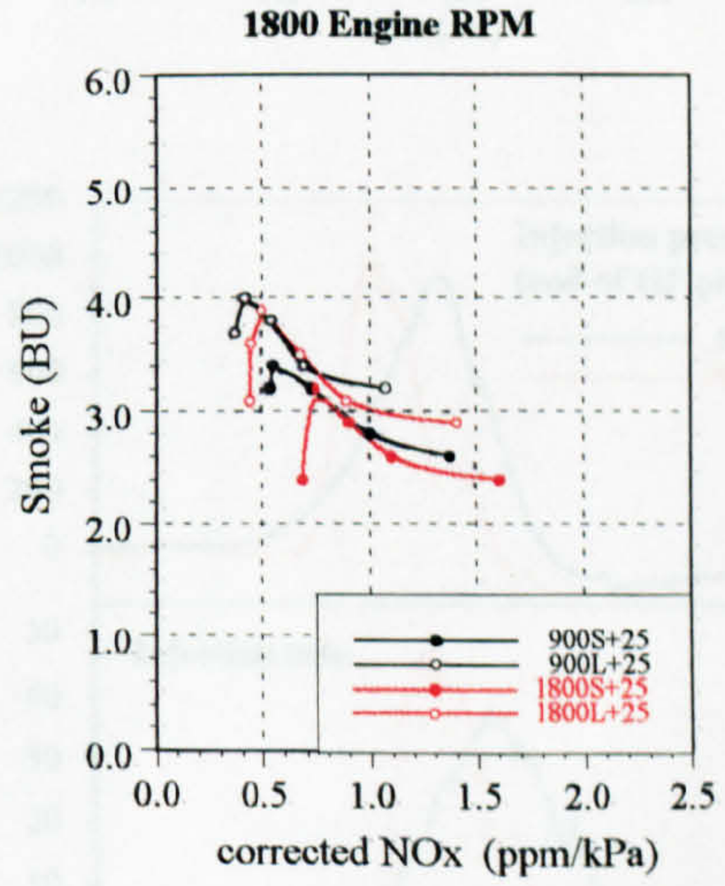
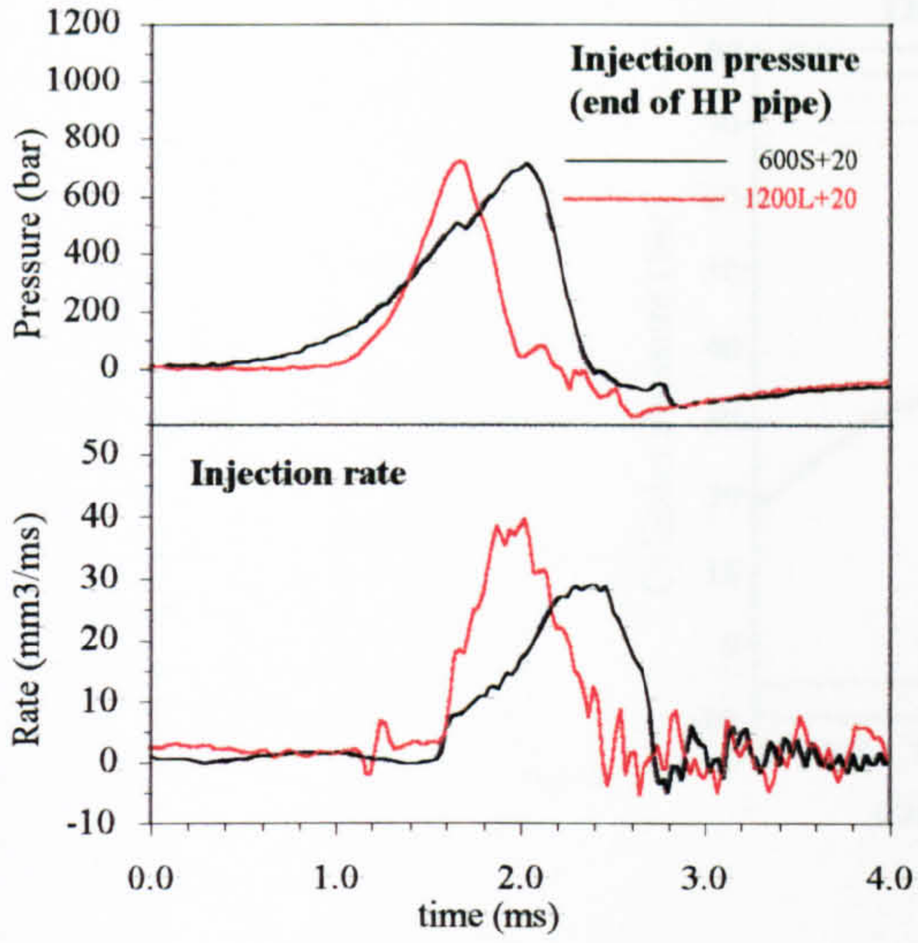
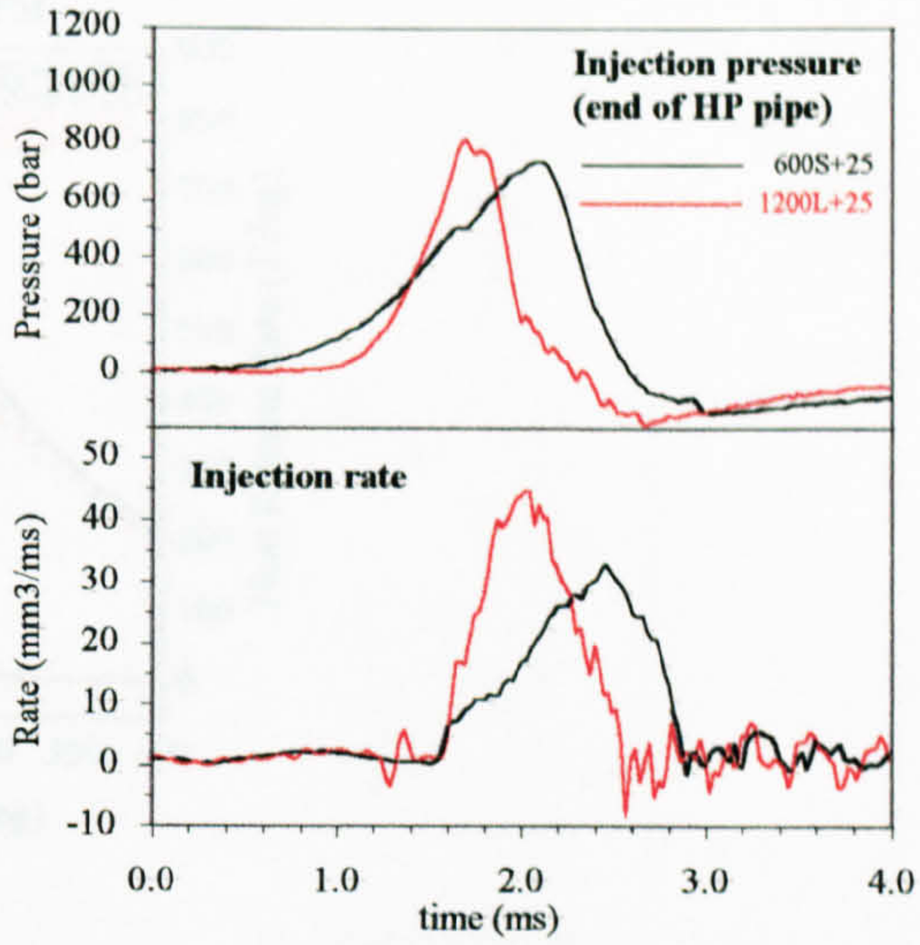
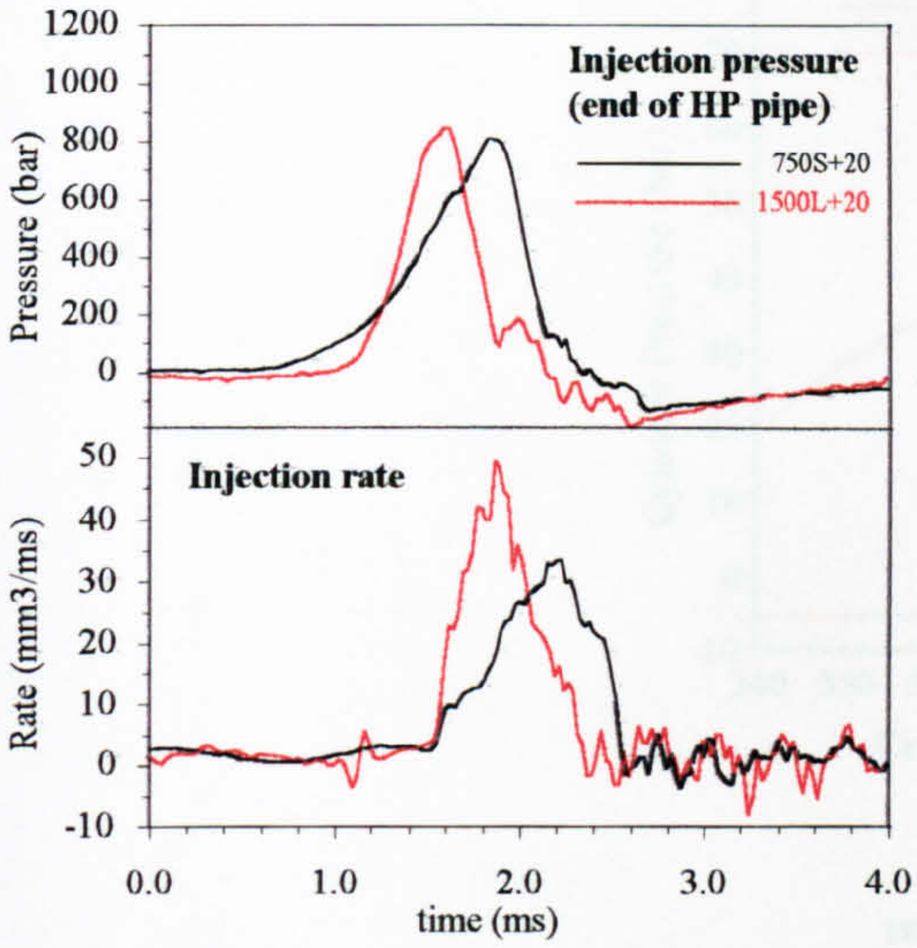
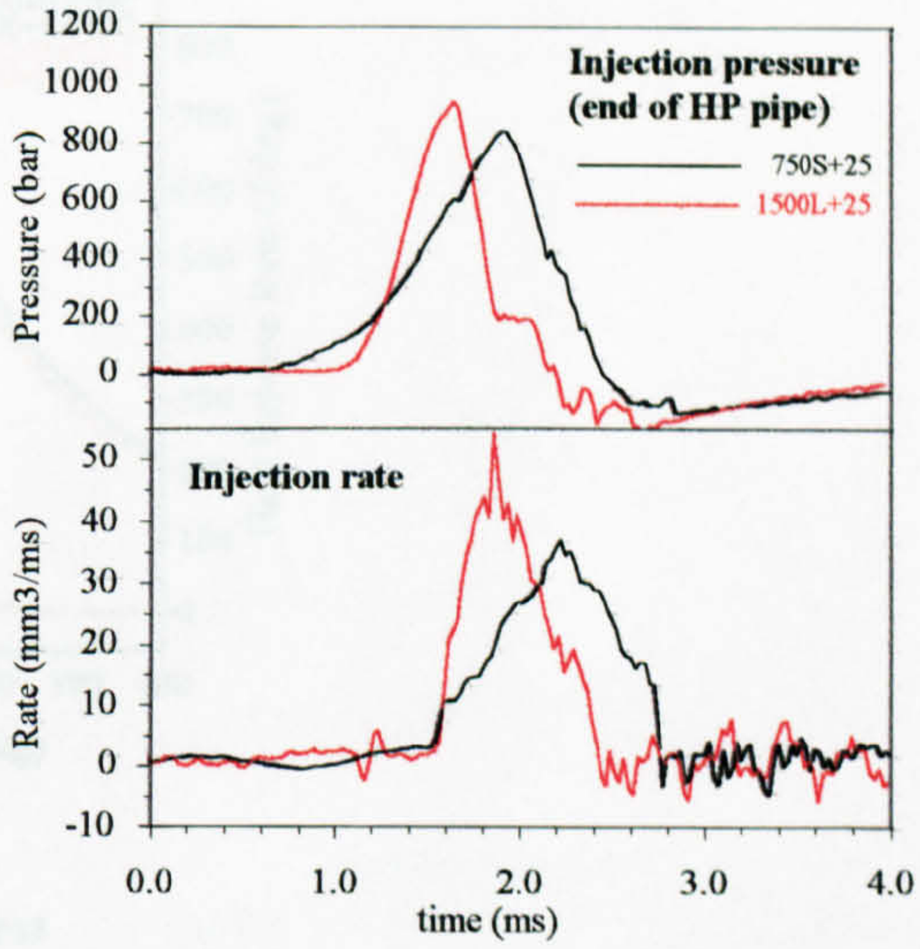


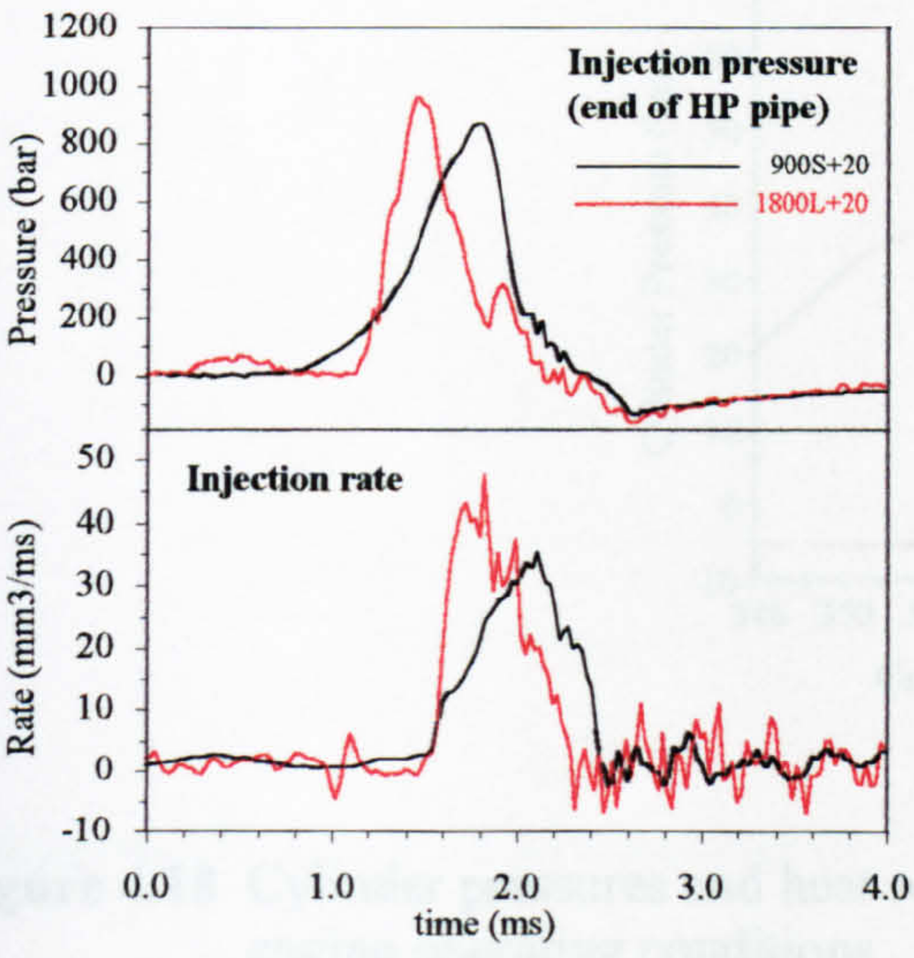
Figure 4.16 Effects of nozzle configuration on smoke-NO_x trade-off curves at various engine operating conditions











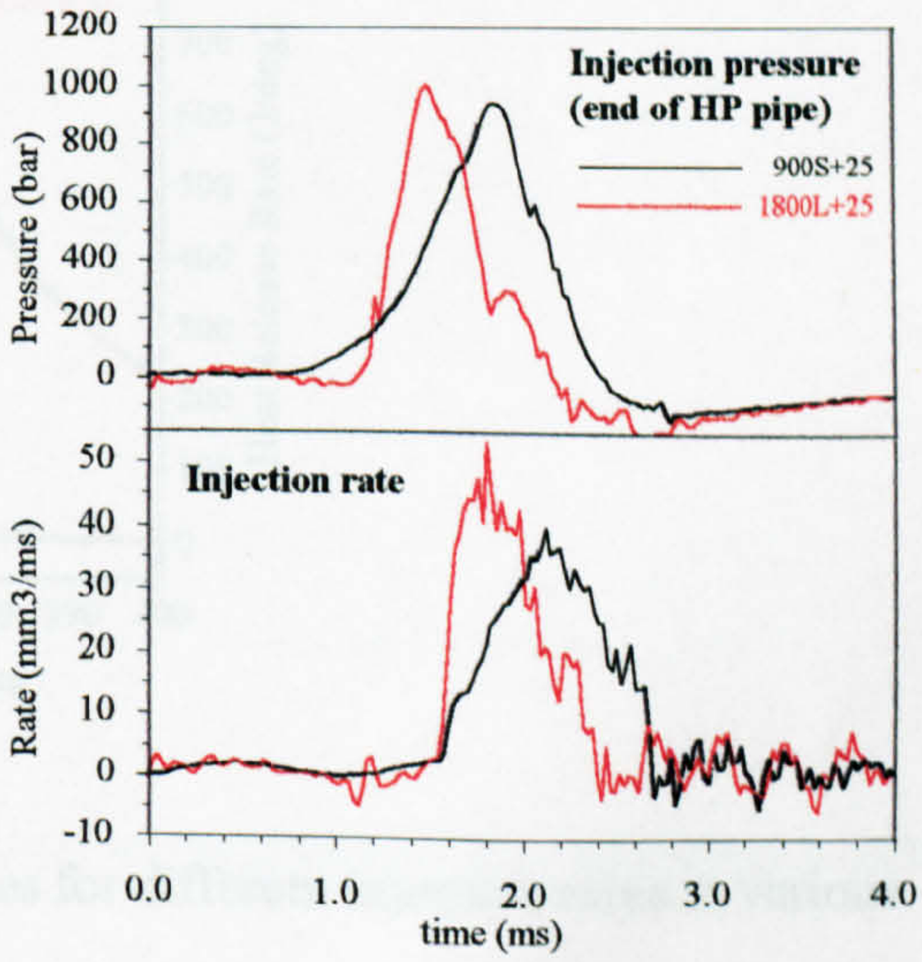


Figure 4.17 Injection pressure and injection rate profiles for the normal pump speed with S nozzle and the doubled pump speed with L nozzle

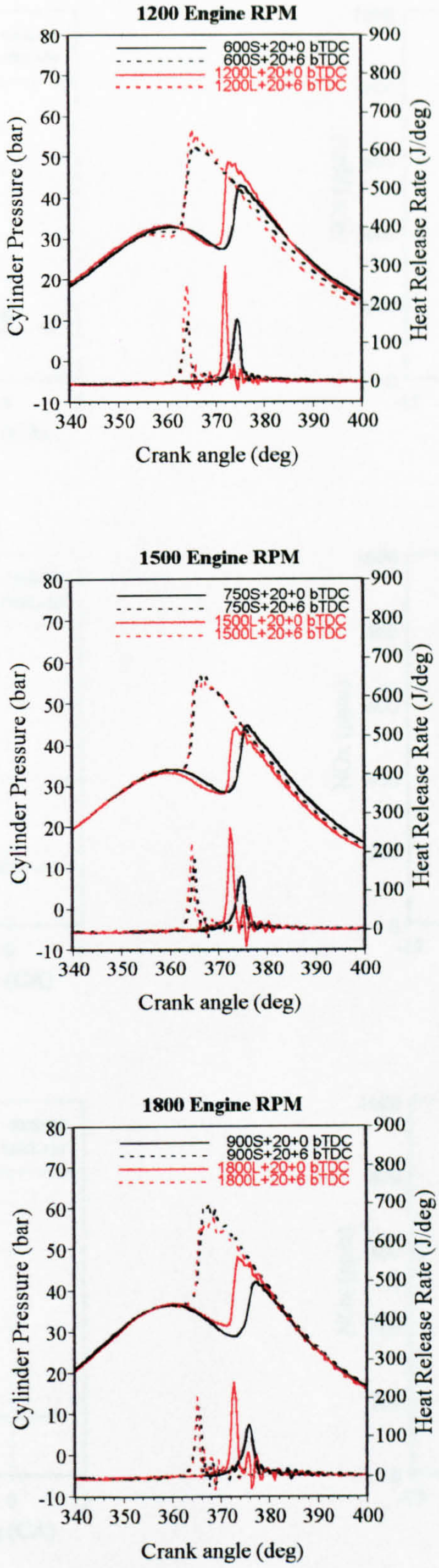
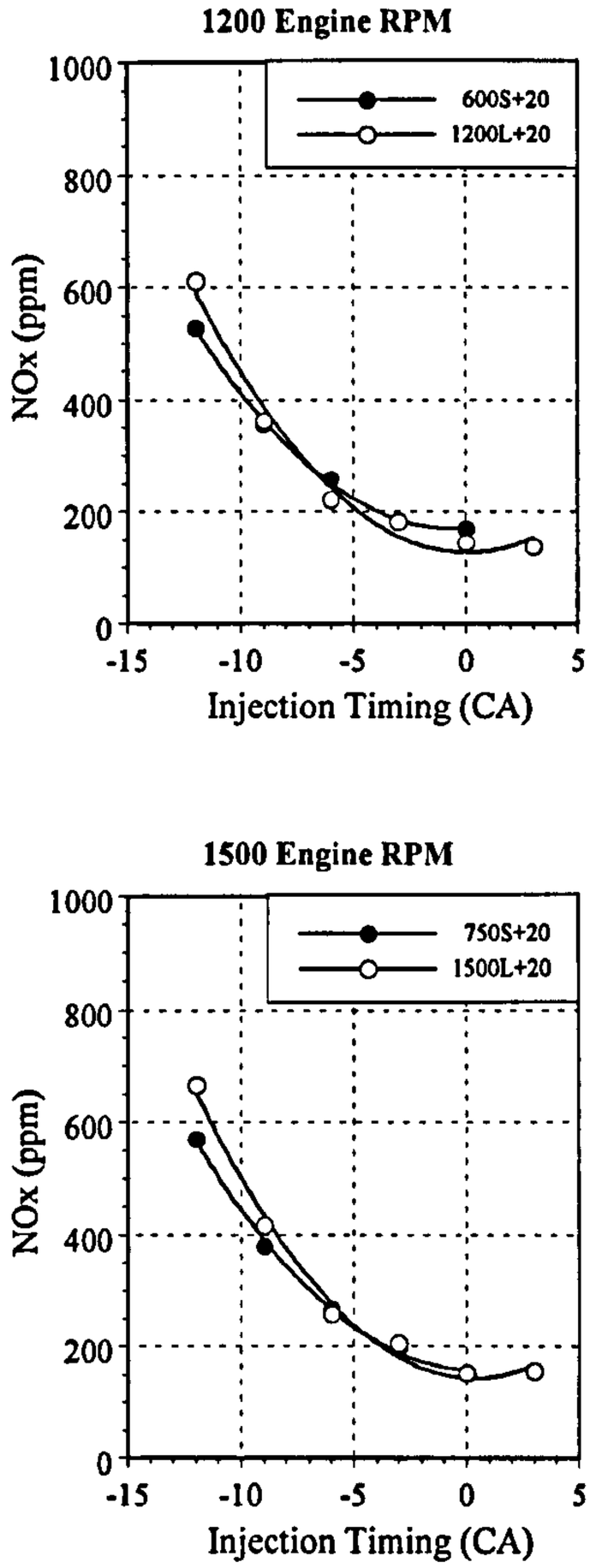
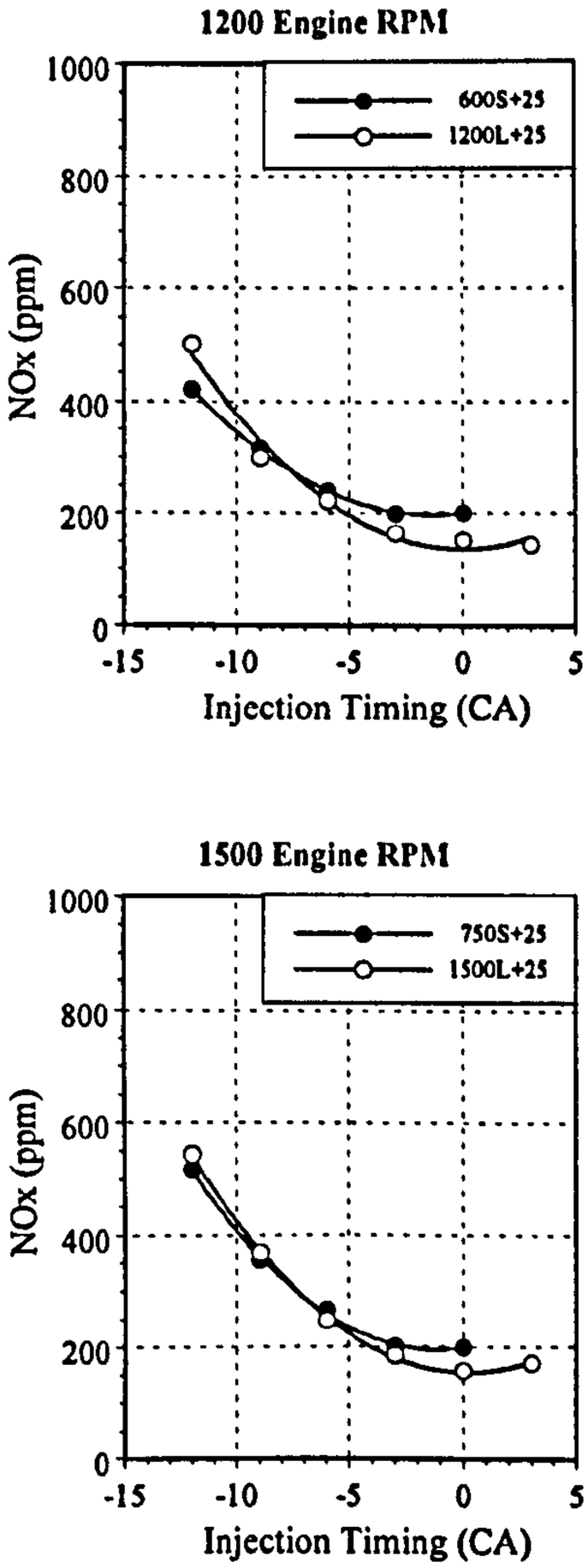
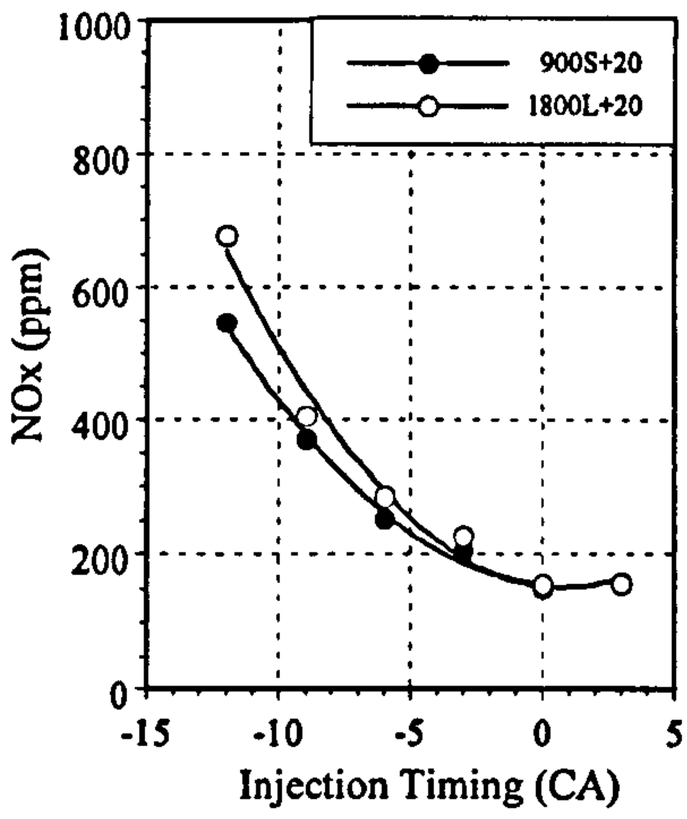


Figure 4.18 Cylinder pressures and heat release rates for different injection rates at various engine operating conditions







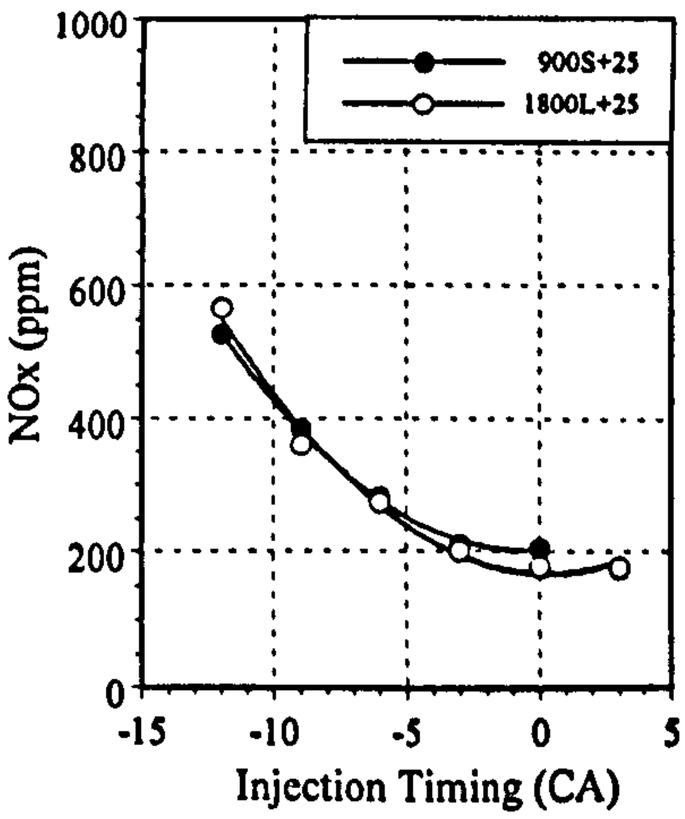


Figure 4.19 Effects of injection rate on NO_x emissions at various engine operating conditions

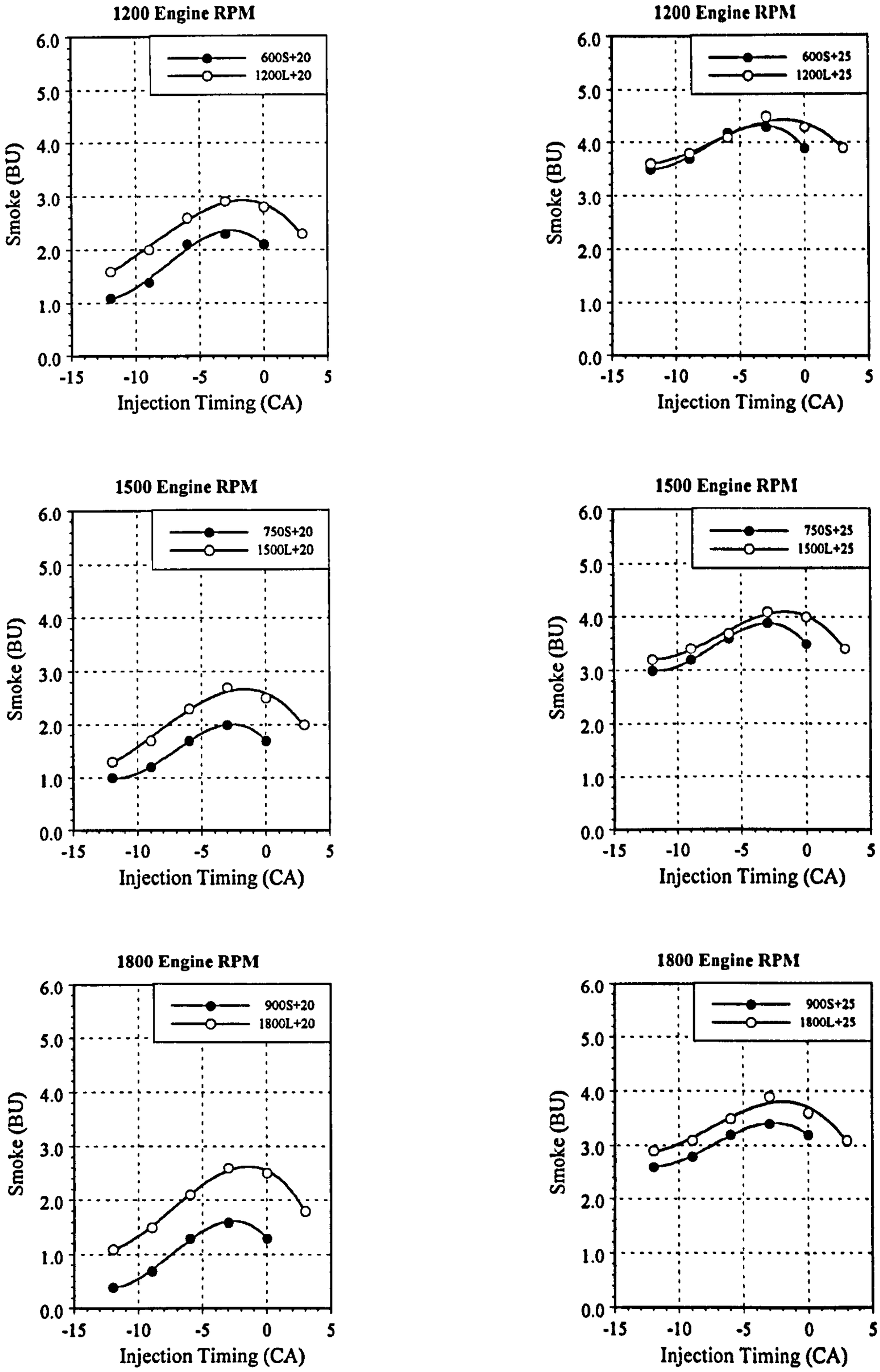


Figure 4.20 Effects of injection rate on smoke emissions at various engine operating conditions

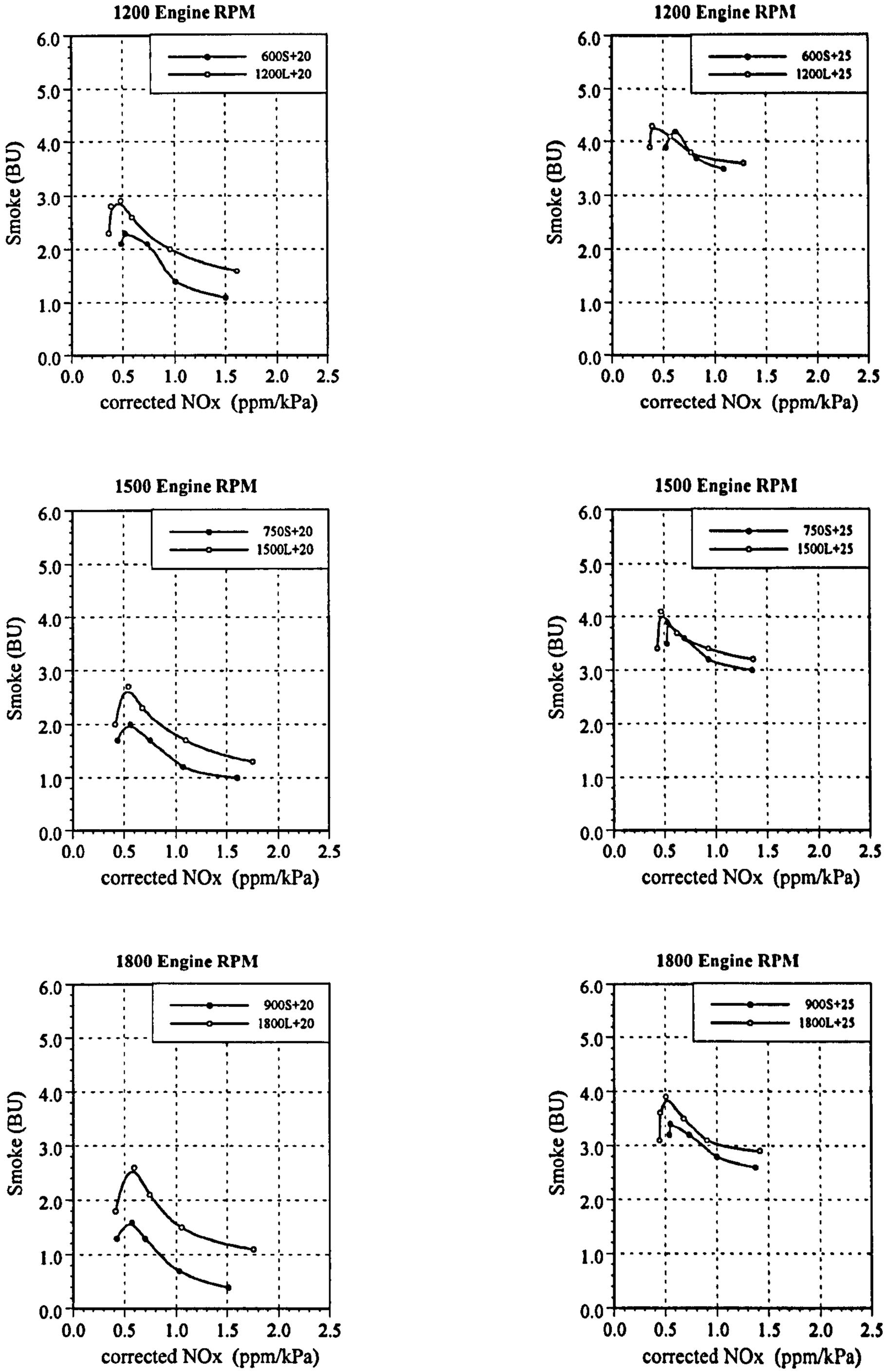
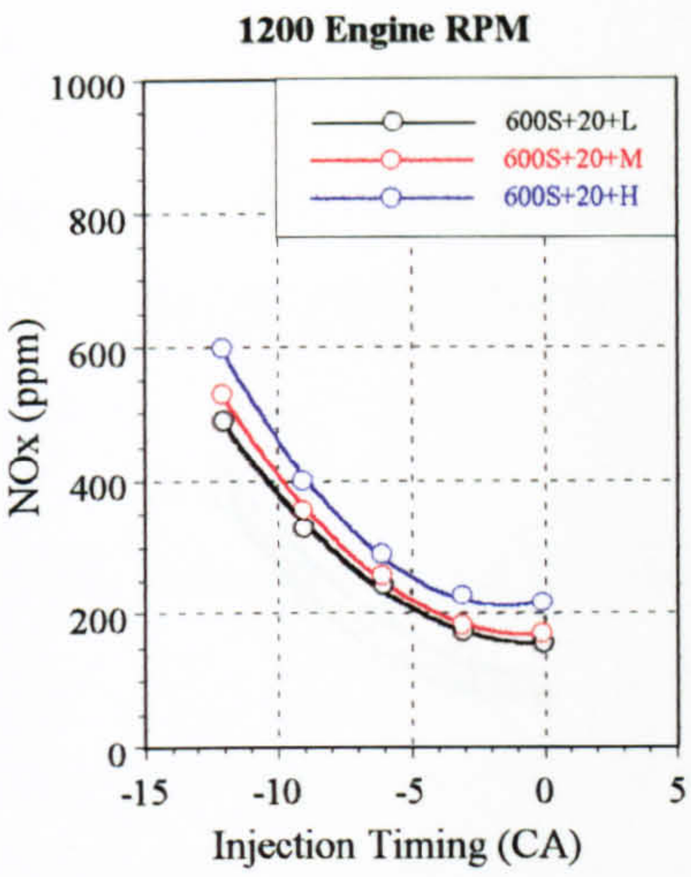
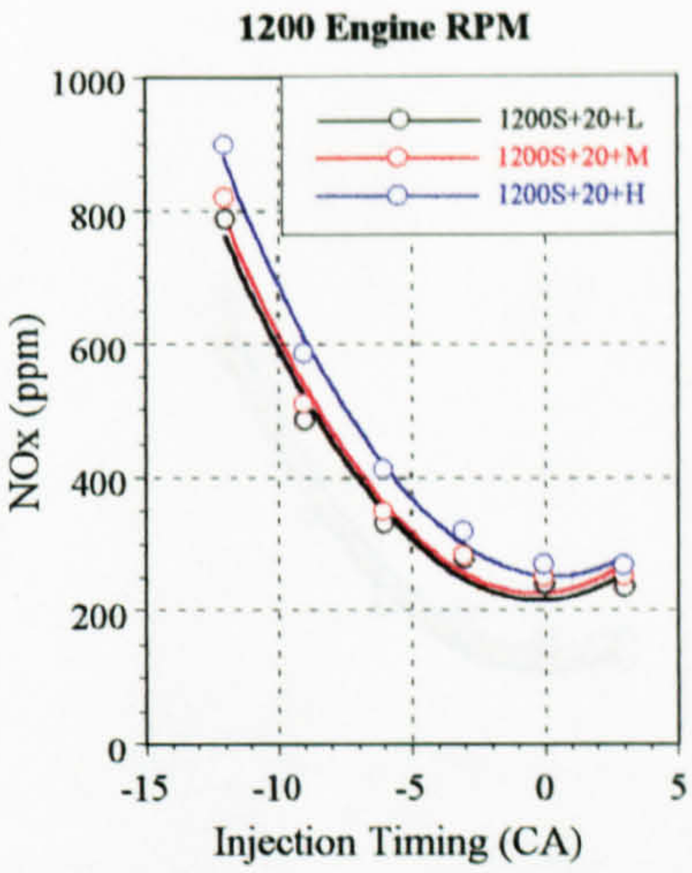
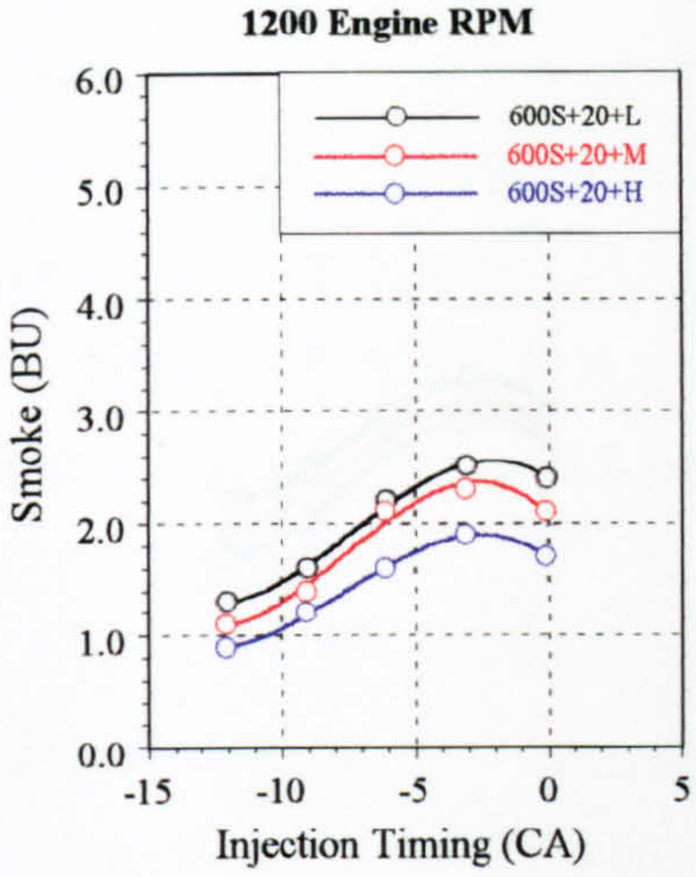
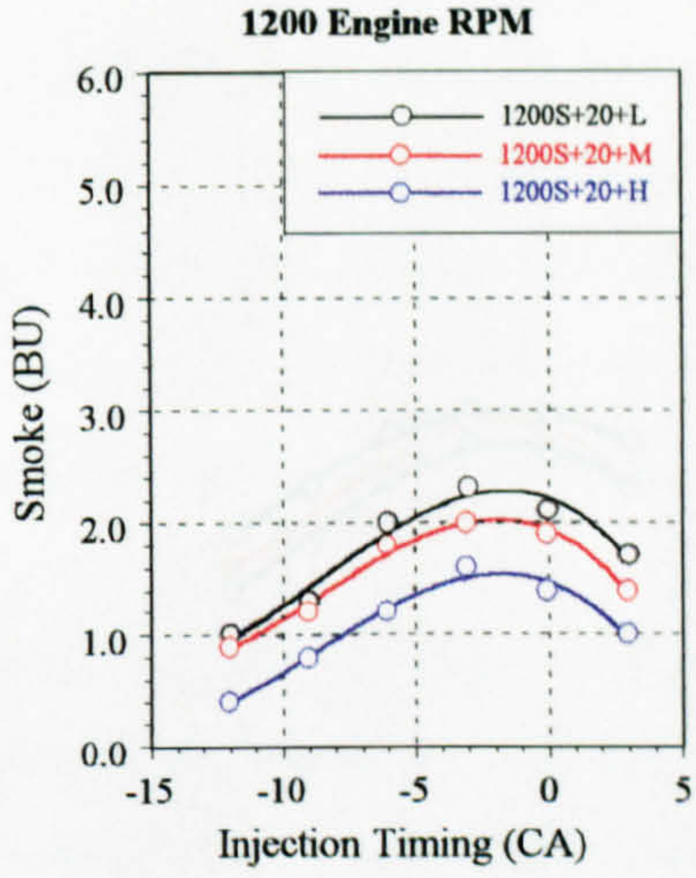


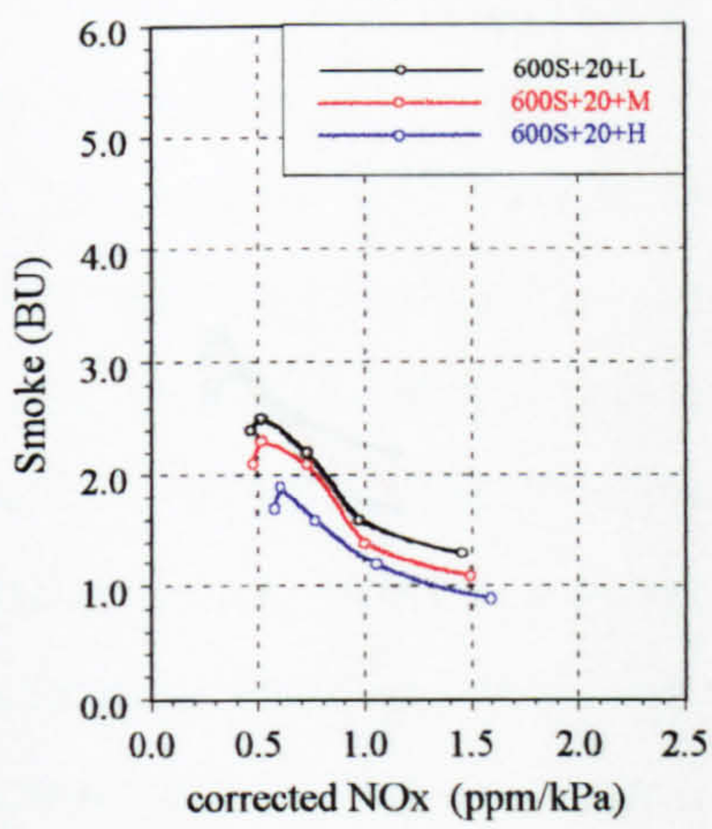
Figure 4.21 Effects of injection rate on smoke-NO_x trade-off curves at various engine operating conditions











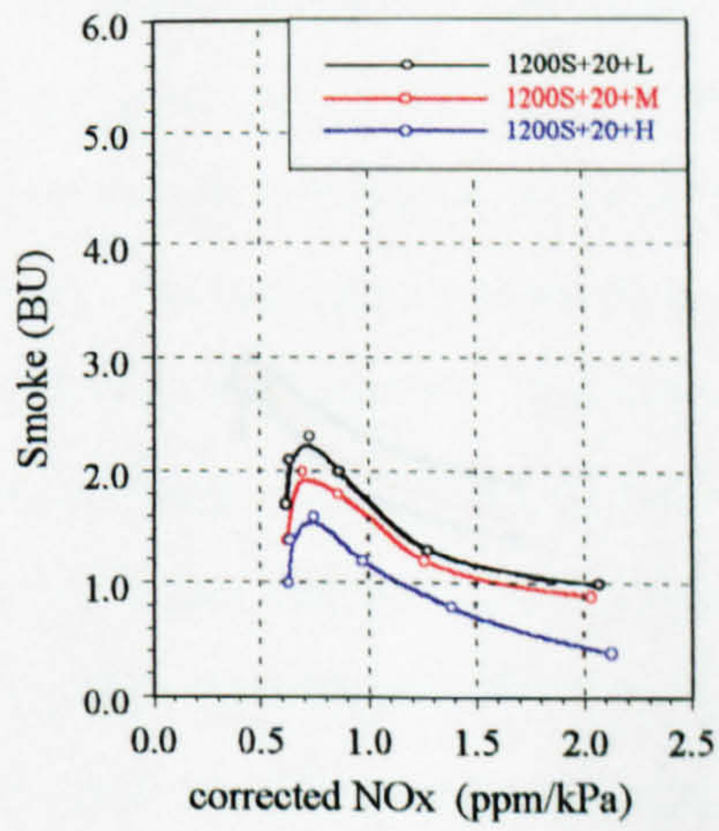
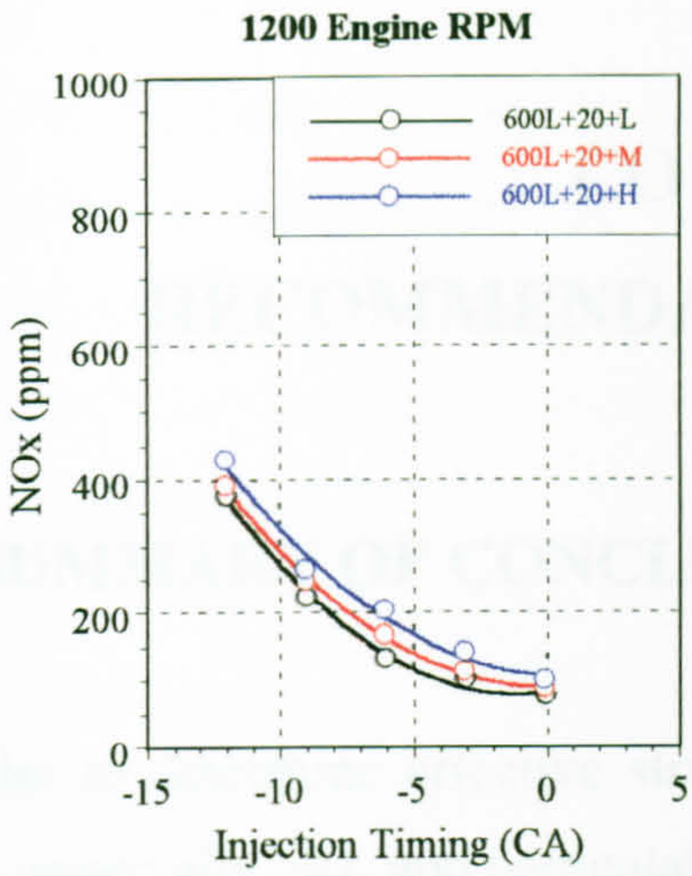
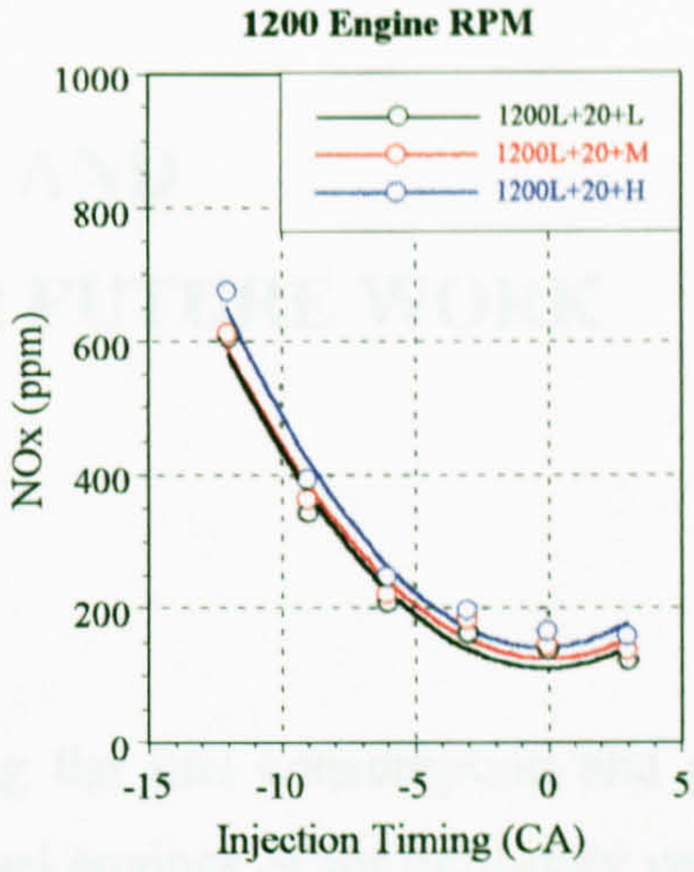
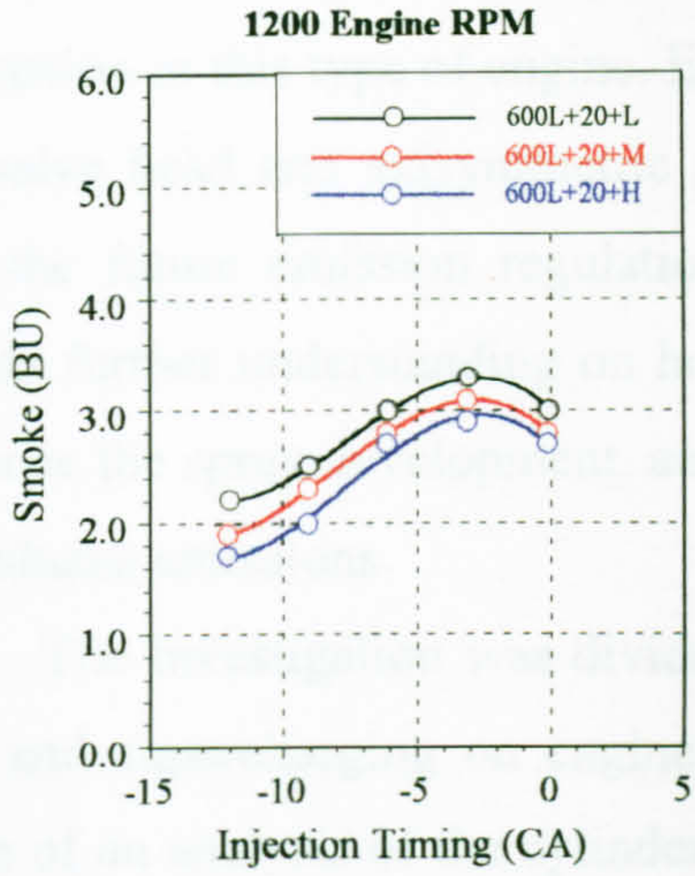
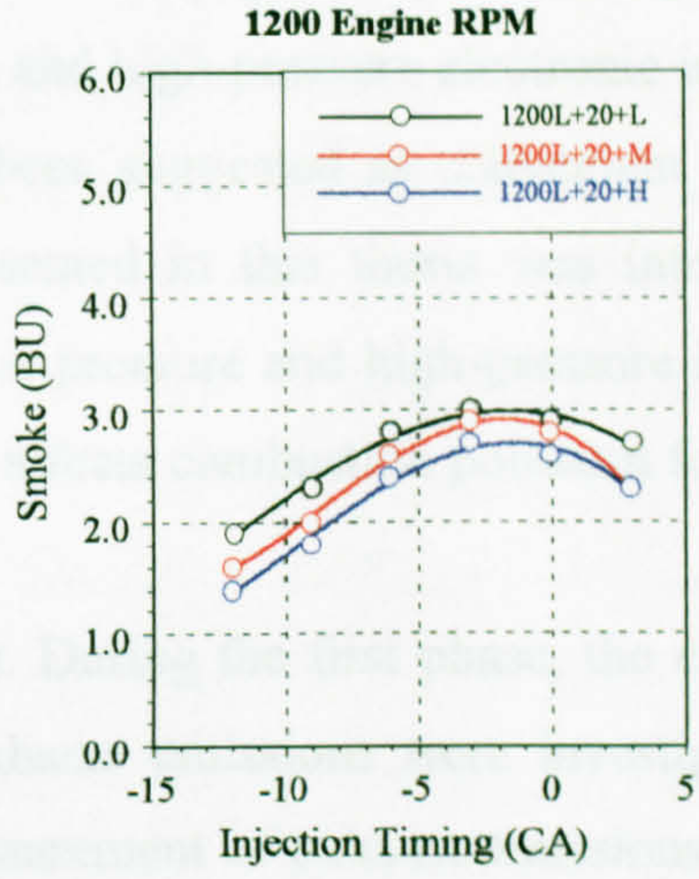


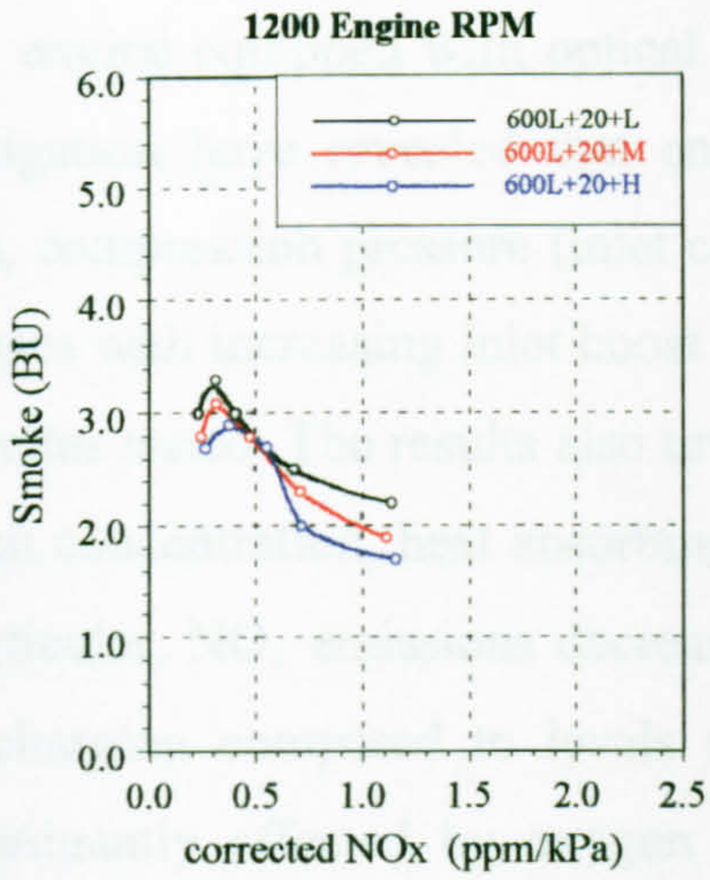
Figure 4.22a Effects of nozzle protrusion into cylinder on exhaust emissions at various engine operating conditions; S nozzle











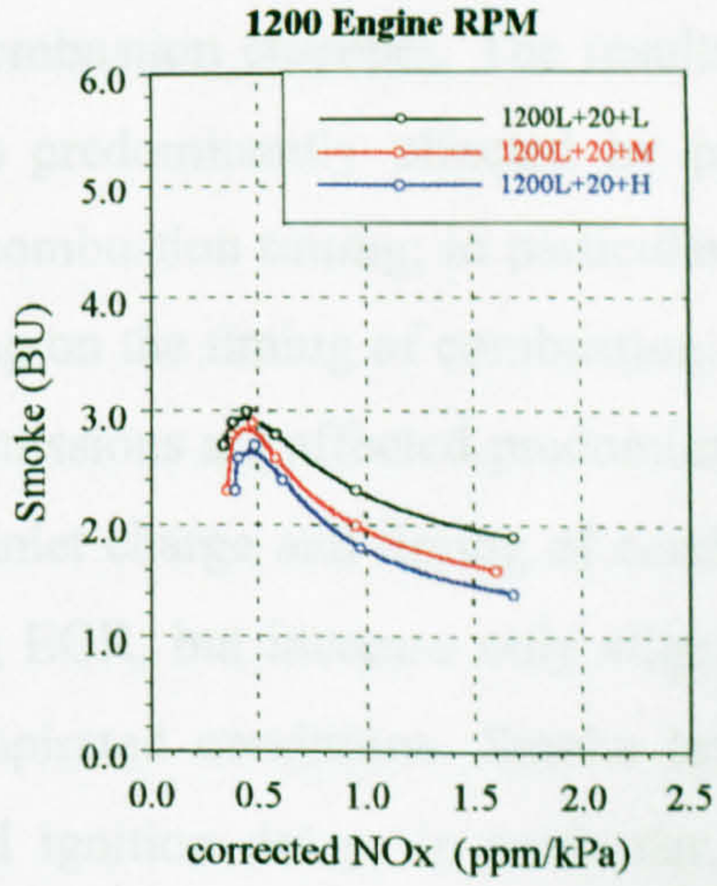


Figure 4.22b Effects of nozzle protrusion into cylinder on exhaust emissions at various engine operating conditions; L nozzle

CHAPTER 5

CONCLUSIONS AND RECOMMENDATIONS FOR FUTURE WORK

5.1 SUMMARY OF CONCLUSIONS

In order to determine effective strategies for reducing the fuel consumption and pollutant levels, especially NO_x and particulates, from HSDI diesel engines of for light-duty vehicles, it is necessary to improve the present understanding of the physical processes governing combustion in this type of engine. EGR, turbocharging and high-pressure electronic injection, four-valve head and axisymmetric piston-bowl have been suggested as convenient ways to meet the future emission regulations. The work presented in this thesis was intended to provide further understanding on how EGR, inlet boost pressure and high-pressure injection influence the spray development, and how this in turn affects combustion pollutant formation and exhaust emissions.

The investigation was divided into two phases. During the first phase, the effects of EGR and supercharging on engine efficiency and exhaust emissions were investigated by means of an analysis of the cylinder pressure, the measurement of exhaust emissions and the visualisation of the sprays and flame in both a four-cylinder and a single-cylinder research DI diesel engine equipped with optical access into the combustion chamber. The results of the investigation have revealed that engine efficiency is predominantly affected by pumping losses, compression pressure (inlet charge mass) and combustion timing; in particular, IMEP increases with increasing inlet boost pressure depending on the timing of combustion over all EGR rates tested. The results also revealed that NO_x emissions are affected predominantly by oxygen concentration, heat absorbing capacity of the inlet charge and timing of combustion; in particular, NO_x emissions decrease with increasing EGR, but increase only slightly with supercharging compared to levels under naturally aspirated conditions. Smoke levels are predominantly affected by oxygen concentration and ignition delay; in particular, smoke increases with increasing EGR, and decreases with increasing swirl ratio and, even more so, with intake boost pressure. Finally, it has been concluded that the combination of EGR and supercharging can offer only advantages in that it allows a significant reduction in the NO_x levels and increase of power output while maximising the suppression of smoke emissions.

As part of the first phase, the LII and LIS techniques were employed for producing better focus on the effects of EGR on in-cylinder soot formation and oxidation during the combustion period. The results have indicated that the soot formation and oxidation are affected by increasing EGR rate due to the lower oxygen concentration. As a result, higher levels of soot were identified in the cylinderafter 400° CAD as EGR rates increased, which agreed well with the smoke measurements obtained in the engine exhaust.

The second phase of the investigation was conducted in a modified Hydra single-cylinder four-valve DI diesel engine equipped with an electronically controlled injection pump which is capable of high-pressure injection up to 1500 bar. Similarly to the first phase of investigation, analysis of cylinder pressures, measurement of exhaust emissions and visualisation of spray and combustion flame development were conducted in order to determine the effects of various injection parameters on engine performance.

The visualisation of the spray showed that a centrally positioned multi-hole vertical injector provided an even distribution of the six sprays, which led to improved air-fuel mixing and minimisation of local hot spots. The obtained images revealed that the higher injection pressure resulted in faster spray tip penetration and led to an earlier impingement of the fuel on the wall and formation of wall jets on each side of the impingement point, which resulted in reduction of the ignition delay. Detailed engine tests have confirmed that the higher injection pressure resulted in a decrease in smoke emissions due to the improved fuel atomisation but an increase in NO_x emissions due to the enhanced air-fuel mixing, assisted by the smaller size of the generated fuel droplets, and an increase in the premixed burn fraction as a result of the higher injection rate, induced by the shortened duration of the pre-needle lift. On the other hand, the higher injection pressure provided a negligible improvement in the NO_x-smoke trade-off curve; this is considered to be due to an imbalance between the high injection pressure and the small size of the nozzle hole which offsets the effect of the improved fuel atomisation on the reduction in smoke levels. The results also showed that an increased fuel delivery gave rise to lower NO_x levels at advanced injection timing and low load conditions, when the initial injection rate and ignition delay remained unchanged. It is considered that this is the result of the increased fuel injected after the start of combustion which absorbed more heat from the in-cylinder gases due to the latent heat of vaporisation. On the other hand, reduction of the size of the nozzle hole resulted in improvements in the NO_x-smoke trade-off curve as a result of the improved fuel atomisation by the increased injection pressure; however, only a small increase in injection rate has been observed unlike raising injection pressure which has a much more significant increase in the injection rate.

Overall, the results revealed that when high pressure-injection is employed, reducing the size of the nozzle hole should also be considered at the same time in order to maintain, in combustion, an appropriate injection rate and duration of injection, satisfying both combustion efficiency and exhaust emission requirements.

5.2 RECOMMENDATIONS FOR FUTURE WORK

Recommended future work ranges from incremental improvements in the experimental systems developed within this thesis, which have been described in Chapters 2 to 4, to the development of new techniques to be applied to the engine under different operating conditions.

Overall, evaluation of factors affecting spray, combustion development and exhaust emissions, such as EGR, swirl, supercharging, injection pressure, cylinder head design and nozzle hole configuration, has already been performed to various degrees of sophistication and completeness. The spray development has been characterised extensively in engines by means of measurement of the spray tip penetration and observation of the spray development after impingement on the wall using high-speed spray visualisation. In this thesis, only liquid phase penetration and dispersion have been investigated. It is thus recommended to extend the work to vapour phase penetration measurement and investigation of spray behaviour after wall impingement using the Mie scattering based imaging technique. In addition, measurement of the fuel droplets size under various engine operating conditions could provide the more detailed information required for quantitative estimation of the effect of various injection parameters on diesel combustion.

Soot formation and oxidation during combustion phase has been investigated within this thesis by experiments based on the LII/LIS technique. To compare in-cylinder soot concentration obtained through optical and mechanical techniques it would, though, be necessary to extend the developed LII/LIS system to allow semi-quantitative or possibly quantitative measurements to be obtained through calibration against a well known test flame (Dec and Espey, 1995). It is also suggested to develop corresponding in-cylinder gas sampling techniques, which are able to provide additional information to the present results on in-cylinder pollutant formation (for example, Shimazaki *et al.*, 1996).

Further detailed parametric studies by means of isolating each factor from the others would be highly desirable to understand and quantify the effect of each factor on engine performance similar to the work of Ladommatos *et al.* (1996a, 1996b, 1998a, 1998b, 1998c)

but complemented by laser diagnostics for the measurement of in-cylinder NO concentration. Particularly, the effects of a four-valve cylinder head and centrally positioned vertical injector on air-fuel mixing process and combustion could be isolated from other parameters. Employing a common rail system would be very effective to isolate the effect of high injection pressure since it allows changing the injection pressure independently from the engine speed. Furthermore, it allows investigating the effect of split injection such as pilot injection and multiple injection, which have been considered as indispensable tools for future diesel engines in order to improve the control of noise, combustion and emissions. Engine performance tests together with high-resolution imaging of the spray and combustion development for both split and multiple injection in realistic engines may provide answers to the many questions raised about the role of these injection factors on diesel spray and combustion. In view of the stringent current and future emissions legislation, an improved understanding of the effect of the above mentioned factors and of the characteristics of exhaust after-treatment devices, such as oxidation catalysts and particulate traps, will be of great value to both academics and industrialists alike.

REFERENCES

K. Akiyama, K. Masunaga, K. Kado and T. Yoshioka (1987), "Cylinder Wear Mechanism in an EGR-Equipped Diesel Engine and Wear Protection by the Engine Oil", SAE Paper 872158

B. Alatas, J. A. Pinson, T.A. Litzinger, D.A. Santavicca (1993), "A Study of NO and Soot Evolution in a DI Diesel Engine via Planar Imaging", SAE Paper 930973

C. A. Amann and D. C. Siegla (1982), "Diesel Particulates-What They Are and Why", *Aerosol Science and Technology*, Elsevier Publishing Co., Inc.

C. Arcoumanis, A. Hatziapostolou and J. H. Whitelaw (1991), "Flow and Combustion in a Hydra Direct-Injection Diesel Engine", SAE Paper 910177

C. Arcoumanis, Z. Hu and J. H. Whitelaw (1994), "Droplet Velocity Measurement in a Four-Cylinder Optical DI Diesel Engine", *Intern. Sym. COMODIA 94*, Japan, pp. 205-211

C. Arcoumanis and P. Cutter (1995a), "Flow and Heat Transfer Characteristics of Impinging Diesel Sprays under Cross Flow Conditions", SAE Paper 950448

C. Arcoumanis, C. Bae, A. Nagwaney and J.H. Whitelaw (1995b), "Effect of EGR on Combustion in an Optical Four Cylinder HSDI Diesel Engine", SAE Paper 950850

C. Arcoumanis, A. Nagwaney, W. Hentschel and S. Ropke (1995c), "Effect of EGR on Spray Development, Combustion and Emissions in a 1.9L Direct-Injection Diesel Engine", SAE Paper 952356

C. Arcoumanis, P. Cutter, D. Foulkes and R. Tabaczynski (1996), "Spray, Combustion and Heat Transfer Studies in a Ricardo Hydra Direct-Injection Engine", IMechE Seminar on Lean Burn Combustion Engines, Paper S433/013

T. A. Baritaud, T. A. Heinze and J. F. Le Coz (1994), "Spray and Self-Ignition Visualization in a DI Diesel Engine", SAE Paper 940681

G. R. Bower and D. E. Foster (1993), "The Effect of Split Injection on Fuel Distribution in an Engine-Fed Combustion Chamber", SAE Paper 930864

P. H. Campbell, K. M. Sinko and B. Chehroudi (1995), "Liquid and Vapour Phase Distributions in a Piloted Diesel Fuel Spray", SAE Paper 950445

J. G. Carter, R. H. Huebner, R. N. Hamm and R. D. Birkhoff (1965), "Optical Properties of Graphite in the Region 1100-3000Å", *Phys. Rev.*, A 137, 639

F. E. Corcione and G. Valentino (1994), "Analysis of In-Cylinder Turbulent Air Motion Dependence on Engine Speed", SAE Paper 940284

F. E. Corcione, G. Mazziotti and B. M. Vaglieco (1996), "Two Dimensional Analysis of Diesel Combustion by Spectral Flame Emissivity Measurements", SAE Paper 960838

G.E. Cossali, A. Gerla, A. Coghe and G. Brunello (1996), "Effect of Gas Density and Temperature on Air Entrainment in a Transient Diesel Spray", SAE Paper 960862

Y. Daisho, N. Uchida, K. Morita, S. Shimogata and T. Saito (1994), "Effects of Supercharging and EGR on Diesel Combustion and Emissions", *Intern. Sym. COMODIA 94*, pp. 281-286

C. J. Dasch (1984), "New Soot Diagnostics in Flames Based on Laser Vaporisation of Soot", *20th Sym. (Intern.) on Combustion*, The Combustion Institute, pp. 1231-1237

J. E. Dec (1992), "Soot Distribution in a DI Diesel Engine Using 2-D Imaging of Laser-Induced Incandescence, Elastic Scattering, and Flame Luminosity", SAE Paper 920115

J. E. Dec, A. O. zur Loye and D. L. Siebers (1991), "Soot Distribution in a DI Diesel Engine Using 2-D Laser-Induced Incandescence Imaging", SAE Paper 910224

J. E. Dec and C. Espey (1992), "Soot and Fuel Distribution in a DI Diesel Engine via 2-D Imaging", SAE Paper 922307

J. E. Dec and C. Espey (1995), "Ignition and early Soot Formation in a DI Diesel Engine Using Multiple 2-S Imaging Diagnostics", SAE Paper 950456

J. E. Dec and E. B. Coy (1996), "OH Radical Imaging in a DI Diesel Engine and the Structure of the Early Diffusion Flame", SAE Paper 960831

J. C. Dent (1980), "Turbulent Mixing Rate - Its Effect on Smoke and Hydrocarbon Emissions from Diesel Engine", SAE paper 800092

M. Dürnholz, G. Eifler and H. Endres (1992), "Exhaust-Gas Recirculation - A Measure to Reduce Exhaust Emissions of DI Diesel Engines", SAE Paper 920725

A. C. Eckbreth (1977), "Effects of Laser-Modulated Particulate Incandescence on Ramen Scattering Diagnostics", *Journal of Applied Physics*, Vol. 48, pp. 4473-4479

S. Endo (1991) "Improvement of Performance for Truck by Multi Valve System", *Proceedings of The Sixth International Pacific Conference on Automotive Engineering*, Vol. 1, pp. 91-102

P. V. Farrell, C. T. Chang and T. F. Su (1996), "High Pressure Multiple Injection Spray Characteristics", SAE Paper 960860

K. Funai, T. Yamaguchi and S. Itoh (1996), "Injection Rate Shaping Technology with Common Rail Fuel System (EDC-U2)", SAE Paper 960107

Y. Fujiwara, F. Shoichi, S. Tosaka and T. Murayama (1984), "Formation of Soot Particulates in the Combustion Chamber of Pre-Combustion Chamber Type Diesel", SAE Paper 840417

Y. Hardalupas, A. M. K. P. Taylor and H. Whitelaw (1992), "Characteristics of the Spray from a Diesel Injector", *Int. J. Multiphase Flow* Vol. 18, No. 2, pp. 159-179, 1992

B. S. Haynes and H. G. Wagner (1981), " Soot Formation", *Prog. Energy Combust. Sci.*, Vol. 7, pp. 229-273, 1981

W. Hentschel and S. Röpke (1993), "Influence of Exhaust Gas Recirculation on Diesel Combustion", *IDEA EFFECT A.3*, periodic report 1.7.93 - 31.12.93

H. O. Herrmann and M. Dürnholz (1995), "Development of a DI Diesel Engine with Four Valves for Passenger Cars", SAE Paper 950808

J. B. Heywood (1988), "Internal Combustion Engine Fundamentals", *McGraw-Hill Book Company,* Intern. *Ed.* 1988

H. Hiroyasu, M. Arai and K. Nakanishi (1980), "Soot Formation and Oxidation in Diesel Engines", SAE Paper 800252

R.W. Horrocks (1993), "Light Duty Diesels - an Update on the Emissions Challenge", *Proc. I. Mech. E. Seminar on 'Worldwide Engine Emission Standards and How to Meet Them'*, London, pp. 155-169

N. Iida (1993), "Surrounding Gas Effects on Soot Formation and Extinction - Observation of Diesel Spray Combustion Using a Rapid Compression Machine", SAE Paper 930603

T. Kamimoto, H. Yokota and H. Kobayashi (1987), "Effect of High Pressure Injection on Soot Formation Processes in a Rapid Compression Machine to Simulate Diesel Flames", SAE Paper 871610

T. Kamimoto, H. Yokota and H. Kobayashi (1989), "A New Technique for the Measurement of Sauter Mean Diameter of Droplets in Unsteady Dense Sprays", SAE Paper 890316

T. Kamimoto and H. Kobayashi (1991), "Combustion Processes in Diesel Engines", *Prog. Energy Combust. Sci.*, Vol. 17, pp. 163-189

T. Karasawa, M. Tanaka, K. Abe, S. Shiga and T. Kurabayashi (1991), "Effect of Nozzle Configurations on the Atomization of Steady Spray", ICLASS-91, July 1991

M. Kerker (1969), "The Scattering of Light and other Electromagnetic Radiation", *Academic Press, New York and London,* pp. 31-39, 1969

N. Khalil, Y. A. Levendis and R. F. Abrams (1995), "Reducing Diesel Particulate and NOx Emissions via Filtration and Particle-Free Exhaust Gas Recirculation", SAE Paper 950736

I. M. Khan, G. Greeves and C. H. T. Wang (1973), "Factors Affecting Smoke and Gaseous Emissions from Direct Injection Engines and a Method of Calculation", SAE Paper 730169

D. B. Kittelson, M. J. Pipho, J. L. Ambs and L. Luo (1988), "In-cylinder Measurements of Soot Production in a Direct-Injection Diesel Engine", SAE Paper 880344

S. Kobory, T. Kamimoto and H. Kosaka (1996), "Ignition, Combustion and Emissions in a DI Diesel Engine Equipped with a Micro-Hole Nozzle", SAE Paper 960321

H. Kosaka, T. Nishigaki, T. Kamimoto and S. Harada (1995), "A Study on Soot Formation and Oxidation in an Unsteady Spray Flame via Laser Induced Incandescence and Scattering Techniques", SAE Paper 952451

H. Kosaka, T. Nishigaki, T. Kamimoto, T. Sano, A. Matsutani and S. Harada (1996), "Simultaneous 2-D Imaging of OH Radicals and Soot in a Diesel Flame by Laser Sheet Techniques", SAE Paper 960834

S. I. Kwon, M. Arai, H. Hiroyasu (1991), "Ignition Delay of a Diesel Spray Injected Into a Residual Gas Mixture", SAE Paper 911841

M. Ladommatos, S. M. Abdelhalim, H. Zhao and Z. Hu (1996a), "The Dilution, Chemical, and Thermal Effects of Exhaust Gas Recirculation on Diesel Engine Emissions-Part1: Effects of Reducing Inlet Charge Oxygen", SAE Paper 961165

M. Ladommatos, S. M. Abdelhalim, H. Zhao and Z. Hu (1996b), "The Dilution, Chemical, and Thermal Effects of Exhaust Gas Recirculation on Diesel Engine Emissions-Part2: Effects of Carbon Dioxide", SAE Paper 961167

N. Ladommatos, S. M. Abdelhalim, H. Zhao and Z. Hu (1998a), "Effects of EGR on Heat Release in Diesel Combustion", SAE Paper 980184

N. Ladommatos, S. M. Abdelhalim, H. Zhao and Z. Hu (1998b), "Effects on Diesel Combustion and Emissions of Reducing Inlet Charge Mass Due to Thermal Throttling with Hot EGR", SAE Paper 980185

N. Ladommatos, S. M. Abdelhalim and H. Zhao (1998c), "Effects of Exhaust Gas Recirculation Temperature on Diesel Engine Combustion and Emissions", Proc. Instn. Mech. Engrs, Vol. 212 Part D, pp 479-500

M. Lapuerta, J.M. Salavert and C. Doménech (1995), "Modelling and Experimental Study About the Effect of Exhaust Gas Recirculation on Diesel Engine Combustion and Emissions", SAE Paper 950216

W. Lee, C. E. Solbrig, T. A. Litzinger and R. J. Santoro (1990), "Planar Laser Light Scattering for the In-Cylinder Study of Soot in a Diesel Engine", SAE Paper 902125

S.C. Lee and C. L. Tien (1981), "Optical Constants of Soot in Hydrocarbon Flames", Proc., *18th International Symposium on Combustion*, The Combustion Institute, Pittsburgh, pp. 1156-1166

Y.A. Levendis, I. Paviatos and R.F. Abrams (1994), "Control of Diesel Soot, Hydrocarbon and NO_x Emissions with a Particulate Trap and EGR", SAE Paper 940460

X. Li and J. S. Wallace (1995a), "A Phenomenological Model for Soot Formation and Oxidation in Direct-Injection Diesel Engines", SAE Paper 952428

X. Li and J. S. Wallace (1995b), "In-Cylinder Measurement of Temperature and Soot Concentration Using the Two-Color Method", SAE Paper 950848

N. Lida and G. T. Sato (1988), "Temperature and Mixing Effects on NO_x and Particulate", SAE Paper 880424

N. Lida (1993), "Surrounding Gas Effects on Soot Formation and Extinction-Observation of Diesel Spray Combustion Using a Rapid Compression Machine", SAE Paper 930603

L. Luo, M. J. Pipho, J. L. Ambs and D. B. Kittelson (1989), "Particle Growth and Oxidation in a Direct-Injection Diesel Engine", SAE Paper 890580

H.T.C. Machanon, S. Shiga, T. Karasawa and H. Kakamura (1994), "The Effect of EGR on Diesel Particulate Emissions", *Intern. Sym. COMODIA 94*, Japan, pp. 287-292

Y. Matsui, T. Kamimoto, S. Matsuoka (1982), "Formation and Oxidation Processes of Soot Particulates in a DI Diesel Engine - An Experimental Study via the Two-Color Method", SAE Paper 820464

L.A. Melton (1984), "Soot Diagnostics Based on Laser Heating", *Applied Optics*, V23, pp. 2201-2208

D.L. Mitchell, J.A. Pinson and T. A. Litzinger (1993), "The Effects of Simulated EGR via Intake Air Dilution on Combustion in an Optically Accessible DI Diesel Engine", SAE 932798

D. T. Montgomery and R. D. Reitz (1996), "Six-Mode Cycle Evaluation of the Effect of EGR and Multiple Injections on Particulate and NOx Emissions from a DI Diesel Engine", SAE Paper 960316

J. D. Naber and D. L. Siebers (1996), "Effects of Gas Density and Vaporization on Penetration and Dispersion of Diesel Sprays", SAE Paper 960034

K. Nakakita, M. Nagaoka *et al.* (1990), "Photographic and Three Dimensional Studies of Diesel Soot Formation Process", SAE Paper 902081

K. B. Neoh, J. B. Howard and A. O. Sarofim (1980), "Soot oxidation in Flames" in *Particulte Carbon Formation During Combustion (D. C. Siegla and G. W. Smith eds.)*, Plenum, New York

K. Nishida, N. Murakami, H. Hiroyasu and S. Saijocho (1985), "A Pulsed-laser Holography Study of the Evaporating Diesel Spray in a High Pressure Bomb", *Intern. Sym. on Diagnostics and Modeling of Combustion in Reciprocating Engines*, Tokyo, pp. 141-148

S. Ohigashi, H. Kuroda (1971), Y. Hayashi and K. Sugihara, "Heat Capacity Changes Predict Nitrogen Oxides Reduction by Exhaust Gas Recirculation", SAE Paper 710010

H. B. Palmer and C. F. Cullis (1965), "The formation of Carbon from Gases", *Chemistry and Physics of Carbon (editor P. L. Walker),* Vol. 1, pp. 265-325, Marcel Dekker, New York

D. A. Pierpont and R. D. Reitz (1995), "Effects of Injection Pressure and Nozzle Geometry on DI Diesel Emissions and Performance", SAE Paper 950604

J. A. Pinson, D. L. Mitchell, R. J. Santoro and T. A. Litzinger (1993), "Quantitative, Planar Soot Measurements in a DI Diesel Engine Using Laser-Induced Incandescence and Light Scattering", SAE Paper 932650

S. L. Plee, T. Ahmad and J. P. Myers (1981), "Flame Temperature Correlation for the Effects of Exhaust Gas Recirculation on Diesel Particulate and NO_x Emissions", SAE Paper 811195

B. Quay, T. W. Lee, T. Ni and R. J. Santoro (1994), "Spatially Resolved Measurements of Soot Volume Fraction Using Laser-Induced Incandescence", *Combustion and Flame 97*, pp. 384-392

H. X. Quoc, J. M. Vignon and M. Brun (1991), "A New Approach of the Two-Color Method for Determining Local Instantaneous Soot Concentration and Temperature in a DI Diesel Combustion Chamber", SAE Paper 910736

K. K. Rao, D. E. Winterbone and E. Clough (1992), "Laser Illuminated Photographic Studies of the Spray and Combustion Phenomena in a Small High Speed DI Diesel Engine", SAE Paper 922203

K. K. Rao, D. E. Winterbone and E. Clough (1993), "Influence of Swirl on High Pressure Injection in Hydra Diesel Engine", SAE Paper 930978

A. Roller, A. Arnold, M. Decker, V. Sick, J. Wolfrum, W. Hentschel and K. P. Schindler (1995), "Non-Intrusive Temperature Measurements during the Compression Phase of a DI Diesel Engine", SAE Paper 952461

S. Röpke, G. W. Schweimer and T. S. Strauss (1995), "NO_x Formation in Diesel Engines for Various Fuels and Intake Gases", SAE Paper 950213

T. Saito, Y. Daisho, N. Uchida, N. Ikeya (1986), "Effects of Combustion Chamber Geometry on Diesel Combustion", SAE Paper 861186

R. A. Santoro, H. G. Semerjian and R. A. Dobbins (1983), "Soot Particle Measurements in Diffusion Flame", Combust. Flame, 51, pp. 203-218 (1983)

T. Shimada, T. Shoji and Y. Takeda (1989), "The Effect of Fuel Injection Pressure on Diesel Engine Performance", SAE Paper 891919

N. Shimazaki, H. Hatanaka, K. Yokota and T. Nakahira (1996), "A Study of Diesel Combustion Process Under the Condition of EGR and High-Pressure Fuel Injection with Gas Sampling Method", SAE Paper 960030

M. Shioji, S. Ito, K. Yamane and M. Ikegami (1995), "A Study of Diesel Combustion and Soot Formation as Observed by High-Speed Photography", Trans. JSME, B61-581, pp. 334-349, 1995

T. Shiozaki, H. Nakajima, H. Yokota and A. Miyashita (1998), "The Visualization and Its Analysis of Combustion Flame in a DI Diesel Engine", SAE Paper 980141

S. Shundoh, T. Kakegawa and K. Tsujimura (1991), "The effect of Injection Parameters and Swirl on Diesel Combustion with High Pressure Fuel Injection", SAE Paper 910489

S. Shundoh, M. Komori, K. Tsujimura and S. Kobayashi (1992), "NO_x Reduction from Diesel Combustion Using Pilot Injection with High Pressure Fuel Injection", SAE Paper 920461

O. I. Smith (1981), "Fundamentals of Soot Formation in Flames with Applications to Diesel Engine Particulate Emissions", *Prog. Energy Combust. Sci.*, Vol. 7, pp. 275-291

T. F. Su, P. V. Farrell and R. T. Nagarajan (1995), "Nozzle Effect on High pressure Diesel Injection", SAE Paper 950083

T. F. Su and P. V. Farrell (1998), " Characterization of High-Injection-Pressure Diesel Sprays with Relation to Particulate and NO_x Emissions", Atomization and Sprays, vol. 8, pp. 83-107, 1998

H. Sugihara, Y. Aoyagi, T. Otani and I. Joko (1992), "Effects of High-Boost Turbocharging on Combustion Characteristics and Improving Its Low Engine Speed Torque", SAE Paper 920046

S. Tajima (1991), "Development of Sequential Twin Turbo System for Rotary Engine", SAE Paper 910624

N. P. Tait and D. A. Greenhalgh, "Proceedings of the Optical Methods and Data Processing" in *Heat Transfer and Fluid Flow Conference,* London, April 1992

P. M. Torpey, M. J. Whitehead and M. Wright, "Experiments in the Control of Diesel Emissions", I. Mech. E. *Symposium on Air Pollution Control in Transportation Engine*, C124-71, 1971

T. C. Tow, D. A. Pierpont and R. D. Reitz (1994), "Reduction Particulates and NO_x Emissions by using Mutiple Injections in a Heavy Duty D. I. Diesel Engine", SAE Paper 940897

D. R. Tree and D. E. Foster (1994), "Optical Measurements of Soot Particle Size, Number Density, and Temperature in a Direct Injection Diesel Engine as a Function of Speed and Load", SAE Paper 940270

K. Tsujimura (1994), "Problems around the Development of Low Emission Diesel Combustion System", *Intern. Sym. on Advanced Spray Combustion*, Hiroshima, Japan, pp. 151-156

H. Tsunemoto and H. Ishitani (1980), "The Role of Oxygen in Intake and Exhaust on NO Emission, Smoke and BMEP of a Diesel Engine with EGR System", SAE Paper 800030

N. Uchida, Y. Daisho and T. Saito (1992), "The Control of Diesel Emissions by Supercharging and Varying Fuel-Injection Parameters", SAE Paper 920117

N. Uchida, Y. Daisho, T. Saito and H. Sugano (1993), "Combined Effects of EGR and Supercharging on Diesel Combustion and Emissions", SAE Paper 930601

D. Verhoeven, J. Vanhemelryck and T. Baritaud (1998), "Macroscopic and Ignition Characteristics of High-Pressure Sprays of Single-Component Fuels", SAE Paper, 981069

R. W. Weeks and W. W. Duley, "Aerosol Particulate Sizes from Light Emission during Excitation by TEA (Transversely Excited Atmospheric Pressure) Carbon Dioxide Laser Pulses", J. Appl. Phys. 45, 4661 (1971)

A. Wiartalla, H. Bäcker and M. Dürnholz (1995), "Influence of Injection System Parameters on Spray Development, Combustion and Soot Formation by Optical Measurement Techniques in a Model Combustion Chamber", SAE 950233

D. S. Whitelaw (1997), "Droplet Atomisation of Newtonian and Non-Newtonian Fluids Including Automotive Fuels", *PhD Thesis*, Imperial College, University of London

R. P. Wilson, E. B. Muir and F. A. Pellicciotti (1974), "Emissions Study of a Single-Cylinder Diesel Engine", SAE Paper 740123

Y. H. Won, T. Kamimoto, H. Kobayashi and H. Kosaka (1991), "2-D Soot Visualization in Unsteady Spray Flame by means of Laser Sheet Scattering Technique", SAE Paper 910223

Y. H. Won, T. Kamimoto and H. Kosaka (1992), "A Study on Soot Formation in Unsteady Spray Flames via 2-D Soot Imaging", SAE Paper 920114

M. K. Yassine, M. K. Tagomori, N. A. Henein and W. Bryzik (1996), "White Smoke Emissions Under Cold Starting of Diesel Engines", SAE Paper 960249

H. Yokota, Y. Kudo, H. Nakajima, T. Kakegawa and T. Suzuki (1997), "A new Concept for Low Emission Diesel Combustion", SAE Paper 970891

F. Yoshizu and M. Nakayama (1991), "Spray Characteristics of a Pilot Injection System Operating in an Idling DI Diesel Engine", ICLASS-91, U.S.A., July 1991

A. J. Yule, S. L. Mo, S. Y. Tham and S. M. Avak (1985), "Diesel Spray Structure", *ICLASS 85*, Paper 11B/2/1, Vol. 1, London, pp. 1-15

A. O. zur Loye, D. L. Siebers and J. E. Dec (1990), "2-D Soot Imaging in a Direct Injection Diesel Engine Using Laser-Induced Incandescence", *Intern. Sym. COMODIA 90*, Japan, pp. 523-528

BIBL
LONDON